AD-A200 136

SECURITY CLASSIFICATION OF THIS PAGE (When Data Entered)

(4)

REPORT DOCUMENTATION PAGE

READ INSTRUCTIONS BEFORE COMPLETING FORM

1. REPORT NUMBER: MAR 1	2. GOVT ACCESSION NO.
3. RECIPIENT'S CATALOG NUMBER	
4. TITLE (and Subtitle): Interaction of Radiation with Matter: Atomic Collision Processes Occurring in the Presence of Radiation Fields"	5. TYPE OF REPORT & PERIOD COVERED: 8/01/87 - 7/31/88
	6. PERFORMING ORG. REPORT NUMBER
7. AUTHOR(s): P.R. Berman	8. CONTRACT OR GRANT NUMBER(s): N00014-87-K-0303
9. PERFORMING ORGANIZATION NAME AND ADDRESS: Prof. P.R. Berman, Physics Dept. - New York University, 4 Washington Place, New York, N.Y. 10003	10. PROGRAM ELEMENT, PROJECT, TASK AREA & WORK UNIT NUMBERS: 4124104....02
11. CONTROLLING OFFICE NAME AND ADDRESS: Office of Naval Research Resident Representative New York, 715 Broadway, New York, N.Y. 10003	12. REPORT DATE: Sept. 15, 1988
	13. NUMBER OF PAGES: 315
14. MONITORING AGENCY NAME & ADDRESS(if different from Controlling Office)	15. SECURITY CLASS. (of this report): Unclassified
	15a. DECLASSIFICATION/DOWNGRADING SCHEDULE

16. DISTRIBUTION STATEMENT (of this Report)

Approved for public release; distribution unlimited

17. DISTRIBUTION STATEMENT (of the abstract entered in Block 20, if different from Report)

18. SUPPLEMENTARY NOTES

19. KEY WORDS (Continue on reverse side if necessary and identify by block number)

Laser Spectroscopy, Optical Collisions, Radiative Collisions, Two-level Atom; Atomic Coherence, Degenerate Four Wave Mixing, Saturation Spectroscopy, Dressed Atom, Photon Echo, Bloch Equations, Collision Kernel; Collisions; Optical Noise.

20. ABSTRACT (Continue on reverse side if necessary and identify by block number)

Work is reported in areas of:-

(1) Laser spectroscopic line shapes
(2) Coherent transients including collisional effects
(3) Laser-assisted collisions
(4) Collision-induced resonant structures in laser spectroscopy
(5) Collision kernels and transport coefficients
(6) Interactions with broadband noise

DD FORM 1 JAN 73 1473 EDITION OF 1 NOV 65 IS OBSOLETE
S/N 0102-LF-014-6601

SECURITY CLASSIFICATION OF THIS PAGE (When Data Entered)

Annual Report (MAR1)

Title: "Theoretical Studies Relating to the Interaction of Radiation with Matter: Atomic Collision Processes Occurring in the Presence of Radiation Fields"

Supported by: The U.S. Office of Naval Research

Contract No: N00014-87-K-0303

Report Period: August 1, 1987 - July 31, 1988

Approved for public release; distribution unlimited.

Research has been carried out in the areas of (1) laser spectroscopic line shapes, (2) coherent transients including collisional effects, (3) laser-assisted collisions, (4) collision-induced resonant structures in laser spectroscopy (5) collision kernels and transport coefficients, and (6) interactions with broadband noise.

1. Laser Spectroscopic Line Shapes (M. Gorlicki, P. Berman)

A collaboration with Duncan Steel (Univ. of Michigan) was initiated to develop the mutual exchange of theoretical and experimental information regarding high resolution laser spectroscopy. The initial problem which was studied involved the four-wave mixing signals generated in Na vapor using lasers having various polarizations. It was theoretically predicted and experimentally verified that, for polarizations in which magnetic state alignment or orientation was not conserved, narrow resonances (characterized by the ground state width) can be observed.[1*,2*] Such resonances could serve as the basis for an optical filter or be used to lock two laser frequencies together. The theory of these resonances involves a calculation of the creation and spontaneous decay of polarization gratings. It has recently been suggested to us that these processes may be important in the cooling of trapped atoms below the Doppler limit.[3]

In a related calculation, we showed that velocity-changing collisions can also lead to narrow resonances in four-wave mixing.[4*] If the ground and excited state collision rates for a two-level atom differ, collisions result in non-conservation of population for a given velocity class of atoms. This lack of population conservation again results in resonances characterized by the ground state width. Recently, Steel was able to use a modified version of our theory to explain experimental results that he has recently obtained.[5]

It might also be mentioned that a theory of collisionally-induced Rayleigh gain which we had developed[6] (but which was only recently published)[7*] has received a great deal of experimental interest. This gain is used to generate new fields in multiwave mixing in both linear and ring configurations.[8]

---

* An asterisk indicates that a reprint or preprint of this article has been forwarded to the Scientific Officer with this report. Reprints of articles have been furnished to DTIC with this report. Preprints or reprints of articles are available on request to anyone receiving this report.

2. Coherent Transients Including Collisional Effects (R. Sung, P. Berman)

We have finished an analysis of an extended-pulse echo experiment carried out by Mossberg's group several years ago.[9] In their qualitatative analysis of the problem, they argued that the strong field in the second excitation pulse could quench collisional effects. We have shown that this interpretation is questionable.[10*,11*] A detailed analytical and numerical solution of the problem of a strong transient field interacting with an ensemble of atoms also subjected to velocity-changing collisions has been carried out. Using this solution, we have analyzed a two-photon echo experiment in which the second pulse's duration is comparable to an atomic decay time. It was found that, even for weak excitation fields, a long second excitation pulse can "quench" collisional effects. This phenomenon is conveniently explained in terms of a set of equivalent stimulated photon echo excitation schemes. For strong fields, the overall explanation of the "quenching" process is not changed significantly, implying that our interpretation of the quenching differs from that of Mossberg's group. The agreement between theory and experiment is good. The techniques that were developed for this problem can be applied to other transient problems involving collisions. A previous article[12*] on the transient probe spectrum for a driven two-level atom has appeared.

3. Laser-Assisted Collisions (P. Berman)

Our modified theory of Laser-Induced Collisional Excitation Transfer (LICET) gives good agreement with most of the LICET experiments carried out to date.[13*,14*,15*] The theory, which includes the contribution of a nearly-resonant intermediate state, has cleared up a long-standing mystery on the detuning dependence of the quasistatic tail of the LICET profile. Work on the model is continuing, in collaboration with A. Bambini (Florence).

In another LICET calculation [in collaboration with F. Schuller (Univ. of Paris - XIII)], we have calculated the magnetic state polarization produced in the quasistatic wing of the LICET profile. The calculation possesses interesting differences from that of collisional redistribution.[15*] We are preparing a manuscript in which the various physical mechanisms giving rise to the final state polarization are examined.

4. Collision-induced Resonances in Laser Spectroscopy (P. Berman)

In collaboration with G. Grynberg (Univ. of Paris), we have developed a unified interpretation of pressure-induced resonances. Both collisionally-aided radiative excitation (CARE) and pressure-induced extra resonances in four-wave mixing (PIER4) are explained on the basis of conservation of energy arguments.[16*] The theory is formulated using both bare - and dressed-state approaches, and some new aspects relating to the quantum statistics of the fields are described. Moreover, we have predicted new classes of experiments, such as fluorescence beats and two-photon ionization, in which collision induced resonant structures should be observed. Duncan Steel has indicated that he might try to carry out the experiments to test the theory.

5. Collision Kernels and Transport Coefficients (G. Rogers, P. Berman)

Our previous work on the relationship between collision kernels and transport coefficients[17,18*] has proven to be useful in analyzing an experiment on Na - rare gas velocity-changing collisions.[19*] Using a theory including the effects of fine-structure changing collisions, we were able to fit all the data with only one free parameter. These results have implications for a successful modeling of the optical piston.[20] We are trying to extend some of this work to relate the coefficients of thermal conductivity and viscosity to the collision kernels encountered in laser spectroscopy.

6. Interactions with Broadband Noise (V. Finkelstein)

Recently, it has been appreciated that broadband noise can be used as a source of femtosecond time resolution.[21] The theory of such processes is complicated owing to the fact that the four-wave mixing interaction used to generate the signals involves the use of a noise pulse and its time-delayed image. The correlations between the pulse and its time-delayed replica create an effective interaction which is non-Markovian. We are working on the theory of this problem in the limit of intense pulses. Ultimately, we hope to compare our theoretical results with the experimental ones of the groups of Hartmann[22] and LeGouët.[23]

References

1. J. Liu, G. Khitrova, D. Steel and P.R. Berman, in Laser Spectroscopy VIII, edited by W. Persson and S. Svanberg (Springer-Verlag, Berlin, 1987)

pp. 291-293; J. Liu, D.G. Steel, P.R. Berman, M. Gorlicki and G. Khitrova, to appear in Proceedings of XVI International Quantum Electronics Conference.

2. P.R. Berman, D.G. Steel, G. Khitrova and J. Liu, Phys. Rev. A38, 252 (1988).
3. See, for example, P.D. Lett, R.N. Watts, C.I. Westbrook, W.D. Phillips, P.L. Gould and H.J. Metcalf, Phys. Rev. Lett. 61, 169 (1988).
4. M. Gorlicki, P.R. Berman and G. Khitrova, Phys. Rev. A37, 4340 (1988).
5. J. Liu and D.G. Steel, to appear in Phys. Rev. A.
6. P.R. Berman, G. Khitrova dnd J.F. Lam in Spectral Line Shapes, edited by F. Rostas (de Gruyter, Berlin, 1985), Vol. 3, p. 337.
7. G. Khitrova, P.R. Berman and M. Sargent, J. Opt. Soc. Amer. B5, 160 (1988).
8. D. Grandclément, G. Grynberg and M. Pinard, Phys. Rev. Lett. 59, 40 (1987); G. Khitrova, J.F. Valley and H.M. Gibbs, Phys. Rev. Lett. 60, 1126 (1988).
9. A.G. Yodh, J. Golub and T.W. Mossberg, Phys. Rev. Lett. 53, 659 (1984).
10. R. Sung and P.R. Berman, submitted to Phys. Rev. A.
11. R. Sung and P.R. Berman, submitted to Phys. Rev. A.
12. N. Lu and P.R. Berman, Phys. Rev. A36, 3845 (1987).
13. A. Agresti, P.R. Berman, A. Bambini and R. Stefenal, Phys. Rev. A38, (1988).
14. P.R. Berman in Atomic and Molecular Processes with Short Intense Laser Pulses, edited by A. Bandrauk (Plenum, New York, 1988) pp. 75-85.
15. P.R. Berman in Spectral Line Shapes, Vol. 4, edited by J. Szudy - to appear.
16. P.R. Berman and G. Grynberg, Phys. Rev. A, to appear.
17. P.R. Berman, J.E.M. Haverkort and J.P. Woerdman, Phys. Rev. A34, 4647 (1986).
18. P.R. Berman, in Workshop on Light-Induced Kinetic Effects in Gases, edited by L.J.F. Hermans (Univ. of Leiden, 1988) pp. 1-8.
19. J.E.M. Haverkort, J.P. Woerdman and P.R. Berman, Phys. Rev. A36, 5251 (1987).
20. H.G.C. Werij, J.E.M. Haverkort and J.P. Woerdman, Phys. Rev. A 33, 3270 (1986).

21. See, for example, T. Kobayashi, T. Hattori, A. Terasaki and K. Kurokowa, Revue Phys. Appl. 22, 1773 (1987), and references therein.

22. R. Beach and S.R. Hartmann, Phys. Rev. Lett. 53, 663 (1984).

23. J. LeGouët, private communication.

PUBLICATIONS

PAPERS SUBMITTED TO REFEREED JOURNALS

(not yet published)

1. P.R. Berman and G. Grynberg, "Theory and Interpretation of Pressure-Induced Resonances", Phys. Rev. A (in press) (additional support from NSF).

2. R. Sung and P.R. Berman, "Collisional Relaxation in an Extended-Pulse Photon-Echo: Weak Field Limit", submitted to Physical Review A (additional support from NSF).

3. R. Sung and P.R. Berman, "Theory of Optical Coherent Transients Including Collisional Effects - Application to an Extended Pulse Photon Echo", submitted to Physical Review A (additional support from NSF).

PAPERS PUBLISHED IN REFEREED JOURNALS

1. N. Lu and P.R. Berman, "Transient Probe Spectra in a Driven Two-Level Atom," Phys. Rev. A36, 3845-3861 (1987).

2. J.E.M. Haverkort, J.P. Woerdman and P.R. Berman, "Experimental Determination of Na-Noble Gas Velocity-Changing and Fine Structure Changing Collision Kernels," Phys. Rev. A36, 5251-5264 (1987).

3. G. Khitrova, P.R. Berman and M. Sargent, "Theory of Pump-Probe Spectroscopy", J. Opt. Soc. Amer. B5, 160-170 (1988).

4. P.R. Berman, D.G. Steel, G. Khitrova and J. Liu, "Effects of Radiative Decay in Four-Wave Mixing Spectroscopy - Narrow Resonances Produced by Nonconservation of Population, Alignment, and Orientation", Phys. Rev. A38, 252-262 (1988).

5. M. Gorlicki, P.R. Berman and G. Khitrova, "Theory of Resonances in Four-Wave Mixing Resulting from Velocity-Changing Collisions", Phys. Rev. A37, 4340-4350 (1988).

6. A. Agresti, P.R. Berman, A. Bambini and R. Stefanel, "Analysis of the Far Wing Behavior in the Spectrum of the LICET Process," Phys. Rev. A38, (1988).

On all papers except No. "6", additional support from NSF is acknowledged.

BOOKS (AND SECTIONS THEREOF) SUBMITTED FOR PUBLICATION

1. J. Liu, D.G. Steel, P.R. Berman, M. Gorlicki and G. Khitrova, "High Resolution Four-Wave Mixing Spectroscopy of Narrow Resonances in Doppler-Broadened Systems," to appear in Proceedings of XVI International Quantum Electronics Conference(additional support from NSF).

2. P.R. Berman, "Three-State Model for Laser-Assisted Collisions", to appear in Spectral Line Shapes, Vol. 4, ed. by J. Szudy.

BOOKS (AND SECTIONS THEREOF) PUBLISHED

1. P.R. Berman, "Light-Induced Collisional Energy Transfer-Revisited," in Atomic and Molecular Processes with Short Intense Laser Pulses, edited by P. Bandrauk (Plenum, New York, 1988) pp. 75-85.

2. J. Liu, G. Khitrova, D. Steel and P.R. Berman, "Narrow Resonances in Four-Wave Mixing Due to Radiative Decay," in Laser Spectroscopy VIII, edited by W. Persson and S. Svanberg (Springer-Verlag, Berlin, 1987 pp. 291-293 (additional support from NSF).

3. P.R. Berman, "On the Connection Between Collision Kernels and Transport Coefficients", in Proceedings of Workshop on Light-Induced Kinetic Effects in Gases, edited by L.J.F. Hermans (Univ. of Leiden, 1988) pp. 1-8 (additional support from NSF).

Laser Spectroscopy VIII

Proceedings of the Eighth International Conference, Åre, Sweden, June 22–26, 1987

Editors:
W. Persson and S. Svanberg

With 315 Figures

Springer-Verlag Berlin Heidelberg New York
London Paris Tokyo

Narrow Resonances in Four-Wave Mixing Due to Radiative Decay

Jing Liu[1], *G. Khitrova*[2], *D. Steel*[1], *and P. Berman*[2]

[1]Departments of Physics and EECS, University of Michigan, Ann Arbor, MI48109, USA

[2]Department of Physics, New York University, New York, NY10003, USA

The early work of Bloembergen and co-workers on pressure induced extra resonances (PIER-4) verified earlier predictions that resonances in nonlinear spectroscopy can result from incomplete cancellation of quantum mechanical amplitudes in the presence of collisions[1]. This work was followed by a demonstration of collision induced narrow resonances in backward nearly degenerate four-wave mixing (NDFWM)[2] which have a similar physical origin.

In the current work, we demonstrate that such resonances can be observed in collisionless systems due to spontaneous emission. In a two level Doppler broadened system, the NDFWM response is characterized by two resonances as a function of the pump-probe detuning, δ. The first resonance, at δ=0, has a linewidth determined by the relaxation of the ground state and excited state. The second resonance, at δ equal to twice the pump-resonance detuning, has a width determined by the decay rate of the dipole coherence. In this work, we are concerned with the first resonance only.

If the system is closed (i.e., the excited state can decay only to the ground state) then the population difference decays at the spontaneous emission rate, and the linewidth of the δ=0 resonance is given by γ_{sp}. However, if the system is "open" (for example, the upper state can radiatively decay to a long lived state other than the initial state such as a different

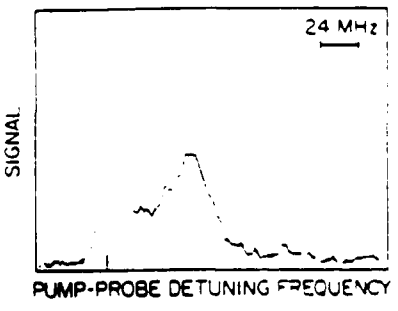

Fig. 1a NDFWM spectra on the $S_{1/2}(F=2)$ to $P_{1/2}(F=2)$ transition.

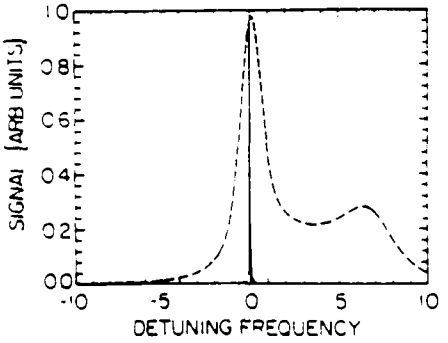

Fig. 1b Calculation normalized to γ_{sp}. The dashed line accounts for Doppler broadening.

hyperfine or Zeeman sublevel of the ground state), then the population difference decays with two components that have decay rates determined by the inverse upper and lower state lifetimes.

These effects are observed in NDFWM measurements of atomic sodium. Fig. 1a shows the NDFWM spectrum recorded on the $S_{1/2}(F=2)$ to $P_{1/2}(F=2)$ transition. In the absence of the $P_{1/2}(F=2)$ decay to the F=1 ground state, the system would be closed and both of the resonances would have the same width, 20 MHz. However, the observed linewidth of the $\delta=0$ resonance is 7 MHz. This width is in excellent agreement with the analysis (Fig. 1b) based on an open system which gives a nonvanishing amplitude for the narrow resonance (solid curve). The dashed line includes Doppler broadening. The results show a long-lived component in the population difference with a width determined by the transit time and residual Doppler effects. (Note, *unlike a coherent Raman effect, all three input beams are nearly resonant with the* $S_{1/2}(F=2)$ *to* $P_{1/2}(F=2)$ *transition.*)

Fig. 2a shows the NDFWM spectrum recorded on the $S_{1/2}(F=2)$-$P_{3/2}(F=3)$ transition. The data shows a new feature which is a dip in the first resonance. To understand this, we note that earlier descriptions have ignored the effects of alignment and orientation which contribute to the response in a system with magnetic subetate degeneracies. For the F=2 to F=3 transition, the population is conserved and the system is closed for population. However, since the field can transfer net orientation or alignment to the atom, one can show the system is not closed. The resulting ground state alignment and orientation lead to a nonvanishing amplitude for the narrow component which manifests itself as a dip in the resonant structure centered at $\delta=0$. The width of this dip is again determined by the inverse transit time and residual Doppler width. For this transition, the sign of the ground state component is opposite to the sign of the upper state component, producing the dip. Agreement with theory is excellent, as shown (for the first resonance) in Fig. 2b.

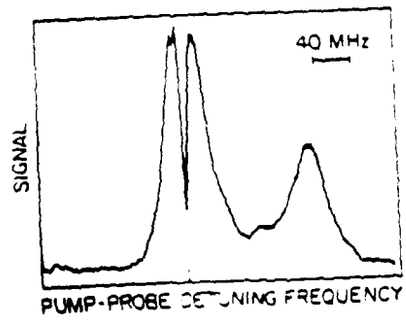

Fig. 2a NDFWM spectrum of the $S_{1/2}(F=2)$ to $P_{3/2}(F=3)$ transition.

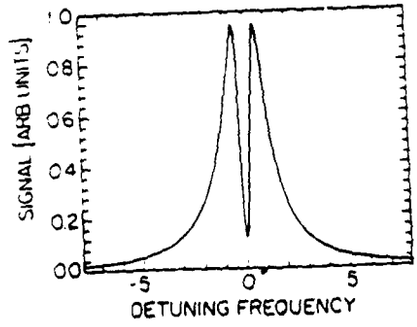

Fig. 2b Calculation of the first resonance, normalized to γ_{sp}.

In summary, these data and analysis show the effects of decay of the excited state to a state other than the initial state of excitation. We anticipate that this understanding will be important in understanding frequency or time domain measurements in other materials such as the spectroscopy of resonant systems in solids.

This work was supported by ARO, ONR, and NSF (PHY8415781).

1. N. Bloembergen, in Laser Spectroscopy, edited by H. Walther and K.W. Rothe (Springer, Berlin, 1979), p340. Yehiam Prior, etal, Phys. Rev. Lett. 48, 111 (1981).
2. J.F. Lam, D.G. Steel, and R.A. McFarlane, Phys. Rev. Lett. 49, 1628 (1982), also 56, 1679 (1986).

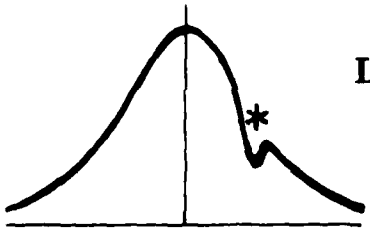

Workshop on

Light-Induced Kinetic Effects in Gases

Leiden, June 2-3, 1988

Organizing Committee:

L.J.F. Hermans (Leiden)
J.P. Woerdman (Leiden)
G. Nienhuis (Utrecht/Leiden)

Workshop secretary:

Anneke Aschoff
Huygens Laboratory
P.O. Box 9504
2300 RA Leiden, The Netherlands
Phone (0)71-275896

Sponsored by:

Rijksuniversiteit Leiden
Koninklijke Nederlandse Akademie van Wetenschappen
Stichting voor Fundamenteel Onderzoek der Materie
Stichting Physica

ON THE CONNECTION BETWEEN COLLISION KERNELS AND TRANSPORT COEFFICIENTS

P.R. BERMAN

New York University, 4 Washington Place, New York, N.Y. 10003

A connection is made between classical transport theory and the usual description of collisional processes in laser spectroscopy. In classical transport theory, collisional processes are described in terms of either transport coefficients or collision integrals. In analyzing the influence of collisions on laser spectroscopic line shapes, collisions are often described in terms of collision kernels. Two sets of equations are obtained relating the collision integrals to the collision kernels. While these two sets of equations are equivalent for any physically realistic kernel, they need not be equivalent if one carries out calculations using phenomenological kernels. If the two methods give similar collision integrals for a phenomenological collision kernel, it may serve as a justification for the use of that kernel. It is shown that the two methods do give very similar results for the Keilson-Storer kernel but give dramatically different results for a "difference" kernel (a kernel that is a function of the difference between the initial and final velocity). The calculations, carried out for a low-density binary gas mixture, provide a link between classical transport theory and the collision kernels commonly used in analyzing experiments in laser spectroscopy. Implications of the results to experimental situations of current interest are explored.

The research described in this report was carried out during my visit to Huygens Laboratory in November, 1985. The work represents a collaborative effort between Drs. Haverkort, Woerdman, and myself. I was fortunate to be able to be a visitor at the University of Leiden, an institution that has in the past, and continues to be, and important center for research in kinetic theory. In this environment, it was possible to combine some of the results I had obtained in analyzing the effects of collisions on laser spectroscopic line shapes with concepts originating in the

transport theory of gases. What emerged from this study was a method for relating the collision integrals and transport coefficients of transport theory to the collision kernels commonly used in spectroscopic line shape analysis.

It is the aim of this report to recall some of the results of that study and to suggest possible paths for continued research in this subject area. Details of the calculations can be found in Reference [1], which is hereafter referred to as I; "Transport Theory" will be abbreviated as "TT", while "the study of collisional processes using laser spectroscopy" will be referred to as "CLS".

Fundamental to both TT and CLS is a knowledge of the intermolecular potential. Armed with expressions for the intermolecular potential, one can proceed, in principle, to calculate the scattering amplitudes and differential scattering cross sections which characterize collisions in a vapor. From the differential scattering cross sections, it is possible to arrive at expressions for the transport coefficients of TT or the collision kernels of CLS. Although TT and CLS share a common language at the level of the differential scattering cross section, there has not been much dialogue between researchers working in these two areas. Undoubtedly, this is due to the different techniques and vocabulary employed in TT and CLS, as well as the different types of physical processes which are probed in both approaches. This lack of "crosstalk" between the two disciplines is unfortunate, since several of the results achieved in TT (CLS) can be used to complement those of CLS (TT).

TT

Owing to density, temperature or velocity gradients within a vapor, physical observables such as momentum and energy are transported from one part of the vapor to another. Such transport processes can be characterized by coefficients of diffusion, thermal conductivity and viscosity. These coefficients can be measured experimentally and can be calculated assuming a specific form for the intermolecular potential. Although the values for the transport coefficients reflect the nature of the intermolecular potential, they are essentially moments of a distribution function and, as such, provide considerably less information than the distribution function itself. In other words, the transport coefficients characterize the non-uniform state of a vapor, but cannot be used to map out the intermolecular potential. This situation is somewhat reminiscent to that encountered in the impact limit of the pressure

broadening of spectral line shapes - the collision-induced line width and shift are sufficient to characterize the line shapes, but, as quantities representing an average over collision parameters, they shed limited light on the intermolecular potential.

In order to calculate the transport coefficients in a systematic manner, one can follow an approximation scheme developed by Chapman and Enskog [2]. For a vapor in thermal equilibrium having a Maxwellian velocity distribution, there is no average transport of momentum, energy, etc., across a given plane in the vapor. Transport results from deviations of the distribution function from Maxwellian. In Chapman-Eskog theory, it is assumed that the distribution function remains close to Maxwellian so that an expansion of the distribution function about a Maxwellian is permissible. This procedure allows one to linearize the Boltzmann equation and to obtain an approximation scheme for calculating both the distribution function and the transport coefficients to arbitrary degrees of accuracy for a given intermolecular potential. For moderate temperature, density and velocity gradients in the vapor, the deviation of the distribution function from Maxwellian is not excessive and the expansion converges rapidly. The transport coefficients are expressed in terms of a few "square bracket integrals" [3] or "effective cross sections" [4] which give the appropriate transport characteristics of the vapor. Moreover, for a well-defined intermolecular potential, the square bracket integrals or effective cross sections can be related to the so-called collision integrals (to be defined below), which represent an integral over a given function of the collision scattering angle. Thus the objective of TT is to obtain expressions for the collision integrals from the intermolecular potentials and then obtain the transport coefficients from the collision integrals.

CLS

In "traditional" line shape studies, collisions are found to broaden and shift absorption and emission profiles. As mentioned above, the broadening and shift parameters can be viewed as somewhat analogous to the transport coefficients. With the advent of laser spectroscopy, additional information about collisions occurring within a vapor can now be derived from line shape studies. In a typical laser spectroscopy experiment, one excites a specific velocity class of atoms using a nearly monochromatic laser source. As a result of collisions within the vapor the velocities of the selected atoms relax back towards a Maxwellian distri-

bution. For experiments done in the time domain, one monitors this relaxation as a function of time [5]. In steady-state experiments, relaxation occurs on a time scale determined by an effective lifetime of the velocity-selected atoms, and one measures a velocity distribution corresponding to relaxation over this time interval [6]. Since the total velocity profile is monitored, considerably more information about collisions is available than from simple line width and shift measurements.

The physical quantity of interest in CLS experiments is the collision kernel $K(\vec{v}' \to \vec{v})$, giving the probability density (in velocity space) per unit time that collisions change the velocity of an atom or molecule from $\vec{v}'$ to $\vec{v}$. There have been several experiments in which the collision kernel has been determined [5], [6]. For theoretical evaluations of the kernel, it is invariably assumed that the velocity-tagged molecule undergoes a collision with perturbers whose velocity distribution is Maxwellian. Since the perturber distribution is assumed to be Maxwellian, one arrives at a linear transport equation for the "active-atom" distribution function. The collision kernel can be expressed as a single integral over the collision scattering angle [7]. Calculations of kernels assuming either classical or quantum-mechanical scattering have been carried out for a number of intermolecular potentials [6], [7].

Relationship between TT and CLS

In lowest order approximation, the coefficient of diffusion $D_{12}^{(0)}$ for a two-component gas is given by

$$D_{12}^{(0)} = \frac{k_B T}{m} \frac{1}{N u_r \sigma\binom{10}{10}_{12}} = \frac{3}{2} \frac{k_B T}{m} \frac{1}{N[\vec{C}_1, \vec{C}_1]_{12}} \tag{1a}$$

$$= \frac{3}{16} \frac{k_B T}{\mu} \frac{1}{N \Omega_{12}^{(1,1)}} , \tag{1b}$$

where k_B is Boltzmann's constant, m is the active-atom mass, N is the total molecular density, u_r is the most probable active-atom - perturber relative speed, T is the absolute temperature $\sigma\binom{10}{10}_{12}$ is an effective cross section defined by Eggermont et al [4], $[\vec{C}_1, \vec{C}_1]_{12}$ is a square-bracket integral defined by Chapman and Cowling [3], μ is the active-atom - perturber reduced mass and $\Omega_{12}^{(i,j)}$ is a collision integral defined by [3]

$$\Omega_{12}^{(\ell,s)} = \frac{k_B T}{2\pi\mu} \int_0^\infty dy \int_0^\infty 2\pi b\, db$$

$$\times e^{-y^2} y^{2s+3} [1 - \cos^{\ell}\chi(b,y)], \qquad (2)$$

where ℓ and s are integers, $\chi(b,y)$ is the scattering angle in the center-of-mass frame, and b is the collision impact parameter.

It is important to note that Eq. (1b) follows from Eq. (1a) when explicit use is made of the relationship

$$\frac{d\sigma}{d\Omega} = \frac{b}{\sin\chi} \frac{db}{d\chi}, \qquad (3)$$

where $d\sigma/d\Omega$ is the differential scattering cross section for active-atom - perturber scattering. If one were to use a <u>phenomenological</u> differential scattering cross section (not derivable from an intermolecular potential), then Eq. (1b) would no longer be valid. Of course, the difference between Eqs. (1a) and (1b), in that case, would be a measure of the suitability of the phenomenological cross section which was assumed. I shall return to this point below.

Using the definition of the effective cross sections and the collision kernel, the following relationship between $\sigma\binom{10}{10}_{12}$ and the collision kernel $K(\vec{v}'\to\vec{v})$ was derived in I:

$$N_p \sigma\binom{10}{10}_{12} = -\frac{2}{3u_r^2} \int d\vec{v} d\vec{v}'\, W(\vec{v}')\, K(\vec{v}'\to\vec{v})\, [\vec{v}'\cdot(\vec{v}-\vec{v}')]\,. \qquad (4)$$

Similar equations relating other $\sigma\binom{i\ j}{i\ j'}_{12}$ to integrals of $K(\vec{v}'\to\vec{v})$ are given in I. Equations (1) and (4) imply that any fit of laser line shapes using a specific kernel should be constrained by available (experimental or theoretical) diffusion data. In this way the number of free parameters used in fitting the lines can be reduced to a minimum [6].

Equation (4) can be evaluated for a number of collision kernels $K(\vec{v}'\to\vec{v})$. For a hard-sphere kernel (derivable from a hard sphere intermolecular potential), one finds $N_p u_r \sigma\binom{10}{10}_{12} = (4/3)(\mu/m)\Gamma_{HS}$, where Γ_{HS} is the collision rate and N_p is the perturber density. For the phenomenological Keilson-Storer kernel [9], given by

$$K_{KS}(\vec{v}'\to\vec{v}) = \frac{\Gamma_{KS}}{(\pi\omega^2)^{3/2}} e^{-(\vec{v}-\alpha\vec{v}')^2/\omega^2} \qquad (5)$$

with

$$\omega^2 = (1 - \alpha^2)\, u^2, \qquad (6)$$

where $0 \leq \alpha < 1$ and u is the most probable active-atom speed, one finds $N_p u_r \sigma\binom{10}{10}_{12} = \Gamma_{KS}(1 - \alpha)$. Finally for a "difference-kernel" defined by

$$K_d(\vec{v}' \to \vec{v}) = \frac{\Gamma_d}{[\pi(\delta u)^2]^{3/2}} e^{-(\vec{v}-\vec{v}')^2/(\delta u)^2} \tag{7}$$

one finds $\sigma\binom{10}{10}_{12} = 0$. The fact that $\sigma\binom{10}{10}_{12} = 0$ for a difference kernel reflects the fact that $\langle \dot{\vec{v}} \rangle = 0$ for distribution functions governed by such a kernel (detailed balance is violated).

A method for providing a consistency check for phenomenological collision kernels was given in I. A second method for relating the collision kernels to the collision integrals was derived. Since this method involves the collision integrals rather than the effective cross sections, it is strictly valid for kernels derivable from an intermolecular potential. By calculating the collision integrals using both methods, one has an implicit test of the validity of the chosen kernel. For collision kernels derivable from an intermolecular potential, the collision integrals evaluated by both methods must be identical. Differences between the collision integrals which arise when the two methods are applied to a phenomenological kernel can serve as a test of the validity of the use of such a kernel.

The two methods give the same value for $\Omega_{12}^{(1,1)}$ for any kernel that satisfies detailed balance. Since the Keilson-Storer kernel does satisfy detailed balance, this result serves as a justification for using it to describe diffusion. For the Keilson-Storer kernel, the two methods give the same rather complicated functional form for $\Omega_{12}^{(2,2)}$, but with an amplitude that differs by about 10%. I do not understand the implications, if any, of this result. For the Keilson-Storer kernel, the two methods lead to a different functional form for $\Omega_{12}^{(1,2)}$; however, the two expressions differ by only 6% to 20% when the value of α in Eq. (6) is suitably chosen. For the difference kernel, the collision integrals vanish by the first method and are non-vanishing (but small) by the second. This result indicates the fundamental problems which can arise when kernels are chosen which do not obey detailed balance.

Viscosity and Thermal Conductivity

The coefficients of viscosity and thermal conductivity for a gas mixture are rather complicated [2]. For a one-component gas, the lowest order approximation to the viscosity $\eta^{(0)}$ and thermal conductivity are given

by [2]
$$\eta^{(0)} = \frac{k_B T}{u_r}\,\frac{1}{\sigma\binom{20}{20}} = \frac{5}{2}\,\frac{k_B T}{u_r}\,\frac{1}{[\vec{C}_1^{0}\vec{C}_1, \vec{C}_1^{0}\vec{C}_1]} \tag{8a}$$

$$= \frac{5}{8}\,\frac{k_B T}{\Omega_1^{(2,2)}} \quad ; \tag{8b}$$

$$\lambda^{(0)} = \frac{5}{2}\,\frac{k_B^2 T}{mu_r}\,\frac{1}{\sigma\binom{11}{11}} = \frac{75}{8}\,\frac{k_B^2 T}{mu_r}\,\frac{1}{[S_{3/2}^{(1)}(C_1^2)\vec{C}_1, S_{3/2}^{(1)}(C_1^2)\vec{C}_1]} \tag{9a}$$

$$= \frac{75}{32}\,\frac{k_B^2 T}{m}\,\frac{1}{\Omega_1^{(2,2)}} \quad . \tag{9b}$$

The lack of subscripts on σ and $[\cdot\cdot,\cdot\cdot]$ imply that these quantities are are evaluated for a one-component gas.

The relations derived in I are not sufficient for an evaluation of these equations. What is needed is an analogous set of relations for a tranfer kernel, in which one measures the probability density that a collision transfers the velocity of an active atom $\vec{v}'$ to a final perturber velocity $\vec{v}$. Such terms are related to square bracket integrals [3] of the form $[f(\vec{C}_1), f(\vec{C}_2)]_{12}$, where f is some arbitrary function. If this analogous set of equations is derived and added to the first set, then a comparison with Eqs. (8) and (9) can be made.

Paths for Continued Research

Since limited research has been dedicated to the specific goal of uniting laser spectroscopy and transport theory, it would seem to me that the choices for continued research in this area are virtually unlimited. Along the lines of I, one could complete the transfer-kernel calculation described above. It is also possible to introduce transport coefficients for atomic electronic-state coherence, state-changing collisions, magnetic-state coherence, etc. One could then develop a series of relations between these somewhat unconventional transport coefficients and the corresponding collision kernels. From the experimental side, one could use lasers to create localized deviations from equilibrium and then probe the relaxation back to equilibrium. In particular, one could produce a $\langle\vec{v}\rangle \neq 0$ for a sample and see if there are deviations from an exponential decay law for $\langle\vec{v}(t)\rangle$. The use of lasers to significantly mobilize atoms and give them some net mass flow has already been elegantly demonstrated in the "optical piston [10].

Acknowledgments

This work is supported by the U.S. Office of Naval Research and the National Science Foundation under Grant No. PHY 8415781.

References

[1] P.R. Berman, J.E.M. Haverkort and J.P. Woerdman, Phys. Rev. A34, 4647 (1985).

[2] Standard texts which treat Chapman-Enskog theory include S. Chapman and T.G. Cowling, The Mathematical Theory of Nonuniform Gases (Cambridge University Press, London, 1970); J.O. Hirshfelder, C.F. Curtiss and R.B. Bird, Molecular Theory of Gases and Liquids (Wiley, New York, 1954); J.H. Ferziger and H.G. Kaper, Mathematical Theory of Transport Processes in Gases (North-Holland, Amsterdam, 1972).

[3] S. Chapman and T.G. Cowling, op. cit.

[4] G.E.J. Eggermont, H. Vestner, and H.F.P. Knapp, Physica 82A, 23 (1976).

[5] See, for example, M. Gorlicki, C. Lerminiaux, and M. Dumont, Phys. Rev. Lett. 49, 1394 (1982); P. Cahuzac and X. Drago, Opt. Comm. 24, 63 (1978); E. Buhr and J. Mlynek, Phys. Rev. A36, 2684 (1987).

[6] See, for example, J.E.M. Haverkort, J.P. Woerdman and P.R. Berman, Phys. Rev. A36, 5251 (1987), and references therein.

[7] J.H. Ferziger and H.G. Kaper, op. cit.; S. Avrillier, Ch. Bordé, J. Picart and N. Tran Minh, J. de Phys. 47, 1213 (1982).

[8] T. Ho and S. Chu, Phys. Rev. A33, 3067 (1986).

[9] J. Keilson and K.E. Störer, J. Appl. Math. 10, 243 (1952).

[10] See, for example, H.G.C. Werij, J.E.M. Haverkort, and J.P. Woerdman, Phys. Rev. A33, 3270 (1986), and references therein.

Experimental determination of Na–noble-gas velocity-changing and fine-structure-changing collision kernels

J. E. M. Haverkort* and J. P. Woerdman
Molecular Physics Department, Huygens Laboratory, University of Leiden, P.O. Box 9504, 2300 RA Leiden, The Netherlands

P. R. Berman
Physics Department, New York University, 4 Washington Place, New York, New York 10003
(Received 13 July 1987)

We report on an experimental investigation of the collision kernels governing the effects of velocity-changing collisions, fine-structure-changing collisions, and their interplay, for Na–noble-gas pairs. The velocity distributions in the two Na excited-state fine-structure levels and in the Na ground-state hyperfine levels have been measured in the presence of a pump laser which produces velocity-selective excitation. For interpretation of these experiments we use a rate-equation model developed in the context of light-induced drift: the velocity-changing collisions are accounted for by a composite Keilson-Storer kernel describing large-angle and small-angle collisions and the fine-structure-changing collisions are treated in the sudden limit. The model is valid for arbitrarily high pump laser intensities and uses only a single adjustable parameter characterizing the small-angle scattering. It is found that the theory describes the experimental velocity distributions in all four Na levels over a wide range of experimental parameters for each Na–noble-gas pair. The relevance of the collision kernels deduced in the present work is discussed in the context of light-induced drift.

I. INTRODUCTION

Recent experiments[1–8] on light-induced drift (LID) have necessitated a closer study of collision kernels of Na–noble-gas systems. The phenomenon of LID can be described in terms of the level-dependent collisional interaction between optically active atoms and a buffer gas. Specifically, the difference between the active atom ground-state and excited-state collisional interaction with the buffer-gas atoms is the source for LID. A description of LID for Na in a noble-gas background requires knowledge about the collision kernels[9–12] associated with all relevant energy levels of the Na atom. When the pump laser is tuned to the $3s \rightarrow 3p$ transition, the two ground-state hyperfine levels ($3s\ ^2S_{1/2}$; $F=1,2$) and the two excited-state fine-structure levels ($3p\ ^2P_{1/2}$, $3p\ ^2P_{3/2}$) are populated by the combined action of the pump laser, spontaneous decay, and fine-structure-changing collisions. Therefore, in this paper we obtain the kernels for velocity-changing collisions (VCC) and fine-structure-changing collisions (FSC) of Na–noble-gas pairs.

We have directly measured the pump-laser-induced deformations of the velocity distributions in these four Na levels. Normally, in LID, one measures only transport effects related to the deformation of the *total* distribution function. By measuring the velocity distributions in all four relevant levels, we obtain information about the ground-state and the excited-state collision kernels which, in turn, can serve as input for a calculation of the drift velocity in LID.[8] We have measured the single-level distribution functions by means of a separate probe laser, tuned near the Na $3p \rightarrow 4d$ transition for excited-state measurements and tuned near the Na $3s \rightarrow 3p$ transition for ground-state measurements.

Previous work on collision kernels for Na–noble-gas mixtures has not been done in the context of LID and has focused on the collision kernel in a single level. The ground-state collision kernel for Na-Ne has been measured by Aminoff *et al.*,[13] but ground-state data for other Na-noble-gas mixtures are lacking. Liao *et al.*[14] have measured the kernel for velocity-changing collisions in a single excited-state fine-structure level for all Na–noble-gas mixtures, neglecting, however, the effect of fine-structure-changing collisions.

A large body of experimental[15] and theoretical work[16–18] has been devoted to the study of fine-structure-mixing collisions. Historically, these fine-structure-changing collisions have first been observed as a sensitized fluorescence signal when one of the fine-structure states of an alkali-metal atom was excited. Since then, the experimental work can be subdivided into gas-cell and molecular-beam experiments.

Most gas-cell experiments[15] yield *velocity-averaged* cross sections for (i) transfer of population, orientation, and alignment between the two fine-structure states of an alkali-metal atom and (ii) decay of orientation or alignment within one such state. As an exception, Apt *et al.*[19,20] obtained the precollision velocity dependence of such mixing cross sections in the gas phase by measuring the transfer fluorescence as a function of laser detuning; however, the information that could be obtained was rather restricted since only one component of the alkali atom velocity distribution before the collision could be Doppler selected and the velocity distribution after the collision could not be analyzed.

Molecular-beam experiments are intrinsically more suitable to determine velocity-dependent data. The differential scattering cross section for excited alkali–noble-gas collisions has been measured by many groups.[21–25] In these experiments, the velocity and the fine-structure level before the collision are selected but the final fine-structure state is usually not resolved, resulting in a final-state-averaged differential scattering cross section. As an exception, Phillips *et al.*[26] were able to analyze also the fine-structure state after the collision. Finally, the initial velocity dependence of the total mixing cross section has been determined in a molecular-beam experiment;[27,28] however, the final-state velocity distribution or scattering angle was not analyzed.

In the experiments which are discussed in this work, we measure elastic and inelastic collision kernels for atomic state populations. For the Na–noble-gas system under investigation, such kernels can be defined as the probability density per unit time that an alkali-metal atom is scattered from $\mathbf{v}'$ to $\mathbf{v}$ while undergoing a transition from state $|J',m_J'\rangle$ to $|J,m_J\rangle$ as a result of collisions with buffer-gas atoms which are assumed to be in thermal equilibrium. We consider, as is usual in laser spectroscopy, a one-dimensional kernel corresponding to the probability that the component of the atomic velocity along the laser beam is changed. Furthermore, in this work, only the total population of a J level will be considered, averaging out the m_J dependence of the kernel. The collision kernel is thus a quantity which is, in a sense, intermediate between the velocity-averaged transfer cross section and the final-state resolved differential scattering cross section.

We emphasize that the main objective of our work is to obtain a complete set of collision kernels for all Na–noble-gas pairs, the Na atom being in the $3s$ ground state or in the $3p$ excited state, for (future) use in LID theory.[8] Therefore, we have chosen relatively simple Keilson-Storer model kernels with only a few free parameters[8,29] the latter will be fixed by the experiments reported in this paper. In principle, for most Na–noble-gas pairs one could obtain better agreement between the calculated and the measured velocity distributions reported in this work by using more elaborate model kernels (i.e., more free parameters) or by using numerical instead of analytical kernels. Such refinement is of limited use in the context of LID and has therefore not been pursuaded; however, our experimental data are presented in such a way that a more refined analysis remains possible.

The structure of this work is as follows. In Sec. II, we present the experimental setup for measuring the velocity distributions in all four relevant Na levels, and some typical experimental results are shown. In Sec. III we briefly review the four-level rate-equation model previously developed[8] and extend it to five levels in order to be able to calculate the experimental probe spectra. Model kernels for velocity and fine-structure-changing collisions are specified in Sec. IV. In Sec. V a comparison is made between the experimental probe spectra and theoretical spectra; the latter have been obtained using the rate-equation model of Sec. III with the kernels of Sec. IV. In Sec. VI we give conclusions also as to the relevance of the present work for LID.

II. EXPERIMENTAL SETUP AND RESULTS

In this section the experimental setup for the measurement of the velocity distributions in all four relevant Na levels is described and some typical results are presented.

As mentioned above, we will consider the five-level scheme shown in Fig. 1(a), in which levels 1 and 2 are the $^2S_{1/2}$, $F=1$ and $F=2$ ground levels, respectively, and levels 0 and 3 are the two $3p$ fine-structure levels $^2P_{1/2}$ and $^2P_{3/2}$. Level 0 is defined as the level which is directly populated by the pump laser and level 3 is the nonresonant fine-structure level; in our notation, levels $^2P_{1/2}$ and $^2P_{3/2}$ are labeled "0" and "3," respectively, for D_1 excitation; the labels are interchanged for D_2 excitation. The $4d\ ^2D_{3/2}$ level is used as the upper level of the probe laser transition and is denoted as level 4. The pump laser, which is responsible for LID, is always

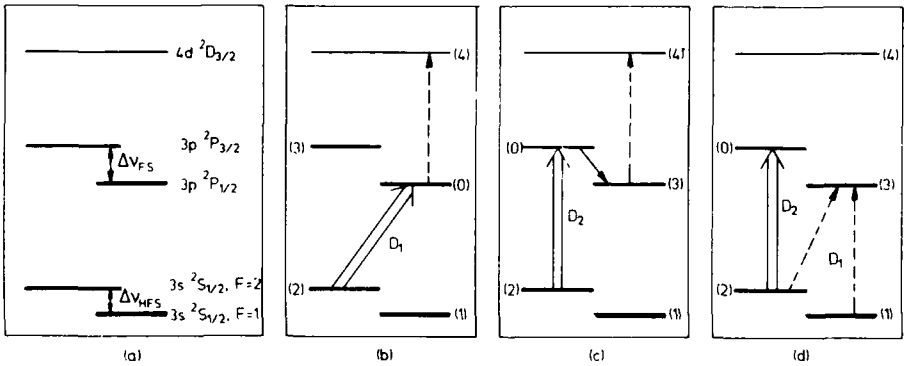

FIG. 1. (a) shows the five-level approximation of the actual Na level scheme. We take into account both ground-state hyperfine levels, both fine-structure levels of the $3p$ excited state (neglecting the $3p$ hyperfine structure), and the $4d$ level. The $3s$ ground-state hyperfine splitting is 1.77 GHz and the $3p$ fine-structure splitting is 510 GHz. (b), (c), and (d) show the pump and probe laser frequencies for measurements of the velocity distributions of the resonant fine-structure level, the nonresonant fine-structure level, and the ground-state levels, respectively. Note that the level numbering is chosen in such a way that level 0 is always the resonant $3p$ level.

tuned into the red wing of the Doppler-broadened $2 \rightarrow 0$ transition, about 1 GHz below line center, but it should be noted that it also weakly excites atoms in the Lorentz tail of the $1 \rightarrow 0$ transition; in fact, this weak excitation turns out to be of prime importance for LID.[8]

The velocity distribution in the *resonant* fine-structure level, level 0, is recorded [Fig. 1(b)] by means of a probe laser which is tuned to the $0 \rightarrow 4$ transition, whereas the velocity distribution in the *nonresonant* fine-structure level, level 3, can be recorded when the probe laser is tuned to the $3 \rightarrow 4$ transition [Fig. 1(c)]. We always use the $3p\ ^2P_{1/2}$ as the lower level for the probe laser transition, because, in this case, complications due to the $4d$ fine-structure splitting are absent since the $^2P_{1/2} \rightarrow {}^2D_{5/2}$ transition is forbidden. Consequently, when we want to switch from resonant to nonresonant fine-structure-level measurements [see Figs. 1(b) and 1(c)], we tune the pump laser from the D_1 to the D_2 line, while keeping the probe laser frequency near the $3p\ ^2P_{1/2} \rightarrow 4d\ ^2D_{3/2}$ transition. In the scheme shown in Fig. 1(b) the two laser-driven transitions share a common level; the resulting complications in interpreting the probe laser spectra are accounted for in Sec. III.

We have also measured the velocity distributions in the two ground-state levels using a probe laser on the $3s \rightarrow 3p$ transition [Fig. 1(d)]. In this case, in order to avoid the complications associated with two laser-driven transitions sharing a common upper level, we have chosen to tune the pump laser to the D_2 line and the probe laser to the D_1 line.

A sketch of the spatial overlap of pump and probe beams is shown in Fig. 2. A pump laser with beam diameter d, much smaller than the diameter D of the cell, induces LID. The relevant velocity distributions can be recorded by means of a probe laser with diameter d' which is running either copropagating, for ground-state measurements, or counterpropagating, for excited-state measurements, with respect to the pump laser beam ($d' < d$). Since $D \gg d$, wall interactions which tend to complicate the transport experiments of LID (Refs. 3 and 4) are absent.

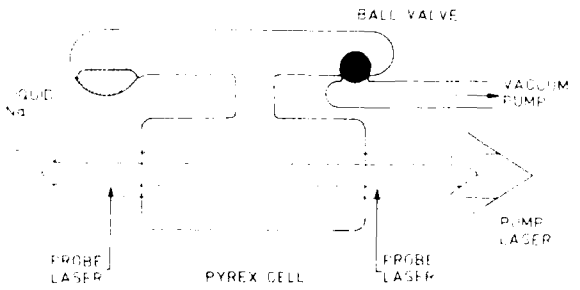

FIG. 2. The Na vapor cell and the geometry of the pump laser beam, which produces LID and the probe laser beams which monitor the velocity distributions responsible for LID. For the excited-state measurements we use a counterpropagating probe beam and for the ground-state measurements a copropagating probe beam. The ball valve is used to admit buffer gas into the cell. The cell is maintained at a temperature of 393 K by an oven (not shown), keeping the Na density at 10^{10} cm^{-3}.

The experimental setup in which the ground-state spectra and excited-state spectra have been measured is shown in Figs. 3 and 4, respectively. We use two Rhodamine 6G dye lasers. The pump laser is a single-frequency ring dye laser (Spectra Physics 380D) which is tuned near 589.0 nm for D_2 excitation and near 589.6 nm for D_1 excitation. The probe laser is a single-frequency standing-wave dye laser (Coherent CR-599-21), tuned near 589.6 nm for ground-state measurements, and near 568.2 nm for excited-state measurements. The intensity of the probe laser beam is actively stabilized using an electro-optic modulator. Both lasers are frequency stabilized and have a linewidth of ≈ 1 MHz. The probe spectra have been digitized using 50 frequency points for excited-state measurements and 200 frequency points for ground-state measurements. The beam profiles inside the Na vapor cell are approximately Gaussian [$d \approx 0.22$ cm, $d' \approx 0.15$ cm full width at half maximum (FWHM)]; they are defined by means of spa-

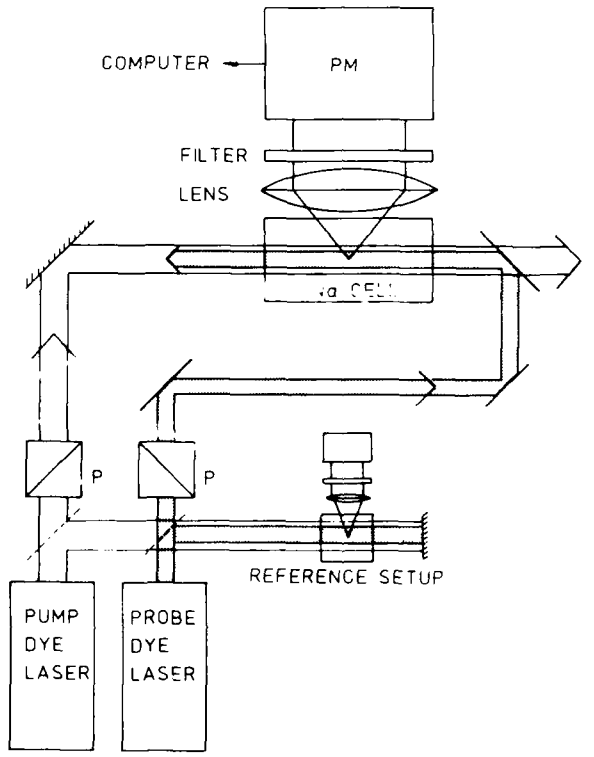

FIG. 3. The experimental setup for excited-state measurements. The excited-state spectra are measured by using a fixed pump laser frequency and by scanning the probe laser frequency over the velocity distribution of the level in study, using a counterpropagating geometry. The 330-nm cascade fluorescence is separated from the strong 589-nm fluorescence by a filter and photon counted by a photomultiplier tube (PM). The frequency calibration setup is basically similar to the main setup, except that both copropagating and counterpropagating geometries are used. The Lamb-dip setup for the calibration of the pump laser frequency is not shown.

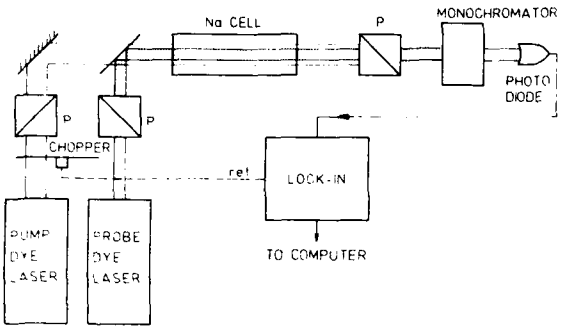

FIG. 4. The experimental setup for ground-state measurements. The ground-state spectra are measured by using a fixed pump laser frequency and scanning the probe laser frequency over the ground-state velocity distributions. The transmitted probe laser beam is separated from the strong pump laser beam using an analyzer in combination with a monochromator and is detected by a photodiode. By chopping the pump laser beam, the pump laser-induced deviation from the ground-state equilibrium distributions is obtained. Not shown are two separate Lamb-dip setups which are used to calibrate the pump and the probe laser frequencies.

tial filters.

The Na–noble-gas mixture is contained in a cylindrical Pyrex cell with an inner diameter of $D=1$ cm and a length of 3 cm (Fig. 2). The cell is connected to a second Pyrex reservoir containing liquid Na. The Na reservoir is connected, via a ball valve, with a larger reservoir at room temperature containing the buffer gas. By controlling the temperature of the Na reservoir, the Na density in the cell is kept at 10^{10} atoms/cm^3, resulting in a maximum light absorption of $\approx 30\%$ at the center of the $2\rightarrow 0$ (D_2) transition. At this Na density, the effects of Na-Na collisions were negligible as compared to the effects of Na–noble-gas collisions. The cell is heated by a quartz tube coated with a transparent semiconducting tin-oxide layer which surrounds the cell and acts as an oven.[30] The noble-gas pressure is monitored by means of a Barocell capacitance manometer.

The experimental setup for the excited-state measurements is shown in Fig. 3. We use a reference setup (Fig. 3) in order to calibrate the probe laser frequency. For the excited-state measurements, the probe laser frequency is monitored by measuring $3s\rightarrow 3p\rightarrow 4d$ two-step excitation spectra. In contrast to the main setup, where only counterpropagating beams are used, both the copropagating and counterpropagating geometries are used in the reference setup. By adding a little amount of buffer gas in the latter frequency calibration cell, the nonresonant fine-structure level is populated by fine-structure-changing collisions. Consequently, both the resonant and the nonresonant excited-state calibration spectra could be measured. During the ground-state measurements, the probe laser frequency was monitored by recording a Lamb-dip spectrum in the reference setup, simultaneously with each ground-state spectrum in the main setup.

The excited-state spectra are recorded by keeping the pump laser frequency fixed and by scanning the probe laser through the velocity distribution of the level under study, using the transitions shown in Figs. 1(b) and 1(c) and monitoring the ultraviolet $4p\rightarrow 3s$ fluorescence (330 nm).

The experimental setup for the ground-state measurements is shown in Fig. 4. The ground-state spectra are recorded by scanning the probe laser through the velocity distribution of the hyperfine level under study, using the $1\rightarrow 3$ or $2\rightarrow 3$ transition, while keeping the pump laser frequency fixed. When the probe laser is tuned to the $1\rightarrow 3$ transition, the copropagating and counterpropagating spectra are equivalent. For experimental convenience, we used the copropagating geometry. We measured the probe laser absorption instead of the probe laser-induced fluorescence, which, in this case, cannot be easily separated from the strong pump laser-induced fluorescence. By choosing mutually orthogonal laser polarizations, the probe beam could be conveniently separated from the much stronger pump beam by means of an analyzer in combination with a monochromator with an instrumental width of 0.2 nm, tuned to the $1\rightarrow 3$ transition [see Fig. 1(d)]. By modulating the pump laser intensity and demodulating the probe absorption synchronously, we obtain a spectrum proportional to the deviation of the ground-state distribution function from equilibrium. We refer to such a spectrum as a ground-state spectrum. In recording these ground-state spectra, we had to avoid the spurious effect of incomplete hyperfine relaxation at the cell wall;[31] this has the same effect as strong velocity-changing collisions. In the present case, this spurious contribution could be suppressed, by choosing the pump beam diameter d much smaller than the cell diameter D.

In Fig. 5(a), as an example, the counterpropagating excited-state spectrum for the resonant fine-structure level is presented for a buffer-gas pressure of 6 Torr of Ne (peak 1). In recording the resonant excited-state spectrum, complications due to the $3p$ hyperfine structure could be eliminated[32] by probing the $^2P_{1/2}$ $(F=1,2)\rightarrow {}^2D_{3/2}$ transition and by using counterpro-

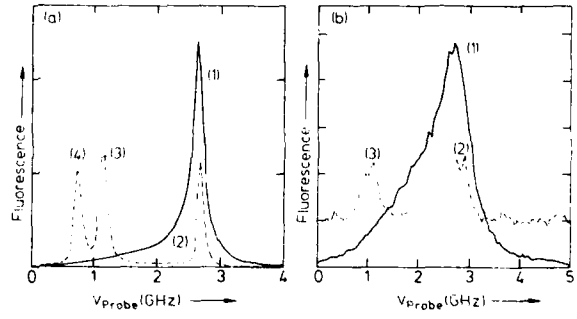

FIG. 5. Resonant (a) and nonresonant (b) excited-state spectra as a function of probe laser detuning at a buffer-gas pressure of 6-Torr argon, a pump laser intensity of 24 mW/cm^2, and a probe laser intensity of 0.2 mW/cm^2. During each measurement, the pump laser frequency was fixed at a detuning of 0.8 GHz below resonance of the $2\rightarrow 0$ transition [see Figs. 1(b) and (c)]. The dashed curve is for frequency calibration. The labels 1–4 are explained in the text.

pagating pump and probe beams; in this geometry, the probe laser is effectively tuned to a two-level transition (neglecting the residual hyperfine splitting of 7 MHz). Using the frequency calibration trace [see Fig. 5(a)], the probe detuning corresponding to a zero Doppler detuning, and thus to a zero axial velocity ($v_z=0$), can be easily obtained. For the $^2P_{1/2}$, $F=1$ (2) level, this detuning corresponds to the position midway between the peaks 2 and 3 (4).

Figure 5(b) shows a similar excited-state spectrum for the nonresonant fine-structure level. The features 2 and 3 in the frequency calibration trace are again due to counterpropagating and copropagating beams, respectively. The full curve is the nonresonant excited-state spectrum at a buffer-gas pressure of 6-Torr Ne; this corresponds to the same experimental conditions as the full curve in Fig. 5(a). By comparing the resonant and the nonresonant spectra, it follows that in this case fine-structure-changing collisions appreciably thermalize the velocity distributions.

We present two typical ground-state spectra in Figs. 6(a) and 6(b), which correspond to a buffer-gas pressure of 0- and 50-mTorr He, respectively. The two dips labeled as 1, correspond to the Bennett hole in the $F=2$ ground state. The two peaks, labeled by 2, correspond to the "Bennett peak" in the $F=1$ ground level which is due to optical hyperfine pumping from levels 2 to 1. In these copropagating spectra, the $^2P_{1/2}$ hyperfine splitting ($\Delta\nu=192$ MHz) is resolved but the $^2P_{3/2}$ hyperfine splittings ($\Delta\nu=15$, 34, 60 MHz) are not resolved.

III. CALCULATION OF THE PROBE SPECTRA

In this section we calculate the two-step excitation spectra produced by an arbitrarily strong fixed-frequency pump laser tuned to the $3s\rightarrow 3p$ transition and a weak probe laser tuned across the $3p\rightarrow 4d$ transition for excited-state measurements or the $3s\rightarrow 3p$ transition for ground-state measurements. We extend the four-level model (levels 0–3) discussed in the context of LID (Ref. 8) by taking into account a fifth level (level 4, see Fig. 1). The probe transition to this fifth level allows one to monitor the velocity distributions of the excited-state levels 0 and 3. The specification of the collision terms which are introduced in the model to describe velocity-changing and fine-structure-changing collisions will be deferred to Sec. IV. In Sec. V we compare the calculated spectra with our experimental spectra.

Following the perturbation approach introduced by Berman *et al.*,[33] we first calculate the velocity distributions in levels 0–3 in the presence of the strong pump laser, the weak probe laser beam being absent. We generalize the approach of Berman *et al.*[33] in the sense that we allow for the Na ground-state hyperfine structure and that we take into account an improved description of the fine-structure-changing collisions (see Sec. IV). The velocity distributions $f_i(v)$ in levels 0–3 are governed by a set of rate equations which is valid for arbitrarily high pump laser intensity. This set of rate equations reads[8]

$$\frac{\partial f_0}{\partial t}=0=R_{10}\left[f_1-\frac{g_1}{g_0}f_0\right]+R_{20}\left[f_2-\frac{g_2}{g_0}f_0\right]$$
$$-A_0f_0+\mathcal{L}_{00}f_0+\mathcal{L}_{03}^{-}f_0+\mathcal{L}_{30}^{+}f_3$$
$$+\Gamma_I[n_0^{(0)}W(\mathbf{v})-f_0]\,, \tag{3.1a}$$

$$\frac{\partial f_1}{\partial t}=0=-R_{10}\left[f_1-\frac{g_1}{g_0}f_0\right]+\alpha_{01}A_0f_0+\alpha_{31}A_3f_3$$
$$+\mathcal{L}_{11}f_1+\Gamma_I[n_1^{(0)}W(\mathbf{v})-f_1]\,, \tag{3.1b}$$

$$\frac{\partial f_2}{\partial t}=0=-R_{20}\left[f_2-\frac{g_2}{g_0}f_0\right]+\alpha_{02}A_0f_0+\alpha_{32}A_3f_3$$
$$+\mathcal{L}_{22}f_2+\Gamma_I[n_2^{(0)}W(\mathbf{v})-f_2]\,, \tag{3.1c}$$

$$\frac{\partial f_3}{\partial t}=0=-A_3f_3+\mathcal{L}_{33}f_3+\mathcal{L}_{30}^{-}f_3+\mathcal{L}_{03}^{+}f_0$$
$$+\Gamma_I[n_3^{(0)}W(\mathbf{v})-f_3]\,. \tag{3.1d}$$

Here A_i is the spontaneous decay rate from level i, g_i is the degeneracy factor of level i, α_{ij} is the branching ratio from level $i\rightarrow j$, $\mathcal{L}_{ii}$ is a collision operator for velocity-changing collisions within level i, $\mathcal{L}_{ij}^{+},\mathcal{L}_{ij}^{-}$ are operators describing gain and loss ($i\leftrightarrow j$) occurring in fine-structure-changing collisions. The transit relaxation rate Γ_I couples the volume within the laser beam with an infinite bath of Na atoms having equilibrium level populations $n_i^{(0)}$ and equilibrium Maxwellian velocity distributions $W(\mathbf{v})$. Explicitly Γ_I is given by[8]

$$\Gamma_I=\frac{(2.405)^2D_g}{R^2}\left[\frac{1}{1+6.8\bar{l}/R}\right]\,, \tag{3.2}$$

where D is the diffusion coefficient,[34] $\bar{l}$ is the mean-free path and R is the radius of the laser beam. The velocity-selective excitation rates R_{i0} are defined as

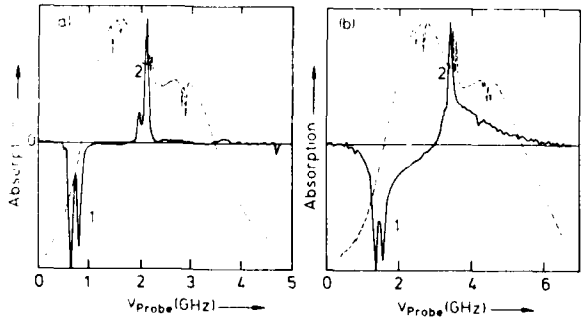

FIG. 6. The ground-state spectra without buffer gas (a) and with 50-mTorr helium (b) as a function of probe laser detuning, at a pump laser intensity of 26 mW/cm^2 and a probe laser intensity of 0.2 mW/cm^2. For frequency calibration, a $3s\rightarrow 3p$ Lamb-dip absorption spectrum has been added (dashed curve).

$$R_{i0}=\tfrac{1}{2}A_0\frac{I}{I_s}\frac{\Gamma_{i0}^2}{\Gamma_{i0}^2+(\Delta_{i0}-kv_z)^2}\ , \tag{3.3a}$$

$$I_s=\frac{\hbar\omega_L A}{2\sigma_H}\ . \tag{3.3b}$$

Here Γ_{i0} is the homogeneous linewidth, Δ_{i0} is the detuning from line center, I_s is the saturation intensity for a two-level system without velocity-changing collisions and σ_H is the homogeneous absorption cross section. The solution of the set of rate equations has been calculated numerically[8] and is denoted as $f_i^{(4)}(v_z)$. The two-step fluorescence excitation spectrum can be calculated from the solution $f_i^{(4)}(v_z)$ of the set of rate equations. It consists of three contributions: a "stepwise" (SW) contribution proportional to the population in level 0 and two "two-quantum" (TQ) contributions proportional to the 1-0 and 2-0 coherences, respectively.[33] The total spectrum is[8]

$$I=I^{\rm SW}+I_{1\to4}^{\rm TQ}+I_{2\to4}^{\rm TQ}\ , \tag{3.4a}$$

$$I^{\rm SW}=\frac{2(\Omega')^2}{A_4+\Gamma_T}{\rm Re}\int dv_z f_0^{(4)}(v_z)L'_{40}(v_z)\ , \tag{3.4b}$$

$$I_{1\to4}^{\rm TQ}=\frac{2(\Omega\Omega')^2}{A_4+\Gamma_T}{\rm Re}\int dv_z[f_1^{(4)}(v_z)-f_0^{(4)}(v_z)]\times L'_{10}(v_z)L'_{40}(v_z)L'_{41}(v_z)\ , \tag{3.4c}$$

$$I_{2\to4}^{\rm TQ}=\frac{2(\Omega\Omega')^2}{A_4+\Gamma_T}{\rm Re}\int dv_z[f_2^{(4)}(v_z)-f_0^{(4)}(v_z)]\times L'_{20}(v_z)L'_{40}(v_z)L'_{42}(v_z)\ , \tag{3.4d}$$

where Ω,Ω' are the Rabi frequencies corresponding to the pump laser and the probe laser fields, respectively. The Lorentzians $L'_{10}(v_z),L'_{41}(v_z)$ and the somewhat more complex line-shape function $L'_{40}(v_z)$ are defined as

$$L'_{10}(v_z)=\frac{\Gamma_{10}+i\delta_{10}}{\Gamma_{10}^2+\delta_{10}^2}\ , \tag{3.5a}$$

$$L'_{41}(v_z)=\frac{\Gamma_{41}-i\delta_{41}}{\Gamma_{41}^2+\delta_{41}^2}\ , \tag{3.5b}$$

$$L'_{40}(v_z)=\frac{\Gamma_{41}+i\delta_{41}}{(\Gamma_{40}+i\delta_{40})(\Gamma_{41}+i\delta_{41})+(1+\alpha)\Omega^2}\ , \tag{3.5c}$$

$$\delta_{10}=\omega_{\rm pump}-(\omega_0-\omega_1)-kv_z\ , \tag{3.5d}$$

$$\delta_{41}=\omega_{\rm pump}+\omega_{\rm probe}-(\omega_4-\omega_1)-(k+\epsilon k')v_z\ , \tag{3.5e}$$

$$\delta_{40}=\omega_{\rm probe}-(\omega_4-\omega_0)-\epsilon k'v_z \tag{3.5f}$$

$$\alpha=\frac{\Gamma_{41}+i\delta_{41}}{\Gamma_{42}+i\delta_{42}}\ . \tag{3.5g}$$

The Lorentzians $L'_{20}(v_z)$ and $L'_{42}(v_z)$ have the same functional form as $L'_{10}(v_z)$ and $L'_{41}(v_z)$ with δ_{10},δ_{41} replaced by δ_{20},δ_{42}. Equations (3.4) and (3.5) are a generalization of the results obtained by Berman *et al.*[33] in the sense that we allow for the hyperfine splitting in the ground state. Moreover, Berman *et al.* only took into account velocity-changing collisions with velocity changes larger than those corresponding to the width of a Bennett hole. This additional assumption, which was necessary in order to obtain analytical results, is not required in our numerical approach.

The nonresonant excited-state spectra involve probe transitions which start from the nonresonant fine-structure level and consequently do not involve any two-quantum contributions since the two transitions do not share a common level. In this case, the probe spectra are simply convolutions of a Lorentzian with the appropriate velocity distributions,

$$I_{3\to4}=\frac{2(\Omega')^2}{A_4+\Gamma_T}\int dv_z f_3^{(4)}(v_z)\frac{\Gamma_{34}}{\Gamma_{34}^2+(\Delta_{34}-kv_z)^2}\ . \tag{3.6}$$

Next, we address the ground-state probe spectra. The copropagating spectrum in which the $F=2$ ground level is common to pump and probe transitions again contains two-quantum contributions (V configuration[35]). Since the ground-state spectra associated with the $F=1$ and $F=2$ levels essentially contain the same information about the ground-state collision kernel, we decided to analyze only the probe spectrum associated with the $F=1$ level, the pump transition always starting from the $F=2$ level. The probe spectrum associated with this nonresonant ground-state velocity distribution is

$$I_{1\to3}=\frac{2(\Omega')^2}{A_3+\Gamma_T}\int dv_z f_1^{(4)}(v_z)\frac{\Gamma_{13}}{\Gamma_{13}^2+(\Delta_{13}-kv_z)^2}\ . \tag{3.7}$$

Finally, in order to compare the theory with experimental spectra, the effects of the $^2P_{1/2}$ and $^2P_{3/2}$ hyperfine structure must be accounted for in the nonresonant excited-state spectra and in the ground-state spectra; for the resonant excited-state spectrum with counterpropagating beams, such effects are minimal due to Doppler cancellation. The probe spectra calculated from Eqs. (3.6) and (3.7) are *ad hoc* convolved with the hyperfine splitting of the $3p$ level in order to obtain the final theoretical expression for comparison with experiment.

IV. KERNELS FOR FINE-STRUCTURE-CHANGING COLLISIONS

In this section kernels which describe both the effects of fine-structure-changing collisions and velocity-changing collisions are presented. We start with a collision model for an active atom with degenerate levels, described by an orbital angular momentum $\mathbf{L}\neq0$ only, the so called L-base model. During a collision of a Na atom with a noble-gas atom, only the angular momentum $\mathbf{L}$ of the Na atom is affected, while the electron spin $\mathbf{S}$ and the nuclear spin $\mathbf{I}$ can be considered as frozen, provided that the collisions occur at a short enough time scale so that $\mathbf{I}$ and $\mathbf{S}$ cannot couple with $\mathbf{L}$.[36,37] In this

limit, the so-called "sudden limit," all physics is contained in the L-base collision model. Subsequently, we consider collisions in the J base in which the levels are split due to the spin-orbit interaction. Assuming that the collisions are sudden, the collisional evolution in the J base can be related to the collisional evolution in the L base. The kernels for fine-structure-changing collisions directly follow from this collision model. Finally, the validity of the sudden approximation is discussed briefly.

In the L-base description, collisions affect not only the velocity of an atom, but also its magnetic quantum number m_L. Both effects can be incorporated in a quantum-mechanical version of the Boltzmann equation[38–40] which describes the collisional evolution of the density-matrix elements $\rho_{mm'}(\mathbf{r},\mathbf{v},t)$ of the active atoms due to collisions with buffer-gas atoms. In general, one has to specify $(2L+1)^4$ collision kernels in order to describe the collisional decay and transfer of populations and coherences within such a level. In order to simplify the discussion, an isotropic distribution of the relative velocities of Na atoms and perturbers is assumed.[41] In this case, the collision operator becomes isotropic and only couples multipole elements of equal rank k. The collision operator in the L base can be written as

$$\frac{\partial}{\partial t}{}^{L}\rho_Q^K = \mathcal{L}_K\,{}^{L}\rho_Q^K(\mathbf{v}) = -\Gamma^{(K)}\,{}^{L}\rho_Q^K(\mathbf{v}) + \int d\mathbf{v}'\,K^{(K)}(\mathbf{v}'\to\mathbf{v})\,{}^{L}\rho_Q^K(\mathbf{v}'), \quad (4.1)$$

where ${}^{L}\rho_Q^K(\mathbf{v})$ are the density-matrix elements in the irreducible tensor notation;[42] $\Gamma^{(K)}$ with $K=0,1,2$ are the collisional relaxation rates in the L base for population, orientation, and alignment, respectively; $K^{(K)}(\mathbf{v}'\to\mathbf{v})$ are the associated collision kernels in the L base, and $\mathcal{L}_K$ the collision operators in the L base.

When the collisions are sudden, the collision model in the J base can be obtained from that in the L base. First, the time evolution of the density-matrix elements in the J base ${}^{J}\rho_q^k$ is related to that of their counterparts in the L base ${}^{L}\rho_Q^K$ using vector coupling algebra. Secondly, the time rate of change of the density-matrix elements in the L base ${}^{L}\rho_Q^K$ can be related to the density-matrix elements ${}^{L}\rho_Q^K$ themselves using Eq. (4.1). Finally, these elements ${}^{L}\rho_Q^K$ can again be related with the elements ${}^{J'}\rho_q^k$ in the J base using vector coupling algebra. Using this procedure, an equation describing the collisional evolution of ${}^{J}\rho_q^k$ in the J base is obtained in terms of a collision model in the L base,

$$\frac{\partial}{\partial t}{}^{J}\rho_q^k = \sum_{J',K,m}(2m+1)(2K+1)(2J+1)(2J'+1)\begin{Bmatrix} L & L & K \\ S & m & J \end{Bmatrix}\begin{Bmatrix} L & L & K \\ S & m & J' \end{Bmatrix}\begin{Bmatrix} J & J & k \\ m & S & L \end{Bmatrix} \times \begin{Bmatrix} J' & J' & k \\ m & S & L \end{Bmatrix}\left[-\Gamma^{(K)}\,{}^{J'}\rho_q^k(\mathbf{v}) + \int K^{(K)}(\mathbf{v}'\to\mathbf{v})\,{}^{J'}\rho_q^k(\mathbf{v}')d\mathbf{v}'\right], \quad (4.2)$$

where $\{\ \}$ are 6-J symbols.[43] In deriving Eq. (4.2) we neglected coherences between the two fine-structure states since these states are not connected by any field.

Using Eq. (4.2), one can obtain rate equations governing the collisional evolution of the velocity distributions in the $^2P_{1/2}$ and $^2P_{3/2}$ excited states of Na. For instance, for population transfer ($k=q=0$, $L=1$, $S=\frac{1}{2}$) we find

$$\frac{\partial}{\partial t}f_{1/2} = \mathcal{L}_1 f_{1/2} + \tfrac{1}{3}(\mathcal{L}_0-\mathcal{L}_1)(f_{1/2}+f_{3/2}), \quad (4.3a)$$

$$\frac{\partial}{\partial t}f_{3/2} = \mathcal{L}_1 f_{3/2} + \tfrac{2}{3}(\mathcal{L}_0-\mathcal{L}_1)(f_{1/2}+f_{3/2}), \quad (4.3b)$$

where f_J is the velocity distribution function for level-J population [$f_J=(2J+1)^{1/2}\,{}^{J}\rho_0^0$] and $\mathcal{L}_0,\mathcal{L}_1$ are the collision operators in the L *base* for total population and orientation, respectively. The operator $\mathcal{L}_2$ for alignment in the L base does not appear in these equations, indicating that $\mathcal{L}_2$ only influences the individual m_J distributions, but not the total J-level population distributions. Equations (4.3) also show that the difference $(\mathcal{L}_0-\mathcal{L}_1)$, which depends on the difference between the population and the orientation collision kernel, is responsible for the fine-structure mixing.

The collision operators $\mathcal{L}_0$ and $\mathcal{L}_1$ can be split into two parts: (i) an elastic collision rate $\Gamma^{\rm el}$, giving the rate at which atoms are scattered out of a certain interval $\mathbf{v},\mathbf{v}+d\mathbf{v}$ and (ii) a gain term characterized by a kernel which describes the transfer from the full velocity space back into the same interval,

$$\mathcal{L}_0 = -\Gamma^{\rm el} + \int d\mathbf{v}'K^{(0)}(\mathbf{v}'\to\mathbf{v}), \quad (4.4a)$$

$$\mathcal{L}_1 = -\Gamma^{\rm el} + \int d\mathbf{v}'K^{(1)}(\mathbf{v}'\to\mathbf{v}), \quad (4.4b)$$

in which $\Gamma^{\rm el}$ is given by

$$\Gamma^{\rm el} = \int d\mathbf{v}'K^{(0)}(\mathbf{v}\to\mathbf{v}') > \int d\mathbf{v}'K^{(1)}(\mathbf{v}\to\mathbf{v}'). \quad (4.5)$$

The equality in Eq. (4.5) represents the conservation of total population in the $L=1$ level. As indicated by the inequality in that equation, the velocity-integrated orientation kernel is *not* conserved. Consequently, the total (velocity-integrated) orientation decays to zero, a result that is not surprising given the fact that, in general, collisions destroy Zeeman coherence.

At this point the kernels $K^{(0)}$ and $K^{(1)}$ should be specified in order to obtain expressions for the transfer kernel and the relaxation kernel in the J base. We will follow the common practice[13,44–46] by more or less arbitrarily subdividing the collisions into different categories, depending on the range of the collisional interaction.

These categories can be linked to the shape of the one-dimensional collision kernel which reflects the change of the component of the velocity along the laser axis. As shown by Gorlicki[44] in a numerical calculation of the Ne*-Ne collision kernel based on a realistic potential, the kernel consists of a strong narrow peak arising from small-angle scattering owing to the long-range part of the potential, that is, symmetric around the initial velocity component, and a broad tail arising from large-angle scattering owing to short-range interactions. Also, Ho and Chu,[46] who combined a semiclassical differential cross section for small-angle scattering with a classical Lennard-Jones differential cross section to describe large-angle scattering, found excellent agreement with a full quantum-mechanical calculation of the differential scattering cross section, showing that a subdivision into large-angle and small-angle scattering can be successful.

In addition to classical scattering as described above, there will be a quantum-mechanical diffractive contribution to the scattering. However, since the diffractive scattering does not contribute to magnetic state reorientation in the L basis, as discussed by Keller and Le Gouët[40] (and, consequently, provides no contribution to fine-structure-changing collisions) and since diffractive scattering for level populations corresponds to velocity changes that are undetectable in our experiment, all effects of diffractive scattering have been neglected in the present work.

Here, the subdivision of the collisions into several categories will be exploited to connect the different parts of the kernel with different regimes of fine-structure mixing. For small impact parameters, large-angle scattering (LAS) occurs which mixes the fine-structure populations completely; the large-angle scattering is described by a Keilson-Storer kernel[8,29,47] $K^{\mathrm{LAS}}(\mathbf{v}'\rightarrow\mathbf{v})$ with a corresponding rate $\Gamma^{\mathrm{LAS}}(\mathbf{v})$. For larger values of the impact parameter, small-angle scattering (SAS) occurs, also described by a Keilson-Storer kernel $K^{\mathrm{SAS}}(\mathbf{v}'\rightarrow\mathbf{v})$ and rate $\Gamma^{\mathrm{SAS}}(\mathbf{v})$. Since calculations based on a van der Waals interaction have shown that all collisions corresponding to classical scattering lead to nearly complete depolarization in the L basis,[40,42] orientation cannot be preserved for these LAS and SAS collisions. Consequently, we assume that the orientation kernel vanishes. The resulting L-base model has kernels and rates given by

$$K^{(0)}=K^{\mathrm{LAS}}+K^{\mathrm{SAS}}\ , \tag{4.6a}$$

$$K^{(1)}=0\ , \tag{4.6b}$$

$$\Gamma^{\mathrm{el}}=\Gamma^{\mathrm{LAS}}+\Gamma^{\mathrm{SAS}}\ , \tag{4.6c}$$

$$\Gamma^{\mathrm{LAS}}=\int d\mathbf{v}'K^{\mathrm{LAS}}(\mathbf{v}\rightarrow\mathbf{v}'),\quad \Gamma^{\mathrm{SAS}}=\int d\mathbf{v}'K^{\mathrm{SAS}}(\mathbf{v}\rightarrow\mathbf{v}')\ . \tag{4.6d}$$

It follows from Eqs. (4.3) that the difference between $K^{(1)}(\mathbf{v}'\rightarrow\mathbf{v})$ and $K^{(0)}(\mathbf{v}'\rightarrow\mathbf{v})$ is responsible for fine-structure mixing. Consequently, according to Eqs. (4.6a) and (4.6b), all collisions corresponding to classical scattering angles contribute to fine-structure mixing. When Eqs. (4.5) and (4.6) are inserted into Eqs. (4.4), we find

$$\begin{aligned}\frac{\partial}{\partial t}f_{1/2}=&-(\Gamma^{\mathrm{LAS}}+\Gamma^{\mathrm{SAS}})f_{1/2}\\&+\tfrac{1}{3}\int d\mathbf{v}'K^{\mathrm{LAS}}(\mathbf{v}'\rightarrow\mathbf{v})[f_{1/2}(\mathbf{v}')+f_{3/2}(\mathbf{v}')]\\&+\tfrac{1}{3}\int d\mathbf{v}'K^{\mathrm{SAS}}(\mathbf{v}'\rightarrow\mathbf{v})[f_{1/2}(\mathbf{v}')+f_{3/2}(\mathbf{v}')]\ ,\end{aligned} \tag{4.7a}$$

$$\begin{aligned}\frac{\partial}{\partial t}f_{3/2}=&-(\Gamma^{\mathrm{LAS}}+\Gamma^{\mathrm{SAS}})f_{3/2}\\&+\tfrac{2}{3}\int d\mathbf{v}'K^{\mathrm{LAS}}(\mathbf{v}'\rightarrow\mathbf{v})[f_{1/2}(\mathbf{v}')+f_{3/2}(\mathbf{v}')]\\&+\tfrac{2}{3}\int d\mathbf{v}'K^{\mathrm{SAS}}(\mathbf{v}'\rightarrow\mathbf{v})[f_{1/2}(\mathbf{v}')+f_{3/2}(\mathbf{v}')]\ .\end{aligned} \tag{4.7b}$$

At this point, the validity of the sudden approximation has to be discussed. Using the experimental values of transfer and relaxation rates of the eight different multipoles of Na in the $3p\ ^2P$ multiplet, which have been measured by Gay and Schneider,[48] we can compare our L-base model with experiment. Assuming that the sudden approximation is valid and using vector coupling algebra, the multipole transfer and relaxation rates in the J base can be related to the orientation relaxation rate $\Gamma^{(1)}$ and the alignment relaxation rate $\Gamma^{(2)}$ in the L base[8(a),49,50]. Using a van der Waals potential to describe the long-range part of the intermolecular potential, these latter two rates are related through $\Gamma^{(1)}/\Gamma^{(2)}=1.12$.[42,51] Using this relation, all eight multipole rates can be expressed in terms of the orientation relaxation rate $\Gamma^{(1)}$. For Na-He, the experimental multipole transfer and relaxation rates[48] can indeed be described by a single parameter $\Gamma^{(1)}$ within 10%, showing that the sudden approximation is valid for this case[8(a)]. However, when the noble gas is changed from He to Xe the deviations due to the sudden approximation increase monotonically[8(a)]. For Na-Xe, the sudden approximation clearly breaks down since the experimental transfer and relaxation rates and the theoretical ones based on $\Gamma^{(1)}$ differ by a factor of 2. Thus, our analysis of the Na-Xe results should be considered as less reliable.

The last point to be addressed is how to relate the four adjustable parameters, the collision rates $\Gamma^{\mathrm{LAS}},\Gamma^{\mathrm{SAS}}$, and the Keilson-Storer strength parameters $\alpha^{\mathrm{LAS}},\alpha^{\mathrm{SAS}}$ to the interaction potentials. By using the hard-sphere value for α^{LAS}, which depends on the mass ratio of active atom and perturber atom only,[52] and experimental data for Γ^{el},[48] two adjustable parameters can be readily eliminated. A third adjustable parameter can be eliminated by using the known value of the diffusion coefficient as is discussed below. The only remaining adjustable parameter α^{SAS} will be fit to the excited-state spectra in Sec. V.

For a composite kernel, the relation between the diffusion coefficient and the collision rates and strength parameters can be obtained by slightly generalizing our previous results for a single kernel.[8(a),53]

$$\frac{kT}{mD^{[0]}} = (1-\alpha^{\mathrm{LAS}})\Gamma^{\mathrm{LAS}} + (1-\alpha^{\mathrm{SAS}})\Gamma^{\mathrm{SAS}} , \tag{4.8}$$

where m is the Na mass. The left member of Eq. (4.8) represents the diffusional collision rate. The question remains as to how to relate the diffusion coefficient $D_{3p}^{[0]}$ in each fine-structure level to the diffusion coefficients which can be calculated for the three excited-state Na–noble-gas interatomic potentials, namely, the $A\,^2\Pi_{1/2}$, $A\,^2\Pi_{3/2}$, and $B\,^2\Sigma_{1/2}$ potentials. Assuming that the sudden limit is valid, the diffusion coefficient is equal for both fine-structure levels and can be expressed as

$$D_{3p}^{[0]} = \tfrac{1}{3}D_{\Sigma}^{[0]} + \tfrac{2}{3}D_{\Pi}^{[0]} , \tag{4.9}$$

where the diffusion coefficients $D_{\Pi}^{[0]}$ and $D_{\Sigma}^{[0]}$ corresponding to the $A\,^2\Pi$ and $B\,^2\Sigma$ potentials have been calculated previously.[34] In this case the validity of the sudden limit is warranted, even in the case of a heavy noble gas as collision partner, if we restrict ourselves to large-angle collisions which determine the diffusion coefficient. This can be deduced[8(a)] by comparison with the quantum calculations of Pascale and Olson[54] for Na-Kr and Na-Xe.

V. COMPARISON OF EXPERIMENT WITH THEORY

A. Excited-state measurements

Experimental excited-state probe spectra for both fine-structure levels have been recorded for all noble gases and for various noble-gas pressures and pump laser intensities. In Figs. 7–11 these experimental spectra are presented together with calculated spectra. We have

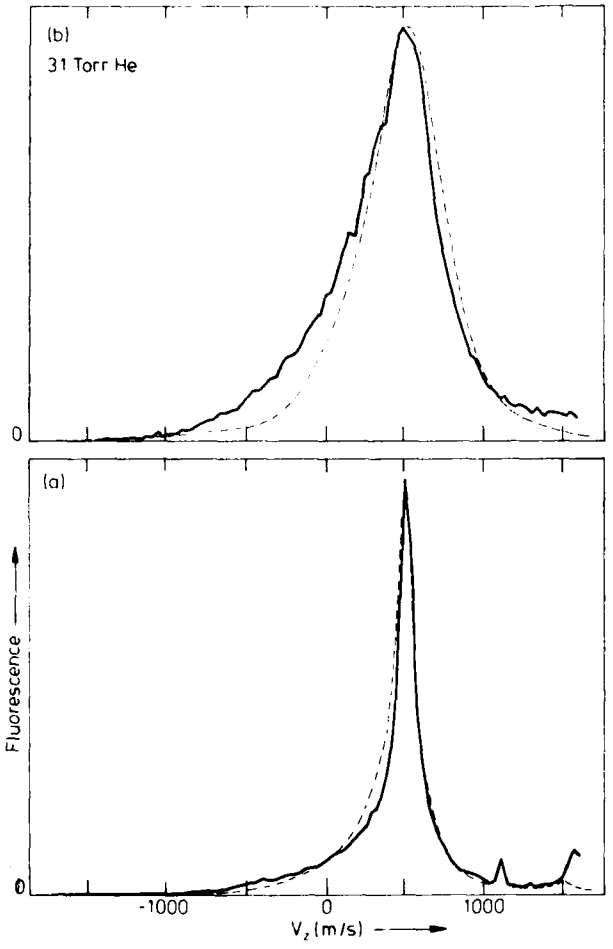

FIG. 7. Resonant (a) and nonresonant (b) excited-state spectra as a function of probe laser detuning ($v_z = \Delta\omega/k$ with respect to the 0→4 or 3→4 transition) for 3.1-Torr helium. Both spectra have been scaled to the same peak height. The solid curve is the experimental spectrum and the dashed curve represents the model calculation. Parameters are as follows: $\alpha^{\mathrm{SAS}} = 0.99$; pump laser intensity 280 mW/cm^2; pump laser detuning 0.8 GHz below line center of the $3s$, $F=2 \rightarrow 3p$ transition; pump laser beam diameter 2.2 mm; probe laser intensity 0.2 mW/cm^2; probe laser beam diameter 1.5 mm; temperature 393 K; and Na density 10^{+10} cm^{-3}.

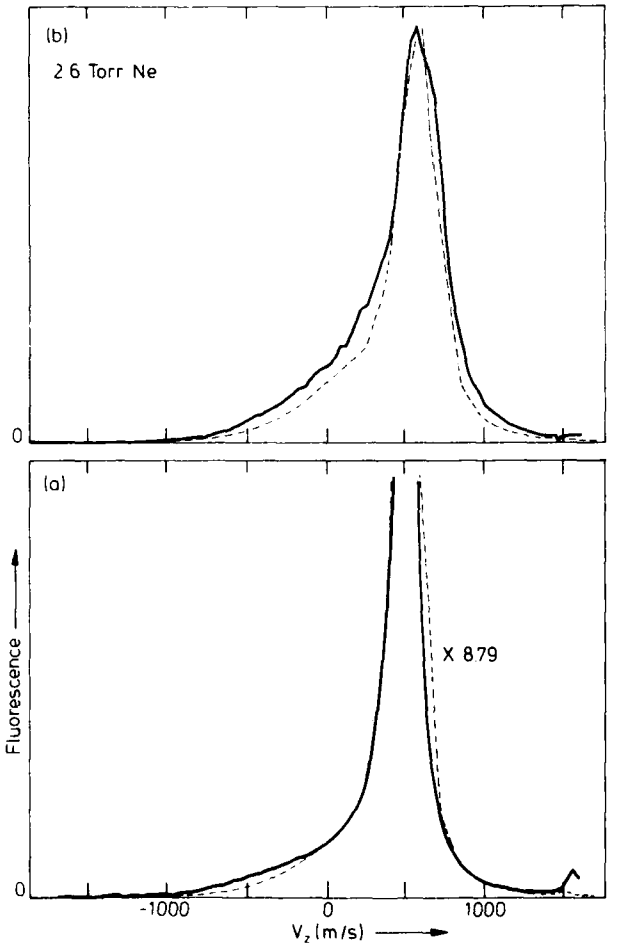

FIG. 8. Resonant (a) and nonresonant (b) excited-state spectra for Na-Ne for $\alpha^{\mathrm{SAS}} = 0.975$, 2.6-Torr neon, and pump intensity 4.77 mW/cm^2. All other parameters are identical to Fig. 7. The peak height of the resonant spectrum has been scaled to be a factor 8.79 larger than the peak height of the nonresonant spectrum.

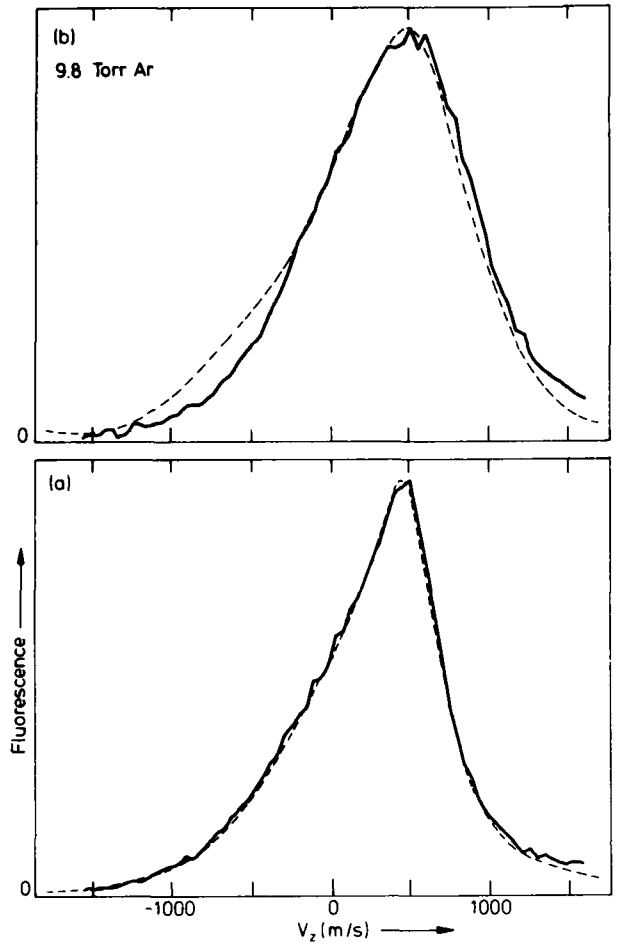

FIG. 9. Resonant (a) and nonresonant (b) excited-state spectra for Na-Ar for $\alpha^{SAS}=0.975$, 9.8-Torr argon, and pump intensity 19 mW/cm^2. All other parameters are identical to Fig. 7.

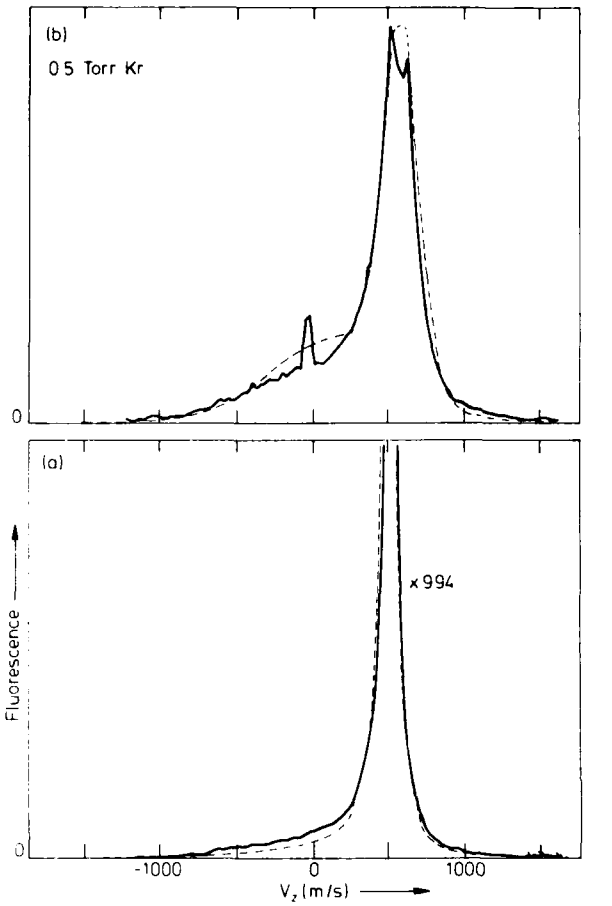

FIG. 10. Resonant (a) and nonresonant (b) excited-state spectra for Na-Kr for $\alpha^{SAS}=0.975$, 0.5-Torr krypton, and pump intensity 36 mW/cm^2. All other parameters are identical to Fig. 7. The peak height of the resonant spectrum has been scaled to be a factor 9.94 larger than the peak height of the nonresonant spectrum.

chosen to present the spectra as a function of the velocity component of the resonant atoms along the laser beam v_z. The resonant velocity is related to the probe laser detuning by $v_z=\Delta\omega/k$, where $\Delta\omega$ denotes the detuning from resonance on the $0\rightarrow 4$ transition. The calculated spectra have been obtained by introducing the excited-state kernels (Eqs. 4.7) into the set of rate equations (Eqs. 3.1). By solving these rate equations numerically,[8] one can obtain the excited-state spectra. As discussed in Sec. IV, the resulting excited-state spectra contain a single adjustable parameter, the Keilson-Storer strength parameter α^{SAS} characterizing small-angle collisions.

An example of the sensitivity of the spectrum to the precise value of α^{SAS} is presented in Fig. 12. The calculated nonresonant spectrum is shown here at 0.5-Torr krypton and a pump laser intensity of 36 mW/cm^2 for $\alpha^{SAS}=0.95$, 0.975, and 1.0. It can be seen that the widths of the two peaks (which are due to the $^2P_{1/2}$ hyperfine splitting) around $v_z=500$ m/s are very sensitive to small changes in α^{SAS}. When $\alpha^{SAS}=1$, the small-angle kernel only mixes the two fine-structure levels, but does not affect the velocities. When α^{SAS} is slightly different from unity, the small-angle kernel significantly broadens the Lorentzian peaks. In Fig. 10(b), the calculated spectrum for $\alpha^{SAS}=0.975$ is compared with the experimental spectrum, showing that $\alpha^{SAS}=0.975$ yields approximately the experimentally observed amount of broadening for a pressure of 0.5-Torr krypton. By comparing Fig. 12 with Fig. 10(b), it is obvious that the choice $\alpha^{SAS}=1$, which would correspond to neglecting the small-angle kernel, does not describe the experimental data. From fitting procedures as described above, we find that the best value of α^{SAS} for all Na–noble-gas mixtures is 0.975 (± 0.01), except for Na-He where it is 0.99 (± 0.005). Although both values are close to unity, the average velocity change per small-angle collision, $\Delta u=\bar{v}[1-(\alpha^{SAS})^2]^{1/2}$ is still appreciable. We find $\Delta u=0.22\bar{v}$ and $\Delta u=0.14\bar{v}$ for $\alpha^{SAS}=0.975$ and $\alpha^{SAS}=0.99$, respectively, which at 1 Torr buffer-gas pressure corresponds to a Doppler-frequency shift of approximately three times the homogeneous linewidth of the stepwise contribution to the spectrum. This is a theoretical confirmation that the small-angle kernel can-

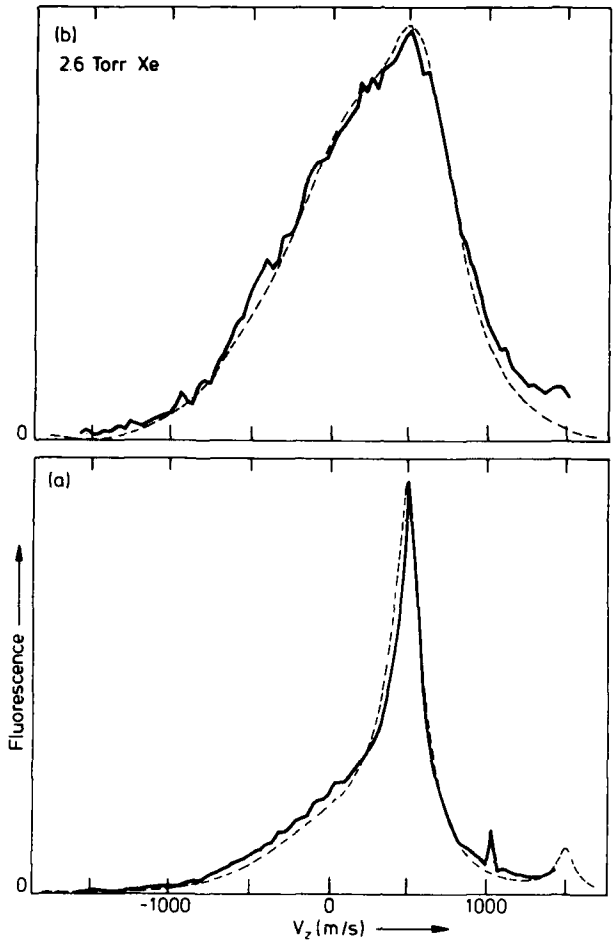

FIG. 11. Resonant (a) and nonresonant (b) excited-state spectra for Na-Xe for $\alpha^{SAS}=0.975$, 2.6-Torr xenon, and pump intensity 1000 mW/cm^2. All other parameters are identical to Fig. 7. Both spectra have been scaled to the same peak height.

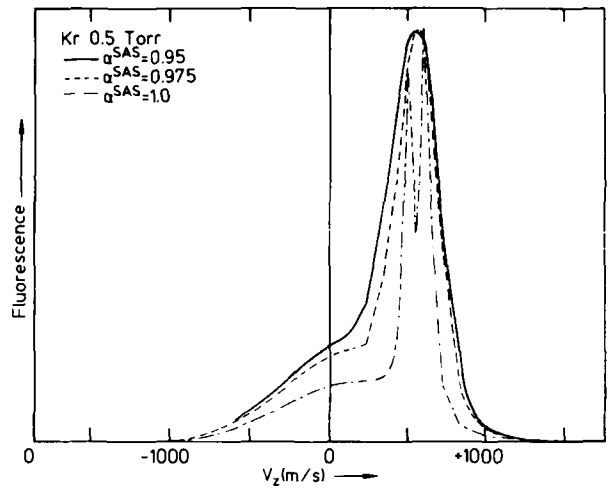

FIG. 12. Theoretical nonresonant excited-state spectra for $\alpha^{SAS}=0.95$, 0.975, and 1.0 (weak collision limit), respectively, showing that small-angle scattering has a considerable influence. The spectra have been calculated for a pressure of 0.5-Torr krypton, $\alpha^{LAS}=0$, a pump laser intensity of 36 mW/cm^2, and a detuning of 0.8 GHz below line center of the $2\rightarrow0$ transition. The velocity v_z is defined by $v_z=\Delta\omega/k$ with respect to the $3\rightarrow4$ transition.

not be neglected, at least not at low buffer-gas pressures. Note that the data was consistent with our assumption that diffractive scattering does not contribute to fine-structure mixing; otherwise, one would have observed narrow peaks in the nonresonant spectrum of order of the homogeneous width.

By comparing the experimental resonant and nonresonant excited-state spectra with the theoretical fits (see Figs. 7–11), we observe an excellent agreement. The theoretical model describes both the resonant and the nonresonant spectra between 0.5 and 10 Torr at various laser intensities, independent of the buffer-gas pressure or the laser intensity. Furthermore, it should be emphasized that no effort has been undertaken to optimize the precise shape of the collision kernel beyond the composite Keilson-Storer kernel. Values for the various parameters α^{LAS}, α^{SAS}, Γ^{LAS}, and Γ^{SAS} are given in Table I.

At this point, we should like to make a comparison with the results of Liao *et al.*[14] These authors measured the resonant excited-state spectra in a setup similar to ours, but they did not measure nonresonant spectra. Their analysis differs from ours in three respects.

(i) They did not include optical hyperfine pumping into their model. Therefore, the relative hyperfine population in the resonant ground-state hyperfine level acted as an additional free parameter in their treatment.

(ii) They did not relate the rate for velocity-changing collisions to the diffusion coefficient, which resulted in still another free parameter.

(iii) The most important difference between their analysis and ours is that they included the fine-structure-changing collisions in an erroneous way, leading to a pressure-dependent cross section for velocity-changing collisions. In their model, the fine-structure-mixing collisions were taken to be independent of the velocity-changing collisions; this choice was motivated by a single measurement of the nonresonant excited-state spectrum from which they (wrongly) concluded that the resonant and nonresonant excited-state spectra have similar shapes. In the L base, their choice is equivalent to the assumption that the population and orientation kernels for velocity-changing collisions (LAS + SAS) are identical. It seems much more realistic to take the orientation kernel identically equal to zero (as we do in this work), since collisions tend to destroy any magnetic state coherence. Based on this unrealistic assumption, they obtain a theoretical rate for velocity-changing collisions *within* the $^2P_{1/2}$ level which is three times larger than in our rate-equation model (Eq. (3.1), where only $\frac{1}{3}$ of all velocity-changing collisions starting in the $^2P_{1/2}$ ends up in the same level and $\frac{2}{3}$ of those collisions are accompanied by a fine-structure change. When analyzing the experimental resonant fine-structure spectrum using their model, one expects to find a cross section for

TABLE I. Parameters of composite Keilson-Storer kernels describing ground-state and excited-state Na–noble-gas collisions. The tabulated values refer to a temperature of 400 K and a buffer-gas pressure of 1 Torr.

	Na + He	Na + Ne	Na + Ar	Na + Kr	Na + Xe
Γ_e^{LAS} (10^6 s^{-1})	12.3	5.17	8.61	9.80	12.8
Γ_e^{SAS} (10^6 s^{-1})	47.7	19.8	26.3	17.9	12.1
α_e^{LAS}	0.8	0.4	0.2	0.0	0.0
α_e^{SAS}	0.99	0.975	0.975	0.975	0.975
Γ_g^{LAS} (10^6 s^{-1})	9.07	4.96	6.84	6.90	8.58
$\Gamma_{g,\mathrm{eff}}^{\mathrm{SAS}}$ (10^6 s^{-1})	0.018	0.019	0.21	0.13	0.08
α_g^{LAS}	0.8	0.4	0.2	0.0	0.0

velocity-changing collisions which is a factor 3 too low for low buffer-gas pressures, when the fine-structure populations are not in equilibrium, and which approaches the correct value for high pressures, when the fine-structure populations are in equilibrium. They indeed observed such an artificial increase of the cross section for velocity-changing collisions with pressure.[14]

B. Ground-state measurements

In Fig. 13 we present experimental ground-state probe spectra and compare them with theoretical ones. We have recorded ground-state spectra for all noble gases keeping the pump laser frequency fixed in the red wing of the $3s\ ^2S_{1/2}$, $F=2\rightarrow 3p\ ^2P_{3/2}$ transition, about 1 GHz below line center, while scanning the probe laser over the $3s\ ^2S_{1/2}$, $F=1\rightarrow 3p\ ^2P_{1/2}$ transition, probing the velocity distribution in the $F=1$ ground-state level. As compared with Fig. 6 where we showed the complete ground-state spectra, in Fig. 13 we show only the parts belonging to the $F=1$ ground-state level. The spectra are presented as a function of the Doppler-selected velocity component v_z along the laser beam, referring to the transition starting from the $F=1$ level. The spectra were recorded at a buffer-gas pressure of 50 mTorr and at pump laser intensities between 4 and 26 mW/cm^2. The two peaks (with amplitudes 1:5) around $v_z=-500$ m/s represent the "Bennett peak" in the $F=1$ ground state; these peaks arise due to optical pumping from the $F=2$ to the $F=1$ level. The splitting of this Bennett peak is due to the $^2P_{1/2}$ hyperfine splitting ($\Delta\nu_{\mathrm{HFS}}=192$ MHz); the $^2P_{3/2}$ hyperfine splitting is not resolved in these spectra. The ratio 1:5 of the peak amplitudes reflects the transition probabilities of the $3s\ ^2S_{1/2}$, $F=1\rightarrow 3p\ ^2P_{1/2}$, $F=1,2$ transitions. The pedestals around $v_z=0$ are due to velocity-changing collisions in the $F=1$ level.

In principle, the theoretical ground-state spectra again contain four free parameters: Γ^{LAS}, Γ^{SAS}, α^{LAS}, α^{SAS}. For Na ground-state ($L=0$) collisions there are no orientation or alignment kernels and rates. Two of the remaining free parameters can be eliminated by using (i) the diffusion coefficient (Eq. 4.8) and (ii) the hard-sphere value for α^{LAS}. For the ground-state case experimental data for Γ^{el} are not available. However, since there is evidence[55] that very weak velocity-changing collisions can be characterized by an effective rate $\Gamma_{\mathrm{eff}}^{\mathrm{SAS}}=\Gamma^{\mathrm{SAS}}(1-\alpha^{\mathrm{SAS}})$, we attempted to fit the data using $\Gamma_{\mathrm{eff}}^{\mathrm{SAS}}$ as a single free parameter. The theoretical spectra are scaled to yield the same maximum peak value as the experimental spectra. Good agreement between theory and experiment was obtained (see Fig. 13) for the values of $\Gamma_{\mathrm{eff}}^{\mathrm{SAS}}$ given in Table I.

We stress that it would go beyond the object of this work to optimize the shape of the collision kernel (that is, going beyond a sum of two Keilson-Storer kernels). However, even without such optimization, the fit between experiment and theory is quite adequate. Since we scaled the experimental spectra to give the same peak height as the experimental ones, our spectra are quite sensitive to the small-angle scattering. Therefore, the deviation of $\Gamma_{\mathrm{eff}}^{\mathrm{SAS}}$ from zero, which we deduce from our experiments, is certainly significant.

Our ground-state measurements are closely related to the work of Aminoff *et al.*,[13] who measured Na ground-state orientation relaxation (Δm_F) due to Na-Ne collisions. Due to the fact that $|\mathbf{F}|$-changing and $\mathbf{F}$-reorientation collisions of Na ground-state atoms in a noble gas do not occur, orientation relaxation is only caused by velocity-changing collisions and their orientation relaxation measurements yield information equivalent to our population relaxation measurements. From an experimental point of view, the major difference between their measurements and ours is that we could use separate dye lasers as pump laser and probe laser. Consequently, we were able to monitor collisions changing the velocity from v_{pump} to v_{probe}, where v_{probe} could be scanned over the entire velocity distribution, keeping v_{pump} constant. Such a scan immediately yields the ground-state velocity distribution. Aminoff *et al.*[13] could only monitor collisions changing the velocity from $-v_{\mathrm{pump}}$ to $+v_{\mathrm{pump}}$, yielding a signal proportional to the product of the (frequency-dependent) Maxwellian pump absorption and the ground-state velocity distribution. Moreover, they had to perform a laborious correction due to a backward reflection of the pump beam which resulted in a second, unintentional pump beam, running through the cell, nearly copropagating with the probe beam. In our data, a contribution due to such a pump laser reflection is also present, but this spurious signal appears spectrally separated from the true pump laser signal and does not interfere with the proper signal, even at high pump laser intensi-

ties. Aminoff *et al.* have fitted their data with a composite kernel being the sum of a Keilson-Storer kernel and a difference kernel. They used five adjustable parameters to fit theory to their experimental data and obtained, for the case of Na-Ne, a rate of velocity-changing collisions which, when transformed into a diffusion coefficient, is a factor of 2 smaller than its accepted value.[53] By using the relation between the collision rates for velocity-changing collisions and the well-known diffusion coefficient, our theoretical spectra are intrinsically consistent with the diffusion coefficients.

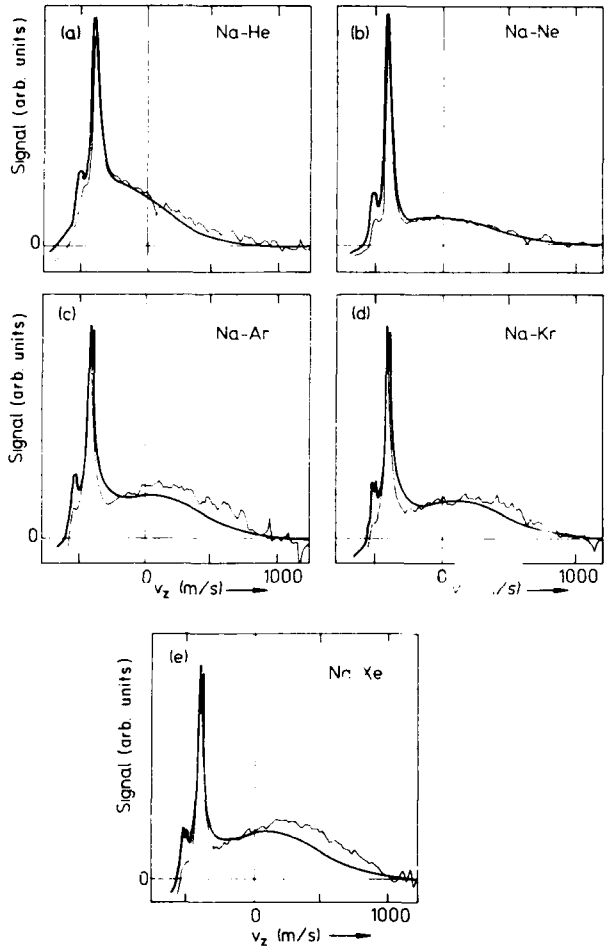

FIG. 13. Ground-state spectra as a function of probe detuning for various buffer gases. In this figure v_z denotes the velocity component along the axis of the laser beam for resonant atoms in the $F=1$ ground-state level. The heavy curves are the model calculations and the thin curves represent the experimental spectra. In the model calculations the only free parameter used is $\Gamma_{g,\text{eff}}^{\text{SAS}}$ (see text); the optimum fits presented here have been obtained with values of $\Gamma_{g,\text{eff}}^{\text{SAS}}$ given in Table I. (a) Results for 0.050-Torr He as a buffer gas. Parameters are as follows: pump laser intensity 26 mW/cm^2; pump laser detuning 0.8 GHz below line center of the $3s$, $F=2\rightarrow 3p$ transition; pump laser beam diameter 2.2 mm; probe laser intensity 0.2 mW/cm^2; probe laser beam diameter 1.5 mm; temperature 393 K; and Na density 10^{10} cm^{-3}. (b) Same as (a) for 0.050-Torr Ne at a pump intensity of 7.4 mW/cm^2. (c) Same as (a) for 0.050-Torr Ar at a pump intensity of 7.9 mW/cm^2. (d) Same as (a) for 0.048-Torr Kr at a pump intensity of 7.9 mW/cm^2. (e) Same as (a) for 0.053-Torr Xe at a pump intensity of 7.4 mW/cm^2.

VI. DISCUSSION AND CONCLUSIONS

We have shown that for all Na–noble-gas pairs, the experimental spectra for both the Na ground state and the Na excited state are adequately described by a straightforward rate equation model for a wide range of experimental parameters. It has been found that the spectra could be fit with a composite Keilson-Storer kernel consisting of a large-angle and a small-angle Keilson-Storer kernel using only the strength of the small-angle collisions as a free parameter. In particular, the nonresonant excited-state spectra are surprisingly sensitive to the small-angle kernel. Given the nature of the approximations made in formulating the theory, the agreement between theory and experiment is remarkably good. In particular, the reduction of the actual level scheme to an effective five-level scheme with the consequential averaging over the magnetic substates and excited-state hyperfine structure is an assumption that warrants additional investigation. Also, the sudden approximation is somewhat marginal, especially for the heavier noble gases. On the other hand, the experimental data seem to be consistent with the assumptions that classical scattering leads to depolarization of the $L=1$ state and that diffractive scattering does not lead to depolarization.

Unlike most previous experiments which focused on the description of velocity-changing collisions within a single level, we have measured the velocity distributions in *all* levels which are populated in the presence of a pump laser tuned to the $3s\rightarrow 3p$ transition. The light-induced drift velocity, which is a consequence of the difference in collisional interaction between the ground-state and the excited-state collisional interaction, can be expressed as a suitably weighted average of all these velocity distributions,

$$v_{\text{drift}}=\sum_{i=0}^{3}\int dv_z v_z f_i(v_z)\ . \tag{6.1}$$

Using the strength parameters for the Keilson-Storer kernel obtained in this work, the drift velocity can be calculated employing collision kernels for velocity-changing and fine-structure-changing collisions which have been proven successful at the spectroscopic level of detail in the present work. As can be seen from Eq. (6.1), the drift velocity is a much cruder quantity than the spectra presented in this work since the calculation of the drift velocity involves a lot of averaging. Consequently, we expect that the model will certainly give a satisfactory description of a transport effect such as light-induced drift; the first quantitative experimental information on the drift velocity[6] indeed yields excellent agreement with the rate-equation model. The consequences of the collision model established in this paper for the phenomenon of light-induced drift, such as the sensitivity of the drift velocity for the shape of the col-

lision kernel and the influence of the fine-structure-changing collision on light-induced drift will be discussed in a subsequent paper.[8(b)]

ACKNOWLEDGMENT

We would like to thank W. A. Hamel for assistance with the experiments and G. Nienhuis for stimulating discussions. This work is part of the research program of the Foundation for Fundamental Research on Matter (FOM) and was made possible by financial support of the Netherlands Organization for the Advancement of Pure Research (ZWO). The research of one of us (P.R.B.) is supported by the U.S. Office of Naval Research and the National Science Foundation under Grant No. PHY-8415781.

---

*Present address: Physics Department, Eindhoven University of Technology, P.O. Box 513, 5600 MB Eindhoven, The Netherlands.

[1]F. Kh. Gel'mukhanov and A. M. Shalagin, Pis'ma Zh. Eksp. Teor. Fiz. **29**, 773 (1979) [JETP Lett. **29**, 711 (1979)].

[2]F. Kh. Gel'mukhanov and A. M. Shalagin, Zh. Eksp. Teor. Fiz. **78**, 1674 (1980) [Sov. Phys.—JETP **51**, 839 (1980)].

[3]H. G. C. Werij, J. P. Woerdman, J. J. M. Beenakker, and I. Kuščer, Phys. Rev. Lett. **52**, 2237 (1984).

[4]H. G. C. Werij, J. E. M. Haverkort, and J. P. Woerdam, Phys. Rev. A **33**, 3270 (1986).

[5]S. N. Atutov, St. Lesjak, S. P. Podjachev, and A. M. Shalagin, Opt. Commun. **60**, 41 (1986).

[6]H. G. C. Werij, J. E. M. Haverkort, P. C. M. Planken, E. R. Eliel, J. P. Woerdman, S. N. Atutov, P. Chapovskii, and F. Kh. Gel'mukhanov, Phys. Rev. Lett. **58**, 2660 (1987).

[7]F. Kh. Gel'mukhanov, J. E. M. Haverkort, S. W. M. Borst, and J. P. Woerdman, Phys. Rev. A **36**, 164 (1987).

[8](a) J. E. M. Haverkort, Ph.D. thesis, University of Leiden, 1987; (b) J. E. M. Haverkort and J. P. Woerdman (unpublished).

[9]P. R. Berman, in *New Trends in Atomic Physics*, 1982 Les Houches Lecture Series, edited by G. Grynberg and R. Storn (North-Holland, Amsterdam, 1984), pp. 451–514.

[10]P. R. Berman, in *Advances in Atomic and Molecular Physics*, edited by D. R. Bates and B. Bederson (Academic, New York, 1977), Vol. 13, pp. 57–112.

[11]P. R. Berman, Ann. Phys. (Paris) **5**, 199 (1980).

[12]R. Vetter and P. R. Berman, Comments At. Mol. Phys. **10**, 69 (1981).

[13]C. G. Aminoff, J. Javanainen, and M. Kaivola, Phys. Rev. A **28**, 722 (1983).

[14]P. F. Liao, J. E. Bjorkholm, and P. R. Berman, Phys. Rev. A **21**, 1927 (1980).

[15]L. Krause, Adv. Chem. Phys. **28**, 267 (1975).

[16]E. E. Nikitin, *Theory of Elementary Atomic and Molecular Processes in Gases* (Clarendon, Oxford, 1974; first published by Khimiya, Moscow, 1970).

[17]E. E. Nikitin, Adv. Chem. Phys. **28**, 317 (1975).

[18]E. E. Nikitin and L. Zülicke, *Selected Topics of the Theory of Chemical Elementary Processes*, Vol. 8 of *Lecture Notes in Chemistry* (Springer Verlag, New York, 1978).

[19]J. Apt and D. E. Pritchard, Phys. Rev. Lett. **37**, 91 (1976).

[20]J. Apt and D. E. Pritchard, J. Phys. B **12**, 83 (1979).

[21]G. M. Carter, D. E. Pritchard, M. Kaplan and T. W. Ducas, Phys. Rev. Lett. **35**, 1144 (1975).

[22]R. Düren and W. Gröger, Chem. Phys. Lett. **61**, 6 (1979).

[23]R. Düren, W. Gröger, E. Hasselbrink, and R. Liedtke, J. Chem. Phys. **74**, 6806 (1981).

[24]F. van den Berg and R. Morgenstern, Chem. Phys. **90**, 125 (1984).

[25]F. van den Berg, R. Morgenstern, and C. Th. J. Alkemade, Chem. Phys. **93**, 171 (1985).

[26]W. D. Phillips, J. A. Serri, D. J. Ely, D. E. Pritchard, K. R. Way, and J. L. Kinsey, Phys. Rev. Lett. **41**, 937 (1978).

[27]W. D. Phillips, C. L. Glaser, and D. Kleppner, Phys. Rev. Lett. **38**, 1018 (1977).

[28]J. M. Mestdagh, J. Cuvellier, J. Berlande, A. Binet, and P. de Pujo, J. Phys. B **13**, 4589 (1980).

[29]J. Keilson and K. E. Storer, Q. Appl. Math. **10**, 243 (1952).

[30]J. P. Woerdman, J. Chem. Phys. **77**, 3726 (1982).

[31]J. E. M. Haverkort, R. W. M. Hoogeveen, and J. P. Woerdman, Opt. Commun. **61**, 109 (1987).

[32]J. E. Bjorkholm and P. F. Liao, Phys. Rev. A **14**, 751 (1976).

[33]P. R. Berman, P. F. Liao and J. E. Bjorkholm, Phys. Rev. A **20**, 2389 (1979).

[34]W. A. Hamel, J. E. M. Haverkort, H. G. C. Werij, and J. P. Woerdman, J. Phys. B **19**, 4127 (1986).

[35]P. R. Berman, Phys. Rep. **43**, 101 (1978).

[36]F. A. Franz and J. R. Franz, Phys. Rev. **148**, 82 (1966).

[37]E. E. Nikitin, J. Chem. Phys. **43**, 744 (1965).

[38]P. R. Berman, Phys. Rev. A **6**, 2157 (1972).

[39]J.-L. Le Gouët and P. R. Berman, Phys. Rev. A **24**, 1831 (1981).

[40]J. C. Keller and J.-L. Le Gouët, Phys. Rev. A **32**, 1624 (1985).

[41]J. E. Thomas, A. P. Ghosh, M. A. Attili, Phys. Rev. A **33**, 3029 (1986).

[42]A. Omont, J. Phys. (Paris) **26**, 26 (1965).

[43]A. Messiah, *Quantum Mechanics* (North-Holland, Amsterdam, 1972).

[44]M. Gorlicki, C. Lerminiaux, and M. Dumont, Phys. Rev. Lett. **49**, 1394 (1982).

[45]Xiwen Zhu, Phys. Rev. A **33**, 251 (1986).

[46]Tak-San Ho and Shih-I Chu, Phys. Rev. A **33**, 3067 (1986).

[47]S. Kryszewski and G. Nienhuis (unpublished).

[48]J.-C. Gay and W. B. Schneider, Z. Phys. A **278**, 211 (1976).

[49]E. I. Dashevskaya and N. A. Mokhova, Chem. Phys. Lett. **20**, 454 (1973).

[50]E. I. Dashevskaya, F. Masnou-Seeuws, R. McCarrol, and E. E. Nikitin, Opt. Spectrosk. **37**, 209 (1974) [Opt. Spectrosc. **37**, 119 (1974)].

[51]P. R. Berman and W. E. Lamb, Phys. Rev. **187**, 221 (1969).

[52]M. Borenstein and W. E. Lamb, Phys. Rev. A **5**, 1311 (1972).

[53]P. R. Berman, J. E. M. Haverkort, and J. P. Woerdman, Phys. Rev. A **34**, 4647 (1986).

[54]J. Pascale and R. E. Olson, J. Chem. Phys. **64**, 3538 (1976).

[55]Ph. Cahuzac, E. Marie, O. Robaux, R. Vetter, and P. R. Berman, J. Phys. B **11**, 645 (1978).

PHYSICAL REVIEW A VOLUME 38, NUMBER 1 JULY 1, 1988

Effects of radiative decay in four-wave-mixing spectroscopy: Narrow resonances produced by nonconservation of population, alignment, and orientation

P. R. Berman
Department of Physics, 4 Washington Place, New York University, New York, New York 10003

D. G. Steel
Departments of Physics and Electrical Engineering, Randall Physics Laboratory, University of Michigan, Ann Arbor, Michigan 48109

Galina Khitrova*
Department of Physics, 4 Washington Place, New York University, New York, New York 10003

Jing Liu
Departments of Physics and Electrical Engineering, Randall Physics Laboratory, University of Michigan, Ann Arbor, Michigan 48109

(Received 28 December 1987)

We present experimental and theoretical results describing the presence of radiative-decay-induced narrow resonances in systems which do not conserve population, alignment, or orientation. We show how spectroscopic line-shape analysis of the nonlinear response can be used to determine all of the relaxation parameters characterizing a two-level atom.

In this paper we demonstrate how spectroscopic line-shape analysis can be used to determine *all* of the relaxation parameters characterizing a "two-level" atom. This problem is investigated in the context of a simple gas-phase collisionless system, but has important implications for interpretation of nonlinear-spectroscopy data in more complicated systems such as solids or liquids. This work also demonstrates the observation of linewidths smaller than the radiative linewidth associated with the two-level transition. The narrow resonances which are observed may serve as the basis for constructing a narrow-band tunable optical filter or for locking two laser frequencies together.

Consider one or more radiation fields driving a transition between atomic levels 1 and 2 (Fig. 1). A simple relaxation scheme has been assumed in which, owing to interactions with a reservoir (such as perturber atoms or spontaneous emission), levels 1 and 2 decay with rates γ_1 and γ_2, respectively, and the 1-2 dipole coherence decays with rate γ_{12}. As a result of spontaneous emission (or some other interaction), level 2 populates level 1 at a rate $\gamma_{2,1}$.

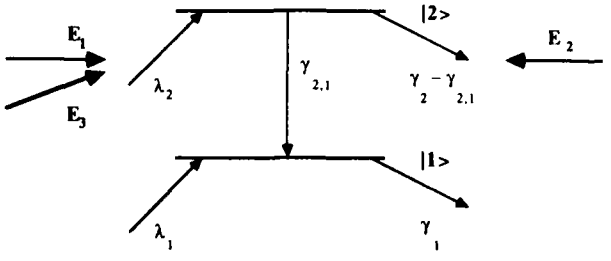

FIG. 1. Simple two-level system with spontaneous emission $\gamma_{2,1}$ from level 2 to 1. Level 1 decays to reservoir at rate γ_1 and level 2 decays to the reservoir at rate $\gamma_2 - \gamma_{2,1}$.

It is often of interest to obtain values for each of the relaxation constants γ_1, γ_2, and γ_{12}. We restrict the discussion to a spectroscopic determination of these parameters and recognize that γ_i represents a general decay to the reservoir which could be due to collisions, radiation, phonons (in a solid), etc., γ_{12} represents the total decay rate of the dipole coherence which has contributions from γ_1 and γ_2, along with contributions arising from other processes (e.g., collisions).

In standard linear spectroscopy, the absorption line shape can be used to obtain γ_{12} only. Increasing the field strength modifies the linewidth parameter so that it depends on all three decay parameters (as well as the field strength). Hence, in principle, strong-field studies could be used to obtain information about γ_i. However, to arrive at spectral line shapes with components whose widths give a direct measure of γ_1, γ_2, and γ_{12}, it is necessary to use at least two fields and examine the *nonlinear response* as a function of frequency.

A general scheme for obtaining such profiles is shown in Fig. 2, in which three fields propagate in an atomic vapor (or other material) and produce a signal via nearly degenerate four-wave mixing (NDFWM). Laser fields 1 and 2 are detuned from the resonant transition frequency by Δ and laser field 3 is detuned by $\Delta+\delta$. As δ is varied, the (nearly) phase-conjugate signal generated in the direction $-\mathbf{k}_3$ is monitored. In general, for Doppler-broadened materials and detunings $|\Delta|$ less than the Doppler width associated with the 1-2 transition, the signal intensity as a function of δ exhibits a spectrum con-

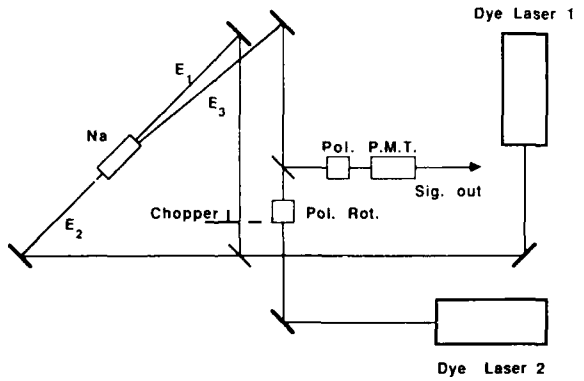

FIG. 2. Experimental configuration for nearly degener 'e four-wave mixing (NDFWM).

sisting of two peaks at $\delta=0$ with widths (FWHM, full width at half maximum) of $2\gamma_1$ and $2\gamma_2$, respectively, and a peak at $\delta=2\Delta$ of width $4\gamma_{12}$.[1,2]

Physically, the first resonance at $\delta=0$ occurs as a result of a two-photon Rayleigh-type process involving the probe beam (field 3, $\mathbf{k}_3$) and the forward pump beam (field 1, $\mathbf{k}_1$), and is actually the superposition of two resonances. The widths of these two resonances centered at $\delta=0$ are determined by γ_1 and γ_2, respectively, because the resonances are associated with the temporal modulation of the state populations at rate δ. The strength of the contribution of state i decreases when δ exceeds γ_i. The resonance at $\delta=2\Delta$ results from the condition that the same velocity-selected atoms interact with both the signal beam (at $-\mathbf{k}_3$) and the forward pump beam. The width of this resonance is determined by the total dephasing rate γ_{12}, reflecting the contributions to the spectral response from both a one-photon (simple absorption) and a three-photon process (absorption of two pump photons and emission of a probe photon, giving rise to the signal beam) which are characterized by the dipole-coherence decay rate. Additional contributions to the resonances are not observed because they are washed out by thermal averaging.

We note that $\gamma_2-\gamma_{2,1}$ is the decay rate of level 2 to the reservoir. In the limit that levels 1 and 2 decay to the reservoir at the same rate, i.e.,

$$\gamma_1=\gamma_2-\gamma_{2,1} \tag{1}$$

(as in the case of a gas-phase atom where γ_1 is determined by the inverse transit time, denoted by γ_t), the resonance having width $2\gamma_1$ does *not* occur. The width of the observed resonance is $2\gamma_2$ where $\gamma_2=\gamma_{2,1}+\gamma_t$. In other words, the resonance having width $2\gamma_1$ is absent whenever the *total population* $\rho_{11}+\rho_{22}$ is *conserved*, except for an overall decay owing to γ_1 (ρ_{ii} is a matrix element of the population density matrix operator). The purpose of this paper is to show both theoretically and experimentally that a narrow resonance having width $2\gamma_1$ can be observed whenever Eq. (1) is violated for either atomic state populations *or* total magnetic state orientation or alignment associated with levels 1 and 2. (This principle can be generalized to account for degeneracies arising from other than rotational symmetries.)

The existence of the narrow resonance due to nonconservation of population is demonstrated on the $2S_{1/2}(F=2)\rightarrow 2P_{1/2}(F=2)$ transition in sodium. Population is not conserved because the excited state can radiatively decay to another hyperfine level in the ground state (optical pumping). The analogous resonance resulting from nonconversation of total orientation or alignment is seen on the $2S_{1/2}(F=2)\rightarrow 2P_{3/2}(F=3)$ transition (a transition which *does* conserve total population.)

These resonances may be compared with the so-called pressure-induced extra resonances (PIER4) predicted and observed by Bloembergen and co-workers,[3] as well as a number of related effects.[4] In most of these situations one deals with either atoms subjected to homogeneous broadening only or to inhomogeneously broadened systems with atom-field detunings $|\Delta|$ much greater than the Doppler width. In those limits, as has been discussed in detail elsewhere,[3,4] both resonances centered at $\delta=0$ (having widths $2\gamma_1$ and $2\gamma_2$, respectively) vanish under suitable conditions. The relationship of our work on inhomogeneously broadened systems to that on PIER4 and related resonances will be noted. In particular, it appears that a destructive interference argument used to describe PIER4 is somewhat artificial when applied to an ensemble-averaged inhomogeneously broadened system.

It should be noted that experiments on inhomogeneously broadened systems with $|\delta|$ less than the Doppler width have been performed previously,[2] but with an emphasis which differs considerably from that presented herein.

I. THEORY

The geometry of the experiment is shown in Fig. 2. Beams 1, 2, and 3 propagate in the cell with wave vectors $\mathbf{k}_1$, $\mathbf{k}_2=-\mathbf{k}_1$, and $\mathbf{k}_3$, respectively. The third beam makes a small angle θ with the first. As we note below, the fact that θ is nonvanishingly small is important in systems inhomogeneously broadened by Doppler motion. The frequency of the laser fields are $\Omega_1=\Omega_2=\Omega$ and $\Omega_3=\Omega+\delta$. One observes the phase-conjugate signal emerging in the direction $\mathbf{k}_s=-\mathbf{k}_3$ (due to phase matching) with frequency $\Omega_s=\Omega-\delta$ as a function of δ.

The physical ideas we wish to emphasize are best illustrated by considering two cases which are simpler than the actual experimental level scheme, but illustrate all of the important physics. In the first case we consider the problem when the fields drive a transition from a ground state with total angular momentum $F=0$ to an $F=1$ excited state. In the second case we consider the problem when the transition is from an $F=1$ ground state to an $F=0$ excited state. In both cases the fields are taken to be linearly copolarized in a direction that defines the quantization axis in the problem. Because of the dipole selection rules, the fields induce a transition between the $F=0$ state and the $m=0$ substate of the $F=1$ state. In both cases the decay rate γ_2 of level 2 is determined totally by the rate of spontaneous emission back to level 1, though in the second case the $m=0$ excited state can decay back to *any* of the three magnetic substates. The signal is proportional to the absolute square of the averaged

density matrix element $\langle \rho_{F_1 0;F_2 0}(-\mathbf{k}_3,\mathbf{v})\rangle$, where F_1 and F_2 refer to the angular momenta of the ground and excited states, respectively, and the average is over the atomic velocity distribution (assumed to be Maxwellian with most probable speed u). The argument $-\mathbf{k}_3$ signifies that we are concerned only with the component of $\rho_{F_1;F_2}$ varying as $e^{i[\mathbf{k}_3\cdot\mathbf{R}+(\Omega-\delta)t]}$, which corresponds to the signal propagating in the $-\mathbf{k}_3$ direction.

Consider first the $F_1=0\rightarrow F_2=1$ level scheme. Using perturbation theory to lowest order in the product of the field amplitudes and neglecting transit-time effects, one can solve the transport equation for the population density matrix operator and obtain the result [see Eqs. (A1) and (A21) of the Appendix and Ref. 5]

$$\rho_{00;10}(-\mathbf{k}_3,\mathbf{v})=i\frac{N_0}{3\sqrt{3}}\chi_1^*\chi_2^*\chi_3 e^{i[\mathbf{k}_3\cdot\mathbf{R}+(\Omega-\delta)t]}[\gamma_{12}+i(\Delta-\delta+\mathbf{k}_3\cdot\mathbf{v})]^{-1}$$
$$\times\sum_{\epsilon=\pm 1}2\{\gamma_2-i[\delta+(\epsilon\mathbf{k}_1-\mathbf{k}_3)\cdot v]\}^{-1}\{[\gamma_{12}-i(\Delta+\delta-\mathbf{k}_3\cdot\mathbf{v})]^{-1}+[\gamma_{12}+i(\Delta-\epsilon\mathbf{k}_1\cdot\mathbf{v})]^{-1}\}, \tag{2}$$

where N_0 is the ground-state density, $\Delta=\Omega-\omega$. ω is the atomic transition frequency, $\chi_i=p_{21}E_i/2\hbar$ $(i=1,2,3)$ is a Rabi frequency (E_i is the laser field amplitude and p_{21} is an atomic-dipole-moment *reduced* matrix element.)

The $\epsilon=1$ term in the sum in Eq. (2) can be viewed as the scattering of field 2 from the "coarse" (spacing approximately equal to $1/|\mathbf{k}_1-\mathbf{k}_3|$) population grating formed by fields 1 and 3. It is common to combine the terms in the second set of curly brackets in Eq. (2) to demonstrate that the resonant denominator $(\gamma_2-i[\delta+(\epsilon\mathbf{k}_1-\mathbf{k}_3)\cdot\mathbf{v}])$ disappears when $\gamma_{12}=\gamma_2/2$ but *not* when $\gamma_{12}\neq\gamma_2/2$, as would occur if collisions were present (PIER4 resonance[3]). A typical interpretation of this effect is based on the fact that the two terms in the second set of curly brackets are associated with two different calculational perturbation sequences of the nonlinear response of the atoms to the applied fields. The different sequences are distinguished by the order in which fields 1 and 3 act. Combining these terms appears to give rise to an interference effect which cancels the γ_2 resonance. This feature of the line shape is especially relevant for stationary atoms ($\mathbf{v}=\mathbf{0}$) or for large detunings ($|\Delta|\gg ku$) when both terms in the second set of curly brackets in Eq. (2) contribute to provide the interference effect. However, for detunings $|\Delta|<ku$ and decay rates $\gamma_{12}<ku$ ("Doppler limit"), the situation is changed. When Eq. (2) is integrated over velocity in the Doppler limit, only the $[\gamma_{12}+i(\Delta-\mathbf{k}_1\cdot\mathbf{v})]$ component of the $\epsilon=1$ term survives the velocity averaging (for all the other terms, the poles all lie in the same half plane, giving a null contribution when a contour integration is carried out).

Since one of the pathways in Eq. (2) no longer contributes, an interpretation of the disappearance of PIER4 effects as a destructive interference of two pathways in a perturbation chain seems somewhat artificial for the *velocity-averaged* atomic ensemble.

Equation (2) is averaged with a Maxwellian $W(\mathbf{v})=(\pi u^2)^{-3/2}\exp[-(v/u)^2]$. Assuming that $(k_1u\theta)^2\ll(\gamma_2)^2$ one finds

$$|\langle\rho_{00;10}(-\mathbf{k}_3,\mathbf{v})\rangle|=\frac{N_0}{3\sqrt{3}}|\chi_1^*\chi_2^*\chi_3|\frac{2\sqrt{\pi}}{k_1u}$$
$$\times\left|\frac{1}{[2\gamma_{12}-i(2\Delta-\delta)]}\frac{2}{(\gamma_2-i\delta)}\right|. \tag{3}$$

There is a resonance at $\delta=2\Delta$ having a width (FWHM) $4\gamma_{12}$ and a resonance at $\delta=0$ having a width $2\gamma_2$.

The line shape changes dramatically if one considers the $F_1=1$ to $F_2=0$ transition. In that case [see Eqs. (A1) and (A21)]

$$|\langle\rho_{10;00}(-\mathbf{k}_3,\mathbf{v})\rangle|=N_0\frac{4}{27\sqrt{3}}|\chi_1^*\chi_2^*\chi_3|\frac{2\sqrt{\pi}}{k_1u}\left|\frac{1}{[2\gamma_{12}-i(2\Delta-\delta)]}\right|\left|\frac{1}{(\gamma_2-i\delta)}+\left\langle\frac{r}{\gamma_1-i[\delta-(\mathbf{k}_3-\mathbf{k}_1)\cdot\mathbf{v}]}\right\rangle\right|, \tag{4}$$

where $r=\frac{1}{3}$ and γ_1 is the ground-state decay rate (determined, for example by transit-time effects), which is assumed to be much smaller than γ_2. The average in Eq. (4) is over the transverse velocity distribution and leads to a residual Doppler broadening (width approximately equal to $k_1u\theta$) for the narrow resonance centered at $\delta=0$. The fact that the two-level system under consideration is not closed (in the sense that $\rho_{00;00}+\rho_{10;10}\neq$ const) leads to a *new resonance* of width $2\gamma_1$ (plus any residual Doppler broadening). Since γ_1 is usually much smaller than γ_2 we observe a narrow spike associated with the resonance.

Although the population of the two-level subsystem is not conserved, the total population of the upper and ground levels *is* conserved, with population transferred to the $m_F=\pm 1$ ground-state levels. In a somewhat more general picture of this problem, one can say that population is conserved, but the total magnetic state alignment of the system is not. The process of field absorption plus spontaneous emission leads to a net gain of alignment. In

general, one can expect narrow (ground-state) resonances when either total (excited plus ground state) population, orientation, or alignment is not conserved. When the more general theory is applied to allow for arbitrary F_1 and F_2 as well as optical hyperfine pumping, the final result still takes the form of Eq. (4), but with a different value of r. Moreover, in one of the transitions studied below, the value of *r can be negative*, producing a *narrow dip* in the *spectral profile.*

In an effort to provide additional physical insight into the origin of the above results, we consider a time-domain description of the interaction, which is justified since the state populations are modulated at frequency δ. In the first case where the total population of the two states involved in the transition is conserved, the applied field creates a population in the excited state and decreases the population in the ground state. This perturbation in the excited state decays by spontaneous emission at rate γ_2. Similarly, the perturbation in the ground state also decays at rate γ_2 due to spontaneous emission from the excited state. However, in the second example, while the excited state decay is still determined by γ_2, the perturbation in the $m=0$ ground state no longer decays at the excited-state decay rate. This is because some of $m=0$ ground-state population, which is excited to the upper state, now decays to the $m=\pm 1$ ground states. Hence, a "residual" perturbation *remains* in the $m=0$ ground state, which decays at rate γ_1.

II. DISCUSSION OF RESULTS

Two transitions in atomic sodium were chosen to test the ideas discussed above: the $3s\,^2S_{1/2}(F=2)-3p\,^2P_{3/2}(F=3)$ transition of the $D2$ line at 589 nm (designated transition A) and the $3s\,^2S_{1/2}(F=2)-3p\,^2P_{1/2}(F=2)$ transition of the $D1$ line at 589.6 nm (designated transition B). The experimental configuration is similar to that described earlier[6] and is shown schematically in Fig. 2. A frequency-stabilized tunable cw dye laser (Coherent 699-21) was tuned to frequency Ω near the resonant frequency of the specific transition to provide the two counterpropagating pump beams (the forward pump at $\mathbf{k}_1$ and the backward pump at $\mathbf{k}_2=-\mathbf{k}_1$, respectively). The probe beam (at $\mathbf{k}_3$) is at frequency $\Omega+\delta$ and was provided by a second frequency-stablized tunable cw dye laser.

The two counterpropagating pump beams were aligned interferometricly to be exactly counterpropagating, while the angle between the forward pump and probe was adjusted to be less than 2 mrad (measured in the plane of incidence) and less than 0.4 mrad (measured out of the plane of incidence). Such care was required in order to avoid having the measurements dominated by residual Doppler broadening which characterized the earlier measurements on the effects of collisions (see Lam, Steel, and McFarlane, 1982 and 1986, in Ref. 2). In order to minimize optical-pumping problems, pump intensities were kept below 2mW/cm^2 and the probe beam was a factor of 2 weaker than the pump beams. (Even at these power levels, it is still not possible to avoid saturation effects in alignment and orientation as we discuss below.)

The forward pump was chopped at approximately 300 Hz and phase-sensitive detection of the signal was accomplished using a lock-in amplifier. The amplifier output was then further processed using a real-time signal averager.

The experiments on transition A were performed with the pump beams detuned 51 MHz above the $3s\,^2S_{1/2}(F=2)-3p\,^2P_{3/2}(F=3)$ transition. This was to reduce hyperfine optical-pumping problems associated with transitions to the adjacent $F=2$ and $F=1$ excited states. Using linearly polarized input beams with the probe-beam polarization orthogonal to the pump beams we observed the line shape shown in Fig. 3(a) (the detector polarization was parallel to the probe polarization.) In this configuration the line shape is sensitive only to alignment and orientation effects. As anticipated above, we observe two peaks: one peak with a central dip at $\delta=0$ and a second peak at $\delta=2\Delta$ with a width given by $4\gamma_{12}$. In the balance of this discussion we will concentrate on understanding the details of the first peak.

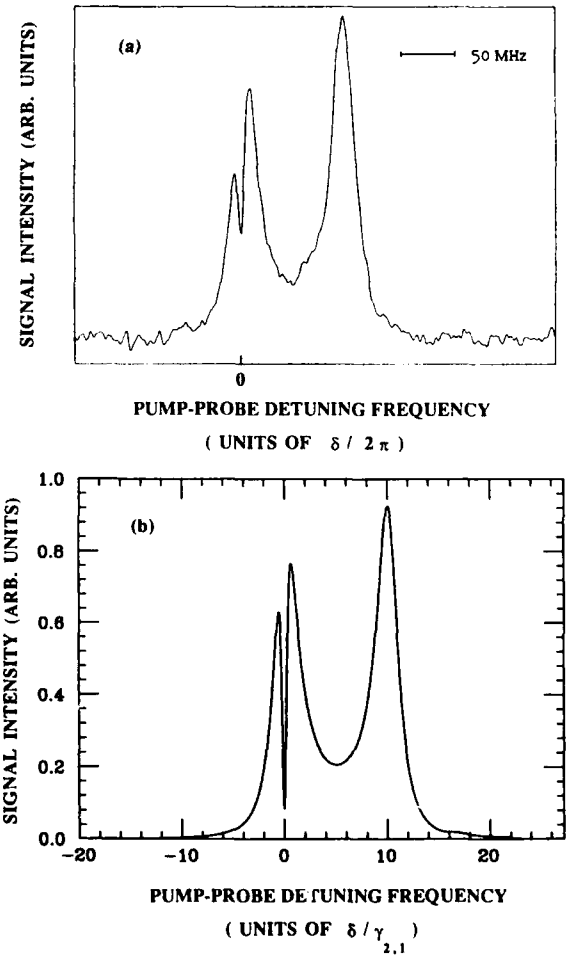

FIG. 3. NDFWM spectrum of the $3s\,^2S_{1/2}(F=2)\rightarrow 3p\,^2P_{3/2}(F=3)$ transition. The optical beams are linearly polarized and the probe beam polarization is orthogonal to the pump beams. (a) Experiment. (b) Theory. The detuning is normalized to $\gamma_{2,1}$ ($\gamma_{2,1}/2\pi=10$ MHz) and $\Delta/2\pi=51$ MHz.

Because of the presence of the magnetic substates, we expect a spectral structure of the form indicated in Eq. (4). This is a direct result of the fact that a given m level in the excited state (excited from a specific m' level in the ground state) can decay to an m'' level in the ground state. However, unlike the simple situation described by a $F=1\rightarrow F=0$ transition, each magnetic ground-state level is coupled to the excited state by the field. The four-wave-mixing signal has a contribution from the alignment and orientation decay of both the ground state and excited states. Since spontaneous decay results in a total ground-state plus excited-state orientation and alignment which is negative, the value of r in Eq. (4) becomes negative. Specifically, the polarization may be calculated using perturbation theory as [see Eq. (A35)—it is always assumed that $(k_1 u\theta)^2 \ll (\gamma_2)^2$]

$$|\mathbf{P}| = \left|\sqrt{2}N_2(\chi^{(1)}_{\frac{3}{2}\frac{1}{2}}\chi^{(2)}_{\frac{3}{2}\frac{1}{2}})^*\chi^{(3)}_{\frac{3}{2}\frac{1}{2}}p_{\frac{3}{2}\frac{1}{2}}5\frac{2\sqrt{\pi}}{k_1 u}\right|\left|\frac{1}{2\gamma_{12}+i(2\Delta-\delta)}\right| \times\left|\left(\frac{7}{20}\right)^2\frac{1}{1050}\left[\frac{47.6}{\gamma_2-i\delta}-\left\langle\frac{5.0}{\gamma_1-i(\delta-\Delta\mathbf{k}\cdot\mathbf{v})}\right\rangle\right]\right|, \tag{5}$$

where $\Delta\mathbf{k}=\mathbf{k}_3-\mathbf{k}_1$. The notation $\chi^{(i)}_{eg}$ corresponds to the previously defined Rabi flopping frequency for field "i" between the excited state e and the ground state g, the angular brackets again indicate a velocity average, and N_2 denotes the $F=2$ ground-state density. For comparison with the experiment, however, we have included in the theory contributions from the $F=2$ to $F=2$ transition along with "crossover" terms that also add to the signal. For weak fields, the measured response is proportional to the modulus squared of the polarization. In arbitrary units, Fig. 3(b) gives $|P|^2$ [from Eq. (A35)] as a function of δ where the detuning is normalized to $\gamma_{2,1}$ and the average has been carried out assuming that $(\mathbf{k}_3-\mathbf{k}_1)\cdot\mathbf{v}\approx k_1 v_x\theta$ with $\theta\approx 1.9$ mrad. In addition, we phenomenologically incorporated approximately 4 Mhz of relative laser jitter into the $\delta=0$ and $\delta=2\Delta$ resonances.[7]

As we see from the qualitative agreement between the data and the theory, the resultant ground-state alignment and orientation produced by decay of the excited state results in a destructive-type contribution to the spectral response [i.e., $r<0$ in Eq. (4) above] producing the observed dip. The width of the dip is determined by residual Doppler broadening and laser jitter. (The relative intensities, though not the widths, of the two resonances depends sensitively on the intensities of the input optical beams. We currently believe this is due to the onset of alignment and orientation saturation effects which are currently not included in the theoretical analysis.)

An analysis similar to that above indicates that an analogous behavior should be observed when all the input beams are copolarized, except the strength of the dip should be weaker because the nonlinear response is dominated by population terms. Namely, the polarization produced on the $F=2$–$F=3$ transition is given by [see Eq. (A36)]

$$|\mathbf{P}| = \left|\sqrt{2}N_2(\chi^{(1)}_{\frac{3}{2}\frac{1}{2}}\chi^{(2)}_{\frac{3}{2}\frac{1}{2}})^*\chi^{(3)}_{\frac{3}{2}\frac{1}{2}}p_{\frac{3}{2}\frac{1}{2}}5\frac{2\sqrt{\pi}}{k_1 u}\right|\left|\frac{1}{2\gamma_{12}+i(2\Delta-\delta)}\right|\left|\left(\frac{7}{20}\right)^2\frac{1}{7875}\left[\frac{384}{\gamma_2-i\delta}-\left\langle\frac{14}{\gamma_1-i(\delta-\Delta\mathbf{k}\cdot\mathbf{v})}\right\rangle\right]\right|. \tag{6}$$

Again, the negative sign in front of the γ_1 resonance results in the dip. However, in fact, the observations show that the dip is absent and a spike is observed. For complete comparison with experiment, it is necessary to include the effects of the $F=2$–$F=2$ transition as well as the crossover terms. In this case, the main effect of the addition of these other terms is to change the relative sign of the γ_1 resonance, leading to a spike rather than a dip in the output. Figures 4(a) and 4(b) compare experiment and theory, where Fig. 4(b) displays the results of Eq. (A36).

In order to confirm the effects of nonconservation of population, we performed experiments on the $3s\,^2S_{1/2}(F=2)$–$3p\,^2P_{1/2}(F=2)$ transition of the $D1$ line at 589.6 nm (the B transition.) The $D1$ line was chosen over the $D2$ line because the excited state hyperfine splitting on the $D1$ line is 189 MHz. The larger splitting reduces the contribution from nearby transitions. (None of the transitions on the $D1$ line conserve population, hence the population-conserving experiment had to be performed on the $D2$ line.) Figure 5(a) shows the experimental data on the $D1$ line using linearly copolarized beams. The polarization is given by Eq. (A37), where unlike an earlier simple analysis,[8] the effects of magnetic substates are included. The theoretical spectral response [Eq. (A37)] is given by

$$|\mathbf{P}| = \left|\sqrt{2}N_2(\chi^{(1)}_{\frac{1}{2}\frac{1}{2}}\chi^{(2)}_{\frac{1}{2}\frac{1}{2}})^*\chi^{(3)}_{\frac{1}{2}\frac{1}{2}}p_{\frac{1}{2}\frac{1}{2}}5\frac{2\sqrt{\pi}}{k_1 u}\right|\left|\frac{1}{2\gamma_{12}+i(2\Delta-\delta)}\right|\left|\left(\frac{5}{20}\right)^2\frac{1}{900}\left[\frac{47.5}{\gamma_2-i\delta}+\left\langle\frac{20.5}{\gamma_1-i(\delta-\Delta\mathbf{k}\cdot\mathbf{v})}\right\rangle\right]\right| \tag{7}$$

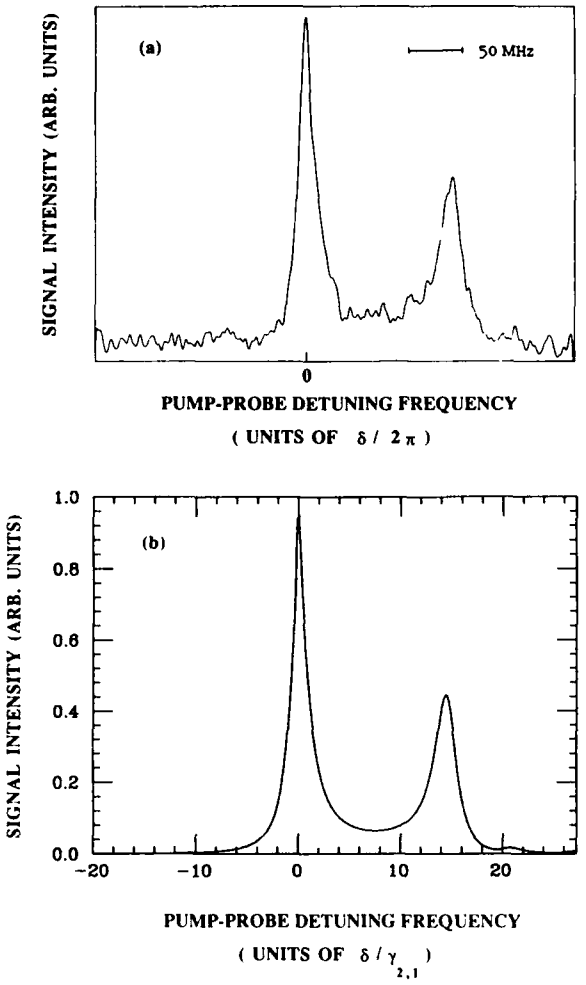

FIG. 4. NDFWM spectrum of the $3s\,^2S_{1/2}(F=2) \rightarrow 3p\,^2P_{3/2}(F=3)$ transition. The optical beams are linearly polarized and the probe beam polarization is parallel to the pump beams. (a) Experiment. (b) Theory. The detuning is normalized to $\gamma_{2,1}$ ($\gamma_{2,1}/2\pi = 10$ MHz) and $\Delta/2\pi = 73$ MHz.

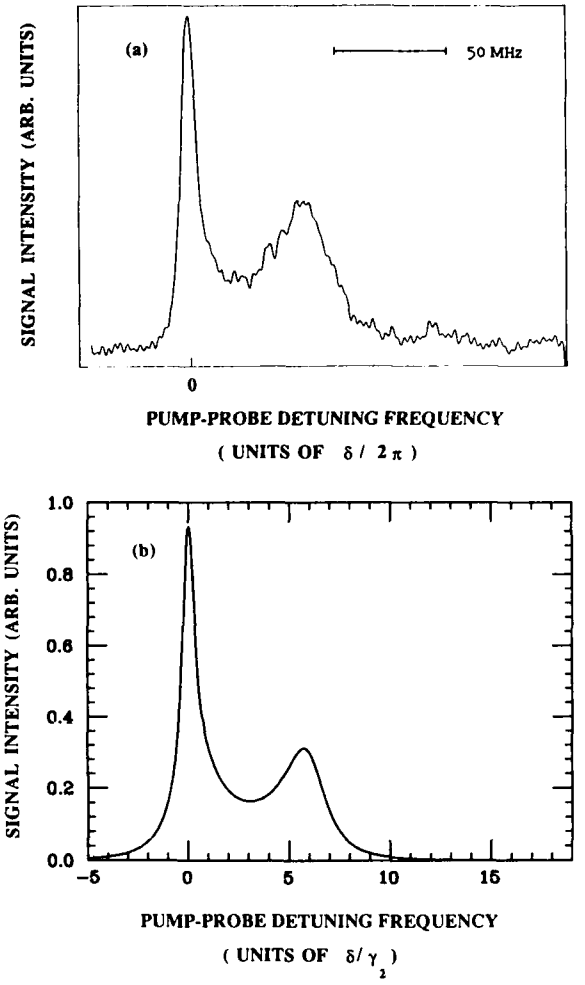

FIG. 5. NDFWM spectrum of the $3s\,^2S_{1/2}(F=2) \rightarrow 3p\,^2P_{1/2}(F=2)$ transition. The opitical beams are linearly polarized and the probe beam polarization is parallel to the pump beams. (a) Experiment. (b) Theory. The detuning is normalized to γ_2 [$\gamma_2/2\pi = 10$ MHz] and $\Delta/2\pi = 30$ MHz.

and is plotted in Fig. 5(b). In contrast to the earlier measurements above, this transition does not conserve population, and population terms dominate the alignment terms, resulting in a spike.

In summary, we have shown that systems which do not conserve population, alignment, or orientation are characterized by a narrow resonance which can either constructively or destructively contribute to the spectral response in four-wave mixing. Based on this work, we see that in principle, it is possible to obtain all three of the decay rates which characterize the transition.

ACKNOWLEDGMENTS

This work was supported by the U.S. Office of Naval Research, the National Science Foundation under Grant No. PHY8415781, and the U.S. Army Research Office Grant No. DAALO3-86-K-0057.

APPENDIX

In this appendix we outline a method for calculating the polarization responsible for phase-conjugate emission. The techniques used to arrive at the results are fairly standard, and details of the method can be found in a number of references.[9] We consider a transition between two manifolds of levels. The quantum numbers which characterize the lower manifold of levels are L_G (total orbital angular momentum), S_G (total spin angular momentum), J_G (coupling of L_G and S_G), I (total nuclear angular momentum), and G (total angular momentum—coupling of J_G and I). The corresponding quantum numbers for the excited manifold of levels are L_H, S_H, J_H, I, and H. Transitions occur between hyperfine levels G of the lower manifold and H of the upper manifold. The labels L_G, S_G, I, and J_G are suppressed in the formulas except when

needed explicitly. The summation convention (all repeated indices appearing on the right-hand side of an equation are summed over, except those which also appear on the left-hand side of the equation) is used throughout. The labels F,F', etc. are hyperfine angular momenta quantum numbers that can refer to either the lower or upper state manifolds of levels.

The atomic state density matrix elements are expanded in an irreducible tensor basis as

$$\rho_Q^K(F,F')=(-1)^{F'-m_{F'}}\langle F,m_F;F',-m_{F'}\mid K,Q\rangle \times\rho(F,m_F;F',m_{F'}) , \tag{A1}$$

where $\langle F_1,m_1;F_2,m_2\mid F,m\rangle$ is a Clebsch-Gordon coefficient. The electric field vector for the applied laser fields is taken as

$$\mathbf{E}(\mathbf{R},t)=\tfrac{1}{2}\mathcal{E}^{(j)}\hat{\boldsymbol{\epsilon}}^{(j)}e^{i(\mathbf{k}_j\cdot\mathbf{R}-\Omega_j t)}+\text{c.c.} \tag{A2}$$

The applied field is a *sum* of fields, each with *complex* amplitude $\mathcal{E}^{(j)}$, complex polarization $\hat{\boldsymbol{\epsilon}}^{(j)}$, propagation vector $\mathbf{k}_j$, and frequency Ω_j. The atom-field interaction energy may be written as

$$V(\mathbf{R},t)=(-1)^q p_q E_{-q}(\mathbf{R},t) , \tag{A3}$$

where

$$p_{\pm1}=\mp\frac{1}{\sqrt{2}}(p_x\pm ip_y),\quad E_{\pm1}=\mp\frac{1}{\sqrt{2}}(E_x\pm iE_y) ,$$
$$p_0=p_z,\quad E_0=E_z , \tag{A4}$$

and p_x,p_y,p_z are components of the atomic-dipole-moment operator. Note that $(p_{\pm1},p_0)$ are components of an irreducible tensor operator of rank 1.

Introducing the standard interaction representation by

$$\rho_Q^K(F,F')=\tilde{\rho}_Q^K(F,F')e^{-i\omega_{FF'}t} \tag{A5}$$

one finds that, owing to the atom-field interaction, density matrix elements evolve as

$$-\dot{\tilde{\rho}}_Q^K(F,F')=\frac{i(-1)^q E_{-q}(\mathbf{R},t)(-1)^{F+F'}}{2\hbar\sqrt{3}}[e^{-i\omega_{F'F''}t}p_{F''F'}\Lambda_{QQ'q}^{KK'1}(F'',F',F)\tilde{\rho}_{Q'}^{K'}(F,F'') - e^{i\omega_{FF''}t}p_{FF''}\Lambda_{QQ'q}^{KK'1}(F'',F,F')(-1)^{K'-K+1}\tilde{\rho}_{Q'}^{K'}(F'',F')] , \tag{A6}$$

where $p_{FF'}$ is a reduced matrix element

$$p_{FF'}=\langle F\|p\|F'\rangle=(-1)^{F-F'}p_{F'F}^* \tag{A7}$$

and

$$\Lambda_{QQ'q}^{KK'1}(F,F',F'')=(-1)^{1+K}[3(2K'+1)]^{1/2}\times\langle K',Q';1,q\mid K,Q\rangle\begin{Bmatrix}K & K' & 1\\ F & F' & F''\end{Bmatrix} , \tag{A8}$$

where the quantity in curly brackets is a 6-j symbol. Any additional contributions to the time rate of change of $\rho_Q^K(F,F')$ from sources other then the applied fields must be added to the rhs (right-hand side) of Eq. (A6).

For the specific problem under investigation, Eq. (A6) is modified as follows.

(1) Incoherent pumping terms

$$\lambda_Q^K(F,F')=\lambda_0^0(F)\delta_{F,F'}\delta_{K,0}\delta_{Q,0}=\frac{\lambda(F)}{(2F+1)^{1/2}}\delta_{F,F'}\delta_{K,0}\delta_{Q,0} \tag{A9}$$

are added to the rhs of Eq. (A6). The quantity $\lambda(F)$ is the rate density (in phase space) at which hyperfine level F is incoherently pumped by sources other than the laser fields.

(2) Decay terms (no sum)

$$-\gamma_{FF'}\tilde{\rho}_Q^K(F,F') \tag{A10}$$

are added to the rhs of Eq. (A6). The decay rate $\gamma_{FF'}$ is defined by

$$\gamma_{FF'}=\tfrac{1}{2}[\gamma(J_F)+\gamma(J_{F'})] , \tag{A11}$$

where $\gamma(J_F)$ is the decay rate for each of the hyperfine levels within a state of given J_F. It is assumed that this (F independent) decay rate results from both spontaneous emission and the finite lifetime the atoms spend in the laser beams.

(3) Spontaneous emission from levels H to G repopulate the G levels. Consequently, a term

$$\gamma^K(H,H';G,G')\tilde{\rho}_Q^K(G,G')\delta_{F,G}\delta_{F',G'} \tag{A12}$$

must be added to the rhs of Eq. (A6). The quantity $\gamma^K(H,H';G,G')$ is defined by

$$\gamma^K(H,H';G,G')=(-1)^{H+K+G'+1}[(2H+1)(2H'+1)]\times\begin{Bmatrix}H & H' & K\\ G' & G & 1\end{Bmatrix}\gamma(H,H';G,G') , \tag{A13}$$

where

$$\gamma(H,H';G,G')=\frac{4}{3\hbar}\left[\frac{\omega_{HG}\omega_{H'G}}{c^2}\right]^{3/2}\times[(2H+1)(2H'+1)]^{-1/2}p_{Gh}p_{G'H'}^* \tag{A14}$$

and ω_{HG} is the H-G transition frequency.

(4) The resonance (or rotating-wave) approximation is made in Eq. (A6) in which terms of order $|(\Omega_j-\omega_{HG})/\omega_{HG}|$ are neglected.

With these additions and approximations, the equations for the time development can be written

$$\dot{\tilde{\rho}}^{K}_{Q}(G,G')=-\gamma_{GG'}\tilde{\rho}^{K}_{Q}(G,G')+\gamma^{K}(H,H';G,G')\tilde{\rho}^{K}_{Q}(H,H')$$
$$+i\chi^{(j)}_{HG'}(-1)^{G+G'}e^{i\mathbf{k}_j\cdot\mathbf{R}}e^{-i(\Omega_j-\omega_{HG'})t}(-1)^{q}\epsilon^{(j)}_{-q}\Lambda^{KK'1}_{QQ'q}(H,G',G)\tilde{\rho}^{K'}_{Q'}(G,H)$$
$$-i(\chi^{(j)}_{HG})^{*}(-1)^{2H+1+K'-K+Q'}e^{i\mathbf{k}_j\cdot\mathbf{R}}e^{i(\Omega_j-\omega_{HG})t}(\epsilon^{(j)}_{q})^{*}\Lambda^{KK'1}_{QQ'q}(H,G,G')[\tilde{\rho}^{K'}_{-Q'}(G',H)]^{*}$$
$$+(2G+1)^{-1/2}\lambda(G)\delta_{G,G'}\delta_{K,0}\delta_{Q,0}\ , \tag{A15a}$$

$$\dot{\tilde{\rho}}^{K}_{Q}(H,H')=-\gamma_{HH'}\tilde{\rho}^{K}_{Q}(H,H')+i(\chi^{(j)}_{H'G})^{*}(-1)^{2G+Q'}e^{-i\mathbf{k}_j\cdot\mathbf{R}}e^{i(\Omega_j-\omega_{H'G})t}(\epsilon^{(j)}_{q})^{*}\Lambda^{KK'1}_{QQ'q}(G,H',H)[\tilde{\rho}^{K'}_{-Q'}(G,H)]^{*}$$
$$-i\chi^{(j)}_{HG}(-1)^{H+H'+K'-K+1}e^{i\mathbf{k}_j\cdot\mathbf{R}}e^{-i(\Omega_j-\omega_{HG})t}(-1)^{q}\epsilon^{(j)}_{-q}\Lambda^{KK'1}_{QQ'q}(G,H,H')\tilde{\rho}^{K'}_{Q'}(G,H')$$
$$+(2H+1)^{-1/2}\lambda(H)\delta_{H,H'}\delta_{K,0}\delta_{Q,0}\ , \tag{A15b}$$

$$\dot{\tilde{\rho}}^{K}_{Q}(G,H)=-\gamma_{GH}\tilde{\rho}^{K}_{Q}(G,H)+i(\chi^{(j)}_{HG'})^{*}(-1)^{G+G'}e^{-i\mathbf{k}_j\cdot\mathbf{R}}e^{i(\Omega_j-\omega_{HG'})t}(\epsilon^{(j)}_{q})^{*}\Lambda^{KK'1}_{QQ'q}(G',H,G)\tilde{\rho}^{K'}_{Q'}(G,G')$$
$$-i(\chi^{(j)}_{H'G})^{*}(-1)^{2G+Q'+K'-K+1}e^{-i\mathbf{k}_j\cdot\mathbf{R}}e^{i(\Omega_j-\omega_{H'G})t}(\epsilon^{(j)}_{q})^{*}\Lambda^{KK'1}_{QQ'q}(H',G,H)[\tilde{\rho}^{K'}_{-Q'}(H,H')]^{*}\ , \tag{A15c}$$

$$\tilde{\rho}^{K}_{Q}(F',F)=(-1)^{F-F'+Q}[\tilde{\rho}^{K}_{-Q}(F,F')]^{*}\ , \tag{A15d}$$

where the polarization components are defined by

$$\epsilon^{(j)}_{\pm1}=\mp\frac{1}{\sqrt{2}}(\epsilon^{(j)}_{x}\pm\epsilon^{(j)}_{y}),\quad \epsilon^{(j)}_{0}=\epsilon^{(j)}_{z}\ , \tag{A16}$$

and the Rabi frequency $\chi^{(j)}_{HG}$ by

$$\chi^{(j)}_{HG}=p_{HG}\mathcal{E}^{(j)}/2\hbar\ . \tag{A17}$$

It is to be noted that the time derivative is to be interpreted as a total derivative, i.e.,

$$\frac{d}{dt}=\frac{\partial}{\partial t}+\mathbf{v}\cdot\nabla\ , \tag{A18}$$

where $\mathbf{v}$ is the atomic velocity.

Equations (A6) and (A15) are quite general and can be used as the starting point for many calculations in nonlinear optics. To calculate the phase-conjugate signal we must solve Eqs. (A15) to third order in the fields. The macroscopic polarization of the sample is given by

$$\mathbf{P}(\mathbf{R},t)=\langle\mathbf{p}\rangle=\frac{1}{\sqrt{3}}\hat{\boldsymbol{\epsilon}}_{Q}(-1)^{H-G}p_{HG}\langle\rho^{1}_{Q}(G,H)\rangle+\text{c.c.}\ , \tag{A19}$$

where

$$\hat{\boldsymbol{\epsilon}}_{\pm1}=\mp\frac{1}{\sqrt{2}}(\hat{\mathbf{x}}\pm i\hat{\mathbf{y}}),\quad \hat{\boldsymbol{\epsilon}}_{0}=\hat{\mathbf{z}}\ , \tag{A20}$$

$\hat{\mathbf{x}}$, $\hat{\mathbf{y}}$, and $\hat{\mathbf{z}}$ are unit vectors, and the average is over the atomic velocity distribution. There are many terms which contribute to $\rho^{1}_{Q}(G,H)$ in third order. For incident fields $\mathbf{E}^{(1)}\equiv(\mathbf{k}_1,\Omega)$, $\mathbf{E}^{(2)}\equiv(-\mathbf{k}_1,\Omega)$, and $\mathbf{E}^{(3)}(\mathbf{k}_3\approx\mathbf{k}_1,\Omega+\delta)$, the phase-conjugate field corresponds to the polarization component which propagates in the $-\mathbf{k}_3$ direction with frequency $\Omega-\delta$. By solving Eqs. (A15) to third order in the fields and using Eq. (A5), one finds the phase-conjugate contribution to $\rho^{1}_{Q}(G,H;\ -\mathbf{k}_3,\mathbf{v})$ to be

$$\rho^{1}_{Q}(G,H;-\mathbf{k}_3,\mathbf{v})=i\sqrt{3}(-1)^{q'+Q}(\epsilon^{(1)}_{q'})^{*}(\epsilon^{(2)}_{q''})^{*}\epsilon^{(3)}_{q}\exp\{i[\mathbf{k}_3\cdot\mathbf{R}+(\Omega-\delta)t]\}$$
$$\times\sum_{j'=1}^{3}(1-\delta_{j,3})\langle1,Q;1,-q''\,|\,K',Q'\rangle\langle1,q';1,\ -q\,|\,K',Q'\rangle[\gamma_{GH}+i(\Delta_{HG}-\delta+\mathbf{k}_3\cdot\mathbf{v})]^{-1}$$
$$\times\left\{\frac{(\chi^{(1)}_{HG'}\chi^{(2)}_{H'G})^{*}\chi^{(3)}_{H'G'}(-1)^{H+G'+2G}\begin{Bmatrix}K' & 1 & 1\\ G & H' & H\end{Bmatrix}\begin{Bmatrix}K' & 1 & 1\\ G' & H' & H\end{Bmatrix}}{(2G'+1)^{1/2}[\gamma_{HH'}-i(\delta-\omega_{H'H}-\mathbf{k}_{3j}\cdot\mathbf{v})]\mu_{jj'}(G',H;G',H';\lambda(G'),\lambda(G'))}\right.$$
$$+\frac{(\chi^{(1)}_{H'G}\chi^{(2)}_{HG'})^{*}\chi^{(3)}_{H'G'}(-1)^{H'-G}\begin{Bmatrix}K' & 1 & 1\\ H & G' & G\end{Bmatrix}\begin{Bmatrix}K' & 1 & 1\\ H' & G' & G\end{Bmatrix}}{(2G+1)^{1/2}[\gamma_{GG'}-i(\delta-\omega_{GG'}-\mathbf{k}_{3j}\cdot\mathbf{v})]\mu_{jj'}(G,H';G',H';\lambda(G),\lambda(G'))}$$
$$\left.-\frac{(\chi^{(1)}_{H'G''}\chi^{(2)}_{HG'})^{*}\chi^{(3)}_{H''G''}(-1)^{2G'+G''+H'}\begin{Bmatrix}K' & 1 & 1\\ H & G' & G\end{Bmatrix}\begin{Bmatrix}K' & 1 & 1\\ G'' & H'' & H'\end{Bmatrix}}{(2G''+1)^{1/2}[\gamma_{G'G}-i(\delta-\omega_{GG'}-\mathbf{k}_{3j}\cdot\mathbf{v})]\mu_{jj'}(G'',H';G'',H'';\lambda(G''),\lambda(G''))}\right\}$$
$$\times\gamma^{K'}(H',H'';G',G)/[\gamma_{H'H''}-i(\delta-\omega_{H''H'}-\mathbf{k}_{jg}\cdot\mathbf{v})]\ , \tag{A21}$$

where

$$\mathbf{k}_{3j}=\mathbf{k}_3-\mathbf{k}_j\ , \tag{A22}$$

$$\Delta_{HG}=\Omega-\omega_{HG}\ , \tag{A23}$$

and

$$[\mu_{jj'}(G,H;G',H';\lambda(G),\lambda(G'))]^{-1}=\delta_{j',j}(2G+1)^{-1}\lambda(G)[Y_{GH}+i(\Delta_{HG}-\mathbf{k}_j\cdot\mathbf{v})]^{-1}/\gamma(J_G)$$
$$+\delta_{j',3}(2G'+1)^{-1}\lambda(G')[\gamma_{G'H'}-i(\Delta_{H'G'}+\delta-\mathbf{k}_3\cdot\mathbf{v})]^{-1}/\gamma(J_{G'})\ . \tag{A24}$$

For simplicity, we have set $\lambda(H)=0$.

The polarization is calculated from Eqs. (A19) and (A21). The incoherent pump rate density is assumed to be of the form

$$\lambda(G)=N_G\gamma(J_G)W(\mathbf{v})\ , \tag{A25}$$

where N_G is the G-state density and $W(\mathbf{v})$ is the equilibrium velocity distribution (in the absence of any applied fields) given by

$$W(\mathbf{v})=(\pi u^2)^{-3/2}\exp(-v^2/u^2)\ , \tag{A26}$$

where u is the most probable atomic speed. We evaluate the polarization corresponding to our experimental conditions, namely: (1) The dominant transition amplitude is between a single hyperfine ground-state level G and the H hyperfine levels of either the $J=\frac{3}{2}$ or the $J=\frac{1}{2}$ excited state; (2) $|\Delta_{HG}|/k_1u\ll1$ and $\gamma_{HG}/k_1u\ll1$, implying that only the $j=1$, $j'=3$ term in the summation in Eq. (A21) contributes when the velocity integration is carried out; (3) $(\mathbf{k}_3-\mathbf{k}_1)\cdot\mathbf{v}\simeq k_1\theta v_x$, where $\mathbf{k}_1=k_1\hat{\mathbf{z}}$ and $\mathbf{k}_3\simeq k_1(\hat{\mathbf{z}}+\theta\hat{\mathbf{x}})$, with $\theta\ll1$; (4) $(k_1u\theta)^2\ll(\gamma_2)^2$.[10] In these limits, using the relationship

$$\langle J_HIH\|p\|J_GIG\rangle=(-1)^{G+J_H+I+1}[(2G+1)(2H+1)]^{1/2}$$
$$\times\begin{Bmatrix}J_G & 1 & J_H\\ H & I & G\end{Bmatrix}\langle J_H\|p\|J_G\rangle \tag{A27}$$

to rewrite all reduced matrix elements in the J basis and the fact that $|\omega_{HH'}/\omega_{HG}|\ll1$, one finds a polarization

$$\mathbf{P}(\mathbf{R},t)=i\exp\{i[\mathbf{k}_3\cdot\mathbf{R}-(\Omega-\delta)t]\}\hat{\boldsymbol{\epsilon}}_Q(2\sqrt{\pi}/k_1u)[N_G/(2G+1)](\chi^{(1)}_{J_HJ_G}\chi^{(2)}_{J_HJ_G})^*\chi^{(3)}_{J_HJ_G}p_{J_HJ_G}$$
$$\times(2H+1)(2H'+1)(2G+1)^2\begin{Bmatrix}J_H & 1 & J_G\\ G & I & H\end{Bmatrix}^2\begin{Bmatrix}J_H & 1 & J_G\\ G & I & H'\end{Bmatrix}^2$$
$$\times(-1)^{q'+Q}\langle 1,Q;1,-q''\,|\,K',Q'\rangle\langle 1,q';1,-q\,|\,K',Q'\rangle$$
$$\times\Bigg\{\begin{Bmatrix}K' & 1 & 1\\ G & H & H'\end{Bmatrix}^2[2\gamma_{GH}+i(2\Delta_{HG}-\delta)]^{-1}[\gamma(J_H)-i(\delta-\omega_{H'H})]^{-1}$$
$$+(-1)^{H'-H}\begin{Bmatrix}K' & 1 & 1\\ H & G & G\end{Bmatrix}\begin{Bmatrix}K' & 1 & 1\\ H' & G & G\end{Bmatrix}[2\gamma_{GH}+i(\Delta_{HG}+\Delta_{H'G}-\delta)]^{-1}$$
$$\times(\alpha^{K'}_{H'H''}\gamma(J_H\rightarrow J_G)[\gamma(J_H)-\gamma(J_G)+i\omega_{H''H'}]^{-1}[\gamma(J_H)-i(\delta-\omega_{H''H'})]^{-1}$$
$$+\langle[\gamma(J_G)-i(\delta-k_1\theta v_x)]^{-1}\rangle\{1-\alpha^{K'}_{H'H''}\gamma(J_H\rightarrow J_G)[\gamma(J_H)-\gamma(J_G)+i\omega_{H''H'}]^{-1}\}\Bigg)\Bigg\}+\text{c.c.}\ , \tag{A28}$$

where

$$\chi^{(j)}_{J_HJ_G}=\langle J_H\|p\|J_G\rangle\mathcal{E}^{(j)}/2\hbar\ , \tag{A29}$$

$$\alpha^{K'}_{H'H''}=(-1)^{1+H'+G}(2H''+1)(2G+1)(2J_{H''}+1)$$
$$\times\begin{Bmatrix}J_{H''} & 1 & J_G\\ G & I & H''\end{Bmatrix}^2\begin{Bmatrix}K' & 1 & 1\\ G & H' & H''\end{Bmatrix}$$
$$\times\begin{Bmatrix}K' & H' & H''\\ 1 & G & G\end{Bmatrix}\begin{Bmatrix}K' & 1 & 1\\ H' & G & G\end{Bmatrix}^{-1}\ , \tag{A30}$$

and

$$\gamma(J_H\rightarrow J_G)=\frac{4}{3\hbar}\left[\frac{\omega_{J_HJ_G}}{c}\right]^3(2J_H+1)^{-1}$$
$$\times|\langle J_G\|p\|J_H\rangle|^2\ . \tag{A31}$$

The remaining average over v_x is easily expressed in terms of the plasma dispersion function as

$$\langle[\gamma - i(\delta - k\theta v_x)]^{-1}\rangle = -\frac{i}{ku\theta} Z\left(\frac{i\gamma+\delta}{ku\theta}\right), \quad \text{(A32)}$$

where Z is defined by

$$Z(\mu) = -\frac{1}{\sqrt{\pi}} \int_{-\infty}^{\infty} dx \frac{e^{-x^2}}{\mu \pm x}, \quad \mathrm{Im}(\mu) > 0 \quad \text{(A33)}$$

with limiting values

$$\begin{aligned} &Z(\mu) \sim i\sqrt{\pi} e^{-[\mathrm{Re}(\mu)]^2}, \quad |\mu| \ll 1, \\ &Z(\mu) \sim -\mu^{-1}, \quad |\mu| \gg 1. \end{aligned} \quad \text{(A34)}$$

For our experiment in sodium, $I = \frac{3}{2}$, $G = 2$; $H = 1,2,3$ ($J_H = \frac{3}{2}$) or $H = 1,2$ ($J_H = \frac{1}{2}$). For the copolarized case all beams are polarized in the z direction and $\epsilon_q^{(i)} = \delta_{q,0}$ ($i = 1,2,3$). For the cross-polarized case, beams 1 and 2 are polarized in the z direction [$\epsilon_q^i = \delta_{q,0}$ ($i = 1,2,$)] and beam 3 in the x direction [$\epsilon_q^{(3)} = (1/\sqrt{2})(\delta_{q,-1} - \delta_{q,1})$].

It is now a straightforward matter to evaluate Eq. (A28) for our experimental conditions. The polarization exhibits resonances at various values of δ. The "direct" resonance at $\delta = 2\Delta_{HG}$ arises from the interaction of fields 1 and 2 with the *same* pair of transition levels, excited state H and lower state G. The resonance at $\delta = (\Delta_{HG} + \Delta_{H'G})$ ($H' \neq H$) is a "crossover" resonance involving the interaction of field 1 with the G-H transition and field 2 with the G-H' transition. Both these resonances have widths characterized by the dipole decay rate γ_{GH}. In addition, there are resonances at $\delta = \omega_{H'H}$, having widths characterized by atomic state population decay rates. For $H = H'$, these are Rayleigh-type resonances involving the interaction of fields 1 and 3 with a single pair of transition levels G-H. For $H \neq H'$, they are Raman-type resonances involving the interaction of fields 1 and 3 with *two* coupled transitions, G-H and G-H', respectively.

For the level scheme of our experiment and for the detunings and frequency range under investigation, the Raman terms do not contribute significantly to the line shape and can be neglected without much error. Moreover, for the experimental detunings chosen, it turns out that the $(G = 2) \rightarrow (H = 1)$ contribution to the $D2$ resonance and the $(G = 2) \rightarrow (H = 1)$ contribution to the $D1$ resonance are negligibly small. With the neglect of the above terms, the calculated polarizations are as follows.

(1) For cross polarized beams on the $D2$ transition [$J = \frac{1}{2}(G = 2) \rightarrow J = \frac{3}{2}(H = 2,3)$], the polarization is

$$\begin{aligned} \mathbf{P}(\mathbf{R},t) = -i\hat{\mathbf{x}} N_2 \exp\{i[\mathbf{k}_3\cdot\mathbf{R} + (\Omega - \delta)t]\} 5 \left(\frac{7}{20}\right)^2 \frac{47.6}{1050} \left(\frac{2\sqrt{\pi}}{k_1 u}\right) (\chi^{(1)}_{\frac{3}{2}\frac{1}{2}} \chi^{(2)}_{\frac{3}{2}\frac{1}{2}})^* \chi^{(3)}_{\frac{3}{2}\frac{1}{2}} p_{\frac{3}{2}\frac{1}{2}} \\ \times \{[2\gamma + i(2\Delta_{32} - \delta)]^{-1} (\bar{\gamma}_2^{-1} - 0.105\bar{\gamma}_1^{-1}) + 0.073[2\gamma + i(2\Delta_{22} - \delta)]^{-1}(-\bar{\gamma}_2^{-1} - 0.37\bar{\gamma}_1^{-1}) \\ + 0.059[2\gamma + i(\Delta_{32} + \Delta_{22} - \delta)]^{-1}(\bar{\gamma}_2^{-1} - 2.19\bar{\gamma}_1^{-1})\} + \text{c.c.}, \end{aligned} \quad \text{(A35)}$$

where

$$\bar{\gamma}_1 = \langle[\gamma(3S) - i(\delta - k_1\theta v_x)]\rangle, \quad \bar{\gamma}_2 = \gamma(3P) - i\delta,$$

and

$$\gamma = \tfrac{1}{2}[\gamma(3S) + \gamma(3P)].$$

The first two terms in (A35) are the "direct" resonances on the 2-3 and 2-2 transitions, respectively, while the third term is the crossover signal involving both the 2-3 and 2-2 transitions.

(2) For copolarized beams on the $D2$ transition [$J = \frac{1}{2}(G = 2) \rightarrow J = \frac{3}{2}(H = 2,3)$], the polarization is

$$\begin{aligned} \mathbf{P}(\mathbf{R},t) = i\hat{\mathbf{z}} N_2 \exp\{i[\mathbf{k}_3\cdot\mathbf{R} + (\Omega - \delta)t]\} 5 \left(\frac{7}{20}\right)^2 \frac{384}{7875} \left(\frac{2\sqrt{\pi}}{k_1 u}\right) (\chi^{(1)}_{\frac{3}{2}\frac{1}{2}} \chi^{(2)}_{\frac{3}{2}\frac{1}{2}})^* \chi^{(3)}_{\frac{3}{2}\frac{1}{2}} p_{\frac{3}{2}\frac{1}{2}} \\ \times \{[2\gamma + i(2\Delta_{32} - \delta)]^{-1} (\bar{\gamma}_2^{-1} - 0.0365\bar{\gamma}_1^{-1}) + 0.138[2\gamma + i(2\Delta_{22} - \delta)]^{-1}(\bar{\gamma}_2^{-1} + 0.432\bar{\gamma}_1^{-1}) \\ + 0.158[2\gamma + i(\Delta_{32} + \Delta_{22} - \delta)]^{-1}(\bar{\gamma}_2^{-1} + 0.649\bar{\gamma}_1^{-1})\} + \text{c.c.}. \end{aligned} \quad \text{(A36)}$$

Note that it is possible for the crossover contribution to change the narrow resonance at $\delta = 0$ from a dip, predicted by the "direct" terms alone, to a peak. This is, in fact, the case for the detunings in our experiment, $\Delta_{32}/2\pi \simeq 73$ MHz, $\Delta_{22}/2\pi \simeq 133$ MHz.

(3) For copolarized beams on the $D1$ transition [$J = \frac{1}{2}(G = 2) \rightarrow J = \frac{1}{2}(H = 2)$], there is a direct contribution only to the polarization given by

$$\begin{aligned} \mathbf{P}(\mathbf{R},t) = i\hat{\mathbf{z}} N_2 \exp\{i[\mathbf{k}_3\cdot\mathbf{R} + (\Omega - \delta)t]\} 5 \left(\frac{5}{20}\right)^2 \frac{47.5}{900} \left(\frac{2\sqrt{\pi}}{k_1 u}\right) (\chi^{(1)}_{\frac{1}{2}\frac{1}{2}} \chi^{(2)}_{\frac{1}{2}\frac{1}{2}})^* \chi^{(3)}_{\frac{1}{2}\frac{1}{2}} p_{\frac{1}{2}\frac{1}{2}} \\ \times [2\gamma + i(2\Delta_{22} - \delta)]^{-1}(\bar{\gamma}_2^{-1} + 0.432\bar{\gamma}_1^{-1}) + \text{c.c.} \end{aligned} \quad \text{(A37)}$$

*Present address: Optical Sciences Center, University of Arizona, Tucson, AZ.

[1]See, for example, M. Ducloy and D. Bloch, J. Phys. (Paris) **42**, 711 (1981); **43**, 57 (1982); R. L. Abrams, J. F. Lam, R. C. Lind, D. G. Steel, and P. F. Liao, in *Optical Phase Conjugation*, edited by R. A. Fisher (Academic, New York, 1983), pp. 211–284, and references therein.

[2]R. K. Raj, D. Bloch, J. J. Snyder, G. Camy, and M. Ducloy, Phys. Rev. Lett. **44**, 1251 (1980); J. F. Lam, D. G. Steel, and R. A. McFarlane, *ibid.* **49**, 1628 (1982); D. G. Steel and R. A. McFarlane, Phys. Rev. A **27**, 1687 (1983); J. F. Lam, D.G. Steel, and R. A. McFarlane, Phys. Rev. Lett. **56**, 1679 (1986).

[3]N. Bloembergen, in *Laser Spectroscopy IV*, edited by H. Walther and K. W. Rothe (Springer, Berlin, 1979), pp. 340–348; Y. Prior, A. R. Bogdan, M. Dagenais, and N. Bloembergen, Phys. Rev. Lett. **46**, 111 (1981).

[4]For a recent review of this subject, see G. Grynberg, in *Spectral Line Shapes*, edited by R. Exton (W. de Gruyter, Berlin, 1987), Vol. 4, pp. 503–521; L. Rothberg, in *Progress in Optics*, edited by E. Wolf (Elsevier, Amsterdam, 1987), pp. 39–101.

[5]G. Khitrova, Ph. D. Thesis, New York University, 1986; G. G. Adonts and D. G. Akopyan, J. Phys. B **18**, 3407 (1985); M. Ducloy and D. Bloch, Phys. Rev. A **30**, 3107 (1984).

[6]D. G. Steel and R. C. Lind, Opt. Lett. **6**, 587 (1981).

[7]Laser jitter is accounted for in a purely phenomenological manner by setting $\gamma_1 \rightarrow \gamma_1+\gamma_1'$, $\gamma_2 \rightarrow \gamma_2+\gamma_2'$, $\gamma_{12} \rightarrow \gamma_{12}+\gamma_{12}'$ in Eq. (5). The primed quantities, which represent the noise contribution, are taken as $\gamma_1'/2\pi=\gamma_2'/2\pi=2.0$ MHz; $\gamma_{12}'/2\pi=1.3$ MHz. This treatment of noise may be justified on the basis of detailed calculations involving uncorrelated pump and probe fields [G. S. Agarwal and J. Cooper, Phys. Rev. A **26**, 2761 (1982)]. To properly account for laser jitter, one must average the instantaneous dipole moment density over velocity, multiply it by its conjugate, and then average over the laser noise [see, for example, G. S. Agarwal, C. V. Kunasz, and J. Cooper, Phys. Rev. A **36**, 143 (1987), and references therein; Y. Prior, I. Schek, and J. Jortner, *ibid.* **31**, 3775 (1985)].

[8]Jing Liu, J. T. Remillard, and D. G. Steel, Phys. Rev. Lett. **59**, 779 (1987).

[9]See, for example, M. Dumont, J. Phys. (Paris) **33**, 971 (1972); A. Omont, *Progress in Quantum Electronics* (Pergamon, Oxford, 1977), Vol. 5, pp. 69–138; C. Feuillade and P. R. Berman, Phys. Rev. A **29**, 1236 (1984); M. Ducloy and D. Bloch, *ibid.* **30**, 3107 (1984); K. Blum, *Density Matrix Theory and Applications* (Plenum, New York, 1981).

[10]If the assumtion $(k_1u\theta)^2 \ll (\gamma_2)^2$ is not made, the expression for the polarization takes on a more complicated form. The transverse velocity v_x appears in resonance denominators involving both γ_{GH} and $\gamma(J_H)$, as well as those involving $\gamma(J_G)$. The polarization then involves a sum of terms of the form

$$\langle [2\gamma_{GH}+i(\tilde{\Delta}-\delta+k_1\theta v_x)]^{-1}[\gamma_a-i(\delta-k_1\theta v_x)]^{-1}\rangle ,$$

where $\tilde{\Delta}=(\Delta_{HG}+\Delta_{H'G})$; $H'=H$ or $H'\neq H$. This may be rewritten as

$$(\gamma_a-2\gamma_{GH}-i\tilde{\Delta})^{-1}\{\langle [2\gamma_{GH}+i(\tilde{\Delta}-\delta+k_1\theta v_x)]^{-1}\rangle - \langle [\gamma_a-i(\delta-k_1\theta v_x)]^{-1}\rangle\} .$$

The resultant average over v_x can be expressed in terms of the plasma dispersion function, as described in the text [Eq. (A32)], giving a term which varies as

$$[\gamma_a-2\gamma_{GH}-i\tilde{\Delta}]^{-1}[-i/(k_1u\theta)]\left[Z\left(\frac{2i\gamma_{GH}-(\tilde{\Delta}-\delta)}{k_1u\theta}\right)-Z\left(\frac{i\gamma_a+\delta}{k_1u\theta}\right)\right] .$$

Under the actual experimental conditions, $k_1u\theta/\gamma_2 \sim 0.25$. This value is sufficiently small to ensure that the residual Doppler width does not contribute significantly to the γ_2 (or $2\gamma_{12}$) resonances. Of course, it is an easy matter to use the exact expressions for improved accuracy. One simply replaces any products of the form

$$[2\gamma_{GH}+i(\tilde{\Delta}-\delta)]^{-1}[\gamma(J_H)-i(\delta-\omega_{H'H})]^{-1}$$

or

$$[2\gamma_{GH}+i(\tilde{\Delta}-\delta)]^{-1}\langle [\gamma(J_G)-i(\delta-k_1\theta v_x)]^{-1}\rangle$$

appearing in Eq. (A28) by the corresponding expression given above involving the plasma dispersion functions.

Theory of resonances in four-wave mixing resulting from velocity-changing collisions

M. Gorlicki,* P. R. Berman, and G. Khitrova†
Physics Department, New York University, 4 Washington Place, New York, New York 10003
(Received 28 December 1987)

A theory of four-wave mixing including effects of velocity-changing collisions is presented. Three fields with frequencies ω, ω, and $\omega+\delta$ are incident on a vapor of "two-level" atoms having upper state b and lower state a. Two of the fields are counterpropagating and the third (of frequency $\omega+\delta$) makes a small angle with one of the others. The frequency ω is a nearly resonant (inside the Doppler width) with the a-b transition frequency. The phase-conjugate signal emitted at frequency $\omega-\delta$ is calculated as a function of δ. Using a simple collision model in which collisions are phase interrupting in their effect on atomic coherence and velocity-changing in their effect on level populations, we discuss the conditions under which resonances characterized by the upper or lower radiative and collision rates can be observed. Assuming that the total $(a+b)$ state population is conserved in the absence of collisions, it is shown that velocity-changing collisions can "open" the system and lead to a resonance characterized by the lower-state width (convoluted with the residual Doppler width). With increasing pressure, the width of this induced resonance structure decreases monotonically. For sufficiently high pressure, the collisional redistribution of velocity classes is complete—the system "recloses" and the narrow resonance disappears. The interplay of the collision-induced opening, line narrowing, and reclosing of the system is discussed, as is the relationship of these narrow resonances to the so-called pressure-induced extra resonances of Bloembergen and co-workers [Indian J. Pure Appl. Phys. **16**, 151 (1978); Phys. Rev. Lett. **46**, 111 (1981)].

I. INTRODUCTION

The phenomenon of pressure-induced extra resonances observed via four-wave mixing is a subject area that has received a great deal of attention following its prediction[1] and experimental verification[2] by Bloembergen and co-workers. Both theoretical and experimental developments in pressure-induced resonances have been reviewed recently.[3]

Pressure-induced resonances refer to resonant structures that appear only in the presence of collisions. They can be observed under a wide variety of experimental configurations. To observe pressure-induced resonances via four-wave mixing in a "two-level" atom, three laser fields having frequencies ω, ω, and $\omega+\delta$ may be used. As the detuning δ is varied, the pressure-induced resonances appear as structures centered at $\delta=0$ with linewidths characterized by the spontaneous decay rates of the two levels. When one of the transition levels is the ground state, it is possible to observe very narrow resonances, whose widths are limited by transit time or residual Doppler broadening.

Most theoretical treatments of the problem have been restricted to homogeneously broadened atomic samples or to situations in which the atom-field detunings are much larger than the Doppler width. Many of the experiments were carried out for this range of detunings. In this limit atoms in all velocity subclasses essentially contribute equally to line-shape formation. If the atom-field detunings are less than the Doppler width, atoms which are Doppler shifted into resonance with the field are preferentially excited. The physical interpretation of the four-wave mixing signals differs significantly for nearly resonant fields (detuning less than the Doppler width) than for the large-detuning case.

There have been a number of experiments carried out with nearly resonant fields.[4,5] A theoretical analysis of these experiments, including effects of velocity-changing collisions and residual Doppler broadening (owing to a slight angle between two of the beams), has not been carried out to our knowledge. Lam *et al.*[5] did discuss the effect of velocity-changing collisions but did not include the residual Doppler broadening. Rothberg and Bloembergen[6] discussed the collisional narrowing of the residual Doppler broadening of the resonances (for the highly detuned case), giving the expected dependence of the resonances's width and amplitude on perturber pressure. Most other theoretical approaches neglect the residual Doppler broadening and treat collisions solely by the introduction of a number of collision rates.

It is the purpose of this paper to analyze collision-induced features that may appear in four-wave-mixing line shapes. We consider a two-level atom subjected to three fields having frequencies ω, ω, $\omega+\delta$ and calculate the signal emitted by the sample at frequency $\omega-\delta$ as a function of δ. The atom-field detuning $\Delta=\omega-\omega_0$ (ω_0 is the atomic transition frequency) is less than the Doppler width associated with the transition.

In particular, we examine in detail the conditions under which one can observe resonances characterized by the natural widths γ_a and γ_b, associated with the lower and upper transition levels, respectively. In the limit that a is the ground state, it will be seen that a resonance with width γ_a can be observed only when the system is "open" (population not conserved). Velocity-changing collisions provide a mechanism for opening the system. The total

population of *each* atomic velocity class need no longer remain "closed" when collisions are present, even if the total (velocity-integrated) population does remain closed. Thus, velocity-changing collisions contribute directly to the resonance having width γ_a. The resonance having width γ_b occurs for open or closed systems, with or without collisions, for nearly resonant tuning.

Velocity-changing collisions not only lead to the appearance of the γ_a resonance, but are also responsible for the narrowing of the residual Doppler broadening. The way in which velocity-changing collisions result in opening, collisional narrowing, and the ultimate closing of the system is explored.

The calculations are carried out in lowest-order perturbation theory, using a highly simplified collision model ("strong" velocity-changing collisions for populations; homogeneous collisional decay for atomic coherence). A preliminary version of this work has appeared.[7]

In the first part of the paper we carry out a straightforward calculation of the four-wave-mixing signal, after having introduced our definitions of open and closed systems. In the second half of the paper we analyze the results, emphasizing the dependence of the γ_a resonance on the opening, narrowing, and ultimate closing produced by velocity-changing collisions.

II. CALCULATION OF THE SIGNAL

The system we consider in this paper is a collection of two-level atoms, interacting in a classical four-wave-mixing geometry with three laser beams, whose electric fields are labeled by $\mathbf{E}_f$ (forward) $\mathbf{E}_b$ (backward), and $\mathbf{E}_p$ (probe), as shown in Fig. 1. Fields $\mathbf{E}_f$ and $\mathbf{E}_b$ have the same frequency ω and are counterpropagating (wave vectors $\mathbf{k}_0$ and $-\mathbf{k}_0$, respectively), while field $\mathbf{E}_p$ has frequency $\omega+\delta$ and has a wave vector $\mathbf{k}$ which is directed along an axis at angle θ to $\mathbf{k}_0$. The $|a\rangle$ (lower) and $|b\rangle$ states are separated in energy by $\hbar\omega_0$. Both of them may be excited levels, although the interesting case, with which we are mainly concerned, is a closed system in which $|a\rangle$ is a ground state and $|b\rangle$ an excited state that can decay radiatively only via spontaneous emission to state $|a\rangle$. For reasons that will become clear in Sec. III, we adopt a slightly modified definition of a closed system. If γ_a and γ_b are, respectively, the radiative lifetimes of $|a\rangle$ and $|b\rangle$, and $\gamma_{b,a}$ is the radiative transfer rate from $|b\rangle$ to $|a\rangle$, the system is said to be closed if

$$\gamma_b=\gamma_{b,a}+\gamma_a \ . \tag{1}$$

Condition (1) implies that there is only one decay rate (which can be zero) for the sum of the populations of states $|a\rangle$ and $|b\rangle$. In other words, the total population is not conserved within an overall decay constant γ_a which may differ from zero. If, for example, states $|a\rangle$ and $|b\rangle$ have the same transit time in the laser beams, condition (1) could hold with γ_a equal to the inverse transit time. The motivation behind this definition of a closed system is discussed in Sec. III.

The atoms form a gas with a classical velocity distribution, and the internal state of a group of atoms having the velocity $\mathbf{v}$ is described by the density operator $\rho(\mathbf{v})$. In the absence of interaction with the lasers, the variation of $\rho(\mathbf{v})$ as a function of $\mathbf{v}$ is proportional to the Gaussian thermal distribution

$$W(\mathbf{v})=\frac{1}{(u\sqrt{\pi})^3}e^{-v^2/u^2} \ , \tag{2}$$

where u is the most probable atomic speed.

These atoms are immersed in a buffer gas of foreign atoms with no active structure. The active-atom density is assumed to be sufficiently low that one need consider only active-atom–foreign-gas-atom collisions. To easily account for these collisions, we make the classical set of assumptions which defines the so-called collisional and radiative impact regime. The validity conditions for the impact approximation can be stated as[8]

$$\begin{aligned}&\tau_c \ll \Omega_i^{-1}, |\omega-\omega_0|^{-1}, |\omega+\delta-\omega_0|^{-1} \ , \\ &\tau_c \ll \Gamma^{-1}, \gamma_b^{-1}, \gamma_a^{-1} \ ,\end{aligned} \tag{3}$$

where τ_c is the duration of a typical collision, Ω_i is any relevant Rabi frequency, and Γ is a macroscopic collisional rate. In this framework the evolutions under collisional and radiative interactions are decoupled and the collisions can be simply described by an additional time derivative in every equation governing a matrix element $\rho_{\alpha\beta}(\mathbf{v})$ $(\alpha=a,b;\beta=a,b)$ given by[9]

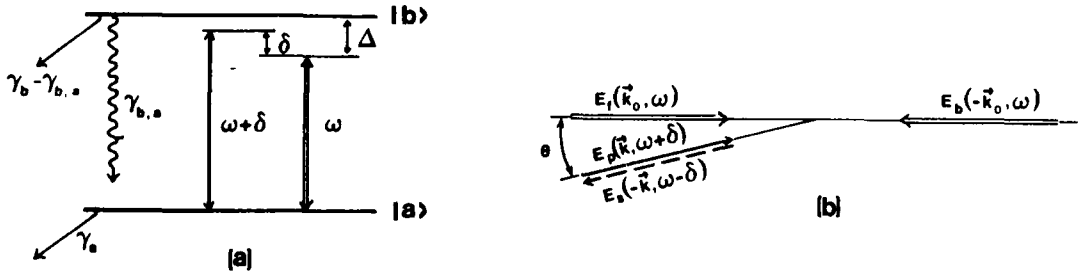

FIG. 1. (a) Level scheme for the system under consideration. For the laser frequencies ω and $(\omega+\delta)$ shown, the detuning $\Delta=(\omega-\omega_0)$ is within the Doppler width of the transition. (b) The geometry of the three input laser beams (E_f,E_b,E_p). The phase-conjugate signal, $E_s(-\mathbf{k},\omega-\delta)$, is shown as a dashed arrow.

$$\left[\frac{\partial}{\partial t}\rho_{\alpha\beta}(\mathbf{v})\right]_{\text{coll}} = -\Gamma^{\text{ph}}_{\alpha\beta}(\mathbf{v})\rho_{\alpha\beta}(\mathbf{v})(\delta_{\alpha a}\delta_{\beta b}+\delta_{\alpha b}\delta_{\beta a}) - \Gamma_{\alpha\beta}(\mathbf{v})\rho_{\alpha\beta}(\mathbf{v}) + \int A_{\alpha\beta}(\mathbf{v}'\rightarrow\mathbf{v})\rho_{\alpha\beta}(\mathbf{v}')d^3v' , \quad (4)$$

where $A_{\alpha\beta}(\mathbf{v}'\rightarrow\mathbf{v})$ is a collision kernel, $\Gamma_{\alpha\beta}(\mathbf{v}) = \int A_{\alpha\beta}(\mathbf{v}\rightarrow\mathbf{v}')d^3\mathbf{v}'$ is a collision rate, and $\Gamma^{\text{ph}}_{\alpha\beta}$ is a (complex) decay rate associated with impact pressure broadening theories involving phase-interrupting collisions.[9] This expression, which accounts for the velocity changes of atoms during collisions, yields a coupling between different velocity classes through the collision kernel $A_{\alpha\beta}(\mathbf{v}'\rightarrow\mathbf{v})$. The kernel, which is directly related to integrals of quantum-mechanical scattering amplitudes, has no general analytical form.

The resulting equations of motion for $\rho_{\alpha\beta}(\mathbf{v})$ cannot be solved analytically unless we model the kernels in a way that permits such a solution. To carry out the illustrative calculations in this paper, we choose simple forms for the kernels as follows.

(1) For the off-diagonal element ρ_{ab}, we neglect the contributions from the second and third terms of Eq. (4). This is a very common approximation, justified when the interaction potentials are somewhat different for the two levels, which is common of atomic optical transitions.[9] We keep only a rate of destruction of ρ_{ab},

$$\left[\frac{\partial}{\partial t}\rho_{ab}(\mathbf{v})\right]_{\text{coll}} = -\Gamma^{\text{ph}}_{ab}\rho_{ab}(\mathbf{v}) , \quad (5)$$

and we furthermore assume that Γ^{ph}_{ab} is real and does not depend upon $\mathbf{v}$.

(2) For the populations ρ_a, we adopt the so-called strong collision model in which the velocity $\mathbf{v}$ of an atom is thermalized, on average, after one collision, regardless of the initial velocity $\mathbf{v}'$. The collision kernel is given by

$$A_\alpha(\mathbf{v}'\rightarrow\mathbf{v}) = \Gamma_\alpha W(\mathbf{v}), \quad \alpha = a,b \quad (6)$$

with Γ_α independent of $\mathbf{v}$.

The equations of motion (in the interaction representation) for the atomic-density matrix elements, including the atom-field and collisional interactions, are

$$\left[\frac{\partial}{\partial t}+\mathbf{v}\cdot\nabla+\bar{\gamma}_b\right]\rho_b(\mathbf{v}) = \lambda_b W(\mathbf{v}) + \left[i\rho_{ab}(\mathbf{v})\sum_\nu \frac{\Omega_\nu}{2}e^{-i\phi_\nu}+\text{c.c.}\right] + \Gamma_b W(\mathbf{v})\bar{\rho}_b ,$$

$$\left[\frac{\partial}{\partial t}+\mathbf{v}\cdot\nabla+\bar{\gamma}_a\right]\rho_a(\mathbf{v}) = \lambda_a W(\mathbf{v}) + \gamma_{b,a}\rho_b(\mathbf{v}) - \left[i\rho_{ab}\sum_\nu \frac{\Omega_\nu}{2}e^{-i\phi_\nu}+\text{c.c.}\right] + \Gamma_a W(\mathbf{v})\bar{\rho}_a , \quad (7)$$

$$\left[\frac{\partial}{\partial t}+\mathbf{v}\cdot\nabla+\bar{\gamma}_{ab}-i\omega_o\right]\rho_{ab}(\mathbf{v}) = i[\rho_b(\mathbf{v})-\rho_a(\mathbf{v})]\sum_\nu \frac{\Omega_\nu}{2}e^{-i\phi_\nu} ,$$

where the summation of ν applies to the three laser beams, $\phi_\nu=\omega_\nu t-\mathbf{k}_\nu\cdot\mathbf{R}$, $\Omega_\nu=\mu_{ab}E_\nu/\hbar$ (Rabi frequency), and λ_b,λ_a account for a possible external incoherent pumping of populations (for a closed system: $\lambda_b,\lambda_a\sim 0$ with $\lambda_a/\gamma_a\sim n_a$, unperturbed population of $|a\rangle$). In Eqs. (7) we have defined

$$\bar{\gamma}_\alpha = \gamma_\alpha+\Gamma_\alpha, \quad \alpha=a,b , \quad (8a)$$

$$\bar{\gamma}_{ab} = \tfrac{1}{2}(\gamma_a+\gamma_b)+\Gamma^{\text{ph}}_{ab} , \quad (8b)$$

$$\bar{\rho}_\alpha = \int d^3v\rho_\alpha(\mathbf{v}), \quad \alpha=a,b . \quad (8c)$$

Equations (7) are solved using a perturbative expansion up to third order in the field amplitudes. Among the 27 contributions to $\rho^{(3)}_{ab}$, two correspond to emission of an electromagnetic wave counterpropagating along the probe direction, with a frequency ω-δ and a wave vector $-\mathbf{k}$ (the so-called phase-conjugated emission). The phase-conjugate contribution to $\rho^{(3)}_{ab}$, obtained from a perturbative solution of Eqs. (7), is[7]

$$\rho^{(3),\text{PC}}_{ab} = \sigma_{ab}e^{i[(\omega-\delta)t+\mathbf{k}\cdot\mathbf{R}]} , \quad (9a)$$

with

$$\sigma_{ab} = -in\frac{\Omega_f\Omega_p^*\Omega_b}{8}[\bar{\gamma}_{ab}+i(\Delta-\delta+\mathbf{k}\cdot\mathbf{v})]^{-1} \times \Big\{ W(\mathbf{v})\{(1+R)[\bar{\gamma}_b-i\delta+i(\mathbf{k}-\mathbf{k}_0)\cdot\mathbf{v}]^{-1}+(1-R)[\bar{\gamma}_a-i\delta+i(\mathbf{k}-\mathbf{k}_0)\cdot\mathbf{v}]^{-1}\} \times\{[\bar{\gamma}_{ab}+i(\Delta-\mathbf{k}_0\cdot\mathbf{v})]^{-1}+[\bar{\gamma}_{ab}-i(\Delta+\delta-\mathbf{k}\cdot\mathbf{v})]^{-1}\} + W(\mathbf{v})\Big\{\bar{\Gamma}_b(1+R)\bar{S}_b[\bar{\gamma}_b-i\delta+i(\mathbf{k}-\mathbf{k}_0)\cdot\mathbf{v}]^{-1} + \bar{\Gamma}_a\left[(1-R)\bar{S}_a+R\left\{\frac{1}{\Gamma_b}-\frac{1}{\Gamma_a}\right\}\bar{\Gamma}_b\bar{S}_b\right][\bar{\gamma}_a-i\delta+i(\mathbf{k}-\mathbf{k}_0)\cdot\mathbf{v}]^{-1}\Big\}\Big\} + (\text{same with } \mathbf{k}_0\rightarrow-\mathbf{k}_0) . \quad (9b)$$

For the sake of compactness, we have introduced in Eqs. (9) the notations

$$R=\frac{\gamma_{b,a}}{\bar{\gamma}_b-\bar{\gamma}_a}\ , \tag{10a}$$

$$\bar{\Gamma}_\alpha=\frac{\Gamma_\alpha}{1-\Gamma_\alpha\int\frac{W(\mathbf{v})d^3v}{\bar{\gamma}_\alpha-i\delta+i(\mathbf{k}-\mathbf{k}_0)\cdot\mathbf{v}}}\ , \tag{10b}$$

$$\bar{\mathcal{S}}_\alpha=\int\frac{W(\mathbf{v})d^3v}{\bar{\gamma}_\alpha-i\delta+i(\mathbf{k}-\mathbf{k}_0)\cdot\mathbf{v}}\left[\frac{1}{\bar{\gamma}_{ab}+i(\Delta-\mathbf{k}_0\cdot\mathbf{v})}+\frac{1}{\bar{\gamma}_{ab}-i(\Delta+\delta-\mathbf{k}\cdot\mathbf{v})}\right]\ , \tag{10c}$$

$$n=\frac{\lambda_b}{\gamma_b}-\left[\frac{\lambda_a}{\gamma_a}+\frac{\gamma_{b,a}\lambda_b}{\gamma_a\gamma_b}\right]\ . \tag{10d}$$

The intensity of phase-conjugate emission is proportional to the absolute square of

$$\bar{\sigma}_{ab}=\int\sigma_{ab}(\mathbf{v})d^3v\ .$$

The integration is carried out within the so-called Doppler limit defined by

$$\bar{\gamma}_a,\bar{\gamma}_b,\bar{\gamma}_{ab}\ll ku,k_0u\ , \tag{11a}$$

$$|\Delta|,|\delta|\ll ku,k_0u\ . \tag{11b}$$

Condition (11a) is satisfied for pressures $\lesssim 100$ Torr. Condition (11b) is satisfied for the nearly resonant atom-field interaction of this problem—it would be violated for the large detunings $|\Delta|\gg ku$ appropriate to many experiments in pressure-induced resonances. As a result of inequalities (11), one can neglect in (9) both the part of the first term varying as $[\bar{\gamma}_{ab}-i(\Delta+\delta-\mathbf{k}\cdot\mathbf{v})]^{-1}$ and the *entire* ($\mathbf{k}_0\rightarrow-\mathbf{k}_0$) term, since, after integration, these terms are smaller by a factor $\bar{\gamma}_{ab}/ku$ than the other contributing terms.

To achieve the three-dimensional integration over $\mathbf{v}$ we choose the coordinate system shown in Fig. 2 with

$$\theta\ll 1\ . \tag{12}$$

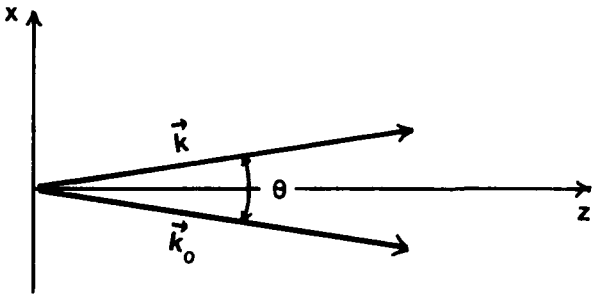

FIG. 2. Axes chosen for performing the velocity integration.

For the range of detunings δ under consideration, we can set $|\mathbf{k}|\approx|\mathbf{k}_0|\equiv K$ so that

$$\mathbf{k}\cdot\mathbf{v}=Kv_z+K\frac{\theta}{2}v_x\ ,$$

$$\mathbf{k}_0\cdot\mathbf{v}=Kv_z-K\frac{\theta}{2}v_x\ ,$$

$$(\mathbf{k}-\mathbf{k}_0)\cdot\mathbf{v}=K\theta v_x\ . \tag{13}$$

Using condition (12), an analytical integration over both v_x and v_z can be easily carried out with the result given by

$$\bar{\sigma}_{ab}=-in\frac{\Omega_f\Omega_p^*\Omega_b}{8}(\bar{\sigma}_{ab}^{\text{out}}+\bar{\sigma}_{ab}^{\text{in}})\ , \tag{14a}$$

$$\bar{\sigma}_{ab}^{\text{out}}=\frac{\sqrt{\pi}}{Ku}(\omega_{ab}^L+\omega_{ab}^{LM})\frac{i}{Ku\theta}\left[\frac{\sqrt{\pi}}{Ku\theta}\right]\times\left[(1+R)\frac{\omega_{ab}^T-\omega_b^T}{\zeta_b-\zeta_{ab}}+(1-R)\frac{\omega_{ab}^T-\omega_a^T}{\zeta_a-\zeta_{ab}}\right]\ , \tag{14b}$$

$$\bar{\sigma}_{ab}^{\text{in}}=\left[\frac{\sqrt{\pi}}{Ku}\right]^2\omega_{ab}^{LM}(\omega_{ab}^L+\omega_{ab}^{LP})(1+R)\mathcal{D}_b\frac{\sqrt{\pi}}{Ku\theta}\omega_b^T+(1-R)\mathcal{D}_a\frac{\sqrt{\pi}}{Ku\theta}\omega_a^T+R\left[\frac{1}{\Gamma_b}-\frac{1}{\Gamma_a}\right]\mathcal{D}_a\mathcal{D}_b\ , \tag{14c}$$

$$\omega_{ab}^L=\omega\left[\frac{-\Delta+i\bar{\gamma}_{ab}}{Ku}\right],\quad \omega_{ab}^T=\omega(\zeta_{ab})=\omega\left[\frac{-2\Delta+\delta+2i\bar{\gamma}_{ab}}{Ku\theta}\right],$$

$$\omega_{ab}^{LM}=\omega\left[\frac{-\Delta+\delta+i\bar{\gamma}_{ab}}{Ku}\right],\quad \omega_a^T=\omega(\zeta_a)=\omega\left[\frac{\delta+i\bar{\gamma}_a}{Ku\theta}\right], \tag{15}$$

$$\omega_{ab}^{LP}=\omega\left[\frac{\Delta+\delta+i\bar{\gamma}_{ab}}{Ku}\right],\quad \omega_b^T=\omega(\zeta_b)=\omega\left[\frac{\delta+i\bar{\gamma}_b}{Ku\theta}\right],\quad \mathcal{D}_\alpha=\frac{\Gamma_\alpha\frac{\sqrt{\pi}}{Ku\theta}\omega_\alpha^T}{1-\Gamma_\alpha\frac{\sqrt{\pi}}{Ku\theta}\omega_\alpha^T}\ ,$$

and the function $\omega(\zeta)$ is defined by[10]

$$\omega(\zeta)=e^{-\zeta^2}[1-\mathrm{erf}(-i\zeta)], \quad \zeta \text{ arbitrary}$$
$$=\frac{i}{\pi}\int_{-\infty}^{+\infty}\frac{e^{-t^2}dt}{\zeta-t} \quad \text{only when } \mathrm{Im}(\zeta)>0 , \quad (16)$$

where $\mathrm{erf}(\zeta)$ is the complex error function.

III. LINE-SHAPE ANALYSIS

The line shape (Eq. 14) may appear to have a rather complicated structure, but it simply reflects the various physical processes simultaneously occurring in the vapor. There is some question as to the best method for analyzing Eq. (14). We chose to use four (related) aspects of the problem and hope that an overall picture emerges from these components. (A) First, we consider the line shape as composed of two contributions—one from atoms have not undergone velocity-changing collisions and one from atoms that have. The former category dominates at low pressure and the latter at high pressure. In this subsection the resonance positions and widths are discussed. (B) Second, we examine the conditions under which resonances having a width characterized by the lower-state spontaneous and collision widths can be observed. It is shown that the existence of such resonances depends critically on the departure of the sum density

$$S(\mathbf{v})=\rho_a(\mathbf{v})+\rho_b(\mathbf{v}) \quad (17)$$

from its equilibrium value. In this subsection a natural definition of a closed system emerges. Moreover, it is seen how the system opens and recloses with increasing peturber pressure, and how the reclosing is linked to the collisional narrowing of the lower-state resonance. (C) Third, we examine briefly the dependence of the resonance characterized by the upper-state spontaneous and collisional decay processes. (D) Finally, we summarize the various line-shape features and give several examples of typical line shapes at various pressures. In Sec. IV the relationship of these line shapes to the pressure-induced extra resonance of Bloembergen and co-workers[1,2] is noted.

A. Line-shape resonances and widths

In the context of the strong collision model, the line shape naturally appears as composed of two terms: $\sigma_{ab}^{\mathrm{out}}$, associated with atoms that have not undergone velocity-changing collisions, and $\sigma_{ab}^{\mathrm{in}}$, associated with atoms that have.

1. *Atoms not having undergone velocity-changing collisions*

The contribution from such atoms is dominant at low pressure when collisions are relatively infrequent (in this case $\sigma_{ab}^{\mathrm{in}}/\sigma_{ab}^{\mathrm{out}}$ is of order Γ_a/ku). For these atoms, the line shape results from the integration over velocity of a component $\sigma_{ab}^{\mathrm{out}}(\mathbf{v})$ which consists of the product of three factors as follows:

$$\sigma_{ab}^{\mathrm{out}}(\mathbf{v})\simeq\frac{1}{\tilde{\gamma}_{ab}+i(\Delta-\delta)+i\mathbf{k}\cdot\mathbf{v}}\,\frac{1}{\tilde{\gamma}_a-i\delta+i(\mathbf{k}-\mathbf{k}_0)\cdot\mathbf{v}}$$
$$\times\frac{1}{\tilde{\gamma}_{ab}+i\Delta-i\mathbf{k}_0\cdot\mathbf{v}}, \quad \alpha=a,b . \quad (18)$$

The third factor represents a single-photon absorption of the forward pump beam; the second factor reflects the evolution within state $|\alpha\rangle$, that is, the probability that the grating formed by the forward pump and probe beams is not affected by velocity-changing collisions; and the first factor represents a "three-photon" process involving the absorption of one forward and one backward pump photon and the emission of a probe photon.

When integrated over velocity, the first and third factors give rise to a resonance centered at $\delta=2\Delta$ with width [full width at half maximum (FWHM)] $4\tilde{\gamma}_{ab}$. This resonance results from a velocity-selective process in which the same velocity classes of atoms are used in both the one-photon and three-photon absorption factors. The second factor in (18) gives rise to "grating resonances" centered at $\delta=0$ with widths that we write symbolically as

$$\Gamma_G(\alpha)=(2\tilde{\gamma}_\alpha)*(Ku\theta) \quad (19)$$

representing the convolution of a Lorentzian having width $2\tilde{\gamma}_\alpha$ with a Gaussian having a characteristic residual width $(Ku\theta)$ (the FWHM of the Gaussian is 1.66 $Ku\theta$). For illustrative purposes, we may consider the case in which

$$\gamma_a \ll Ku\theta, \quad Ku\theta \ll \gamma_b \quad (20)$$

implying that

$$\Gamma_G(b)\simeq 2\tilde{\gamma}_b=2(\gamma_b+\Gamma_b) , \quad (21a)$$

$$\Gamma_G(a)\simeq(2\tilde{\gamma}_a)*(Ku\theta) . \quad (21b)$$

The upper state grating has a width $2(\gamma_b+\Gamma_b)$ while the lower-state grating has a width given by the convolution of $2(\gamma_a+\Gamma_a)$ and $Ku\theta$. At low pressure and for small residual Doppler broadening, the lower-state grating resonance can be much narrower than the upper-state one. These features are shown in Fig. 3.

2. *Atoms having undergone velocity-changing collisions*

Any atom having undergone a velocity-changing collision is thermalized. Consequently, any correlation between the velocity classes participating in the one-photon and three-photon absorption processes is *lost*. In analogy with Eq. (18), the contribution from atoms having undergone velocity-changing collisions arises from the velocity integration (over v_z and v_z') of a term that can be written as

$$\sigma_{ab}^{\mathrm{in}}(\mathbf{v})\sim\frac{1}{\tilde{\gamma}_{ab}+i(\Delta-\delta)+ikv_z}\sigma_G(\delta,\alpha,v_x)$$
$$\times\frac{1}{\tilde{\gamma}_{ab}+i\Delta-ik_0v_z'} , \quad (22)$$

where v_z' and v_z are uncorrelated. The factor $\sigma_G(\delta,\alpha,v_x)$

is a term that is responsible for a collisional or "Dicke" narrowing of the grating resonances.[11] On averaging over velocity, the first and third factors give rise to very broad "resonant" structures, characterized by the full Doppler width.[12] The grating resonance associated with state $|\alpha\rangle$ has a width which starts at $\Gamma_G(\alpha)=(2\gamma_\alpha)*(Ku\theta)$ [Eq. (19)] at low pressure and monotonically decreases to a final width equal to $2\gamma_\alpha$. The condition for collisional narrowing to this final width $2\gamma_\alpha$ is

$$\frac{\Gamma_\alpha}{Ku\theta} \gg 1 . \tag{23}$$

If $\gamma_b \gg Ku\theta$, the excited-state grating width (for this contribution from atoms which have undergone velocity-changing collisions) is always equal to $2\gamma_b$. For the lower state, assuming $\gamma_a \ll Ku\theta$, the grating width starts at 1.66 $(Ku\theta)$ for low pressure and reduces to $2\gamma_a$ for pressures such that $\Gamma_a/Ku\theta \gg 1$.

These line-shape features are shown in Fig. 4. The contributions from atoms having undergone velocity-changing collisions become dominant at high pressure, where atoms undergo many collisions within their natural lifetimes. A quantitative condition for "high" pressure can be written

$$\frac{\Gamma_\alpha}{\gamma_\alpha} > \frac{Ku}{\bar{\gamma}_{ab}}, \quad \alpha=a,b \tag{24}$$

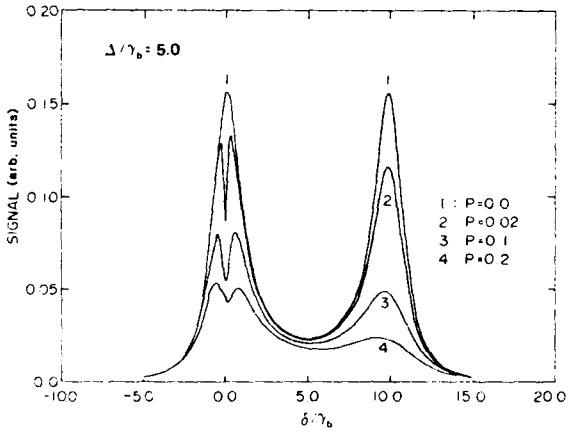

FIG. 3. Four-wave-mixing signal intensity (arbitrary units) as a function of pump-probe detuning δ. All frequencies are in units of γ_b; for the figures shown, $\Delta=5.0$, $Ku\theta=0.1$, $Ku=100$, $\gamma_a=0.01$. The collision rates are taken as $\Gamma_a=\Gamma_{ab}=4\Gamma_b$, $P=\Gamma_b/\gamma_b=0.0$, 0.02, 0.1, 0.2 corresponding to different (dimensionless) pressures. At zero pressure, there are resonances at $\delta=0$ and $\delta=2\Delta$ having widths (FWHM) equal to 2.0. As the perturber pressure increases from zero, this system "opens" and a narrow structure (corresponding to $\bar{\sigma}_{ab}^{\text{out}}$ of the text) appears whose width is $2(\gamma_a+\Gamma_a)$ convoluted with the residual Doppler width $Ku\theta$. This narrow resonance broadens with increasing pressure. At these relatively low pressures, only the contribution from $\bar{\sigma}_{ab}^{\text{out}}$ is dominant, although the marked asymmetry of the $P=0.2$ dip is due to the fact that $\bar{\sigma}_{ab}^{\text{in}}$ is beginning to make a non-negligible contribution to the line shape.

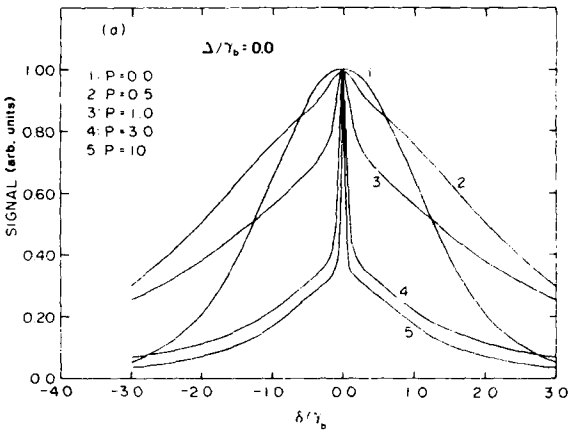

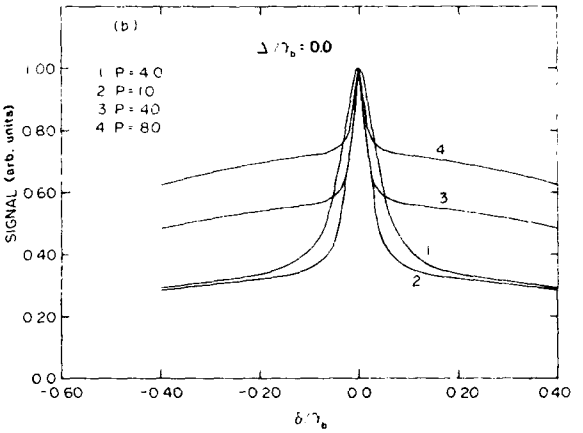

FIG. 4. Graphs of four-wave-mixing signal intensity (arbitrary units) as a function of pump-probe detuning δ. All frequencies are in units of γ_b; for the figures shown, $\gamma_a=0.01$, $\Delta=0.0$, $Ku\theta=1.0$, $Ku=100$, and $\Gamma_a=\Gamma_{ab}=4\Gamma_b$, with $P=\Gamma_b/\gamma_b=(0.001, 0.5, 1.0, 3.0, 10)$ in Fig. 4(a) and $P=(4, 10, 40, 80)$ in Fig. 5(b). These figures are intended to illustrate collisional narrowing and the "reclosing" of the system, which is why a somewhat larger value of $Ku\theta=1.0$ γ_b was chosen. At zero pressure the linewidth is the convolution of a Lorentzian having width $2\gamma_b$ with a Gaussian having width 1.66 $Ku\theta$. As the pressure increases, the system "opens" and the contribution from $\bar{\sigma}_{ab}^{\text{in}}$ begins to become important, leading to a new narrow resonance characterized by the ground-state width (convoluted with $Ku\theta$). (The $\bar{\sigma}_{ab}^{\text{out}}$ component giving rise to the narrow dip seen in Fig. 3 is negligible for the parameters chosen for these graphs.) With increasing pressure, the "broad" and narrow resonances approach their asymptotic widths $2\gamma_b$ and $2\gamma_a$, respectively, as a result of collisional narrowing. There is a range of pressures where the ratio of the narrow to broad resonance amplitude is approximately constant; at still higher pressures, the reclosing of the system leads to an asymptotic disappearance of the narrow resonance. Note that in Fig. 4(b) the scale has been expanded so that the broad resonance (of width $2\gamma_b$) appears only as an approximately constant background. All curves have been normalized to the same value at $\delta=0$; in absolute terms, the signal decreases with increasing pressure approximately as P^{-1}.

which states that the number of collisions within a radiative lifetime is large enough to redistribute velocity selected atoms excited in a range ($Ku = \pm\tilde{\gamma}_{ab}$) over the entire Doppler width Ku. The *redistribution* inequality (24) is linked to the reclosing of the system as is shown below. A schematic picture of the velocity redistribution is shown in Fig. 5.

B. Resonances characterized by lower-state radiative and collisional rates

In order to determine the conditions under which grating resonances characterized by the lower-state width are seen, it is useful to recall Eq. (7c) in which one finds that

$$\rho_{ab}(\mathbf{v}) \propto [\rho_b(\mathbf{v}) - \rho_a(\mathbf{v})] . \tag{25}$$

In terms of the sum density

$$S(\mathbf{v}) = \rho_a(\mathbf{v}) + \rho_b(\mathbf{v}) ,$$

expression (25) can be written

$$\rho_{ab}(\mathbf{v}) \propto [2\rho_b(\mathbf{v}) - S(\mathbf{v})] . \tag{26}$$

Up to second order in the fields, $\rho_b(\mathbf{v})$ depends only on the excited-state parameters. *Thus, any contribution to ρ_{ab} in third order in the fields which depends on the*

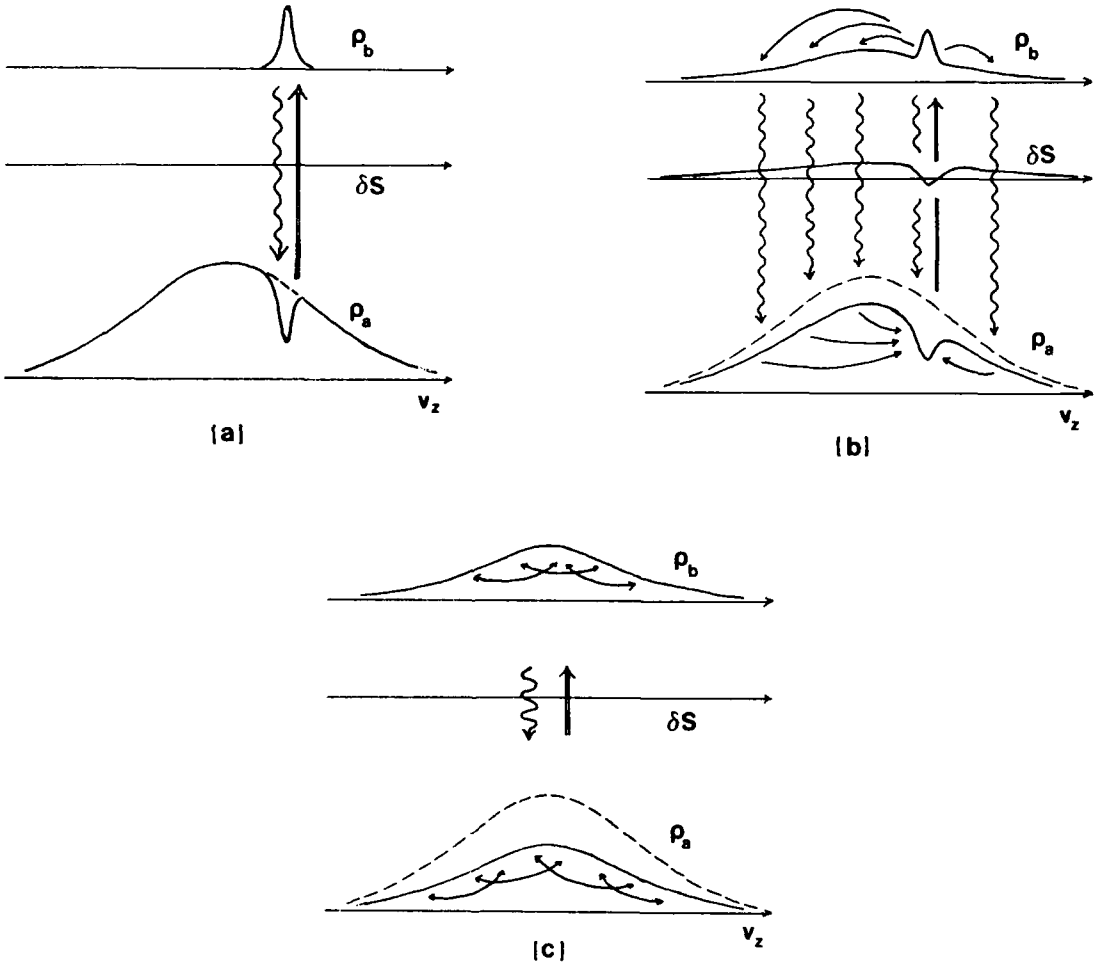

FIG. 5. Schematic representation of the opening and reclosing of the system in velocity space. The graphs shown in each of (a), (b), and (c) give the longitudinal velocity distribution for state a, $\rho_a(\mathbf{v})$, for state b, $\rho_b(\mathbf{v})$, and the deviation $\delta S(\mathbf{v})$ of the sum density $[\rho_a(\mathbf{v}) + \rho_b(\mathbf{v})]$ from its equilibrium value in the absence of applied fields. (a) At zero pressure, excitation and decay occurs within a given velocity class and $\delta S(\mathbf{v}) = 0$, assuming that the system is "closed," as defined in the text. (b) With increasing pressure, collisions redistribute some of the velocity-selected atoms over the entire thermal width. For different collision rates in the two states, the closed nature of the system is lost, as is evidenced by a nonvanishing $\delta S(\mathbf{v})$. (c) At very high pressure, such that the redistribution in each level is complete, the system has "reclosed," and, as at zero pressure, once again finds $\delta S(\mathbf{v}) = 0$. In this limit, there is no longer any velocity selection and excitation and decay occurs over the entire thermal distribution. In each diagram, the dashed curve corresponds to the equilibrium distribution $\rho_a(\mathbf{v})$ in the absence of the fields. The upward arrows represent excitation by the fields, the downward curly arrows represent radiative decay, and the sideways arrows represent velocity redistribution.

lower-state decay rates must come from a second-order nonvanishing contribution to $S(\mathbf{v})$. The sum density serves as a measure of resonances characterized by the lower-state decay rates.

To zeroth order in the fields, the sum density calculated from Eqs. (7) is

$$S^{(0)}(\mathbf{v})=\frac{\lambda_a}{\gamma_a}+\frac{\lambda_b}{\gamma_b}\frac{\gamma_{b,a}}{\gamma_a}+\frac{\lambda_b}{\gamma_b} . \tag{27}$$

To second order in the fields, the sum density contains contributions from all combinations of two of the fields. The part of $S^{(2)}(\mathbf{v})$ responsible for phase-conjugate emission may be written

$$[S^{(2)}(\mathbf{v})]_{\rm PC}=S_+^{(2)}(\mathbf{v})e^{i[(\mathbf{k}-\mathbf{k}_0)\cdot\mathbf{R}-\delta t]}+\text{c.c.} \tag{28}$$

When this is substituted into Eq. (7), one finds that $S_+^{(2)}(\mathbf{v})$ satisfies

$$\begin{aligned}[\bar{\gamma}_a-i\delta+i(\mathbf{k}-\mathbf{k}_0)\cdot\mathbf{v}]S_+^{(2)}(\mathbf{v})&\\ =-(\gamma_d+\Gamma_d)\rho_{b+}^{(2)}+\int A_d(\mathbf{v}'\to\mathbf{v})\rho_{b+}^{(2)}(\mathbf{v}')d^3v'&\\ +\int A_a(\mathbf{v}'\to\mathbf{v})S_+^{(2)}(\mathbf{v}')d^3v' ,&\end{aligned} \tag{29}$$

where

$$\gamma_d=\gamma_b-\gamma_{b,a}-\gamma_a , \tag{30}$$

$$\Gamma_d=\Gamma_b-\Gamma_a , \tag{31}$$

$$A_d(\mathbf{v}'\to\mathbf{v})=A_b(\mathbf{v}'\to\mathbf{v})-A_a(\mathbf{v}'\to\mathbf{v}) , \tag{32}$$

and $\rho_{b+}^{(2)}(\mathbf{v})$ is the second-order component of $\rho_b^{(2)}(\mathbf{v})$ which contributes to the phase-conjugated emission. If $S_+^{(2)}(\mathbf{v})$ vanishes, the line shape to third order cannot depend on the lower-state decay rates. Thus, the existence of resonances characterized by γ_a or Γ_a depends on a nonvanishing $S_+^{(2)}(\mathbf{v})$.

If there are no velocity-changing collisions [$\Gamma_\alpha=0$, $A_\alpha(\mathbf{v}'\to\mathbf{v})=0$], $S_+^{(2)}(\mathbf{v})$ vanishes only if

$$\gamma_d=\gamma_b-\gamma_{b,a}-\gamma_a=0 . \tag{33}$$

Equation (33) is the condition (1) we adopted for a closed system, since it implies no deviation from the zeroth-order sum density. In the following discussion, we assume that (33) holds. In that case, $S_+^{(2)}(\mathbf{v})$ satisfies

$$\begin{aligned}[\bar{\gamma}_a-i\delta+i(\mathbf{k}-\mathbf{k}_0)\cdot\mathbf{v}]S_+^{(2)}(\mathbf{v})-\int A_a(\mathbf{v}'-\mathbf{v})S_+^{(2)}(\mathbf{v}')d^3v'&\\ =-\Gamma_d\rho_{b+}^{(2)}+\int A_d(\mathbf{v}'\to\mathbf{v})\rho_{b+}^{(2)}(\mathbf{v}')d^3v' .&\end{aligned} \tag{34}$$

It is seen that all inhomogeneous terms in Eq. (34) vanish if the collision kernels for the two states are identical. This result is independent of the specific form of the collision kernel, and is not restricted to the strong collision kernel used in this work. For identical collision kernels, $\Gamma_d=0$, $S_+^{(2)}(\mathbf{v})=0$, and there is no opening of the system. This result is easy to understand. For identical kernels, collisions redistribute atoms in all the velocity classes in the upper and lower levels in the same manner, on average. This implies that the total population of each velocity subclass is dynamically conserved and the system remains "closed." Thus, the existence of resonances characterized by ground-state decay rates necessarily depends on a difference between the upper- and lower-state kernels [assuming, as we do, that condition (33) or (1) holds]. This conclusion is illustrated in Fig. 6.

If $\Gamma_d\neq0$, at low pressure the system "opens" as a result of velocity-changing collisions and narrow resonances can be seen (if they are not masked by the residual Doppler broadening, that is, if $Ku\theta<\gamma_a$). As the pressure increases to the point when condition (24) is applicable, the velocity distributions in both ground and excited states are rethermalized, $\rho_a(\mathbf{v})$, $\rho_b(\mathbf{v})\propto W(\mathbf{v})$. In this limit, it is easily seen from Eq. (34) that $S_+^{(2)}(\mathbf{v})=0$, i.e., the system has reclosed. In going from low to high pressure, collisional narrowing of the lower-state grating resonance can be seen.

It can be shown from Eq. (34) and the second-order solution of Eq. (7) for $\rho_b^{2+}(\mathbf{v})$ that the amplitude of that part of $S_+^{(2)}(\mathbf{v})$ which contributes to the resonance having width equal to [2(γ_a + collisionally narrowed residual width)] is proportional to $(Ku\theta)^2/\Gamma_a\gamma_\alpha$. This is precisely the same factor that determines the collisionally narrowed residual width (see below). Thus, the degree of reclosing of the system is interrelated with the collisional narrowing of the system.

C. Upper-state grating resonance

At low pressure, the upper-state grating resonance has width $\Gamma_G(b)=(2\bar{\gamma}_b)*(Ku\theta)\simeq2\bar{\gamma}_b$ if $Ku\theta\ll\bar{\gamma}_b$. This is the contribution from atoms which have not experienced velocity-changing collisions. As the pressure grows, eventually reaching the limit (24), the term arising from atoms having undergone velocity-changing collisions dominates the line shape. This term has width equal to $2\gamma_b$.

D. Line-shape summary

At low pressure, the line shape is determined by atoms that have *not* undergone any collision. There is a resonance of width $4\bar{\gamma}_{ab}$ centered at $\delta=2\Delta$ and one of width

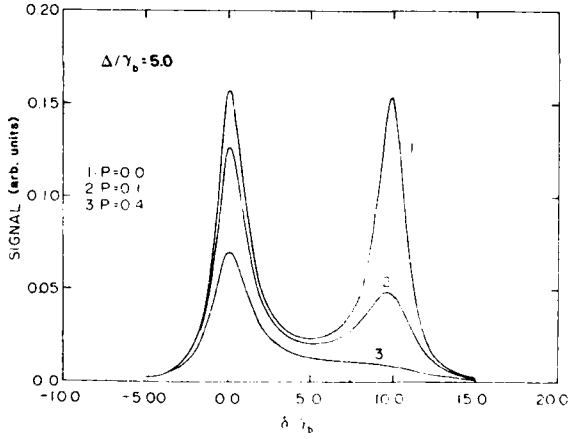

FIG. 6. Graphs similar to those of Fig. 3, but with $\Gamma_a=\Gamma_b$. In this limit of equal collision rates for the two levels, the system never "opens" and the narrow resonance is not seen.

$(2\bar{\gamma}_b)*(Ku\theta)$ centered at $\delta=0$. If the system is "open," owing to $\Gamma_d\neq 0$, there is an additional narrow resonance centered at $\delta=0$, having width $(2\bar{\gamma}_a)*(Ku\theta)$. These features are illustrated in Fig. 3. As the pressure grows, the no-collision terms ($\bar{\sigma}_{ab}^{\text{out}}$) broaden and diminish in (relative) amplitude. The major contribution begins to come from atoms that have undergone velocity-changing collisions. The resonance at $\delta=2\Delta$ vanishes and the resonances centered at $\delta=0$ have widths which reduce toward their asymptotic values of $2\gamma_a$ and $2\gamma_b$, respectively.

At "high" pressure, such that $\Gamma_{ab},\Gamma_a,\Gamma_b \gg (Ku\theta)$ and $\Gamma_a \gg \gamma_a$, $\Gamma_b \gg \gamma_b$, the line shape takes on the asymptotic form

$$\bar{\sigma}_{ab}=-i\frac{\Omega_f\Omega_p^*\Omega_b}{8}(\bar{\sigma}_{ab}^{\text{out}}+\bar{\sigma}_{ab}^{\text{in}}) , \tag{35a}$$

$$\bar{\sigma}_{ab}^{\text{out}} \underset{\sim}{\rightarrow} \left[\frac{\sqrt{\pi}}{Ku}\right](\omega_{ab}^{L}+\omega_{ab}^{LM})\left[\frac{1}{2(\gamma_{ab}+\Gamma_{ab})+2i\Delta-i\delta}\,\frac{1}{\gamma_b+\Gamma_b-i\delta}\left[2+\frac{\gamma_d+\Gamma_d}{\gamma_a+\Gamma_a-i\delta}\right]\right] , \tag{35b}$$

$$\begin{aligned}\bar{\sigma}_{ab}^{\text{in}} \underset{\sim}{\rightarrow} \left[\frac{\sqrt{\pi}}{Ku}\right]^2(\omega_{ab}^{L}+\omega_{ab}^{LP})\omega_{ab}^{LM}\Bigg\{&-\frac{\gamma_d+\Gamma_d}{(\gamma_a+\Gamma_a-i\delta)(\gamma_b+\Gamma_b-i\delta)}\\&+\frac{1}{\gamma_b+\frac{(Ku\theta)^2}{2\Gamma_b}-i\delta}\left[2\left\{\frac{\Gamma_b}{\gamma_b+\Gamma_b-i\delta}\right\}\right.\\&\left.+\frac{1}{\gamma_a+\frac{(Ku\theta)^2}{2\Gamma_a}-i\delta}\left[\gamma_d-(1-R)\frac{(Ku\theta)^2}{2\Gamma_a\Gamma_b}\Gamma_d\right]\right]\Bigg\} ,\end{aligned} \tag{35c}$$

where for convenience, we recall that γ_d and Γ_d are defined by

$$\gamma_d=\gamma_b-\gamma_{b,a}-\gamma_a ,$$

$$\Gamma_d=\Gamma_b-\Gamma_a .$$

From Eq. (35) one easily verifies that the redistributed component $\bar{\sigma}_{ab}^{\text{in}}$ dominates as soon as

$$\frac{(\gamma_{ab}+\Gamma_{ab})\Gamma_b}{Ku\gamma_b}\gg 1 , \tag{36}$$

which is condition (24) arrived at in Sec. III A, using simple physical arguments. The narrowing of the line shape can be seen in $\bar{\sigma}_{ab}^{\text{in}}$, where the widths of the dominant terms are given by $[\gamma_a+(Ku\theta)^2/2\Gamma_\alpha]$, $\alpha=a,b$. Moreover, for a closed system as defined by condition (1) ($\gamma_d=0$), the amplitude of the state $|a\rangle$ (lower) resonance asymptotically approaches zero (for any finite $\gamma_a\neq 0$) as $(Ku\theta)^2/2\Gamma_a\gamma_a$. This is the same factor that determines how the resonance width approaches its asymptotic value γ_a. In other words, when the narrowing is complete, the system is also reclosed and the narrow resonance disappears.

It is interesting to note that as long as $(Ku\theta)^2/2\Gamma_a>\gamma_a$, the narrow resonance keeps a constant amplitude with respect to the γ_b peak, as can be seen in $\bar{\sigma}_{ab}^{\text{in}}$ rewritten as

$$\bar{\sigma}_{ab}^{\text{in}}\simeq\frac{1}{\gamma_b+\frac{(Ku\theta)^2}{2\Gamma_b}-i\delta}\left|2+\left[\frac{\Gamma_a}{\Gamma_b}-1\right]\frac{\frac{(Ku\theta)^2}{2\Gamma_a}}{\frac{(Ku\theta)^2}{2\Gamma_a}-i\delta}\right| .$$

For $\gamma_a\ll\gamma_b$ there is a wide range of pressures for which the ratio of the amplitudes of the resonances associated with states $|a\rangle$ and $|b\rangle$ remains constant. The ratio of amplitudes is governed by the ratio Γ_a/Γ_b. These features are shown in Fig. 4.

IV. DISCUSSION

In this paper we have examined the phase-conjugate four-wave-mixing signal that is produced when three nearly resonant (detunings within the Doppler width of the atomic transition) fields having frequencies ω, ω, and $\omega+\delta$ are incident on an ensemble of two-level atoms. The two fields having frequency ω are counterpropagating and the third field makes a small angle θ with one of these fields. We have seen that for a system which is "closed" in the absence of collisions [i.e., $(\gamma_b-\gamma_{b,a}-\gamma_a)=0$, see Fig. 1], velocity-changing collisions can play a critical role in determining the strength of the phase-conjugate emission as a function of δ. In particular, these collisions are responsible for the detailed structure of the "Rayleigh-type" resonances which appear, centered at $\delta=0$. In the absence of collisions, the $\delta=0$ resonance has a width equal to $2\gamma_b$ (convoluted with the residual Doppler width $Ku\theta$). At low pressure this width is increased owing to velocity-changing collisions. Moreover, since velocity-changing collisions "open" the system for each velocity subclass, a new resonance centered at $\delta=0$ having width $2\gamma_a$ (convoluted with $Ku\theta$) appears. If $\gamma_a\ll\gamma_b$, this new resonance can be much narrower than the resonance of width $(2\gamma_b)$ in the absence of collisions. As the pressure increases, collisional narrowing of the residual Doppler width of the

resonances occurs and the resonance widths decrease monotonically towards their asymptotic values of $(2\gamma_b)$ and $(2\gamma_a)$, respectively. At the same time, the system is "reclosing" since collisions are redistributing the velocity-selected atoms over the entire Maxwellian velocity distribution. When the system is fully reclosed, the γ_a resonance disappears, just as in the absence of collisions.

It seems useful to emphasize that, although they occur simultaneously and are related to the same residual widths $(Ku\theta)^2/2\Gamma_a$, the collisional narrowing and the reclosing are two different phenomena. Collisional narrowing occurs only because there is a spatial phase factor which enters in the line-shape formation. In "traditional" collisional narrowing, the phase factor is associated with an atomic coherence (optical or otherwise) and the narrowing can occur when the collisions reduce this atomic mean-free path to the point where it is less than the wavelength needed to excite this atomic coherence. In the present case, however, the relevant phase is that of the population gratings created within a *single* level by the lasers. Line shapes which are collisionally narrowed have widths which asymptotically approach their homogeneous widths, with a residual component that decreases as $(\Delta v)^2/\Gamma$, where Δv is the relevant inhomogeneous broadening and Γ a collision rate. The population gratings discussed in this work are spatially modulated in the transverse direction. Consequently, the narrowing occurs relative to that direction, with a corresponding inhomogeneous width equal to $Ku\theta$.

In contrast to the collisional narrowing, the reclosing of the system does not depend intrinsically on the existence of a spatial phase. The reclosing is simply related to the velocity distribution within each level. The radiation fields create a nonequilibrium velocity distribution in each level and collisions tend to restore the atoms to equilibrium. The system recloses when the collision rate is much larger than the radiative transfer rate [see condition (36)]. The reclosing occurs not only for the population gratings discussed above, but also for the nonmodulated parts of ρ_a and ρ_b. Moreover, it occurs in the longitudinal as well as in the transverse directions. It can be easily shown that the sum density $S(\mathbf{v})$ which measures the degree of openess of the system, tends to zero with increasing pressure asymptotically as $[(1/\Gamma_b)-(1/\Gamma_a)]$ for all its components, modulated or not. On the other hand, for the population gratings, there is a dependence of the reclosing on $Ku\theta$ which is absent for the unmodulated component of the population. One may say that, at high pressure, there is an additional effective lifetime $(Ku\theta)^2/2\Gamma_a$ for the population grating associated with state $|\alpha\rangle$, so that condition (1) defining a closed system is replaced by

$$G_d=\left[\gamma_b+\frac{(Ku\theta)^2}{2\Gamma_b}\right]-\gamma_{b,a}-\left[\gamma_a+\frac{(Ku\theta)^2}{2\Gamma_a}\right]$$

$$=\gamma_d+\frac{(Ku\theta)^2}{2\Gamma_a\Gamma_b}\Gamma_d=0\ .$$

It is precisely this factor G_d which enters the expression for the amplitude of the narrow peak in $\bar{\sigma}^{\text{in}}_{ab}$. In summary, we see that although the amplitude of the narrow peak is determined by the factor $(Ku\theta)^2/2\Gamma_a$ [and $(Ku\theta)^2/2\Gamma_b$], and the residual width of the narrow peak is determined also by the same factor $(Ku\theta)^2/2\Gamma_a$, the origin of these two effects is different.

The collision-induced resonant structures discussed in this work differ somewhat from the pressure-induced extra resonances (PIER4) studied by Bloembergen and coworkers.[1,2] In PIER4, the atom-field detunings were always *outside* the Doppler width of the transitions. As such, velocity-changing collisions played no role in the opening or closing of the system, as defined in this paper. Moreover, there is no velocity selection in the excitation process since *all* atoms are detuned well outside the Doppler width. As a consequence, there is *no* resonance centered at $\delta=0$ in the absence of collisions for a closed system. A resonant structure centered at $\delta=0$ having width $2\bar{\gamma}_b$ (convoluted with $Ku\theta$) appears and *grows* with increasing perturber pressure, but no resonant structure with width $2\bar{\gamma}_a$ (convoluted with $Ku\theta$) emerges, since the system remains closed for each velocity subclass (as there is no velocity selection in the excitation process). In contrast to these results, for nearly resonant tuning (detuning within the Doppler width), resonant structures centered at $\delta=0$ *always* exist, even in the absence of collisions. The overall amplitude of these resonance structures decreases with increasing pressure, in contrast to PIER4. Moreover, again in contrast to PIER4, collisions lead to an additional resonance having width $2\gamma_a$ (convoluted with $Ku\theta$), owing to the fact that velocity-changing collisions open the system for each velocity subclass. The differences between PIER4 and four-wave mixing using nearly resonant tuning can be traced to velocity-selective excitation which is present in the latter and absent in the former.

Finally, we should like to comment on the experimental implications of our work. Several studies of the role of velocity-changing collisions on four-wave-mixing line shapes for nearly resonant tuning have been carried out.[5] Many of the features predicted in this work have been observed in those experiments (pressure-induced narrow resonant structures centered at $\delta=0$, collisional narrowing), but a quantitative comparison with theory has not yet been attempted (the theory must be extended to include effects of magnetic degeneracy or the experiments will have to be done using an atom other than sodium[5]). A systematic experimental study of the collisional modification of four-wave-mixing line shapes for nearly resonant tuning in Na is in progress,[13] and it is hoped that this study will serve as a test for the theory.

ACKNOWLEDGMENTS

This work is supported by the U.S. Office of Naval Research and the National Science Foundation Grant No. PHY8415781. M. Gorlicki wishes to thank Dr. P. Berman for his support and New York University for its hospitality during this work. The Laboratoire de Physique des Lasers is a laboratory associated with the Centre National de la Recherche Scientifique.

*Permanent address: Laboratoire de Physique des Lasers, Universite Paris-Nord, F-93430 Villetaneuse, France.

†Current address: Optical Sciences Center, University of Arizona, Tucson, AZ 85721.

[1]N. Bloembergen, H. Loten, and R. T. Lynch, Jr., Indian J. Pure Appl. Physics **16**, 151 (1978).

[2]Y. Prior, A. R. Bogdan, M. Dagenais, and N. Bloembergen, Phys. Rev. Lett. **46**, 111 (1981).

[3]L. Rothberg, in *Progress in Optics*, edited by E. Wolf (Elsevier, Amsterdam, 1987), pp. 39–101; G. Grynberg, in *Spectral Line Shapes*, edited by R. Exton (W. de Gruyter, Berlin, 1987), pp. 503–521, Vol. 4.

[4]R. K. Raj, D. Bloch, J. J. Snyder, G. Camy, and M. Ducloy Phys. Rev. Lett. **44**, 1251 (1980).

[5]J. F. Lam, D. G. Steel, and R. A. McFarlane, Phys. Rev. Lett. **49**, 1628 (1982); **56**, 1679 (1986); D. G. Steel and R. A. McFarlane, Phys. Rev. A **27**, 1217 (1983); **27**, 1687 (1983).

[6]L. Rothberg and N. Bloembergen, Phys. Rev. A **30**, 820 (1984).

[7]G. Khitrova, Ph.D. dissertation, New York University, 1986.

[8]See, for example, R. G. Breene, Jr., *The Shift and Shape of Spectral Lines* (Pergamon, New York, 1961); I. I. Sobelman, L. A. Vainshtein, and E. A. Yukov, *Excitation of Atoms and Broadening of Spectral Lines* (Springer-Verlag, Berlin, 1981), Chap. 7.

[9]See P. R. Berman, in *New Trends in Atomic Physics*, edited by G. Grynberg and R. Stora (North-Holland, Amsterdam, 1984), pp. 451–514, and references therein.

[10]M. Abramowitz and I. A. Stegun, *Handbook of Mathematical Functions* (Dover, New York, 1965), Chap. 7.

[11]R. H. Dicke, Phys. Rev. **89**, 472 (1953); see, also, P. R. Berman, Appl. Phys. (Germany) **6**, 283 (1975), and references therein.

[12]If all decay rates are less than the Doppler width, the frequency dependence of the broad resonances is $\exp\{-[(\delta-\Delta)/Ku]^2\}\exp[-(\Delta/Ku)^2]$.

[13]D. Steel (private communication).

Reprinted from Journal of the Optical Society of America B, Vol. 5, page 160, January 1988

Theory of pump–probe spectroscopy

Galina Khitrova

Optical Sciences Center, University of Arizona, Tucson, Arizona 85721

Paul R. Berman

Department of Physics, New York University, New York, New York 10003

Murray Sargent III

Optical Sciences Center, University of Arizona, Tucson, Arizona 85721

Received July 6, 1987; accepted September 29, 1987

We calculate the two-level pump–probe absorption coefficient including both upper-to-lower-level decay and level decays to a still lower-lying reservoir level. The probe-absorption profile can have arbitrary ratios of the natural linewidth and detuning to the Doppler width. We observe and explain new line-shape features that occur when the two main levels decay to the reservoir level at different rates.

1. INTRODUCTION

Pump–probe spectroscopy is a technique that has been used in high-resolution spectroscopy to obtain information about physical properties of atomic systems. In a standard pump–probe experiment involving a single atomic transition, one measures the probe-absorption profile when an arbitrarily strong pump field drives the same transition. In the past, calculations of probe-absorption profiles have been performed by several groups.[1-10]

A detailed theoretical investigation of the probe-absorption line shape including coherent effects was undertaken by Baklanov and Chebotaev[1] and by Haroche and Hartman.[2] The probe-absorption line shape can be calculated by evaluating the probe-field-induced dipole moment using master equations in which the pump field is treated to all orders. Previous calculations have been performed for stationary atoms[2,4,6,8] or for moving atoms in the so-called Doppler limit (Doppler $\gg$ decay rates).[1,3]

Absorption spectra for strongly driven stationary atoms exhibit the interesting phenomena of probe-field amplification[2,4,6,8] at certain probe-field detunings from resonance. This negative absorption occurs with no population inversion and has been investigated by several authors.[4,7,8,11] Doppler-limit calculations for unidirectional[1] and oppositely[4] traveling waves and moving atoms have been carried out by Baklanov and Chebotaev (no probe amplification was predicted). Experimental curves obtained by Wu and coworkers[9] using an atomic beam agree with the stationary-atom theory for both zero[4,8] and nonzero[8] pump detunings.

The present paper extends these calculations to allow for arbitrary ratios of natural linewidth and detuning to the Doppler width. This theory accounts for contributions from all velocity subclasses of atoms not only those that are Doppler shifted into resonance (Doppler limit). We also include both upper-to-lower-level decay and level decays to a reservoir level. By including them we are able to obtain new line-shape features when the reservoir decay constants differ. As in the references mentioned above, our treatment is semiclassical, that is, the fields are treated classically, and the atoms are treated quantum mechanically. The effects of one or two quantized probe waves and a possible Lorentzian broadening have been studied by Sargent *et al.*[12] and Holm *et al.*[13] Their coefficients reduce to the present semiclassical absorption coefficient for stationary atoms and for corunning waves in the Doppler limit.

Expanding the solution in powers of the pump-field intensity, one can predict the appearance of a narrow resonance (characterized by the lower-level width) for different combinations of level- and dipole-decay rates. This resonance is closely related to the pressure-induced extra resonance in four-wave mixing (PIER4) resonance predicted by Bloembergen *et al.*[14,15] in four-wave mixing and studied by a number of groups.[16,19-24]

2. PROBE-WAVE ABSORPTION COEFFICIENT

We consider a medium subjected to a saturating wave of frequency ν_2 and study the transmission of a weak (nonsaturating) probe wave of frequency ν_1 as diagrammed in Fig. 1. We assume that the saturating-wave intensity is constant throughout the interaction region, and we ignore transverse variations. Our two-wave electric field has the form[25]

$$E(\mathbf{r},t)=\frac{1}{2}\sum_{n=1}^{2}\mathcal{E}_n(\mathbf{r})\exp[i(\mathbf{K}_n\cdot\mathbf{r}-\nu_n t)]+\text{c.c.}, \qquad (1)$$

where the mode amplitudes $\mathcal{E}_n(\mathbf{r})$ are in general complex and $\mathbf{K}_n$ are the wave-propagation vectors. This field induces the complex polarization

$$P(\mathbf{r},t)=\frac{1}{2}\sum_{n=1}^{2}\mathcal{P}_n(\mathbf{r})\exp[i(\mathbf{K}_n\cdot\mathbf{r}-\nu_n t)]+\text{c.c.}, \qquad (2)$$

0740-3224/88/010160-11$02.00

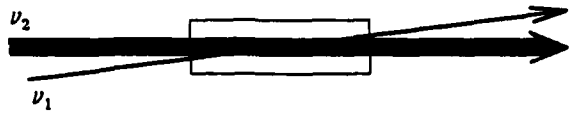

Fig. 1. Basic probe-saturator saturation spectroscopy configuration.

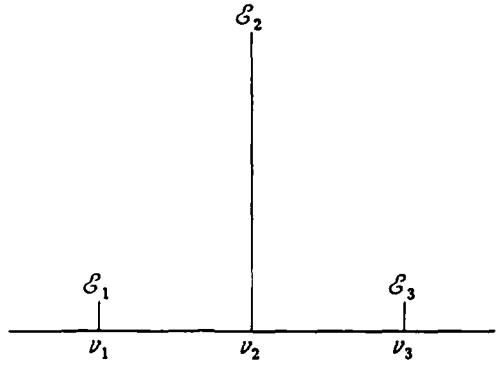

Fig. 2. Spectrum of the multiwave fields used in this paper. The probe wave has frequency ν_1 and is taken to be weak (nonsaturating), while the ν_2 wave may have an arbitrarily large intensity. Pump-scattering off-population pulsations induced by the pump–probe beat frequency induces a polarization at the frequency ν_3. This component couples weak modes in three- and four-wave mixing.

where $\mathcal{P}_n(\mathbf{r})$ is a complex polarization coefficient that yields index and absorption or gain characteristics for the probe and saturator waves. The polarization $P(\mathbf{r}, t)$ in general has other components, but we are interested only in those given by Eq. (2). For example, in homogeneously broadened media, strong wave interactions induce components not only at the frequencies ν_1 and ν_2, but at $\nu_1 \pm k(\nu_2 - \nu_1)$ as well, where k is an integer. To distill the components $\mathcal{P}_n(\mathbf{r})$ out of $P(\mathbf{r}, t)$, we can use the mode factors $\exp(i\mathbf{K}_n \cdot \mathbf{r})$, provided that they differ sufficiently from one another in distances for which the amplitudes vary noticeably. For nearly parallel (or parallel) waves, the mode functions do not vary sufficiently rapidly, and one must separate components by their temporal differences, for example, by heterodyne techniques. In this configuration, the conjugate wave at the frequency $\nu_3 = \nu_2 + (\nu_2 - \nu_1)$ is phase matched and builds up, involving a somewhat more complicated calculation than that given in this paper (Fig. 2).

The problem reduces to determining the probe's polarization $\mathcal{P}_1(\mathbf{r})$, from which the absorption coefficient is determined from the equation

$$\alpha_1 = \frac{iK_1\mathcal{P}_1}{\epsilon_0\mathcal{E}_1}. \tag{3}$$

One might guess that this absorption coefficient is simply a probe Lorentzian multiplied by a population difference saturated by the saturator wave. However, an additional contribution enters because of population pulsations. Specifically, the nonlinear populations respond to the superposition of the modes to give pulsations at the beat frequency

$$\Delta = \nu_2 - \nu_1. \tag{4}$$

Because we suppose the probe does not saturate, the pulsations occur only at $\pm\Delta$, a point proved below. These pulsations act as modulators (or like Raman shifters), putting sidebands onto the medium's response to the ν_2 mode. One of these sidebands falls precisely at ν_1, yielding a contribution to the probe-absorption coefficient. The other sideband would influence the absorption at the frequency ν_3.

In this section we derive the complete nonsaturating probe-absorption coefficient for the expanded two-level scheme depicted in Fig. 3. This scheme is sufficiently general to include the standard excited-state configuration used in typical laser media as well as the upper-to-ground-lower-level decay scheme often used in saturation spectroscopy. In particular it allows us to consider the effects of differing decays $\gamma_a \neq \gamma_b$, which lead to resonances analogous to the PIER resonances in the work of Bloembergen *et al.*[14,15]

The calculation is a semiclassical version of the corresponding two-mode quantized field case given in Refs. 12 and 13, here including possible Doppler shifts due to moving atoms. The polarization $P(\mathbf{r}, t)$ of Eq. (2) is given in terms of the population matrix by

$$P(\mathbf{r}, t) = \wp \int dv W(v)\rho_{ab}(\mathbf{r}, v, t) + \text{c.c.}, \tag{5}$$

where $W(v)$ is the velocity-distribution function. The equations of motion for the population matrix are

$$\left(\frac{\partial}{\partial t} + \mathbf{v}\cdot\nabla\right)\rho_{ab} = -(i\omega + \gamma)\rho_{ab} + i\hbar^{-1}\mathcal{V}_{ab}(z, t)(\rho_{aa} - \rho_{bb}), \tag{6}$$

$$\left(\frac{\partial}{\partial t} + \mathbf{v}\cdot\nabla\right)\rho_{aa} = \Lambda_a\rho_{cc} - (\gamma_a + \Gamma)\rho_{aa} - (i\hbar^{-1}\mathcal{V}_{ab}\rho_{ba} + \text{c.c}), \tag{7}$$

$$\left(\frac{\partial}{\partial t} + \mathbf{v}\cdot\nabla\right)\rho_{bb} = \Lambda_b\rho_{cc} + \Gamma\rho_{aa} - \gamma_b\rho_{bb} + (i\hbar^{-1}\mathcal{V}_{ab}\rho_{ba} + \text{c.c.}), \tag{8}$$

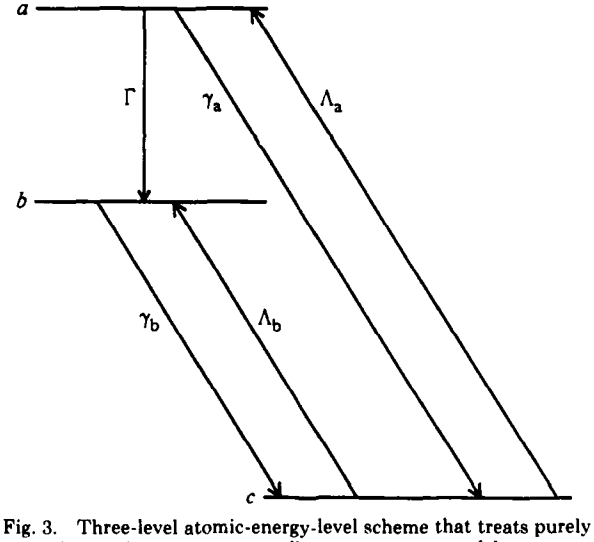

Fig. 3. Three-level atomic-energy-level scheme that treats purely excited-state interactions as well as upper-to-ground lower-state interactions in a uniform way.

$$\left(\frac{\partial}{\partial t} + \mathbf{v}\cdot\nabla\right)\rho_{cc} = -(\Lambda_a + \Lambda_b)\rho_{cc} + \gamma_b\rho_{bb} + \gamma_a\rho_{aa}. \tag{9}$$

As shown in Fig. 3, Λ_a and Λ_b are pump constants from level c to levels a and b, respectively, γ_a and γ_b are the corresponding decay constants, Γ is the decay constant from level a to level b, and γ is the dipole-decay constant given by $(\gamma_a + \gamma_b + \Gamma)/2 + \gamma_{ph}$, where γ_{ph} is a possibly nonzero contribution due to phase-interrupting collisions. In addition, we have the trace condition

$$\rho_{aa} + \rho_{bb} + \rho_{cc} = 1. \tag{10}$$

Using Eq. (10) and the steady-state solution of Eq. (9), we can eliminate ρ_{cc} from Eqs. (7) and (8) and eliminate ρ_{aa} from Eq. (8). For example, we have the relations

$$\rho_{cc} = 1 - \rho_{aa} - [(\Lambda_a + \Lambda_b)\rho_{cc} - \gamma_a\rho_{aa}]/\gamma_b = \frac{\gamma_b - \rho_{aa}(\gamma_b - \gamma_a)}{\gamma_b + \Lambda_a + \Lambda_b}.$$

This reduces Eq. (7) to

$$\left(\frac{\partial}{\partial t} + \mathbf{v}\cdot\nabla\right)\rho_{aa} = \lambda_a - \gamma_a'\rho_{aa} - (i\hbar^{-1}\mathcal{V}_{ab}\rho_{ba} + \text{c.c}), \tag{11}$$

where

$$\gamma_a' = \gamma_a + \Gamma + \frac{\Lambda_a(\gamma_b - \gamma_a)}{\gamma_b + \Lambda_a + \Lambda_b}, \tag{12}$$

$$\lambda_a = \frac{\Lambda_a\gamma_b}{\gamma_b + \Lambda_a + \Lambda_b}. \tag{13}$$

Similarly for the lower-level population ρ_{bb}, we find

$$\left(\frac{\partial}{\partial t} + \mathbf{v}\cdot\nabla\right)\rho_{bb} = \lambda_b - \gamma_b'\rho_{bb} + (i\hbar^{-1}\mathcal{V}_{ab}\rho_{ba} + \text{c.c.}), \tag{14}$$

where

$$\gamma_b' = \gamma_b + \frac{\Gamma(\gamma_b + \Lambda_a + \Lambda_b) + \Lambda_b(\gamma_a - \gamma_b)}{\gamma_a + \Lambda_a + \Lambda_b}, \tag{15}$$

$$\lambda_b = \frac{\Lambda_b\gamma_a + \Gamma(\Lambda_a + \Lambda_b)}{\gamma_a + \Lambda_a + \Lambda_b}. \tag{16}$$

Hence the population-matrix equations of motion (6), (11), and (14) have the same form as those for gas-laser theory but include a more general excitation-decay scheme. In this paper we consider mainly two limiting cases of this excitation–decay scheme. In the upper-to-ground-lower-level decay configuration, $\gamma_a = \gamma_b = 0$, and the Λ_a and Λ_b dependences in Eqs. (12), (13), (15), and (16) drop out, giving $\gamma_a' = \gamma_b' = \Gamma$, $\lambda_a = 0$, and $\lambda_b = \Gamma$. For the excited-state cases considered in this paper, we can neglect Λ_a and Λ_b when compared with the decay rates, since the reservoir-level ρ_{cc} probability is then assumed to be much larger than the excited-state probabilities ρ_{aa} and ρ_{bb}. This assumption gives $\gamma_a' = \gamma_a + \Gamma$, $\lambda_a = \Lambda_a$, $\gamma_b' = \gamma_b(1 + \Gamma/\gamma_a)$, and $\lambda_b = \Lambda_b + \Gamma(\Lambda_a + \Lambda_b)/\gamma_a$. A nice feature of this three-level model is that it allows one to move continuously among various limiting cases.

The interaction energy-matrix element $\mathcal{V}_{ab}$ corresponding to Eq. (1) is given in the rotating-wave approximation by

$$\mathcal{V}_{ab} = -\frac{\wp}{2}\sum_{n=1}^{2}\mathcal{E}_n(\mathbf{r})\exp[i(\mathbf{K}_n\cdot\mathbf{r} - \nu_n t)]. \tag{17}$$

To determine the response of the medium to this multimode field, we analyze, using a Fourier transform, the polarization component ρ_{ab} of the population matrix as well as the populations themselves. We have

$$\rho_{ab} = N\exp[i(\mathbf{K}_1\cdot\mathbf{r} - \nu_1 t)] \times \sum_{m=-\infty}^{\infty} p_{m+1}\exp\{im[(\mathbf{K}_2 - \mathbf{K}_1)\cdot\mathbf{r} - \Delta t]\}, \tag{18}$$

where the unsaturated population difference

$$N = \frac{\lambda_a}{\gamma_a'} - \frac{\lambda_b}{\gamma_b'}. \tag{19}$$

The population-matrix elements $\rho_{\alpha\alpha}$ have the corresponding Fourier expansions

$$\rho_{\alpha\alpha} = N\sum_{k=-\infty}^{\infty} n_{\alpha k}\exp\{-ik[(\mathbf{K}_2 - \mathbf{K}_1)\cdot\mathbf{r} - \Delta t]\}, \qquad \alpha = a, b. \tag{20}$$

It is further convenient to define the population difference $D(\mathbf{r}, t)$ with the expansion

$$D(\mathbf{r}, t) \equiv \rho_{aa}(\mathbf{r}, t) - \rho_{bb}(\mathbf{r}, t) = N\sum_{k=-\infty}^{\infty} d_k\exp\{-ik[(\mathbf{K}_2 - \mathbf{K}_1)\cdot\mathbf{r} - \Delta t]\}, \tag{21}$$

where $d_k \equiv n_{ak} - n_{bk}$. We now substitute these expansions into the population-matrix equations of motion and identify coefficients of common exponential-frequency factors. We suppose that $\mathcal{E}_1$ does not saturate, that is, it appears only once. We show that in this approximation that only p_1, p_2, and p_3 occur in the polarization expansion [Eq. (18)] and that only d_0 and $d_{\pm 1}$ appear in the population-difference expansion [Eq. (21)]. Physically this simplification occurs because once a product of $\mathcal{E}_1$ and $\mathcal{E}_2$ creates the pulsations $d_{\pm 1}$, then only $\mathcal{E}_2$ can interact. One obtains the polarization sidebands of ν_2 at frequencies ν_1 and ν_3, which subsequently combine with ν_2 only to give back $d_{\pm 1}$ components.

We calculate the coefficient of $\exp(i\mathbf{K}_2\cdot\mathbf{r} - i\nu_2 t)$ for the saturator wave by neglecting the nonsaturating probe field. We find

$$i(\mathbf{v}\cdot\mathbf{K}_2 - \nu_2)p_2 = -(i\omega + \gamma)p_2 - i(\wp\mathcal{E}_2/2\hbar)d_0,$$

that is,

$$p_2 = -i(\wp/2\hbar)\mathcal{E}_2\mathcal{D}_2 d_0, \tag{22}$$

where the complex denominator $\mathcal{D}_2$ is the $n = 2$ case of

$$\mathcal{D}_n = \frac{1}{\gamma + i(\omega + \mathbf{v}\cdot\mathbf{K}_n - \nu_n)} = \frac{1}{\gamma + i(\Delta_n + \mathbf{v}\cdot\mathbf{K}_n)}, \tag{23}$$

where the mode detuning

$$\Delta_n = \omega - \nu_n. \tag{24}$$

The coefficient of $\exp(i\mathbf{K}_1 \cdot \mathbf{r} - i\nu_1 t)$ for the probe wave includes an extra term, $\mathcal{E}_2 d_1$,

$$i(\mathbf{v}\cdot\mathbf{K}_1 - \nu_1)p_1 = -(i\omega + \gamma)p_1 - i(\wp/2\hbar)[\mathcal{E}_1 d_0 + \mathcal{E}_2 d_1],$$

giving

$$p_1 = -i(\wp/2\hbar)\mathcal{D}_1[\mathcal{E}_1 d_0 + \mathcal{E}_2 d_1]. \tag{25}$$

The extra $\mathcal{E}_2 d_1$ term gives the scattering of $\mathcal{E}_2$ into the $\mathcal{E}_1$ mode by the population-pulsation component d_1. p_0 remains zero when only d_0 and $d_{\pm 1}$ are nonzero, since it is proportional to $\mathcal{E}_1 d_1$, involving at least two $\mathcal{E}_1$'s.

The component p_3 does have a value, namely,

$$p_3 = i(\wp/2\hbar)\mathcal{D}_3\mathcal{E}_2 d_{-1}, \tag{26}$$

in which $\mathbf{K}_3 = 2\mathbf{K}_2 - \mathbf{K}_1$, while $p_{j>3}$ vanishes since $d_{-(k>1)}$ would be involved.

We calculate the dc-population-difference Fourier component $d_0 = n_{a0} - n_{b0}$ saturated by the saturator wave $\mathcal{E}_2$ alone. Substituting Eq. (20) into Eq. (11), we have

$$0 = \lambda_a/N - \gamma_a' n_{a0} + [i(\wp\mathcal{E}_2/2\hbar)p_2^* + \text{c.c.}],$$

yielding with Eq. (22)

$$n_{a0} = \lambda_a/N\gamma_a' - (2\gamma_a'\gamma)^{-1}|\wp\mathcal{E}_2/\hbar|^2\mathcal{L}_2 d_0. \tag{27}$$

Here $\mathcal{L}_2$ is the dimensionless Lorentzian

$$\mathcal{L}_2 = \gamma^2/[\gamma^2 + (\omega + \mathbf{v}\cdot\mathbf{K}_2 - \nu_2)^2]. \tag{28}$$

The $\mathcal{E}_1$ contributions are ignored, since we assume that $\mathcal{E}_1$ does not saturate. The dc-population component n_{b0} is given by Eq. (27) with $a \to b$ and a change of sign. This gives the population-difference component

$$d_0 = -1 - I_2\mathcal{L}_2 d_0,$$

that is,

$$d_0 = -1/(1 + I_2\mathcal{L}_2), \tag{29}$$

where the dimensionless intensity

$$I_2 = |\wp\mathcal{E}_2/\hbar|^2 T_1 T_2, \tag{30}$$

$T_2 \equiv 1/\gamma$ is the dipole lifetime, and T_1 is the population-difference lifetime:

$$T_1 = \frac{1}{2}\left(\frac{1}{\gamma_a'} + \frac{1}{\gamma_b'}\right). \tag{31}$$

Proceeding with the population-pulsation terms n_{a1}, n_{b1}, and d_1, we have

$$i\Delta' n_{a1} = -\gamma_a' n_{a1} + i(\wp/2\hbar)[\mathcal{E}_1 p_2^* + \mathcal{E}_2 p_3^* - \mathcal{E}_2^* p_1],$$

giving

$$n_{a1} = -\mathcal{D}_a(\Delta')(\wp/2\hbar)^2[\mathcal{E}_1\mathcal{E}_2^*(\mathcal{D}_1 + \mathcal{D}_2^*)d_0 + |\mathcal{E}_2|^2(\mathcal{D}_1 + \mathcal{D}_3^*)d_1], \tag{32}$$

where

$$\mathcal{D}_a' = \frac{\gamma_b + \Lambda_a + \Lambda_b + i\Delta'}{(\gamma_b + i\Delta')(\gamma_a + i\Delta') + \Lambda_a(\gamma_b + i\Delta') + \Lambda_b(\gamma_a + i\Delta') + (\gamma_b\Lambda_a + \Lambda_b + i\Delta')\Gamma}, \tag{33}$$

where Δ' is given by

$$\Delta' = \Delta - \mathbf{v}\cdot(\mathbf{K}_2 - \mathbf{K}_1) \tag{34}$$

and where we have used the fact that $d_{-1} = d_1^*$. For corunning waves, $\Delta' \simeq \Delta$, since $K_2\nu \simeq K_1\nu$. Similarly n_{b1} is given by n_{a1} by changing sign and replacing $\mathcal{D}_a'$ by $\mathcal{D}_b'$, given by

$$\mathcal{D}_b' = \frac{\gamma_a + \Lambda_a + \Lambda_b + i\Delta'}{(\gamma_b + i\Delta')(\gamma_a + i\Delta') + \Lambda_a(\gamma_b + i\Delta') + \Lambda_b(\gamma_a + i\Delta') + (\gamma_b + \Lambda_a + \Lambda_b + i\Delta')\Gamma}. \tag{35}$$

Solving for $d_1 = n_{a1} - n_{b1}$, we have

$$d_1 = -\frac{[\mathcal{D}_a(\Delta') + \mathcal{D}_b(\Delta')](\wp/2\hbar)^2\mathcal{E}_1\mathcal{E}_2^*(\mathcal{D}_1 + \mathcal{D}_2^*)d_0}{1 + |\mathcal{E}_2/2\hbar|^2[\mathcal{D}_a(\Delta') + \mathcal{D}_b(\Delta')](\mathcal{D}_1 + \mathcal{D}_3^*)}$$

$$= -\frac{(\wp/\hbar)^2\mathcal{E}_1\mathcal{E}_2^* T_1 T_2 \mathcal{F}(\Delta')\frac{\gamma}{2}(\mathcal{D}_1 + \mathcal{D}_2^*)}{1 + I_2\mathcal{F}(\Delta')\frac{\gamma}{2}(\mathcal{D}_1 + \mathcal{D}_3^*)} d_0, \tag{36}$$

where the dimensionless complex population-pulsation factor

$$\mathcal{F}(\Delta') = (2T_1)^{-1}[\mathcal{D}_a(\Delta') + \mathcal{D}_b(\Delta')]. \tag{37}$$

This factor approaches unity as $\Delta' \to 0$.

Our calculation is self-consistent, since only d_0 and $d_{\pm 1}$ can obtain nonzero values from p_1, p_2, p_3, and vice versa. Combining the pulsation component [Eq. (36)] with the polarization component [Eq. (25)], setting $\mathcal{P}_1 = 2\wp N p_1$, and using Eq. (3), we find the complex absorption coefficient

$$\alpha_1 = \alpha_0 \int d\upsilon W(\upsilon)\frac{\gamma\mathcal{D}_1}{1 + I_2\mathcal{L}_2} \times\left[1 - \frac{I_2\mathcal{F}(\Delta')\frac{\gamma}{2}(\mathcal{D}_1 + \mathcal{D}_2^*)}{1 + I_2\mathcal{F}(\Delta')\frac{\gamma}{2}(\mathcal{D}_1 + \mathcal{D}_3^*)}\right], \tag{38}$$

where the homogeneous-broadening linear absorption coefficient α_0 is given by

$$\alpha_0 = \frac{K_1 N\wp^2}{\hbar\epsilon_0\gamma}. \tag{39}$$

Equation (38) has the same form as previous derivations but applies to the more general level scheme of Fig. 3 and can be used to calculate probe absorption by Doppler-broadened media with a probe wave propagating in any direction with respect to the saturator wave.

The general formula [Eq. (31)] for the population-difference decay time T_1 and the corresponding population-pulsation factor $\mathcal{F}(\Delta')$ simplify in the limits of the pure two-level system ($\rho_{cc} = 0$), and excited-state systems such that $\rho_{cc} \simeq 1$, while ρ_{aa}, $\rho_{bb} \ll 1$. For the latter, we note that since the pump and decay probability flows have the same general size, γ_a and $\gamma_b \gg \Lambda_a$ and Λ_b. Hence Eq. (31) reduces to

$$T_1 = \frac{1}{2}\frac{1}{\gamma_a + \Gamma}\left(1 + \frac{\gamma_a}{\gamma_b}\right), \tag{40}$$

and Eq. (37) reduces to

$$\mathcal{F}(\Delta') = \frac{1}{2T_1}\frac{1}{\gamma_a + \Gamma + i\Delta'}\left(1 + \frac{\gamma_a + i\Delta'}{\gamma_b + i\Delta'}\right). \tag{41}$$

The limiting value of T_1 for a closed two-level system is recovered by setting γ_a, $\gamma_b \to 0$, such that $\gamma_a/\gamma_b \to 1$. In general, if $\gamma_a = \gamma_b$, Eq. (41) reduces to

$$\mathcal{F}(\Delta') = \frac{1}{T_1(\gamma_a + \Gamma + i\Delta')},$$

a simple resonant behavior studied in detail in the past. However if $\gamma_a \neq \gamma_b$, Eq. (41) shows that $\mathcal{F}$ has an extra beat-frequency dependence because the level populations decay at different rates as far as the population difference is concerned. This fact leads to a new kind of special resonance treated in this paper. Grynberg[23,24] and Pinard[23] also considered an extra resonance in two-wave mixing due to radiation decay as well as to collision broadening.

Physically, one can interpret this resonance intuitively by thinking of the populations as forced, damped, anharmonic oscillators with a zero-resonance frequency. Because they are nonlinear oscillators, they respond to the superposition of two nondegenerate fields by pulsating at the field beat frequency. If the applied fields propagate in different directions, the nonlinear population pulsations are accompanied by a spatial variation, which is typically called spatial hole burning or an induced grating. More precisely, the populations respond to the walking plane-wave field fringe with the dependence $\cos[(\mathbf{K}_2 - \mathbf{K}_1)\cdot\mathbf{r} - (\nu_2 - \nu_1)t]$. Since, unlike the induced dipole, the populations have a zero-resonance frequency, they inevitably lag behind any nonzero forcing frequency such as the possibly Doppler-shifted probe saturator beat note Δ' of Eq. (34). The faster the populations decay, the wider their frequency response and hence the smaller the lag. The Γ contribution to the level decays affects both populations in the same way and hence leads to identical induced gratings for any Δ'. However, if $\gamma_a \neq \gamma_b$, the populations lag different amounts as functions of Δ' [compare Eqs. (33) and (35)], thereby leading to a resonance behavior in the population difference.

In addition, the two-level analogs to the PIER resonances follow from Eq. (38) for $\gamma_a = \gamma_b$ when evaluated to second order in the pump amplitude. In this approximation, Eq. (38) reduces to

$$\alpha_1 = \alpha_0 \int d\upsilon W(\upsilon)\gamma\mathcal{D}_1[1 - I_2\mathcal{L}_2 - I_2\mathcal{F}(\Delta')\gamma(\mathcal{D}_1 + \mathcal{D}_2^*)/2]. \tag{42}$$

Combining the complex denominators $\mathcal{D}_1 + \mathcal{D}_2^*$, we find

$$\alpha_1 = \alpha_0 \int d\upsilon W(\upsilon)\gamma\mathcal{D}_1\left[1 - I_2\mathcal{L}_2 - 2x^2\mathcal{D}_1\mathcal{D}_2^* \times\left(1 + \frac{\epsilon}{\Gamma + \gamma_a + i\Delta'}\right)\right], \tag{43}$$

where $\epsilon = 2\gamma - \Gamma - \gamma_a$ and $x = |\wp\mathcal{E}_2/2\hbar|$ is one half of the Rabi flopping frequency. Here we see that the Δ' dependence of the dipole resonance sum $\mathcal{D}_1 + \mathcal{D}_2^*$ cancels out the Δ' dependence given by the population-difference factor $\mathcal{F}(\Delta')$ if $\Gamma = 2\gamma$ and $\gamma_a = \gamma_b = 0$, which is valid for pure radiative decay. This cancellation is imperfect either if pressure is introduced, causing 2γ to exceed Γ (pressure-induced extra resonance), or if the pump is too intense to permit the use of second-order perturbation theory. In these cases, we expect to see a beat-frequency resonance.

We refer to the system as closed if there are no population transfers to external reservoirs ($\Lambda_a = \Lambda_b = \gamma_a = \gamma_b = 0$) and there are no collisions. This case occurs for pure radiative decay from the upper to the ground lower level. This case satisfies the condition $\Gamma = 2\gamma$ and hence exhibits no Δ' dependence up to third order.

As for the $\gamma_a \neq \gamma_b$ induced resonance, we can gain some understanding of the $\Gamma \neq 2\gamma$ induced resonance in terms of forced, damped, anharmonic oscillators. Specifically, two kinds of second-order population pulsation contribute to the $\mathcal{F}$ term in Eq. (42), one starting with a first-order dipole ρ_{ab} component induced by the probe field and one with a ρ_{ba} component induced by pump. The sum of these contributions produces the complex Lorentzian sum $\mathcal{D}_1 + \mathcal{D}_2^*$. This sum has a phase shift equal to the sum of the individual phase shifts minus that for the beat note Δ' with a decay constant 2γ. The population-difference phase shift also results from the beat note Δ', but with a decay rate Γ. Hence, if Γ equals 2γ, the two phase shifts add to zero. In effect the population-pulsation response lags as usual because of the finite temporal response of the population difference, but this phase lag is canceled by a corresponding phase lead that is due to the interference between the probe- and pump-induced dipoles. As soon as these phase shifts differ, the Δ' dependence fails to cancel out. Furthermore, in higher order, the saturation denominator containing $\mathcal{F}$ in Eq. (38) yields a Δ' dependence even when those in the numerator cancel one another.

Similar results occur in three-wave mixing of two weak fields and a pump. This mixing includes amplitude- and frequency-modulation spectroscopy. In our notation, the coupling coefficient χ_1 appearing in the three-wave coupled-mode equation (neglecting phase matching)

$$\frac{d\mathcal{E}_1}{dz} = -\alpha_1\mathcal{E}_1 + \chi_1\mathcal{E}_3^* \tag{44}$$

has the value

$$\chi_1 = -\alpha_0 \int d\nu\, W(\upsilon)\frac{\gamma\mathcal{D}_1}{1 + I_2\mathcal{L}_2} \times \frac{(\wp\mathcal{E}_2/\hbar)^2 T_1\gamma^{-1}\mathcal{F}(\Delta')\frac{\gamma}{2}(\mathcal{D}_2 + \mathcal{D}_3^*)}{1 + I_2\mathcal{F}(\Delta')\frac{\gamma}{2}(\mathcal{D}_1 + \mathcal{D}_3^*)}, \tag{45}$$

where the conjugate-wave frequency $\nu_3 = \nu_2 + \nu_2 - \nu_1$. This result follows by carrying out the derivation above with three fields in Eq. (1). It is straightforward to see that Eq. (45) has the same Δ' dependences as the absorption coefficient α_1 of Eq. (38). For four-wave mixing with counterpropagating pump waves, the formulas become more complex. Homogeneously broadened treatments have been given in Refs. 18, 26, and 27, and Doppler-broadened treatments have been considered in Refs. 28 and 29. In particular, averages over the pump spatial holes have to be carried out.

However, the suppression Δ' dependences discussed above survive this average.

The observations on population-difference resonances are based directly on the absorption formula [Eq. (38)] and its third-order approximation, which is quite general. We now consider a number of special cases, starting with a homogeneously broadened medium.

3. HOMOGENEOUSLY BROADENED OPERATION

For homogeneously broadened media, we can drop the v dependence in Eq. (38), including that in the $\mathcal{D}$'s, in $\mathcal{L}_2$, and in Δ'. Our discussion focuses on large detunings, but similar features occur for detunings less than the natural linewidth. We are interested in some simple analytic approximations to the absorption coefficient [Eq. (38)] that reveal simple resonant features. We then illustrate these features numerically.

Consider first the real part of the second-order complex probe-absorption coefficient given by Eq. (42). For $\gamma_a = \gamma_b = 0$, pump detunings $|\Delta_2| \gg \gamma$, and beat frequencies Δ of the order of γ, we can approximate the $\mathcal{D}_n$ of Eq. (23) by $-i/\Delta_2$. Hence the real part of Eq. (43) reduces to

$$\mathrm{Re}\{\alpha_1^{(3)}\} \simeq \alpha_0 \frac{2\epsilon x^2}{\Delta_2^3} \frac{\Delta}{\Gamma^2 + \Delta^2}, \tag{46}$$

which has a dispersive line shape. Such dispersionlike absorption resonances are well known in two-level saturation spectroscopy. They are dispersionlike instead of Lorentzian because the dipole is being driven way off its resonance leading to a phase lag or lead of $\pi/2$. This resonance vanishes if ϵ vanishes, that is, if $\Gamma = 2\gamma$.

It no longer vanishes if we expand Eq. (38) to the next order in the pump intensity and assume the resonance condition $\Gamma = 2\gamma$. For similar detuning values and Δ of the order of γ, we find the fifth-order contribution (first order in probe, fourth order in pump)

$$\mathrm{Re}\{\alpha_1\} \simeq \mathrm{Re}\{\alpha_1^{(5)}\} \simeq -\alpha_0 \frac{2x^4\gamma}{\Delta_2^5} \frac{\gamma\Delta}{\Gamma^2 + \Delta^2}. \tag{47}$$

In addition in this order, there is a resonance in the vicinity of $\Delta_3 \simeq 0$ from the $\mathcal{D}_3^*$ term [and hence from p_3 of Eq. (26)] in the denominator of Eq. (38). This resonance occurs for $\Delta \simeq \Delta_2$. This corresponding contribution is

$$\mathrm{Re}\{\alpha_1\} \simeq \mathrm{Re}\{\alpha_1^{(5)}\} \simeq -\alpha_0 \frac{x^4}{\Delta_2^4} \frac{\gamma^2}{\gamma^2 + \Delta_3^2} \tag{48}$$

and originates from three-photon processes that induce a polarization p_3 at the conjugate-wave frequency ν_3. More specifically, the pump-wave scattering off the population pulsations contributes to two side modes, one being the probe itself and the other being the conjugate wave. The contribution in Eq. (48) is sometimes called a Raman resonance and reveals probe amplification at the expense of the pump field. Several authors[2,4,6,11,17,18] have predicted amplification of a weak probe field by a strongly saturated resonance medium in spite of an uninverted population. This amplification was observed by Wu *et al.*[9] It results from constructive scattering of the pump off population pulsations into the probe wave. Figure 4 illustrates the stimulated Rayleigh and Raman resonances given by Eqs. (46)–(48).

Consider next an open system with arbitrarily large pump intensity for which $\gamma_b \ll \gamma_a$, $\gamma \ll \Delta_2$, and consider beat frequencies Δ of the order of γ_b. For simplicity, we further neglect Γ, which just modifies the saturation intensity in these approximations. Then T_1 of Eq. (40) reduces to $1/2\gamma_b$, $\mathcal{F}$ of Eq. (41) reduces to $\gamma_b/(\gamma_b + i\Delta)$, and Eq. (38) reduces to

$$\alpha_1 = -i\alpha_0 \frac{\gamma\mathcal{D}_1}{1 + 4x^2\gamma/\Delta_2^2\gamma_b} \left[1 - \frac{4x^2\gamma/\Delta_1\Delta_2}{\gamma_b(1 + 4x^2\gamma/\gamma_b\Delta_1\Delta_2) + i\Delta}\right], \tag{49}$$

where $x = |\wp\mathcal{E}_2/2\hbar|$ is one half of the Rabi flopping frequency. Dropping the remaining differences between the Δ_n, we find the real part of α_1 to be

$$\mathrm{Re}\{\alpha_1\} \simeq \alpha_0 \frac{\gamma/\Delta_2^2}{1 + 2x^2\gamma/\gamma_b\Delta_2^2} \times \left[1 - \frac{4\Delta x^2/\Delta_2}{\gamma_b^2(1 + 4x^2\gamma/\gamma_b\Delta_2^2)^2 + \Delta^2}\right]. \tag{50}$$

To second order in the pump field, we neglect $4x^2\gamma/\gamma_b\Delta_2^2$ compared to 1 in the denominators. This decision gives the still simpler formula

$$\mathrm{Re}\{\alpha_1\} \simeq \alpha_0 \frac{\gamma}{\Delta_2^2} \left[1 - \frac{4\Delta x^2/\Delta_2}{\gamma_b^2 + \Delta^2}\right]. \tag{51}$$

The first term is the linear probe absorption. The second term has a dispersive line shape as a function of the beat frequency Δ and is due to scattering of the pump wave off the population pulsations. In these limits, amplification (negative absorption) occurs when

$$\frac{4\Delta(x^2/\Delta_2)}{\gamma_b^2 + \Delta^2} > 1. \tag{52}$$

In particular, for $\Delta \simeq \gamma_b$ we have gain for $2x^2/\gamma_b\Delta_2 > 1$. Since our perturbation expansion is valid only for $x^2\gamma/\gamma_b\Delta_2^2$

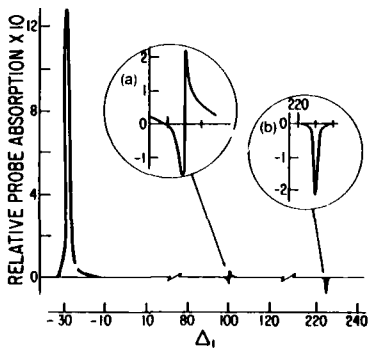

Fig. 4. Probe absorption line shape as a function of probe detuning for the stationary atom limit and a nearly closed system ($\gamma_a = \gamma_b = 0.001$, $\Gamma = 1$, $\gamma = 0.501$, $x = 40$, $\Delta_2 = 100$ pump detuning). All frequency parameters in this and subsequent figures are in units of the total upper-level spontaneous decay rate $\gamma_a + \Gamma$, which is set equal to unity. Linear absorption, Rayleigh (a), and Raman (b) resonances are identifiable. The same dimensionless units are used for relative probe absorption in all the following figures, and $\Delta_1 = \nu_1 - \omega$, $\Delta_2 = \nu_2 - \omega$, which differs from the text by a minus sign.

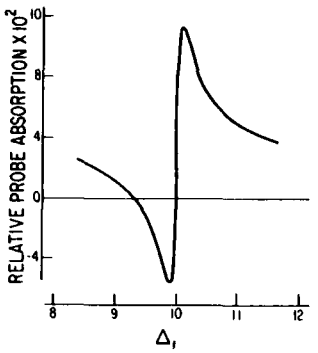

Fig. 5. Rayleigh resonance for stationary atoms in the perturbation limit for an open system $\gamma_b = 0.101$, $\gamma_a = 1.001$, $\Gamma = 0$, $\gamma = 0.551$, $x = 2$, and $\Delta_2 = 10$. No such resonance (to order x^2) occurs for a closed system (see text).

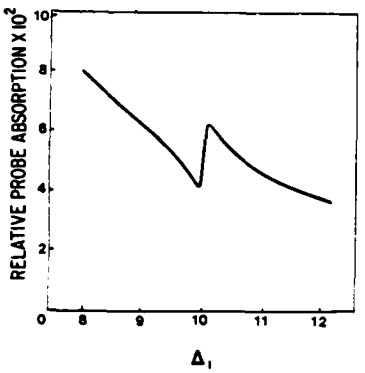

Fig. 6. Same as Fig. 5 but for a weaker pump field of $x = 0.5$. Perturbation theory is valid. There is a resonance structure but no amplification.

$\ll 1$, we find that γ/Δ_2 must be $\ll 1$, which is consistent with our original approximations. This result shows that already in third-order perturbation theory, the scattering off population pulsations is larger than the linear absorption at this detuning. Gain in the absence of population inversion is well known for larger pump intensities.[2,4,6]

Corresponding results of a numerical evaluation of Eq. (38) are shown in Figs. 5 and 6 and are in good agreement with our analytic approximations. Note that alternatively we could have taken $\Gamma + \gamma_a \ll \gamma_b$. The same formulas [Eqs. (49)–(51)] result, with γ_b replaced by $\Gamma + \gamma_a$. In the first case, the population difference lifetime T_1 is given by $1/\gamma_b$, and in the second case it is given by $1/(\Gamma + \gamma_a)$. The resonance in both cases is characterized by the corresponding T_1 limit. This discussion has centered on cases for large pump detuning, but similar resonances also occur within the homogeneous linewidth.

4. MOVING ATOMS

We now calculate the probe-absorption coefficient [Eq. (38)] for an atomic medium assuming a Maxwellian distribution of atomic velocities given by

$$W(v) = \frac{1}{u\sqrt{\pi}} \exp(-v^2/u^2), \tag{53}$$

where u is the average atomic speed. The absorption coefficient [Eq. (38)] can be written in the form

$$\alpha_1 = -i\alpha_0 \int dv W(v) \frac{\gamma}{Kv + \Delta_1 - i\gamma} \times \left[1 - \frac{I_2\gamma^2}{(Kv + \Delta_2 + i\gamma')(Kv + \Delta_2 - i\gamma')}\right] - \alpha_0 \frac{I_2\mathcal{J}(\Delta)\gamma^2}{2} \int dv W(v) \frac{\gamma + i\Delta_2 + iKv}{\gamma'^2 + (\Delta_2 + Kv)^2} \times \frac{2\gamma + i\Delta}{\beta^2 + (\Delta_2 + Kv)^2} \frac{\gamma - i\Delta_3 - iKv}{\gamma + i\Delta_1 + iKv}, \tag{54}$$

where

$$\beta^2 = (\gamma + i\Delta)[\gamma + i\Delta + \gamma I_2 \mathcal{J}(\Delta)], \tag{55}$$

$$\gamma' = \gamma\sqrt{1 + I_2}. \tag{56}$$

The approximation made for obtaining Eq. (54) is the neglect of the term $(\mathbf{K}_2 - \mathbf{K}_1) \cdot \mathbf{v}$ compared to γ. This action is justified for unidirectional waves, since $(K_2 - K_1)v$ is typically of the order of $10^{-6}\gamma$. In actual experiments, the pump and probe typically propagate in slightly different directions, leading to a residual Doppler width of the order 0.1γ. We neglect corrections of this sort in the following. This represents a major difference from the counterpropagating-wave case for which the Doppler shifts add, rather than subtract, and the $(\mathbf{K}_2 - \mathbf{K}_1) \cdot \mathbf{v}$ terms play a decisive role.

We make use of the plasma-dispersion function defined as

$$Z(\mu) = -\int_{-\infty}^{\infty} dx \frac{\pi^{-1/2} e^{-x^2}}{\mu \pm x}, \tag{57}$$

with $\mathrm{Im}\{\mu\} > 0$. When we use the method of partial fractions, the velocity integral of Eq. (54) can be reduced to a sum involving functions Z_2, Z_3, and Z_4, which, as defined in Appendix A, can each be written as a sum of plasma-dispersion functions defined by Eq. (57).

The general result as a sum of Z, Z_2, Z_3, and Z_4 functions is

$$\alpha_1^* = -i\frac{\alpha_0\gamma}{Ku} Z(\mu_1) + \frac{\alpha_0 I_2\gamma^3}{2\gamma'(Ku)^2}[Z_2(\mu_1\mu_6; -1) + Z_2(\mu_1\mu_5; 1)] - \alpha_0 \frac{I_2\gamma^2(2\gamma - i\Delta)\mathcal{J}^*}{4\beta^*(Ku)^2} \Bigg(Z_2(\mu_1\mu_4; -1) + Z_2(\mu_1\mu_3; 1) + \frac{\Delta}{Ku}[Z_3(\mu_1\mu_4\mu_2; -1-1) + Z_3(\mu_1\mu_3\mu_2; 1-1)] - i\frac{I_2\gamma^2}{2\gamma' Ku} \Big\{ Z_3(\mu_1\mu_6\mu_4; -1-1) + Z_3(\mu_1\mu_5\mu_4; 1-1) + Z_3(\mu_1\mu_5\mu_3; 1\,1) + Z_3(\mu_1\mu_6\mu_3; -1+1) + \frac{\Delta}{Ku}[Z_4(\mu_1\mu_6\mu_4\mu_2; -1-1-1) + Z_4(\mu_1\mu_5\mu_3\mu_2; 1-1-1) + Z_4(\mu_1\mu_6\mu_3\mu_2; -1\,1-1) + Z_4(\mu_1\mu_5\mu_3\mu_2; 1\,1-1)] \Big\} \Bigg), \tag{58}$$

where

$$\mu_1 = (i\gamma + \Delta_1)/Ku, \qquad \mu_2 = (i\gamma - \Delta_2)/Ku,$$
$$\mu_3 = (i\beta + \Delta_2)/Ku, \qquad \mu_4 = (i\beta - \Delta_2)/Ku,$$
$$\mu_5 = (i\gamma' + \Delta_2)/Ku, \qquad \mu_6 = (i\gamma' - \Delta_2)/Ku. \tag{59}$$

The general form of our result allows us to consider a number of limiting cases. First, we can reproduce a result previously obtained in the Doppler limit.

5. DOPPLER LIMIT

The Doppler limit is achieved when all decay constants (γ_b, γ_a, Γ, γ), detunings ($|\Delta_n|$, $|\Delta|$), and the Rabi frequency $2x$ are much smaller than the Doppler width Ku. Using the Doppler-limit expressions given in Appendix A for Z_2, Z_3, and Z_4 and after long but straightforward calculations, we obtain

$$\alpha_1 = \alpha_0' \exp[-(\Delta_1/Ku)^2] \times \left\{1 - \frac{\gamma^2 I_2}{\gamma'(\gamma' + \gamma + i\Delta)} - \frac{\gamma I_2}{2} \frac{(2\gamma + i\Delta)\mathcal{F}(\Delta)}{\gamma'^2 - \beta^2} \times \left[\frac{(\gamma' + \gamma)(\gamma' - \gamma - i\Delta)}{\gamma'(\gamma' + \gamma + i\Delta)} - \frac{(\beta + \gamma)(\beta - \gamma - i\Delta)}{\beta(\beta + \gamma + i\Delta)}\right]\right\}, \tag{60}$$

where the inhomogeneous broadening linear-absorption coefficient α_0' is defined by

$$\alpha_0' = \sqrt{\pi}\alpha_0\gamma/Ku. \tag{61}$$

This result is the same as that of Baklanov and Chebotaev,[1] except that Γ is included in $\mathcal{F}$, β, and T_1 and hence in the dimensionless intensity I_2. Including the Γ accounts for spontaneous emission from level a to level b and allows us to investigate open and closed systems (no population loss to the external reservoir and no collisions present). The Doppler-limit results can also be obtained by direct integration of Eq. (38) using the residue method in the complex plane.[1]. In the Doppler limit, velocity-selected atoms provide the major contributions to the line shape, and the slowly varying atomic-velocity distribution functions can be evaluated at the selected velocity.

In the weak-pump-field limit, the probe-absorption profile consists of a broad Gaussian of width Ku containing a Doppler-free hole with width $\Gamma + \gamma_a$ (or 2γ or γ_b). Keeping only first-order terms in I_2, one can obtain for a closed system

$$\alpha_1 = \alpha_0' \exp[-(\Delta_1/Ku)^2]\left[1 - \frac{I_2\gamma(2\Gamma + i\Delta)}{(\Gamma + i\Delta)^2}\right]. \tag{62}$$

To explain this perturbation-theory result, we return to Eq. (54) and note that atoms having velocities

$$Kv = \Delta_2,$$
$$Kv = \Delta_2 \pm \Delta,$$
$$Kv = \Delta_1 \tag{63}$$

are resonant with the applied fields. The contribution to the probe absorption comes from atoms with velocities that simultaneously satisfy at least two of the equalities [Eqs. (63)]. In each case this leads to a resonance at ($\Delta_1 = \Delta$, i.e., $\Delta = 0$). The $\Delta = 0$ resonance comes from satisfying velocity-selection rules [Eqs. (63)], and this result is in agreement with the analytical expression of Eq. (62) (see Fig. 7).

For Rabi frequencies satisfying $Ku > x > \gamma_b$, the perturbation limit is no longer valid, but the Doppler limit still holds. The velocity-selection conditions, obtained from Eq. (54) in this limit are

$$Kv = \Delta_2 \pm \sqrt{\Delta^2 - 4x^2},$$
$$Kv = \Delta_1,$$
$$Kv = \Delta_2. \tag{64}$$

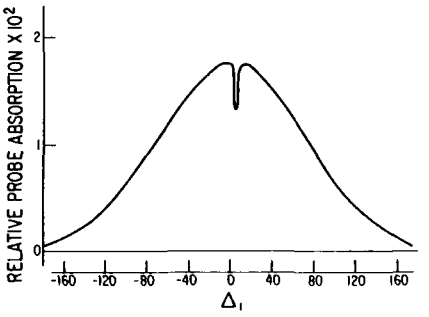

Fig. 7. Probe-absorption line shape for moving atoms in the Doppler limit ($Ku = 100$, $x = 0.2$, $\Delta_2 = 5$), a closed system ($\gamma_b = 0.001$, $\gamma_a = 0.001$, $\Gamma = 1$, $\gamma = 0.501$), and the perturbation-theory limit [$\chi \ll \gamma$]. The dip near $\Delta_2 = \Delta_1$ results from velocity selected atoms. All subsequent figures are for the closed systems.

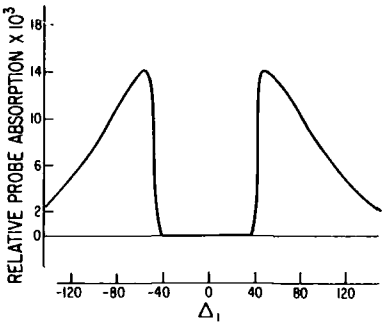

Fig. 8. Probe-absorption line shape in the Doppler limit but for a moderately strong field ($x = 20$, $Ku = 100$, $\Delta_1 = 0$). A dead zone can be seen centered around $\Delta_1 = \Delta_2 = 0$ of width $4x$. In this detuning range no atoms can satisfy the velocity-selection criteria to be resonant with the Stark-shifted transition frequencies.

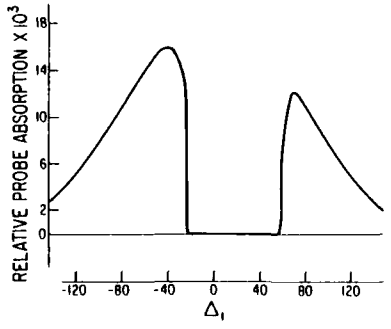

Fig. 9. Same as Fig. 8 but for a pump detuning of $\Delta_2 = 20$, which shifts the center of the dead zone.

If one first considers zero detuning, the condition of $Kv = \pm(\Delta_1^2 - 4x^2)^{1/2}$ can be satisfied only for $\Delta_1 > 2x$ or $\Delta_1 < -2x$ for which no resonant atoms will exist. This means that in the region of detuning $|\Delta_1| < 2x$ the absorption coefficient is equal to zero. As can be seen in Fig. 8, there is a symmetric dead zone in the Gaussian profile. For arbitrary pump detuning Δ_2 the velocity-selection condition requires that $\Delta_2 > 2x$ and $\Delta_2 < -2x$ for absorption to occur. Consequently, the dead zone is shifted from the center by Δ_2, as can be seen in Fig. 9. The size of the dead zone depends on the field strength; by changing x and keeping Δ fixed, one can actually move the borders of dead zone, as illustrated in Fig. 9.

For the strong-pump field, the Doppler-limit results do not contain any probe amplification (gain in the profile) and show no narrow Doppler-free resonances related to the ground- or excited-state width.

6. ABSORPTION LINE SHAPE AND DETUNING DEPENDENCE

We are now in a position to consider cases that were not obtainable in previous calculations, namely, those in which the detuning Δ_2 is of order Ku and the pump field is quite strong, $2x \simeq Ku$. The line shape consists of the contributions from atoms with all possible velocities, not only those from atoms whose velocities Doppler shift their frequencies into resonance with the fields. As can be seen in Fig. 10, there is a Doppler-limit contribution to the line shape; however, internal structure can also be seen in a place where the dead zone used to be. To be able to provide a physical explanation of the line shape, we consider a perturbative development of the profile for a relatively weak pump field.

Expanding the general solution in powers of x^2, we obtain a linear absorption term $(x^2)^0$, which is Doppler broadened since the resonance condition $\omega - \nu_1 = -Kv$ can be satisfied for a range of detunings $|\omega - \nu_1| \lesssim Ku$. The nonlinear $(x^2)^1$ term gives a Rayleigh resonance about $\Delta \simeq 0$ that remains Doppler free, since both waves are Doppler shifted nearly equal amounts. The condition $\nu_1 - Kv = \nu_2 - Kv$ implies that the beat frequency $\Delta \equiv \nu_2 - \nu_1 \simeq 0$. This is true only for copropagating fields. If pump and probe fields are propagating in opposite directions, then this resonance condition gives $|\nu_1 - \nu_2| < 2Ku$, that is, a broad resonance. For the next nonlinear term, $(x^2)^2$, the Raman resonance becomes velocity broadened, since the resonance condition can be satisfied when $(\nu_2 - Kv) - (\nu_1 - Kv) + (\nu_2 - Kv) = \omega$, that is, when $(2\nu_2 - \nu_1 - \omega) < Ku$.

It is now possible to see how the total line shape has been formed. With zero detuning, the line shape for ($x = 50$, $Ku = 25$) is shown in Fig. 11. This intermediate case was impossible to obtain with the previous limits and shows the transition from homogeneous broadening to inhomogeneous broadening. As can be seen in Fig. 11, a Doppler-limit contribution does occur and is similar to that of Fig. 8. However, we can see additional structure in a place where the dead zone used to be. Our line shape accounts for the negative probe absorption, which occurs in the $(-2x < \Delta_1 < 2x)$ region. This is definitely a non-Doppler-limit contribution. It can be traced to a contribution from all atoms that satisfy the velocity-independent stimulated Rayleigh-resonance condition whenever $\Delta \simeq 0$.

The amplification occurs in the dead zone $(-2x < \Delta_1 < 2x)$, as in the homogeneously broadened case in Fig. 4. Thus the dead zone provides openings in the inhomogeneously broadened profile that allow us to see the Doppler-free contributions. The disadvantage of the zero-detuning case is that it is impossible to distinguish contributions from different resonances (they all are at the same place, $\Delta_1 = \Delta = 0$) and to obtain any information about ground- and excited-state widths.

Consider now the large-detuning case ($Ku \simeq 2\Delta_2$). The Doppler-limit contribution occurs only for $(\Delta > 2x)$ and $(\Delta < -2x)$ (the position of the dead zone is shifted from the center

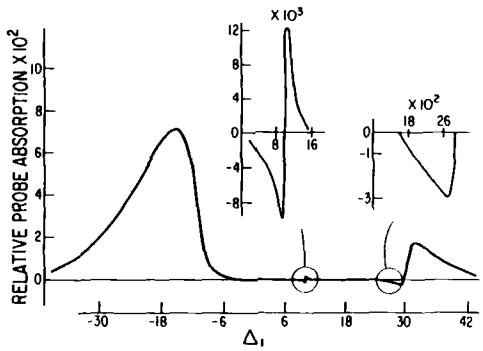

Fig. 10. Probe-absorption line shape when the Doppler limit is no longer valid, with $x = 10$, $Ku = 20$, $\Delta_2 = 10$. Structure is now seen in the dead zone (Rayleigh and Raman resonances), although the Doppler-limit contribution is still evident.

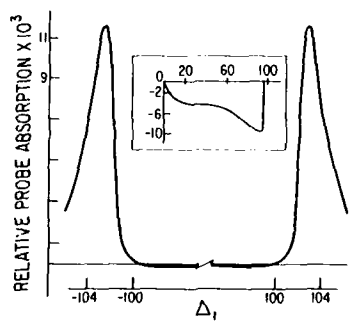

Fig. 11. Probe-absorption line shape for the zero-pump-detuning case with $Ku = 25$, $x = 50$. Owing to contributions from atoms with all velocities, negative absorption occurs in the area that is a dead zone in the Doppler limit.

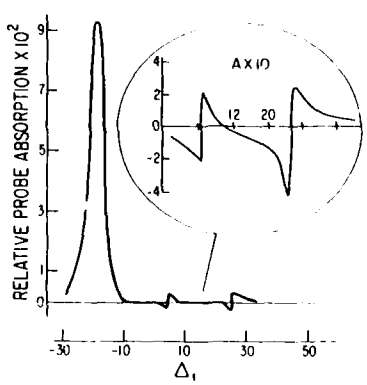

Fig. 12. Line shape for $Ku = 10$, $x = 10$, $\Delta_2 = 5$. Contributions from atoms with all velocities can be seen, including a Rayleigh resonance at $\Delta_1 = \Delta_2$ and Raman dip in the area where the dead zone used to be.

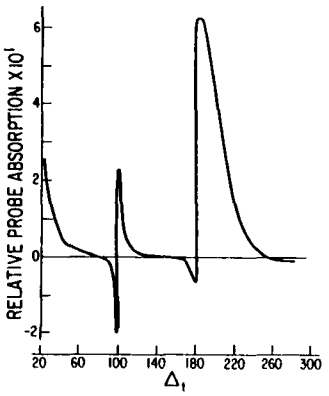

Fig. 13. Line shape for $Ku = 100$, $x = 40$, $\Delta_2 = 100$. The substructure occurring in the area of the dead zone is shown in detail. One can see that the Doppler-limit contribution dominates the Raman dip.

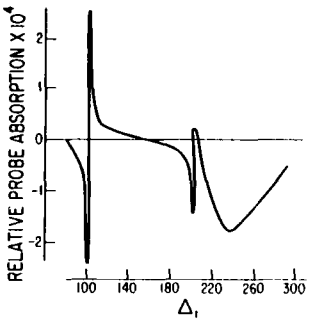

Fig. 14. Same as Fig. 13 except for the increased field strength, $x = 50$. The Raman dip dominates the Doppler-limit contribution.

We have seen that, by changing the field strength, we can move the border of the dead zone. At the same time the shape of the Raman dip itself is only slightly affected, since it is Doppler broadened. For the case $x = 40$, $\Delta_2 = Ku = 100$ (Fig. 13), the Doppler contribution dominates over the Raman dip, and there is only a small gain before a large Doppler-limit contribution, which appears exactly at ($\Delta_1 = 2x + \Delta_2 = 180$) (Fig. 13). Comparing with the stationary atom line shape (Fig. 4), we can see that the stimulated Rayleigh resonance remains the same but that the Raman resonance is changed substantially. If we now increase the field strength (all other parameters remaining the same), the line shape changes dramatically, the border of the dead zone moves ($x = 50$, $\Delta_1 = 200$), and the Raman gain dominates the profile (see Fig. 14). There is a narrow dip just before the dead-zone border, then a small peak occurring exactly at the border, and, finally, additional gain that occurs in the detuning range of the Doppler-limit contribution. Consequently, by properly choosing the field strength, we can divide the Raman gain into two parts. Thus we can vary the pump intensity to produce Doppler-free structures in the openings of a Doppler-limit profile. The line profiles displayed in Figs. 7–14 indicate that both velocity-selected and non-velocity-selected atoms can make important contributions to the probe absorption for different values of the detunings, decay rates, and pump-field strength.

APPENDIX A

This appendix defines the higher-order functions Z_n used in Eq. (58) and evaluates them in terms of the plasma-dispersion function $Z(\mu)$ of Eq. (57). They are

$$Z_2\left(\mu_1\mu_2;\begin{matrix}\epsilon_2\\ \epsilon_1\end{matrix}\right) = \int_{-\infty}^{\infty} \frac{W(v)\mathrm{d}v}{(\mu_1 + \epsilon_1 v/u)(\mu_2 + \epsilon_2 v/u)}, \tag{A1}$$

$$Z_3\left(\mu_1\mu_2\mu_3;\begin{matrix}\epsilon_2\ \epsilon_3\\ \epsilon_1\ \epsilon_1\end{matrix}\right) = \int_{-\infty}^{\infty} \frac{W(v)\mathrm{d}v}{(\mu_1 + \epsilon_1 v/u)(\mu_2 + \epsilon_2 v/u)(\mu_3 + \epsilon_3 v/u)}, \tag{A2}$$

$$Z_4\left(\mu_1\mu_2\mu_3\mu_4;\begin{matrix}\epsilon_2\ \epsilon_3\ \epsilon_4\\ \epsilon_1\ \epsilon_1\ \epsilon_1\end{matrix}\right) = \int_{-\infty}^{\infty} \frac{W(v)\mathrm{d}v}{(\mu_1 + \epsilon_1 v/u)(\mu_2 + \epsilon_2 v/u)(\mu_3 + \epsilon_3 v/u)(\mu_4 + \epsilon_4 v/u)}. \tag{A3}$$

by Δ_2). For ($\Delta_1 < -2x + \Delta_2$), there is a Doppler-limit contribution that just adds to the velocity-broadened linear absorption peak. An interesting feature is the Rayleigh resonance ($\nu_1 = \nu_2$), which is Doppler free and can be seen in the dead-zone region. In the strong-field limit, the Rayleigh resonance exists for both open and closed systems (Fig. 12).

Another interesting structure that occurs in the dead-zone region is a broad dip that terminates at exactly the dead-zone border (see Fig. 12). The origin of this dip can be traced to the velocity-broadened Raman resonance dip, which is competing with the Doppler-limit contribution (Fig. 12). As for purely homogeneous broadening, it is a three-photon process that is responsible for the probe amplification, but it is possible to observe this gain in the profile only because it occurs in the dead-zone region. One actually can change the shape of the gain by considering that the location of the Doppler-limit contribution depends on the field strength ($\Delta_1 \geq \Delta_2 + 2x$).

In terms of Eq. (58), they are given by

$$Z_2(\mu_1\mu_2;\epsilon) = \frac{Z(\mu_2) - Z(\mu_1)}{\mu_2 - \epsilon\mu_1}, \tag{A4}$$

$$Z_3(\mu_1\mu_2\mu_3;\epsilon\epsilon') = \frac{Z_2(\mu_1\mu_3;\epsilon') - \epsilon Z_2(\mu_2\mu_3;\epsilon/\epsilon')}{\mu_2 - \epsilon\mu_1}, \tag{A5}$$

$$Z_4(\mu_1\mu_2\mu_3\mu_4;\epsilon\epsilon'\epsilon'') = \frac{Z_3(\mu_1\mu_3\mu_4;\epsilon'\epsilon'') - \epsilon Z_3(\mu_2\mu_3\mu_4;\epsilon/\epsilon'\ \epsilon''/\epsilon)}{\mu_2 - \epsilon\mu_1}. \tag{A6}$$

ACKNOWLEDGMENTS

This research was supported in part by the U.S. Office of Naval Research, in part by the U.S. Army Research Office, in part by the U.S. Air Force Office of Scientific Research,

and in part by the National Science Foundation under grant PHY-8415781. It is based in part on the Ph.D. dissertation of G. Khitrova (New York University, New York, 1986).

REFERENCES AND NOTES

1. E. V. Baklanov and V. P. Chevotaev, Sov. Phys. JETP **34,** 490 (1972).
2. S. Haroche and F. Hartman, Phys. Rev. A **6,** 1280 (1972).
3. E. V. Baklanov and V. P. Chebotaev, Sov. Phys. JETP **33,** 300 (1971).
4. B. R. Mollow, Phys. Rev. A **5,** 2217 (1972).
5. M. Sargent III and P. E. Toschek, Appl. Phys. **11,** 107 (1976).
6. M. Sargent III, Phys. Rep. **43,** 223 (1978).
7. G. S. Agarwal, Phys. Rev. A **19,** 923 (1979).
8. G. Nienhuis, J. Phys. B **14,** 1693 (1981).
9. F. Y. Wu, S. Ezekiel, M. Ducloy, and B. R. Mollow, Phys. Rev. Lett. **38,** 1077 (1977).
10. R. W. Boyd and S. Mukamel, Phys. Rev. A **29,** 1973 (1984).
11. C.Cohen-Tannoudji and S. Feynaud, J. Phys. B **10,** 345 (1977).
12. M. Sargent III, D. A. Holm, and M. S. Zubairy, Phys. Rev. A **31,** 3112 (1985).
13. D. A. Holm, M. Sargent III, and L. Hoffer, Phys. Rev. A **32,** 963 (1985).
14. N. Bloembergen and L. J. Rothberg, in *Spectral Line Shapes*, F. Rostas, ed. (de Gruyter, Berlin, 1985), Vol. 3, p. 265.
15. N. Bloembergen, A. R. Bogdan, and M. C. Downer, in *Laser Spectroscopy V*, A. R. W. McKellar, T. Oka, and B. P. Stoicheff, eds. (Springer-Verlag, Heidelberg, 1981).
16. P. R. Berman, G. Khitrova, and J. F. Lam in *Spectral Line Shapes*, F. Rostas, ed. (de Gruyter, Berlin, 1985), Vol. 3, p. 337.
17. J. L. Carlsten, A. Szöke, and M. G. Raymer, Phys. Rev. A **15,** 1029 (1977).
18. R. W. Boyd, M. G. Raymer, P. Narum, and D. Harter, Phys. Rev. A **24,** 411 (1981).
19. Y. Prior, A. R. Bogdan, M. Dagenais, and N. Bloembergen, Phys. Rev. Lett. **46,** 111 (1981).
20. G. S. Agarwal and N. Nayak, J. Opt. Soc. Am. B **1,** 164 (1984).
21. L. J. Rothberg and N. Bloembergen, Phys. Rev. A **30,** 820 (1984).
22. G. Grynberg, E. Le Bihan, and M. Pinard, J. Phys. **47,** 1321 (1986).
23. G. Grynberg and M. Pinard, Europhys. Lett. **1,** 129 (1986).
24. G. Grynberg, Ann. Phys. **11,** 125 (1986).
25. For a more pedagogical derivation of a simpler two-level model, see R. W. Boyd and M. Sargent III, J. Opt. Soc. B **4,** 99 (1987).
26. T. Fu and M. Sargent III, Opt. Lett. **4,** 366 (1979).
27. See R. L. Abrams et al, in *Optical Phase Conjugation*, R. A. Fisher, ed. (1983), and references therein.
28. S. M. Wandzura, Opt. Lett. **4,** 208 (1979).
29. M. Ducloy and D. Bloch, J. Phys. **42,** 711 (1981).

PHYSICAL REVIEW A VOLUME 36, NUMBER 8 OCTOBER 15, 1987

Transient probe spectra in a driven two-level atom

Ning Lu and P. R. Berman
Department of Physics, New York University, 4 Washington Place, New York, New York 10003
(Received 15 May 1987)

We analyze the transient probe spectra that arise when two-level atoms in an atomic beam are excited by a "pump" laser field and are probed by a step-function weak field on the same atomic transition. The temporal relaxation of the probe spectra to their steady-state values is found to depend critically on the initial atom–pump-field dressed-state populations and coherences. The transient spectra may be composed of absorption-emission structure that is totally absent in the steady-state limit. A simple physical interpretation of the spectra is given in terms of a conventional dressed-atom picture. In addition, we study the effects of collisions on transient probe spectra and investigate the transient buildup of several collision-induced features in the spectra.

I. INTRODUCTION

Pump-probe spectroscopy is a useful method for studying the interaction of laser fields with atoms. The problem of a weak "probe" field and an arbitrarily strong "pump" field driving the same transition of "two-level" atoms in an atomic beam[1–9] or in a vapor[2,5,9,10] has been studied since the early 1970's. Much knowledge has been obtained for the probe absorption in the steady-state limit. Two well-known results obtained in an atomic beam for a strong pump field are (1) the steady-state probe absorption spectrum consists of one absorption component and one emission component for an off-resonant pump field and (2) for a resonant pump field, the probe spectrum exhibits a complicated absorption-emission structure of relatively small amplitude. Some features of the probe spectrum can be conveniently explained in terms of a conventional "dressed-atom" description of the atom-field interaction.[4] In the conventional dressed-atom approach, eigenstates of the atom plus pump field serve as the basis states for the system. The absorption and emission components of the probe spectrum are viewed as arising from transitions between these dressed states.

Other interesting features of the steady-state probe spectrum relate to the effects of collisions on the spectrum.[5,6,8,9] (1) For a large pump detuning, a small-amplitude dispersion structure occurs centered at $\Omega_2=\Omega_1$ (Ω_1 and Ω_2 are the pump and probe frequencies, respectively) when the atoms undergo collisions.[9,11] (2) In the case of a nearly resonant "weak" pump field interacting with atoms whose coherence decay rate is much larger than their population decay rates, a narrow hole[5,8,9] is created in the probe-absorption line shape centered at $\Omega_2=\Omega_1$.

Recently, we developed a theory of *transient* probe spectra for another pump-probe problem—one in three-level atoms.[12] We assumed that three-level atoms in an atomic beam were prepared with arbitrary initial conditions and then exposed at $t=0$ to a strong pump field and a weak probe field each tuned close to resonance with one of two coupled transitions. As expected, we found that all transient probe spectra ultimately evolved to the well-known steady-state Autler-Townes doublet structure.[13] However, we found that transient probe spectra in three-level atoms may differ dramatically for different initial atomic conditions. In particular, the transient probe spectra arising from atoms initially prepared in a pure dressed state and in a superposition of dressed states are quite different. Experimental verification of our predictions has been achieved recently.[14] We also calculated the transient spectrum of resonance fluorescence arising from strongly driven two-level atoms when the atoms are initially prepared in pure dressed states of the atom-field Hamiltonian.[15] Again, it is quite different from transient fluorescence spectra when atoms are initially in their ground states (superposition of dressed states).[16] It is our purpose in this paper to study the transient probe spectra of driven two-level atoms in a homogeneously broadened medium We find that the transient probe spectra considered here also differ dramatically for atoms initially prepared in a pure dressed state and in a superposition of dressed states. Moreover, novel spectral components can be observed in the transient regime.

A qualitative discussion of transient probe spectra with a strong pump field is presented in Sec. II. We develop the general formalism and give expressions for the probe spectra in Sec. III. In Sec. IV we study the effects of initial conditions on transient probe spectra in the strong-pump-field case. The transient buildup of a collision-induced narrow hole in the weak-pump-field case is studied in Sec. V, while the transient buildup of collision-induced dispersion structure in the large pump detuning case is viewed in Sec. VI.

II. QUALITATIVE DESCRIPTION OF TRANSIENT PROBE SPECTRA IN A STRONGLY DRIVEN TWO-LEVEL ATOM

In studying the strong interaction of atoms with laser fields, a dressed-atom picture (DAP) provides a good approach to the problem and allows one to gain physical insight.[4,12] Our calculation for the transient pump-probe

problem in a two-level atom is carried out with the use of a *classical* description of the laser fields. The corresponding physical interpretation, however, is conveniently explained in a conventional DAP.[4] In the conventional DAP, a fully quantum-mechanical description of the atom-field interaction is used. For a two-level atom interacting with a strong, nearly resonant monochromatic laser field (pump field), the energy-level structure in the conventional DAP appears as an infinite set of equally spaced doublets. The dressed states $|A_n\rangle$ and $|B_n\rangle$ in a given doublet are linear combinations of the states $|1,n\rangle$ and $|2,n-1\rangle$, where n indicates the photon number for the field and 1 and 2 refer to atomic states. The energy difference between the center of two neighboring dressed-state doublets is $\hbar\Omega_1$, where Ω_1 is the laser frequency. Corresponding to the classical laser fields used in the actual calculation, the mean photon number $\bar{n}$ is much larger than the width Δn of photon-number distribution, which, in turn, is much larger than 1,

$$\bar{n} \gg \Delta n \gg 1 . \tag{2.1}$$

Consequently, for photon number n within the width Δn of its distribution centered at $\bar{n}$, the energy splitting between the two states $|B_n\rangle$ and $|A_n\rangle$ within each doublet is almost independent of n and can be identified as $\hbar\omega_{BA}=\hbar(\chi_1^2+\Delta_1^2)^{1/2}$, where $\Delta_1=\omega_{21}-\Omega_1$ is the atom-field detuning (ω_{21} is the atomic transition frequency), $\chi_1=\mathbf{p}_{21}\cdot\mathcal{E}_1/\hbar$ (chosen to be real and positive) is the Rabi frequency associated with a classical laser field of the form $\mathcal{E}_1\exp[-i(\Omega_1 t-\mathbf{k}_1\cdot\mathbf{r}+\phi_1)]/2+\text{c.c.}$ and has been chosen to be real and positive, and $\mathbf{p}_{21}$ is an atomic dipole matrix element. It is assumed that the frequency splitting ω_{BA} of two states $|B_n\rangle$ and $|A_n\rangle$ is much larger than both the population relaxation rate of state 2, γ_2, and the coherence relaxation rate of the atom, γ_{21}. One need only consider the transition between two adjacent doublets to deduce the probe-absorption spectrum. Because of mixing of atomic states in each of the dressed states, all transitions connecting the two doublets are allowed.

In the DAP, the probe absorption spectrum arises from transitions of the probe field between dressed states. In steady state, probe absorption is proportional to both the transition rate between two dressed states in two neighboring doublets and the population difference between the lower and upper states. The relative populations of the two states within a doublet depends on the pump-field strength and atom–pump-field detuning Δ_1. On the other hand, the populations of states $|A_n\rangle$ and $|B_n\rangle$ vary negligibly with n (i.e., $\rho_{A_{n-1}A_{n-1}}\approx\rho_{A_nA_n}\approx\rho_{A_{n+1}A_{n+1}}$, $\rho_{B_{n-1}B_{n-1}}\approx\rho_{B_nB_n}\approx\rho_{B_{n+1}B_{n+1}}$). When the pump field is tuned below the atomic transition frequency ($\Delta_1>0$), there is more population in the lower dressed state of a doublet than in the upper one in steady state. Furthermore, the transition rate between states $|A_n\rangle$ and $|B_{n+1}\rangle$ is larger than that between states $|B_n\rangle$ and $|A_{n+1}\rangle$ when $\Delta_1>0$. Consequently, the steady-state probe spectrum for $\Delta_1>0$ consists of one absorption component at $\Omega_2=\Omega_1+\omega_{BA}$ and one emission component at $\Omega_2=\Omega_1-\omega_{BA}$, with the absorption component having a larger intensity than the emission one, as illustrated in Fig. 1(a). In the limit $|\Delta_1|\gg\chi_1$ the absorption component corresponds simply to the linear absorption of the probe. When the pump field is tuned exactly on resonance with the atomic transition ($\Delta_1=0$), the lower and upper dressed states have the same population in steady state (all transition rates between dressed states are also the same). Consequently, in the so-called secular approximation[4] of the dressed-atom theory in which the probe spectrum is viewed solely as arising from transitions between pairs of dressed states, the probe spectrum vanishes owing to the equal populations of the dressed states [Fig. 1(b)]. This result is true only to order γ_{21}/ω_{BA}—a calculation to first order in γ_{21}/ω_{BA} leads to a complicated emission-absorption spectrum.

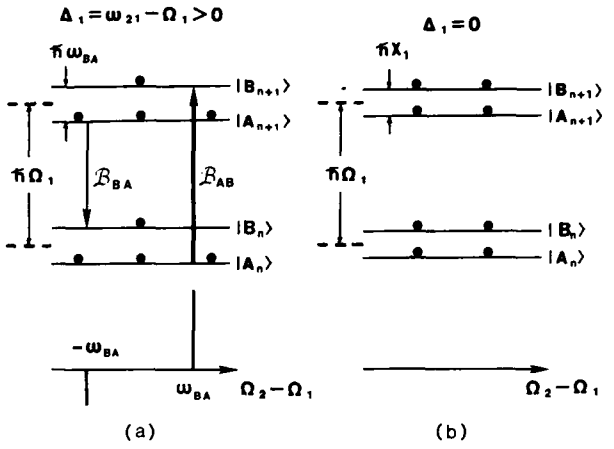

FIG. 1. Steady-state probe transitions in the conventional DAP and the corresponding absorption spectrum of a two-level atom for strong excitation (a) by an off-resonant pump field $\Delta_1>0$ and (b) by an exactly resonant pump field. In (b) all dressed states have the same populations in steady state. A thicker transition line indicates a larger transition rate ($\mathcal{B}_{\mu\nu}$), which are related to transition matrix elements.

The transient spectra must evolve to these steady-state distributions. As has been noted previously,[12,14,15] the transient probe spectra in a strongly driven two-level atom may be strongly influenced by the initial conditions of dressed states. We consider two kinds of initial conditions: (a) atoms initially prepared in pure dressed states and (b) atoms initially in their ground state. Under appropriate methods, pure-dressed-state initial condition can be achieved.[12,17–19] Since the steady-state probe-absorption spectra display different structure for off-resonant and resonant pump fields, we discuss the transient probe spectra for the two cases independently.

A. Off-resonant pump field $\Delta_1\neq 0$

For an off-resonant pump field, atoms prepared initially in the lower dressed state $|A_n\rangle$ and in the upper dressed state $|B_n\rangle$ need to be considered. For $\Delta_1>0$ and atoms prepared initially in the lower dressed state

$|A_n\rangle$ [i.e., $\Sigma_n \rho_{A_n A_n}(0)=1$, $\rho_{B_n B_n}(0)=\rho_{A_n B_n}(0)=0$], transient probe spectrum at early times consists of an absorption component at $\Omega_2=\Omega_1+\omega_{BA}$ and an emission component at $\Omega_2=\Omega_1-\omega_{BA}$ [see Fig. 2(a)]. As in the steady-state limit, the emission component is smaller than the absorption component in the transient regime. This result can be attributed to the fact that dressed-state preparation in state $|A_n\rangle$ for $\Delta_1>0$ corresponds to more population in bare (atomic) state 1 than bare state 2. For $\Delta_1>0$ and atoms prepared initially in the upper dressed state $|B_n\rangle$ [i.e., $\Sigma_n \rho_{B_n B_n}(0)=1$, $\rho_{A_n A_n}(0)=\rho_{A_n B_n}(0)=0$], the transient probe spectrum at early times consists of an emission component at $\Omega_2=\Omega_1+\omega_{BA}$ and an absorption component at $\Omega_2=\Omega_1-\omega_{BA}$ [see Fig. 2(b)]. In contrast to the steady-state limit, however, the emission component is *larger* than the absorption component. The fact that emission is larger than absorption at early times can be attributed to the fact that dressed-state preparation in state $|B_n\rangle$ for $\Delta_1>0$ corresponds to more population in bare state 2 than in bare state 1. As time goes on, the dressed-state populations change as a result of atomic relaxation and optical pumping, eventually going over into the steady-state limit. Consequently, the initial emission component at $\Omega_2=\Omega_1+\omega_{BA}$ becomes an absorption component, while the initial absorption component at $\Omega_2=\Omega_1-\omega_{BA}$ becomes an emission component. (The central component at $\Omega_2=\Omega_1$ is always absent because of the nearly equal populations of dressed states $|A_n\rangle$ and $|A_{n+1}\rangle$, and $|B_n\rangle$ and $|B_{n+1}\rangle$.)

In Fig. 3 we show calculated transient probe spectra at the three dressed-state transition frequencies for parameters $\chi_1=20\gamma_2$, $\Delta_1=0.3\chi_1$, $\gamma_{21}=\gamma_2/2$ and initial conditions (a) $\sum_n \rho_{A_n A_n}(0)=1$ and (b) $\sum_n \rho_{B_n B_n}(0)=1$. (Calculations are presented in Secs. III and IV.) The components build up to their steady-state values without significant oscillation. The absence of large-scale oscillation can be attributed to the absence of coherence in the initial condition, $\rho_{A_n B_n}(0)=0$, as will become clear later. It is also related to the fact that pure-dressed-state preparation corresponds to the situation that the Bloch vector $\mathbf{B}=(u,v,w)$ is initially parallel (or antiparallel) to the driving field vector $\mathbf{\Omega}_B=(-\chi_1,0,\Delta_1)$, where u, v, and w are related to atomic density matrix elements $\tilde{\rho}_{ij}$ in the pump-field–interaction representation[20] by

$$\begin{aligned} u &= \tilde{\rho}_{12}+\tilde{\rho}_{21}\ , \\ v &= i(\tilde{\rho}_{21}-\tilde{\rho}_{12})\ , \\ w &= \tilde{\rho}_{22}-\tilde{\rho}_{11}\ , \\ \tilde{\rho}_{11}+\tilde{\rho}_{22} &= 1\ . \end{aligned} \tag{2.2}$$

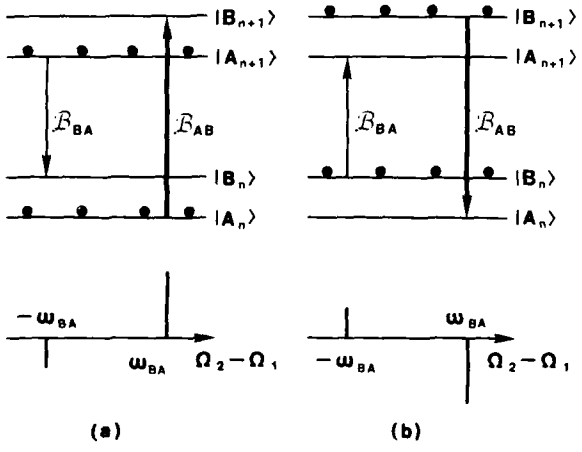

FIG. 2. Probe transitions and the corresponding absorption spectrum of a two-level atom at times immediately following a sudden excitation by a strong, off-resonant laser field $\Delta_1>0$ for atoms initially prepared (a) in the lower dressed state $|A_n\rangle$ and (b) in the upper dressed state $|B_n\rangle$. Thicker transition lines indicate larger transition rates.

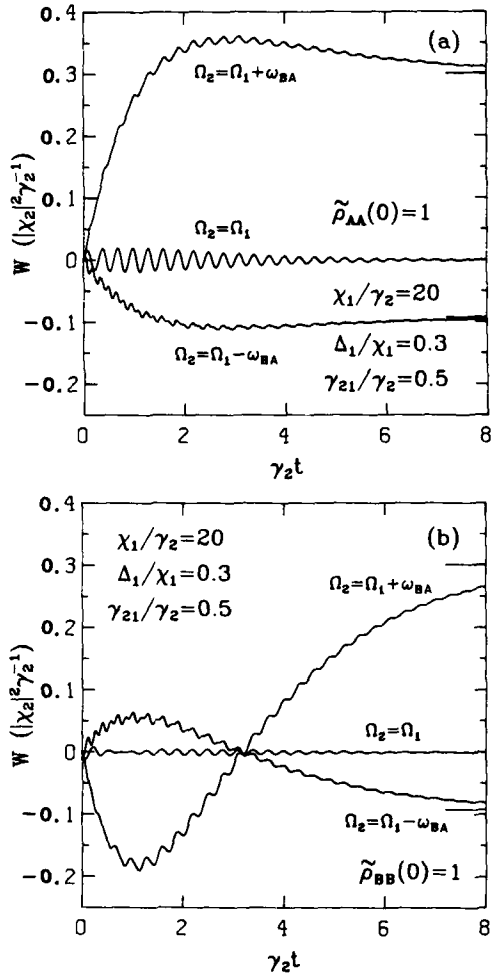

FIG. 3. Transient probe absorption at the three dressed-state transition frequencies $\Omega_2=\Omega_1\pm\omega_{BA}$ and $\Omega_2=\Omega_1$ as a function of $\gamma_2 t$ for an off-resonant pump field with $\chi_1/\gamma_2=20$, $\Delta_1/\chi_1=0.3$, $\gamma_{21}=\gamma_2/2$ and atoms initially prepared (a) in the lower dressed state $|A_n\rangle$, i.e., $\tilde{\rho}_{AA}(0)=\sum_n \rho_{A_n A_n}(0)=1$, and (b) in the upper dressed state $|B_n\rangle$, i.e., $\tilde{\rho}_{BB}(0)=\sum_n \rho_{B_n B_n}(0)=1$, where $\tilde{\rho}_{\mu\nu}$ and $\rho_{\mu_n \nu_{n'}}$ are the semiclassical and conventional dressed-state density matrix elements, respectively. The short lines on the right-hand side indicate the steady-state values, which are independent of initial conditions.

Since the Bloch vector satisfies the equation $d\mathbf{B}/dt=\mathbf{\Omega}_B\times\mathbf{B}=0$, the Bloch vector $\mathbf{B}$ is "locked" to the driving vector $\mathbf{\Omega}_B$ and does not precess as it approaches its steady-state value. The small oscillations appearing in Fig. 3 arise from nonsecular contributions of order γ_2/χ_1 (see Sec. IV B). As the ratio χ_1/γ_2 increases, the amplitude of the oscillations decreases.

For an atom initially in the ground state 1, $\tilde{\rho}_{11}(0)=1$, the initial condition corresponds to the superposition of dressed states $\rho_{A_nA_n}(0)\neq 0$, $\rho_{B_nB_n}(0)\neq 0$, $\rho_{A_nB_n}(0)\neq 0$. The coherence $\rho_{A_nB_n}(0)\neq 0$ leads to oscillations in the buildup of the absorption and emission component as well as a transient oscillatory probe absorption centered at $\Omega_2=\Omega_1$. The central component at $\Omega_2=\Omega_1$ appears for such an initial condition even though the populations of states $|\mu_n\rangle$ and $|\mu_{n+1}\rangle$ $(\mu=A,B)$ are always almost identical in the transient regime. The transient probe spectrum at early times is illustrated in Fig. 4. The central component is unusual in that it never appears in the steady-state spectrum. In Fig. 5 we display calculated transient buildup of probe spectral peaks with the same parameters as in Fig. 3 for the initial condition $\tilde{\rho}_{11}(0)=1$. In this case, spectral components approach their steady-state values in an oscillatory fashion. This oscillation can be viewed as quantum beats from the dressed states. In terms of the Bloch vector picture, it is related to the precession of the Bloch vector $\mathbf{B}$ around the driving field vector $\mathbf{\Omega}_B=(-\chi_1,0,\Delta_1)$. One interesting feature is the alternative absorption and amplification of the probe field in the central component $\Omega_2=\Omega_1$.

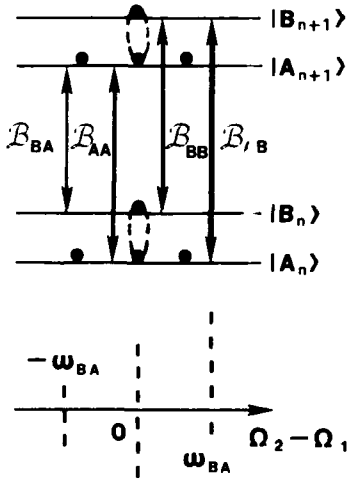

FIG. 4. Probe transitions and the corresponding absorption spectrum of a two-level atom at times immediately following a sudden excitation by a strong, off-resonant laser field $\Delta_1>0$ for atoms initially prepared in a superposition of dressed states. Thicker transition lines indicate larger transition rates ($\mathcal{B}_{\mu\nu}$). Dashed lines indicate oscillating spectral components.

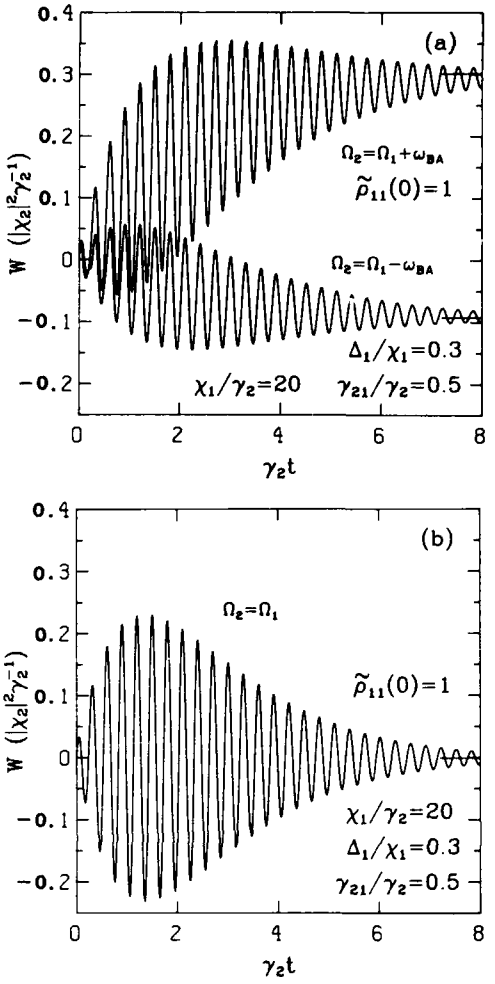

FIG. 5. Transient buildup of the three probe absorption peaks as a function of $\gamma_2 t$ for an off-resonant pump field with $\chi_1/\gamma_2=20$, $\Delta_1/\chi_1=0.3$, $\gamma_{21}=\gamma_2/2$ and atoms initially in the ground state 1, i.e., $\tilde{\rho}_{11}(0)=1$. Two side components at $\Omega_2=\Omega_1\pm\omega_{BA}$ are displayed in (a) while the central component at $\Omega_2=\Omega_1$ is shown in (b). The short lines on the right-hand side indicate the steady-state values.

B. Resonant pump field $\Delta_1=0$

For a resonant pump field, all transition rates connecting two neighboring pairs of dressed states are equal. Consequently, absorption and emission components have the same intensity for atoms prepared initially in a pure dressed state [see Fig. 6(a)]. The absorption and emission components in the resonant pump field case appear in the transient regime only. As the dressed-state populations evolve to their steady-state values, the absorption and emission components vanish, as shown in Fig. 1(b).

If the atom is initially in the ground state 1, $\tilde{\rho}_{11}(0)=1$ [i.e., $\rho_{A_nA_n}(0)=\rho_{B_nB_n}(0)=-\rho_{A_nB_n}(0)$ and $\sum_n\rho_{A_nA_n}(0)=\frac{1}{2}$], the transient spectrum consists entirely of oscillatory components centered at zero absorption since dressed states $|A_n\rangle$ and $|B_n\rangle$ now are equally populated [see Fig. 6(b)]. As the dressed-state coherence de-

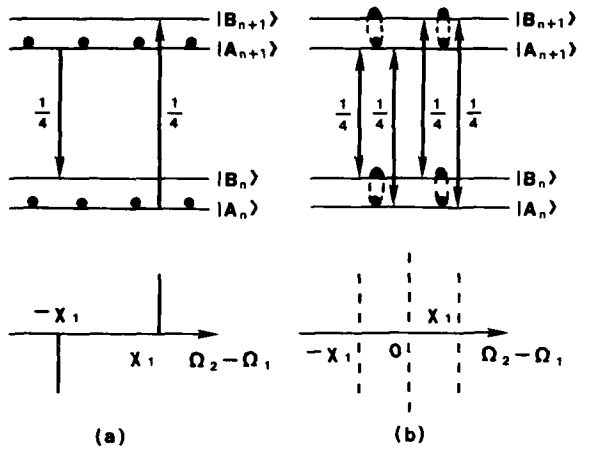

FIG. 6. Probe transitions and the corresponding absorption spectrum of a two-level atom at times immediately following a sudden excitation by a strong, resonant laser field for atoms initially prepared (a) in the lower dressed state $|A_n\rangle$ and (b) in a superposition of dressed states. All transition rates between dressed states are the same ($\mathcal{B}_{\mu\nu}=\frac{1}{4}$). Dashed lines indicate oscillating spectral components.

cays away, all three components vanish.

We show calculated transient behavior of the probe spectral peaks for parameters $\chi_1=20\gamma_2$, $\gamma_{21}=\gamma_2/2$ for initial conditions (a) $\sum_n \rho_{A_n A_n}(0)=1$ and (b) $\tilde{\rho}_{11}(0)=1$ in Fig. 7. The qualitative features of the probe spectra discussed above are clearly illustrated in this figure. Small oscillations seen in Fig. 7(a) will vanish as the ratio χ_1/γ_2 increases.

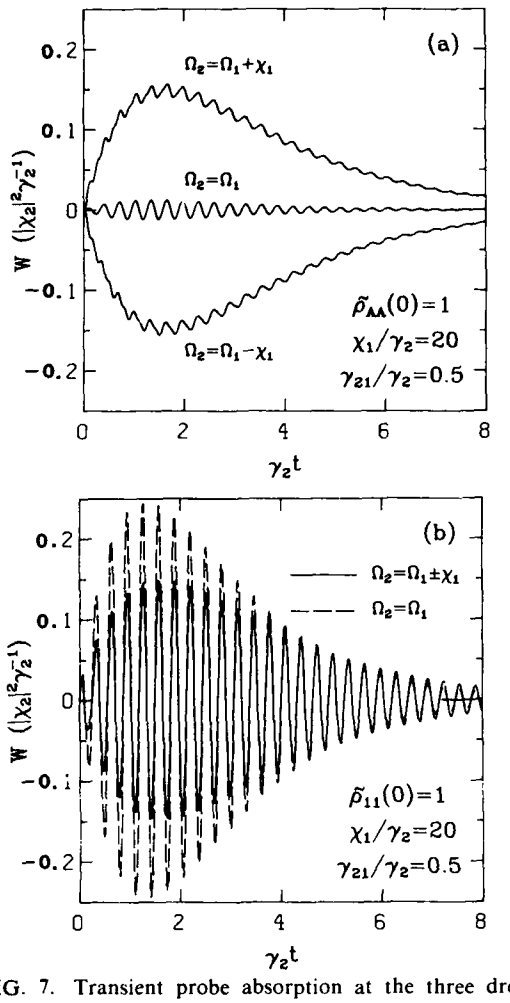

FIG. 7. Transient probe absorption at the three dressed-state transition frequencies $\Omega_2=\Omega_1\pm\chi_1$ and $\Omega_2=\Omega_1$ as a function of $\gamma_2 t$ for a resonant pump field with $\chi_1/\gamma_2=20$, $\gamma_{21}=\gamma_2/2$ and atoms initially prepared (a) in the lower dressed state $|A_n\rangle$, i.e., $\tilde{\rho}_{AA}(0)=\sum_n \rho_{A_n A_n}(0)=1$, and (b) in the ground state 1, $\tilde{\rho}_{11}(0)=1$. In (b), the probe absorption is the same (solid line) at the two side components $\Omega_2=\Omega_1\pm\chi_1$ owing to the resonant pump field and the symmetry in the dressed-state initial condition. Their steady-state value (short line) is indistinguishable from that of the component at $\Omega_2=\Omega_1$, both of which are very close to zero.

III. GENERAL FORMALISM AND SOLUTION

We consider a composite classical laser field of the form

$$\mathbf{E}(\mathbf{r},t)=\tfrac{1}{2}\{\mathcal{E}_1\exp[-i(\Omega_1 t-\mathbf{k}_1\cdot\mathbf{r}+\phi_1)] + \mathcal{E}_2\exp[-i(\Omega_2 t-\mathbf{k}_2\cdot\mathbf{r}+\phi_2)]\}+\text{c.c.} \tag{3.1}$$

interacting with two-level atoms in a homogeneously broadened medium (for example, in an atomic beam such that $\mathbf{k}_1\cdot\mathbf{v}=\mathbf{k}_2\cdot\mathbf{v}=0$, where $\mathbf{v}$ is atomic velocity). The frequency separation between levels 2 and 1 is ω_{21}, and level 2 decays back to the ground state 1 at spontaneous rate γ_2. In a pump-field–interaction representation[20] and bare-atom picture, the density matrix equation of the system can be written as

$$\frac{d\tilde{\rho}}{dt}=[L+S(t)]\tilde{\rho}\,, \tag{3.2}$$

where a density-matrix-element column vector $\tilde{\rho}$ is defined as

$$\tilde{\rho}=\begin{bmatrix}\tilde{\rho}_{11}\\ \tilde{\rho}_{22}\\ \tilde{\rho}_{12}\\ \tilde{\rho}_{21}\end{bmatrix}, \tag{3.3}$$

and matrices L and $S(t)$ are defined by

$$L=\begin{bmatrix}0 & \gamma_2 & -\frac{1}{2}i\chi_1 & \frac{1}{2}i\chi_1\\ 0 & -\gamma_2 & \frac{1}{2}i\chi_1 & -\frac{1}{2}i\chi_1\\ -\frac{1}{2}i\chi_1 & \frac{1}{2}i\chi_1 & -\gamma_{21}+i\Delta_1 & 0\\ \frac{1}{2}i\chi_1 & -\frac{1}{2}i\chi_1 & 0 & -\gamma_{21}-i\Delta_1\end{bmatrix}, \tag{3.4a}$$

$$S(t)=\begin{vmatrix} 0 & 0 & -\frac{1}{2}i\tilde{\chi}_2 e^{-i\delta t} & \frac{1}{2}i\tilde{\chi}_2^* e^{i\delta t} \\ 0 & 0 & \frac{1}{2}i\tilde{\chi}_2 e^{-i\delta t} & -\frac{1}{2}i\tilde{\chi}_2^* e^{i\delta t} \\ -\frac{1}{2}i\tilde{\chi}_2^* e^{i\delta t} & \frac{1}{2}i\tilde{\chi}_2^* e^{i\delta t} & 0 & 0 \\ \frac{1}{2}i\tilde{\chi}_2 e^{-i\delta t} & -\frac{1}{2}i\tilde{\chi}_2 e^{-i\delta t} & 0 & 0 \end{vmatrix} , \tag{3.4b}$$

with

$$\chi_1=\mathbf{p}_{21}\cdot\mathcal{E}_1/\hbar , \tag{3.5a}$$

$$\chi_2=\mathbf{p}_{21}\cdot\mathcal{E}_2/\hbar , \tag{3.5b}$$

$$\tilde{\chi}_2=\chi_2\exp[i(\mathbf{k}_2\cdot\mathbf{r}-\phi_2)-i(\mathbf{k}_1\cdot\mathbf{r}-\phi_1)] , \tag{3.5c}$$

$$\Delta_1=\omega_{21}-\Omega_1 , \tag{3.6a}$$

and

$$\delta=\Omega_2-\Omega_1 , \tag{3.6b}$$

where $\mathbf{p}_{21}$ ($=\langle 2|\mathbf{p}|1\rangle$) is the dipole moment between levels 2 and 1, and χ_1 has been chosen to be real and positive. Note that, for constant pump field $\mathcal{E}_1$ and probe field $\mathcal{E}_2$ considered in this paper, L is a constant matrix while S is time dependent.

It is assumed that the probe field is sufficiently weak so that its Rabi frequency satisfies the inequality

$$|\chi_2| \ll \gamma_2,\gamma_{21},\chi_1 . \tag{3.7}$$

By using Eq. (3.2) and expanding $\tilde{\rho}$ as

$$\tilde{\rho}=\tilde{\rho}^{(0)}+\tilde{\rho}^{(1)}+\cdots , \tag{3.8}$$

where $\tilde{\rho}^{(m)}$ is of order $|\chi_2|^m$, one finds that $\tilde{\rho}^{(0)}$ and $\tilde{\rho}^{(1)}$ satisfy equations

$$\frac{d\tilde{\rho}^{(0)}}{dt}=L\tilde{\rho}^{(0)} , \tag{3.9a}$$

$$\frac{d\tilde{\rho}^{(1)}}{dt}=L\tilde{\rho}^{(1)}+S\tilde{\rho}^{(0)} . \tag{3.9b}$$

We limit the solution to terms of order $|\chi_2|$. Since L is a constant matrix and the initial condition is $\tilde{\rho}^{(j)}(0)=\delta_{j0}\tilde{\rho}(0)$, the formal solution of Eqs. (3.9) are

$$\tilde{\rho}^{(0)}(t)=e^{Lt}\tilde{\rho}(0)=Ve^{\Lambda t}V^{-1}\tilde{\rho}(0) , \tag{3.10a}$$

$$\tilde{\rho}^{(1)}(t)=\int_0^t e^{L(t-t')}S(t')\tilde{\rho}^{(0)}(t')dt' = V\int_0^t e^{\Lambda(t-t')}V^{-1}S(t')Ve^{\Lambda t'}dt'V^{-1}\tilde{\rho}(0) , \tag{3.10b}$$

where Λ is a diagonal matrix with diagonal matrix elements being eigenvalues λ_j of matrix L,

$$\Lambda_{ij}=\delta_{ij}\lambda_j , \tag{3.11a}$$

and V is a matrix whose columns correspond to the eigenvector $\mathbf{y}^{(j)}$ of L associated with eigenvalue λ_j,

$$V=(\mathbf{y}^{(1)},\mathbf{y}^{(2)},\mathbf{y}^{(3)},\mathbf{y}^{(4)}) . \tag{3.11b}$$

The density matrix element $\tilde{\rho}_{21}^{(1)}$ can be written in the form

$$\tilde{\rho}_{21}^{(1)}(t)=\tilde{\chi}_2 H(t)e^{-i\delta t}+\tilde{\chi}_2^* Q(t)e^{i\delta t} , \tag{3.12}$$

where $H(t)$ and $Q(t)$ are two time-dependent functions and neither $H(t)$ nor $Q(t)$ depends on $\mathbf{k}_1$ or $\mathbf{k}_2$. The transient probe absorption can be identified by examining the density matrix element ρ_{21},

$$\rho_{21}(t)=\tilde{\rho}_{21}^{(0)}(t)\exp[-i(\Omega_1 t-\mathbf{k}_1\cdot\mathbf{r}+\phi)]+\chi_2 H(t)\exp[-i(\Omega_2 t-\mathbf{k}_2\cdot\mathbf{r}+\phi_2)] +\chi_2^* Q(t)\exp\{-i[(2\Omega_1-\Omega_2)t-(2\mathbf{k}_1-\mathbf{k}_2)\cdot\mathbf{r}+2\phi_1-\phi_2]\} . \tag{3.13}$$

One sees that $H(t)$ gives the probe response which propagates in the $\mathbf{k}_1$ direction while $Q(t)$ gives a four-wave-mixing response which propagates in the $2\mathbf{k}_1-\mathbf{k}_2$ direction. Consequently, the probe absorption is identified with $H(t)$ and is proportional to a quantity $W(t)$ defined by

$$W(t)=2\,\mathrm{Im}[\chi_2^*\chi_2 H(t)] . \tag{3.14}$$

The general expression for $H(t)$ is quite complicated. We are interested in the solution of the problem when

$$\omega_{BA}\equiv(\chi_1^2+\Delta_1^2)^{1/2}\gg\gamma_2,\gamma_{21} , \tag{3.15}$$

i.e., in the case of a strong pump field or large pump detuning or both. To first order in γ_2/ω_{BA} or γ_{21}/ω_{BA}, we get from Eqs. (3.10) and (3.12)

$$H(t)=\frac{1}{2}\sum_{l=-1}^{1}\sum_{m=-1}^{2}C_{lm}Z_{lm}(t) , \tag{3.16}$$

where the $Z_{lm}(t)$ give various transient resonant structures and C_{lm} give the corresponding weights. Explicit expressions for $Z_{lm}(t)$ and C_{lm} are presented in Appendix A.

The transient probe spectra have the property

$$W(t;\delta,\Delta_1 u(0),v(0),w(0)) = W(t;-\delta,-\Delta_1,-u(0),v(0),w(0)) , \tag{3.17}$$

where u, v, and w are defined in Eqs. (2.2). Consequently, one can restrict the study of probe-absorption spectra to positive Δ_1.

In *steady state*, it follows from Eqs. (3.14), (3.16), and (A1)–(A6) that

$$W(\infty)=|\chi_2|^2\,\mathrm{Im}\left[\frac{C_{-1,0}}{\Gamma_2-i(\delta+\omega_{BA})}+\frac{C_{00}}{\Gamma_1-i\delta}+\frac{C_{10}}{\Gamma_2-i(\delta-\omega_{BA})}\right], \tag{3.18}$$

where

$$\begin{pmatrix}C_{-1,0}\\C_{00}\\C_{10}\end{pmatrix}=ia\cos\theta\begin{pmatrix}-\sin^4(\frac{1}{2}\theta)\\0\\\cos^4(\frac{1}{2}\theta)\end{pmatrix}+\tfrac{1}{2}a(\epsilon_{21}-\epsilon_0\cos^2\theta)\sin^2\theta\begin{pmatrix}-\sin^2(\frac{1}{2}\theta)\\-\cos\theta\\\cos^2(\frac{1}{2}\theta)\end{pmatrix}, \tag{3.19}$$

$$\Gamma_1=\gamma_{21}+\gamma_0\cos^2\theta\,, \tag{3.20a}$$

$$\Gamma_2=\tfrac{1}{2}(\gamma_2+\gamma_{21}-\gamma_0\cos^2\theta)\,, \tag{3.20b}$$

$$\gamma_0=\gamma_2-\gamma_{21}\,, \tag{3.20c}$$

$$\cos\theta=\Delta_1/\omega_{BA},\quad \sin\theta=\chi_1/\omega_{BA},\quad 0\le\theta\le\pi\,, \tag{3.21}$$

$$a=[\cos^2\theta+(\gamma_{21}/\gamma_2)\sin^2\theta]^{-1}=\gamma_2/\Gamma_1\,, \tag{3.22}$$

$$\epsilon_2=\gamma_2/\omega_{BA},\quad \epsilon_{21}=\gamma_{21}/\omega_{BA},\quad \epsilon_0=\gamma_0/\omega_{BA}\,. \tag{3.23}$$

The quantity Γ_2 is the relaxation rate of dressed-state density matrix elements $\rho_{A_nB_n}$, and Γ_1 is that of $\rho_{A_nA_n}-\rho_{B_nB_n}$. As expected, in steady state $W(\infty)$ is independent of initial atomic conditions. It obeys the symmetry relation

$$W(\infty;\delta,\Delta_1)=W(\infty;-\delta,-\Delta_1)\,. \tag{3.24}$$

Clearly, the steady-state probe spectrum is symmetric about $\delta=0$ only if $\Delta_1=0$.

In the case of resonant pump field ($\Delta_1=0$), analytic expressions for W to all orders in γ_2/χ_1 and γ_{21}/χ_1 can be obtained and are presented in Appendix B.

IV. EFFECTS OF INITIAL ATOMIC CONDITIONS ON TRANSIENT PROBE SPECTRA WITH A STRONG PUMP FIELD

In Sec. III results are given in terms of bare-state density matrix elements. To discuss the transient spectra with a strong pump field, it is convenient to introduce dressed-state density matrix elements. There are two kinds of dressed states. One is the conventional dressed states[4,21] in which laser fields are quantized, the other is semiclassical dressed states[18,22] in which the laser fields are treated classically. A physical interpretation of probe-absorption spectra is conveniently given in the conventional DAP, as discussed in Sec. II. The conventional dressed-state density matrix elements are related to the bare-state ones through the semiclassical dressed-state density matrix elements. The semiclassical dressed-state density matrix elements are related to the bare-state ones by[23]

$$\begin{aligned}\tilde\rho_{AA}&=\tfrac{1}{2}(1+u\sin\theta-w\cos\theta)\,,\\ \tilde\rho_{BB}&=\tfrac{1}{2}(1-u\sin\theta+w\cos\theta)\,,\\ \tilde\rho_{AB}&=\tilde\rho^{\,*}_{BA}=\tfrac{1}{2}(u\cos\theta+iv+w\sin\theta)\,,\end{aligned} \tag{4.1}$$

where θ is defined in Eq. (3.21).

The classical pump field given in Eq. (3.1) can be represented in the conventional DAP by a coherent state[24] $|\alpha\rangle$ in the field mode specified by the wave vector $\mathbf{k}_1$ of the pump field. Correspondingly, the relation between the semiclassical dressed-state density matrix elements $\tilde\rho_{\mu\nu}$ and the conventional ones $\rho_{\mu_n\nu_{n'}}$ may be approximated as

$$\tilde\rho_{\mu\nu}=\sum_n\rho_{\mu_n\nu_n}\,, \tag{4.2}$$

and[25]

$$\rho_{\mu_n\nu_n}=\tilde\rho_{\mu\nu}\frac{|\alpha|^{2n}}{n!}e^{-|\alpha|^2}\,, \tag{4.3}$$

with $|\alpha|\gg1$ to satisfy Eq. (2.1).

In terms of the initial values for semiclassical dressed-state density matrix elements, the symmetry relation (3.17) can be rewritten as

$$W(t;\delta,\Delta_1,\tilde\rho_{AA}(0),\tilde\rho_{AB}(0))=W(t;-\delta,-\Delta_1,\tilde\rho_{BB}(0),\tilde\rho_{AB}(0))\,. \tag{4.4}$$

The coefficients C_{lm} $(m=-1,1,2)$ of the transient resonant structures $Z_{lm}(t)$ appearing in Eq. (3.16) can also be rewritten by using Eqs. (A2) and (4.1). To lowest nonvanishing order in γ_{21}/ω_{BA}, one finds

$$\begin{pmatrix}C_{-1,2}\\C_{02}\\C_{12}\end{pmatrix}=i[\tilde\rho_{AA}(0)-\tilde\rho_{BB}(0)-a\cos\theta]\times\begin{pmatrix}-\sin^4(\frac{1}{2}\theta)\\-\frac{1}{4}i\epsilon_0\sin^2(2\theta)\\\cos^4(\frac{1}{2}\theta)\end{pmatrix}, \tag{4.5a}$$

$$\begin{pmatrix}C_{11}\\C_{01}\\C_{1,-1}\end{pmatrix}=-i\tilde\rho_{AB}(0)\sin\theta\begin{pmatrix}\cos^2(\frac{1}{2}\theta)\\\sin^2(\frac{1}{2}\theta)\\2i\epsilon_2\cos^6(\frac{1}{2}\theta)\end{pmatrix}, \tag{4.5b}$$

$$\begin{pmatrix}C_{1,1}\\C_{1,-1}\\C_{0,-1}\end{pmatrix}=-i\tilde\rho_{BA}(0)\sin\theta\begin{pmatrix}\sin^2(\frac{1}{2}\theta)\\-2i\epsilon_2\sin^6(\frac{1}{2}\theta)\\\cos^2(\frac{1}{2}\theta)\end{pmatrix}, \tag{4.5c}$$

where ϵ_0 and ϵ_2 are given in Eq. (3.23).

A. Steady-state probe spectrum in and beyond the secular approximation

Before studying transient probe-absorption spectrum, we first reexamine the steady-state probe spectrum. As shown in Eqs. (3.18) and (3.19) the steady-state spectrum is independent of initial atomic conditions. To zeroth order in $\epsilon_{21}=\gamma_{21}/\omega_{BA}$ (secular approximation), it consists of an absorption peak and an emission peak for an off-resonant pump field ($\Delta_1\neq 0$). For a resonant pump field ($\Delta_1=0$), the probe spectrum vanishes to zeroth order in ϵ_{21}. These features are illustrated in Fig. 8, where the spectrum shown for $\Delta_1=0$, although nonvanishing, is smaller than that shown for $\Delta_1\neq 0$ by a factor of order ϵ_{21}.

These features can be explained quantitatively in the conventional DAP (see Fig. 1). We first note that the steady-state density matrix elements in the semiclassical DAP may be obtained from Eqs. (4.1), (2.2), and (3.2)–(3.4) as (to order ϵ_{21})

$$\begin{aligned}&\tilde{\rho}^{(0)}_{AA}(\infty)-\tilde{\rho}^{(0)}_{BB}(\infty)=a\cos\theta\ ,\\ &\tilde{\rho}^{(0)}_{AB}(\infty)=-\tfrac{1}{2}ia\epsilon_{21}\sin\theta\ .\end{aligned}\tag{4.6}$$

The probe transition rate between two dressed states is proportional to the absolute square of the dipole matrix element of the two states,[26]

$$\begin{aligned}|\langle B_{n+1}|\mathbf{p}\cdot\hat{\mathcal{E}}_2|A_n\rangle|^2&=|\mathbf{p}_{21}\cdot\hat{\mathcal{E}}_2|^2\cos^4(\tfrac{1}{2}\theta)\\&\equiv|\mathbf{p}_{21}\cdot\hat{\mathcal{E}}_2|^2\mathcal{B}_{AB}\ ,\\ |\langle A_{n+1}|\mathbf{p}\cdot\hat{\mathcal{E}}_2|B_n\rangle|^2&=|\mathbf{p}_{21}\cdot\hat{\mathcal{E}}_2|^2\sin^4(\tfrac{1}{2}\theta)\\&\equiv|\mathbf{p}_{21}\cdot\hat{\mathcal{E}}_2|^2\mathcal{B}_{BA}\ ,\\ |\langle B_{n+1}|\mathbf{p}\cdot\hat{\mathcal{E}}_2|B_n\rangle|^2&=|\mathbf{p}_{21}\cdot\hat{\mathcal{E}}_2|^2\sin^2(\tfrac{1}{2}\theta)\cos^2(\tfrac{1}{2}\theta)\\&\equiv|\mathbf{p}_{21}\cdot\hat{\mathcal{E}}_2|^2\mathcal{B}_{BB}\ ,\\ |\langle A_{n+1}|\mathbf{p}\cdot\hat{\mathcal{E}}_2|A_n\rangle|^2&=|\mathbf{p}_{21}\cdot\hat{\mathcal{E}}_2|^2\sin^2(\tfrac{1}{2}\theta)\cos^2(\tfrac{1}{2}\theta)\\&\equiv|\mathbf{p}_{21}\cdot\hat{\mathcal{E}}_2|^2\mathcal{B}_{AA}\ ,\end{aligned}\tag{4.7}$$

where $\hat{\mathcal{E}}_2$ is the unit vector of the probe field amplitude $\mathcal{E}_2$ and $\mathcal{B}_{\mu\nu}$ is a dimensionless transition rate between states $|\mu_n\rangle$ and $|\nu_{n+1}\rangle$. We can approximate the transient probe spectrum $W(t)$ as the sum of the secular approximation $W^{(0)}(t)$ to $W(t)$ (of order $|\chi_2|^2\gamma_2^{-1}$) and a first-order correction $W^{(1)}(t)$ (of order $|\chi_2|^2\omega_{BA}^{-1}$),

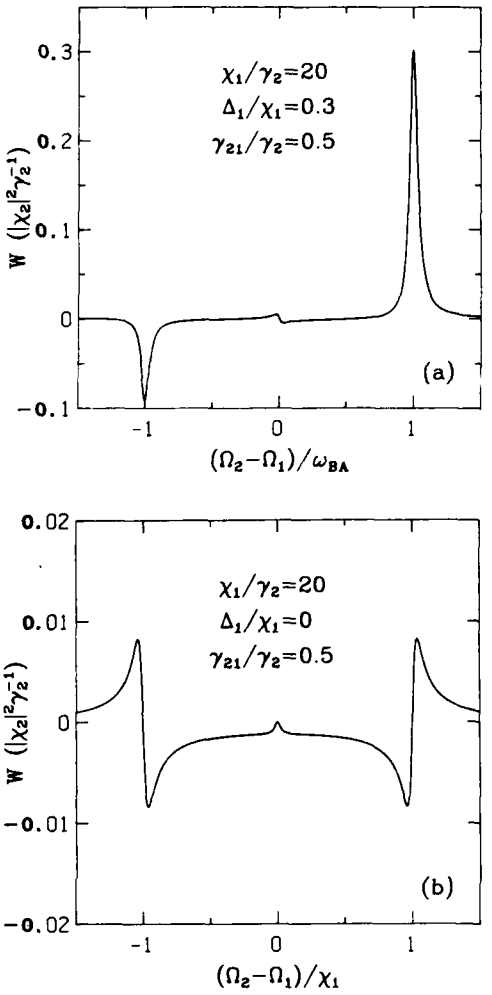

FIG. 8. Steady-state probe absorption spectra for a "closed" two-level atom driven by a strong pump field with $\chi_1/\gamma_2=20$, $\gamma_{21}=\gamma_2/2$ and (a) $\Delta_1=0.3\chi_1$, (b) $\Delta_1=0$. Note that the spectral amplitude is greatly reduced when the pump field is resonant.

$$W(t)\approx W^{(0)}(t)+W^{(1)}(t)\ .\tag{4.8}$$

The steady-state probe-absorption spectrum is given in Eqs. (3.18)–(3.23). Using Eqs. (4.2), (4.6), and (4.7), one can write the contribution in the secular approximation as

$$W^{(0)}(\infty)=|\chi_2|^2\sum_{\mu,\nu=A,B}\sum_n\mathcal{B}_{\mu\nu}\,\mathrm{Re}\frac{\rho^{(0)}_{\mu_n\mu_n}(\infty)-\rho^{(0)}_{\nu_{n+1}\nu_{n+1}}(\infty)}{\Gamma_{\mu\nu}-i(\Omega_2-\omega_{\nu_{n+1}\mu_n})}\ ,\tag{4.9a}$$

and the contribution beyond the secular approximation[27] as[28]

$$W^{(1)}(\infty)=|\chi_2|^2\sum_{\mu,\nu=A,B}\sum_n(\mathcal{B}_{\mu\nu}\mathcal{B}_{\mu'\nu})^{1/2}\,\mathrm{Re}\frac{i\epsilon_0\sin\theta\cos\theta[\rho^{(0)}_{\mu_n\mu_n}(\infty)-\rho^{(0)}_{\mu'_n\mu'_n}(\infty)]-2\rho^{(0)}_{\mu'_n\mu_n}(\infty)}{\Gamma_{\mu\nu}-i(\Omega_2-\omega_{\nu_{n+1}\mu_n})}\ ,$$

$$\mu'=A,B,\quad \mu'\neq\mu\ .\tag{4.9b}$$

where $\Gamma_{AA}=\Gamma_{BB}=\Gamma_1, \Gamma_{AB}=\Gamma_{BA}=\Gamma_2$ [see Eqs. (3.20)], and $\omega_{\nu_{n+1}\mu_n}$ is the frequency difference between dressed states $|\nu_{n+1}\rangle$ and $|\mu_n\rangle$ and takes values Ω_1 or $\Omega_1\pm\omega_{BA}$. Equation (4.9a) is valid to zeroth order in ϵ_{21}. To first order in ϵ_{21} or ϵ_0 atomic relaxation adds three dispersion structures[1] to the steady-state probe spectrum for an off-resonant pump field. The dispersion structures at $\Omega_2=\Omega_1\pm\omega_{BA}$ slightly shift these resonances while that at $\Omega_2=\Omega_1$ may be seen explicitly[3] in Fig. 8(a). For a *resonant* pump field (all dressed-state populations equal), the entire spectrum is of order ϵ_{21} and is made up of two dispersion structures[7] located separately at $\Omega_2=\Omega_1\pm\chi_1$ [Fig. 8(b)], which is related to $\rho^{(0)}_{A_nB_n}(\infty)$ only [see Eq. (4.9b)].

B. Transient buildup of probe spectral peaks in the secular approximation

For the study of transient probe spectra, we consider two kinds of initial conditions—atoms initially prepared (1) in a pure dressed state and (2) in a superposition of dressed states (for example, the ground state 1).

The probe spectral peaks occur at[29] $\delta=\Omega_2-\Omega_1=0, \pm\omega_{BA}$ as can be seen by examining the coefficients C_{lm} [Eqs. (3.19) and (4.5)]. The probe absorption $W(t)$ is of order $|\chi_2|^2\gamma_2^{-1}$ at these frequencies. To this order (i.e., in the secular approximation), the buildup of probe absorption and emission peaks may be obtained from Eqs. (3.14), (3.16), (3.19), (4.5), and (A1) as the sum of a nonoscillatory contribution $\bar{W}(t)$ and oscillatory contribution $\tilde{W}(t)$. For atoms prepared initially in a pure dressed state $|\mu_n\rangle$ ($\mu=A,B$), i.e., $\tilde{\rho}_{\mu\mu}(0)=1$,

$$W^{(0)}(t)=\bar{W}_\mu(t)=\begin{cases}F_\mu(t)\cos^4(\frac{1}{2}\theta), & \delta=\omega_{BA}\\ 0, & \delta=0\\ -F_\mu(t)\sin^4(\frac{1}{2}\theta), & \delta=-\omega_{BA},\end{cases} \tag{4.10}$$

where

$$F_A(t)=|\chi_2|^2\left\{\frac{1-e^{-\Gamma_2 t}}{\Gamma_2}a\cos\theta + \frac{e^{-\Gamma_1 t}-e^{-\Gamma_2 t}}{\Gamma_2-\Gamma_1}(1-a\cos\theta)\right\}, \tag{4.11a}$$

$$F_B(t)=|\chi_2|^2\left\{\frac{1-e^{-\Gamma_2 t}}{\Gamma_2}a\cos\theta - \frac{e^{-\Gamma_1 t}-e^{-\Gamma_2 t}}{\Gamma_2-\Gamma_1}(1+a\cos\theta)\right\}. \tag{4.11b}$$

In the secular approximation the ratio of the peak amplitudes at $\delta=\pm\omega_{BA}$ is independent of time and depends on θ (or Δ_1/χ_1) [see also Figs. 3 and 7(a)].

For atoms initially in the ground state 1, $\tilde{\rho}_{11}(0)=1$ [i.e., $\tilde{\rho}_{AA}(0)=(1+\cos\theta)/2$, $\tilde{\rho}_{BB}(0)=(1-\cos\theta)/2$, $\tilde{\rho}_{AB}(0)=-(\sin\theta)/2$],

$$W^{(0)}(t)=\bar{W}_1(t)+\tilde{W}_1(t), \tag{4.12a}$$

$$\bar{W}_1(t)=\begin{cases}F_1(t)\cos^4(\frac{1}{2}\theta), & \delta=\omega_{BA}\\ 0, & \delta=0\\ -F_1(t)\sin^4(\frac{1}{2}\theta), & \delta=-\omega_{BA},\end{cases} \tag{4.12b}$$

$$\tilde{W}_1(t)=\begin{cases}G_1^{+}(t)\cos^2(\frac{1}{2}\theta), & \delta=\omega_{BA}\\ G_1^{0}(t), & \delta=0\\ G_1^{+}(t)\sin^2(\frac{1}{2}\theta), & \delta=-\omega_{BA},\end{cases} \tag{4.12c}$$

where

$$F_1(t)=|\chi_2|^2\cos\theta\left\{a\frac{1-e^{-\Gamma_2 t}}{\Gamma_2} - (a-1)\frac{e^{-\Gamma_1 t}-e^{-\Gamma_2 t}}{\Gamma_2-\Gamma_1}\right\}, \tag{4.13a}$$

$$G_1^{\pm}(t)=\tfrac{1}{2}|\chi_2|^2\sin^2\theta\frac{e^{-\Gamma_1 t}-e^{-\Gamma_2 t}}{\Gamma_2-\Gamma_1}\cos(\omega_{BA}t), \tag{4.13b}$$

$$G_1^{0}(t)=\tfrac{1}{2}|\chi_2|^2\sin^2\theta te^{-\Gamma_2 t}\cos(\omega_{BA}t). \tag{4.13c}$$

Note that $G_1(t)$ is proportional to $|\tilde{\rho}_{AB}(0)|$, which implies that the transient oscillations can be traced to a nonvanishing initial value for the dressed-state coherence.

When the pump field is exactly resonant, the probe response in the secular approximation takes a much simpler form. To order $|\chi_2|^2\gamma_2^{-1}$, the probe response may be obtained (a) for initial condition $\tilde{\rho}_{AA}(0)=1$ from Eqs. (4.10) and (4.11) as

$$W^{(0)}(t)=\begin{cases}\pm f(t), & \delta=\pm\omega_{BA}\\ 0, & \delta=0\end{cases} \tag{4.14}$$

and (b) for initial condition $\tilde{\rho}_{11}(0)=1$ from Eqs. (4.12) and (4.13) as

$$W^{(0)}(t)=\begin{cases}f(t)\cos(\omega_{BA}t), & \delta=\pm\omega_{BA}\\ \frac{1}{2}|\chi_2|^2te^{-\Gamma_2 t}\cos(\omega_{BA}t), & \delta=0,\end{cases} \tag{4.15}$$

where

$$f(t)=\frac{1}{4}\frac{e^{-\Gamma_1 t}-e^{-\Gamma_2 t}}{\Gamma_2-\Gamma_1}|\chi_2|^2. \tag{4.16}$$

These expressions give a quantitative description (to order $|\chi_2|^2\gamma_2^{-1}$) of transient buildup of the probe spectral peaks, which are displayed in Figs. 3, 5, and 7. The transient behavior of the probe peaks arising from atoms initially in level 1 is accurately represented by the secular approximation $W^{(0)}(t)$ to the total absorption spectrum $W(t)$. For atoms prepared initially in a pure dressed state, however, the contribution $W^{(1)}(t)$ beyond the secular approximation is observable as small oscillations superimposed on the nonoscillatory contribution of $W^{(0)}(t)$.

As discussed qualitatively in Sec. II transient probe spectral components can be viewed in the secular approximation as arising from transitions between dressed

states even in the transient case. We also see above that the nonoscillatory contribution $\bar{W}$ is associated with the population difference between a lower dressed state $|\mu_n\rangle$ and an upper dressed state $|\nu_{n+1}\rangle$, while the oscillatory contribution $\tilde{W}$ is related to the coherence between the dressed states, $\rho_{A_nB_n}(t)$. To gain further physical insight for the transient behavior of the probe spectral peaks, we rewrite their expressions with arbitrary initial conditions in terms of physical quantities of the conventional DAP. We first obtain the semiclassical dressed-state density matrix elements by using Eqs. (4.1), (2.2), and (3.10a) as (to zeroth order in ϵ_{21}),

$$\tilde{\rho}_{AA}^{(0)}(t)-\tilde{\rho}_{BB}^{(0)}(t) =[\tilde{\rho}_{AA}(0)-\tilde{\rho}_{BB}(0)-a\cos\theta]e^{-\Gamma_1 t}+a\cos\theta , \tag{4.17a}$$

$$\tilde{\rho}_{AB}^{(0)}(t)=\tilde{\rho}_{AB}(0)e^{(-\Gamma_2+i\omega_{BA})t} , \tag{4.17b}$$

which are consistent with the steady-state limit of Eq. (4.6). It is then possible to use Eqs. (4.2), (4.7), and (4.17) to recast the peak amplitude of probe component at $\Omega_2=\omega_{\nu_{n+1}\mu_n}$ as (to order $|\chi_2|^2\gamma_2^{-1}$)

$$W^{(0)}(t)=\bar{W}(t)+\tilde{W}(t) , \tag{4.18}$$

$$\bar{W}(t)=|\chi_2|^2\sum_{\mu,\nu}\sum_n \mathcal{B}_{\mu\nu}\int_0^t e^{-\Gamma_{\nu\mu}(t-t')}[\rho_{\mu_n\mu_n}^{(0)}(t')-\rho_{\nu_{n+1}\nu_{n+1}}^{(0)}(t')]dt', \quad \Omega_2=\omega_{\nu_{n+1}\mu_n} , \tag{4.19a}$$

$$\begin{aligned}\tilde{W}(t)&=-2|\chi_2|^2\,\mathrm{Re}\sum_{\mu,\nu}\tilde{\rho}_{\mu\mu'}(t)(\mathcal{B}_{\mu\nu}\mathcal{B}_{\mu'\nu})^{1/2}\int_0^t\exp[-(\Gamma_{\nu\mu'}-\Gamma_{\mu\mu'})(t-t')]dt'\\ &=-|\chi_2|^2\,\mathrm{Re}\sum_{\mu,\nu}\sum_n\int_0^t\{\exp[-(\Gamma_{\nu\mu'}+i\omega_{\mu\mu'})(t-t')](\mathcal{B}_{\mu\nu}\mathcal{B}_{\mu'\nu})^{1/2}\rho_{\mu_n\mu_n'}^{(0)}(t')\\ &\quad+\exp[-(\Gamma_{\nu'\mu}+i\omega_{\nu'\nu})(t-t')](\mathcal{B}_{\mu\nu'}\mathcal{B}_{\mu\nu})^{1/2}\rho_{\nu_{n+1}\nu_{n+1}}^{(0)}(t')\}dt' ,\end{aligned}$$

$$\mu',\nu'=A,B, \quad \mu'\neq\mu, \quad \nu'\neq\nu, \quad \Omega_2=\omega_{\nu_{n+1}\mu_n} , \tag{4.19b}$$

where $\sum_{\mu,\nu}$ implies summation over two transitions for the $\Omega_2=\Omega_1$ component, $\mathcal{B}_{\mu\nu}$ are defined in Eqs. (4.7), $\omega_{AB}=-\omega_{BA}$, and $\omega_{\nu_{n+1}\mu_n}$ has been explained after Eq. (4.9). Equations (4.19) show that, for a transition between two states $|\mu_n\rangle$ and $|\nu_{n+1}\rangle$, (a) the nonoscillatory contribution $\bar{W}(t)$ is still proportional to the transition rate $B_{\mu\nu}$ of the transition but, different from the steady-state limit, it is proportional to time-integrated population difference of the two states, and (b) the amplitude of oscillation from $\tilde{W}(t)$ is proportional to $|\tilde{\rho}_{AB}(0)|$ and $(\mathcal{B}_{\mu\nu}\mathcal{B}_{\mu'\nu})^{1/2}$, where μ' represents the other dressed state in the doublet containing $|\mu_n\rangle$. The nonoscillatory contribution $\bar{W}(t)$ at $\Omega_2=\Omega_1$ always vanishes. The ratio of the nonoscillatory contribution $\bar{W}(t)$ at $\Omega_2=\Omega_1+\omega_{BA}$ to that at $\Omega_2=\Omega_1-\omega_{BA}$ is independent of time and initial conditions and equals $-\mathcal{B}_{AB}/\mathcal{B}_{BA}=-\cot^4(\theta/2)$, the same as in the steady state.

C. Transient probe spectra

A simple quantitative expression (to order $|\chi_2|^2\gamma_2^{-1}$) for the entire transient probe spectrum can also be obtained in terms of physical quantities in the conventional DAP. Using Eqs. (4.2), (4.7), and (4.17), one can recase the general expressions for the transient probe spectra given in Eqs. (3.14), (3.16), (3.19), (4.5), and (A1) in the form

$$\begin{aligned}W^{(0)}(t)=|\chi_2|^2\,\mathrm{Re}\sum_{\mu,\nu=A,B}\sum_n\int_0^t&\exp\{[-\Gamma_{\nu\mu}+i(\Omega_2-\omega_{\nu_{n+1}\mu_n})](t-t')\}\\ &\times\{\mathcal{B}_{\mu\nu}[\rho_{\mu_n\mu_n}^{(0)}(t')-\rho_{\nu_{n+1}\nu_{n+1}}^{(0)}(t')]-(\mathcal{B}_{\mu'\nu}\mathcal{B}_{\mu\nu})^{1/2}\rho_{\mu_n'\mu_n}(t')\\ &-(\mathcal{B}_{\mu\nu}\mathcal{B}_{\mu'\nu'})^{1/2}\rho_{\nu_{n+1}\nu_{n+1}'}(t')\}dt', \quad \mu',\nu'=A,B, \quad \mu'\neq\mu, \quad \nu'\neq\nu .\end{aligned} \tag{4.20}$$

Equation (4.20) is general expressions for transient probe spectra in the secular approximation (i.e., to leading order $|\chi_2|^2\gamma_2^{-1}$) valid for any initial condition.

Equations (4.9) and (4.18)–(4.20) are given in the conventional DAP. Similar expressions in the semiclassical DAP are readily obtained by changing $\omega_{\nu_{n+1}\mu_n}$ to $\omega_{\nu\mu}+\Omega_1$ ($\omega_{AA}=\omega_{BB}=0$) and deleting photon-number subscripts and the summation over n from those expressions of the conventional DAP. The semiclassical version of Eqs. (4.18)–(4.20) can be verified from the first principle if one finds $\tilde{\rho}_{21}^{(1)}$ in the semiclassical DAP.

In the following illustrative examples for transient probe spectra we set $\gamma_{21}=\gamma_2/2$ (no collisions, such as in an atomic beam).

1. *Off-resonant pump field*

We use expressions for probe absorption given in Eqs. (3.14) and (3.16) and Appendix A. The full transient probe absorption spectra for atoms initially in a pure

dressed state are given in Fig. 9 corresponding to the same initial atomic conditions and parameters as in Fig. 3. As is clearly shown in Fig. 9, for atoms initially prepared in a pure *dressed* state, absorption-emission doublet is reached in an essentially nonoscillatory manner. For atoms initially in the ground state, $\tilde{\rho}_{11}(0)=1$, the full transient probe spectrum is given in Fig. 10 corresponding to the same initial atomic condition and parameters as in Fig. 5. One sees that the steady-state spectrum is reached in an oscillatory manner. Moreover, at the center of the probe spectrum $\Omega_2=\Omega_1$, a transient absorption-emission component is produced for atoms initially prepared in a pure atomic state, but not for atoms initially prepared in a pure dressed state. This component is associated with the dressed-state coherence $\tilde{\rho}_{AB}(t)\neq 0$. As implied by Eq. (4.19b), the oscillation of spectral components reflects the oscillation of $\tilde{\rho}_{AB}(t)$, which further indicates[30] the precession of the Bloch vector **B** about the driving vector $\mathbf{\Omega}_B$.

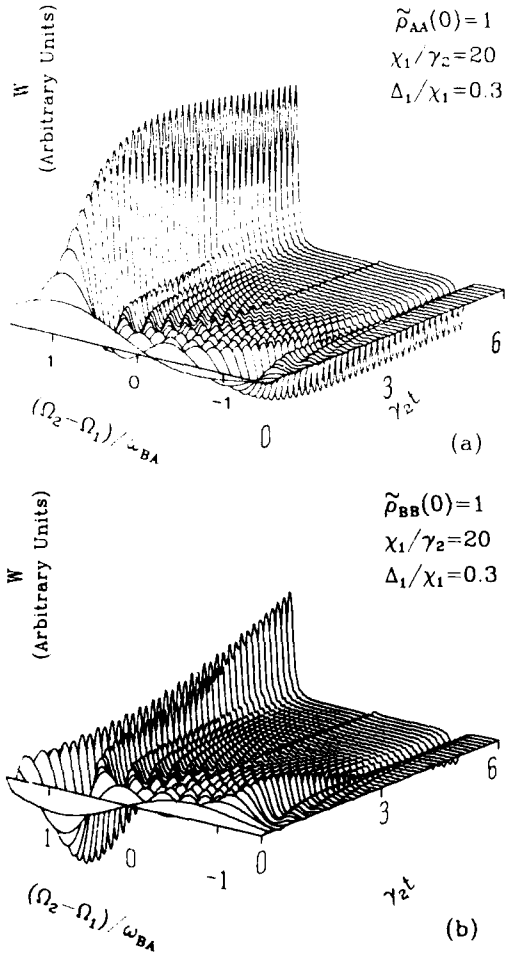

FIG. 9. Transient probe-absorption spectra as a function of both $(\Omega_2-\Omega_1)/\omega_{BA}$ and time $\gamma_2 t$ for the same situation and initial conditions as in Fig. 3, namely, $\chi_1/\gamma_2=20$, $\Delta_1/\chi_1=0.3$, and (a) $\tilde{\rho}_{AA}(0)=1$, (b) $\tilde{\rho}_{BB}(0)=1$. The transient probe response has not yet arrived at its steady-state limit, which is independent of initial conditions and is given in Fig. 8(a).

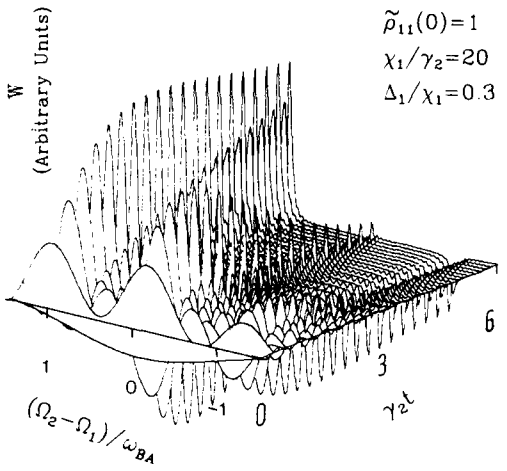

FIG. 10. Same as in Fig. 9 but for a different initial condition, $\tilde{\rho}_{11}(0)=1$. The transient behavior at the peaks is displayed in Fig. 5.

2. *Resonant pump field*

We use the expression given in Appendix B to plot the probe-absorption spectrum for a resonant pump field. The full transient probe-absorption spectra are given in Fig. 11, corresponding to the same initial atomic conditions and parameters as in Fig. 7. One sees that the transient spectrum arising from atoms initially prepared in a pure dressed state is an asymmetric absorption-emission doublet which evolves towards the symmetric steady-state limit shown in Fig. 8(b). The transient spectrum arising from atoms initially prepared in a pure atomic state consists of three oscillatory components centered at frequency $\Omega_2=\Omega_1$, $\Omega_1\pm\chi_1$ which also eventually decay to the steady-state limit [see Fig. 8(b)].

V. EFFECTS OF COLLISIONS ON TRANSIENT PROBE SPECTRA WITH A RESONANT PUMP FIELD

Collisions can add new features to the probe-absorption line shape. To study the effects of collisions in a vapor, the above calculation should be generalized to account for the atomic motion. Although such a generalization is not given in this paper, our results can still be used to investigate a particular collision-induced feature in the probe spectra. This feature occurs in the vicinity of $\Omega_2=\Omega_1$ and is related to a beat frequency created in atomic state populations at frequency $\delta=\Omega_2-\Omega_1$. With allowance for atomic motion δ is replaced by $\delta(\mathbf{v})=(\Omega_2-\mathbf{k}_2\cdot\mathbf{v})-(\Omega_1-\mathbf{k}_1\cdot\mathbf{v})=\delta-(\mathbf{k}_2-\mathbf{k}_1)\cdot\mathbf{v}$. For nearly copropagating waves $\mathbf{k}_2\approx\mathbf{k}_1$ one finds $\delta(\mathbf{v})\approx\delta$ so that atomic motion does not significantly affect the resonant structure at $\delta=0$. Thus, even by studying the "stationary" atom case ($\mathbf{k}_1\cdot\mathbf{v}=\mathbf{k}_2\cdot\mathbf{v}=0$), we will obtain information about collision-induced resonances at $\delta\approx 0$ applicable to atomic vapor.

The probe response in the presence of a "weak" pump field is given by Eqs. (B2)–(B5) in Appendix B for a *resonant* pump field. For the study of collisions, we limit the initial atomic conditions to atoms in the ground state 1. Consequently, the discussion in this section is limited to the initial atomic condition $\tilde{\rho}_{11}(0)=1$, resonant pump field $\Delta_1=0$, and a weak pump field satisfying

$$\chi_1^2 \ll \gamma_2\gamma_{21}, \tfrac{1}{4}(\gamma_{21}-\gamma_2)^2 . \tag{5.1}$$

When inequality (5.1) holds, the steady-state probe-absorption profile with a resonant pump field is [see Eqs. (B2)–(B5)]

$$W(\infty) = |\chi_2|^2 \left| \frac{\gamma_{21}}{\gamma_{21}^2+\delta^2} - \frac{\chi_1^2(\gamma_{21}-\frac{1}{2}\gamma_2)\gamma_2}{\gamma_{21}(\gamma_{21}-\gamma_2)^2(\gamma_2^2+\delta^2)} \right| , \tag{5.2}$$

which is basically a Lorentzian profile of full width at half maximum (FWHM) $2\gamma_{12}$ and height $|\chi_2|^2\gamma_{21}^{-1}$. In the presence of collisions ($\gamma_{21}>\gamma_2/2$), a collision-induced narrow hole of FWHM $2\gamma_2$ and depth $(\chi_1^2/\gamma_2\gamma_{21})(|\chi_2|^2\gamma_{21}^{-1})$ (relative depth $\chi_1^2/\gamma_2\gamma_{21}$) appears at the center of the probe-absorption profile.[5,8,9] In the absence of collisions, this hole is absent and one has the linear absorption profile for the probe (to order $|\chi_2|^2\gamma_{21}^{-1}$).

We plot the full transient probe spectra for parameters (a) $\chi_1=0.1\gamma_{21}$, $\gamma_2=0.1\gamma_{21}$ and (b) $\chi_1=0.07\gamma_{21}$, $\gamma_2=0.05\gamma_{21}$ in Fig. 12. For a clearer illustration, the transient buildup at hole center ($\Omega_2=\Omega_1$) and hole "borders" ($\Omega_2\approx\Omega_1\pm2\gamma_2$) are plotted in Fig. 13. One sees that probe-absorption spectrum is symmetric and the hole is formed after $t\gtrsim\gamma_2^{-1}$. The probe absorption at line center first rises rapidly at rate γ_{21}. Then it relaxes slowly to the steady-state line shape at rate γ_2. The transient probe spectrum can be expressed approximately as

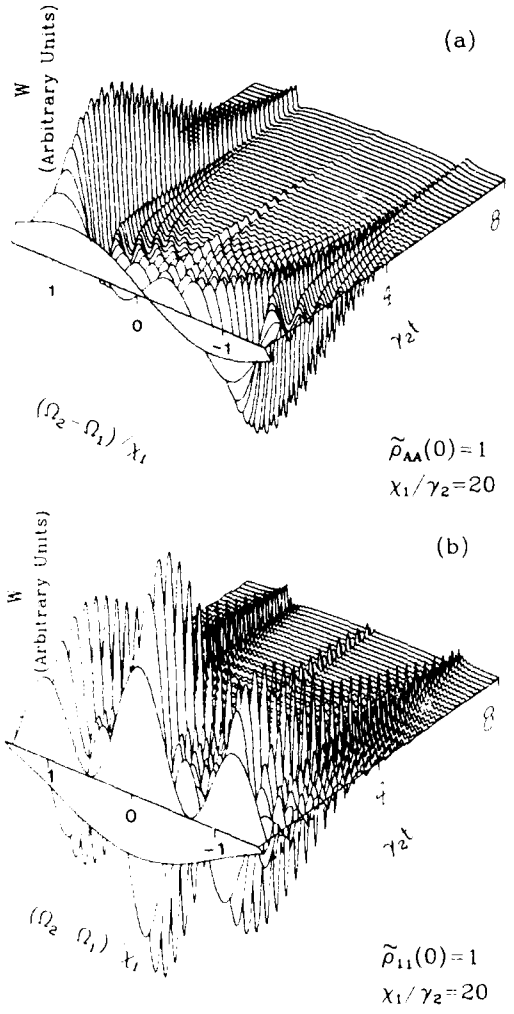

FIG. 11. Transient probe-absorption spectra for a resonant pump field as a function of probe detuning $(\Omega_2-\Omega_1)/\chi_1$ and time $\gamma_{21}t$ for the same parameters and initial condition as in Fig. 7, namely, $\chi_1/\gamma_2=20$, and (a) $\rho_{AA}(0)=1$, (b) $\tilde{\rho}_{11}(0)=1$. The transient probe response has not yet arrived at the steady-state spectrum, which is independent of initial conditions and is displayed in Fig. 8(b). The spectrum in (b) is symmetric about zero probe detuning ($\Omega_2=\omega_{21}$).

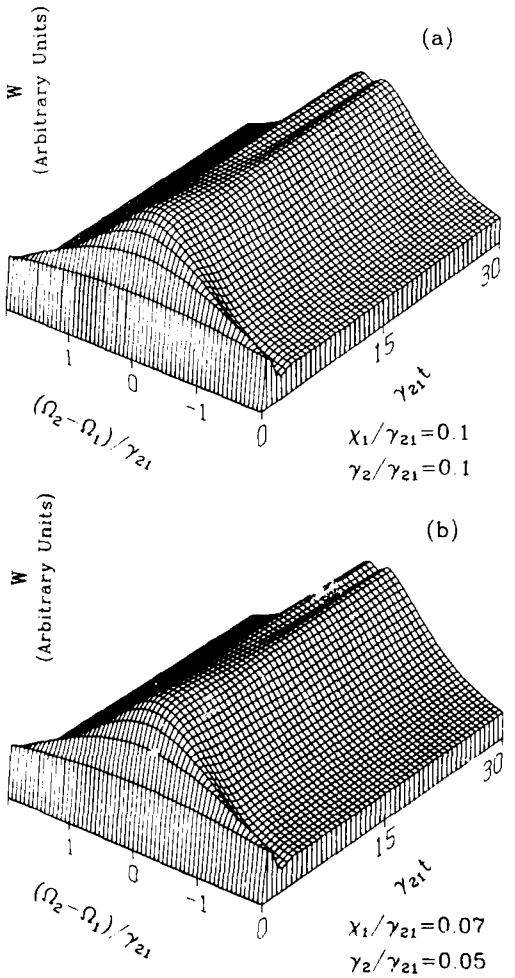

FIG. 12. Transient spectra of probe absorption for a weak, resonant pump field as a function of both probe detuning $(\Omega_2-\Omega_1)/\gamma_{21}$ and time $\gamma_{21}t$ with initial condition $\tilde{\rho}_{11}(0)=1$ and parameters (a) $\chi_1/\gamma_{21}=0.1$, $\gamma_2/\gamma_{21}=0.1$; (b) $\chi_1/\gamma_{21}=0.07$, $\gamma_2/\gamma_{21}=0.05$.

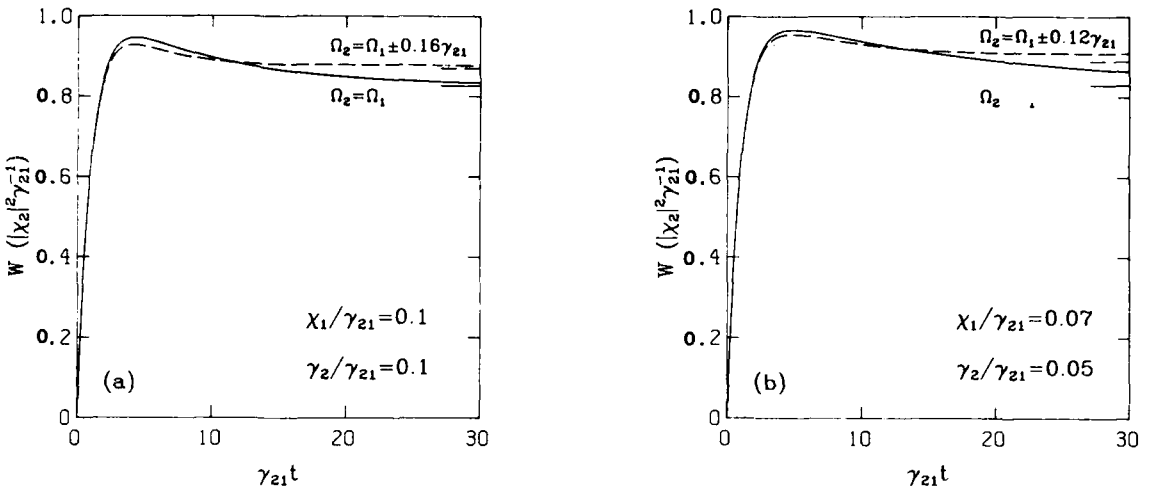

FIG. 13. The transient response at hole center $\Omega_2=\Omega_1$ and hole borders (a) $\Omega_2=\Omega_1\pm0.16\gamma_{21}$, (b) $\Omega_2=\Omega_1\pm0.12\gamma_{21}$ for the same situation and initial condition as in Fig. 12. A hole border is that frequency for which there is a local maximum in the steady-state probe-absorption spectrum. The short lines on the right-hand side indicate the steady-state values.

$$W(t)\approx|\chi_2|^2\left\{\frac{\gamma_{21}}{\gamma_{21}^2+\delta^2}\left[1+\frac{\chi_1^2\exp(-\gamma_2 t)}{2\gamma_2\gamma_{21}}\right]-\frac{\chi_1^2(\gamma_{21}-\frac{1}{2}\gamma_2)}{\gamma_{21}(\gamma_{21}-\gamma_2)^2}\,\frac{\gamma_2-[\gamma_2\cos(\delta t)-\delta\sin(\delta t)]\exp(-\gamma_2 t)}{\gamma_2^2+\delta^2}\right\}\quad\text{for }\exp(-\tfrac{1}{2}\gamma_{21}t)\ll1\ . \tag{5.3}$$

VI. EFFECTS OF COLLISIONS FOR LARGE PUMP DETUNING

The steady-state probe-absorption spectrum is given by Eq. (3.18). For large pump detunings $\Delta_1^2\gg\chi_1^2$, it consists of a large linear absorption peak at $\Omega_2\approx\omega_{21}$, a "Raman" emission peak at $\Omega_2\approx2\Omega_1-\omega_{21}$ and a dispersion structure at $\Omega_2=\Omega_1$. The dispersion structure arises from atomic relaxation and is described by the term $\mathrm{Im}[C_{00}/(\Gamma_1-i\delta)]$ in Eq. (3.18). For large detunings,

$$(\chi_1/\Delta_1)^2\ll1,\quad\gamma_2/\gamma_{21}\ , \tag{6.1}$$

C_{00} can be written as

$$C_{00}\approx-\frac{\chi_1^2}{2\Delta_1}\left\{\left[\frac{2\gamma_{21}-\gamma_2}{\omega_{BA}}\right]\left[1-\frac{\gamma_{21}\chi_1^2}{\gamma_2\Delta_1^2}\right]+\frac{\gamma_{21}}{\omega_{BA}}\,\frac{\chi_1^2}{\Delta_1^2}\right\}\ . \tag{6.2}$$

Consequently, the dispersion structure is of order $(\gamma_{21}/\omega_{BA})(\chi_1/\Delta_1)^2$ (relative to the linear absorption peak) in the presence of collisions and of order $(\gamma_{21}/\omega_{BA})(\chi_1/\Delta_1)^4$ in the absence of collisions. To order $(\chi_1/\Delta_1)^2$ it appears only when $\gamma_{21}\neq\gamma_2/2$.

The discussion in this section for transient spectra is limited to initial condition $\tilde\rho_{11}(0)=1$ and the large pump detuning condition (6.1). Among 12 terms of $\mathrm{Im}[C_{lm}Z_{lm}(t)]$ [see Eqs. (3.16), (A1), and (A2)], four ($lm=00;02;0,\pm1$) are resonant at $\Omega_2=\Omega_1$. None of the four terms, however, gives a dispersion structure at early times. Only for later times does $\mathrm{Im}(C_{00}Z_{00})$ give a dispersion structure. Explicitly, at early times,

$$W(t)=|\chi_2|^2\exp(-\gamma_{21}t)\left\{\frac{\chi_1^2}{2\delta\Delta_1}-\frac{\chi_1^2}{2\Delta_1}(\sin(\omega_{BA}t)-\sin\{[\omega_{BA}-\mathrm{sgn}(\Delta_1)\delta]t\})+\frac{\sin\{[\omega_{BA}-\mathrm{sgn}(\Delta_1)\delta]t\}}{\omega_{BA}}\right\}$$

$$\text{for }\gamma_{21}t\lesssim1,\quad|\delta|\ll\omega_{BA}\ . \tag{6.3}$$

The transient probe absorption is of order $|\chi_2|^2\gamma_2^{-1}(\chi_1/\Delta_1)^2$ at $\Omega_2=\Omega_1$, which is much larger than that of steady state [of order $|\chi_2|^2\gamma_2^{-1}(\gamma_{21}/\omega_{BA})(\chi_1/\Delta_1)^2$]. The transient probe spectra under the condition (6.1) oscillates many cycles before it is damped out by relaxation. Consequently, we show only full transient probe spectra at two sets of times shifted from each other by $\pi/(2\omega_{BA})$. We plot the transient probe spec-

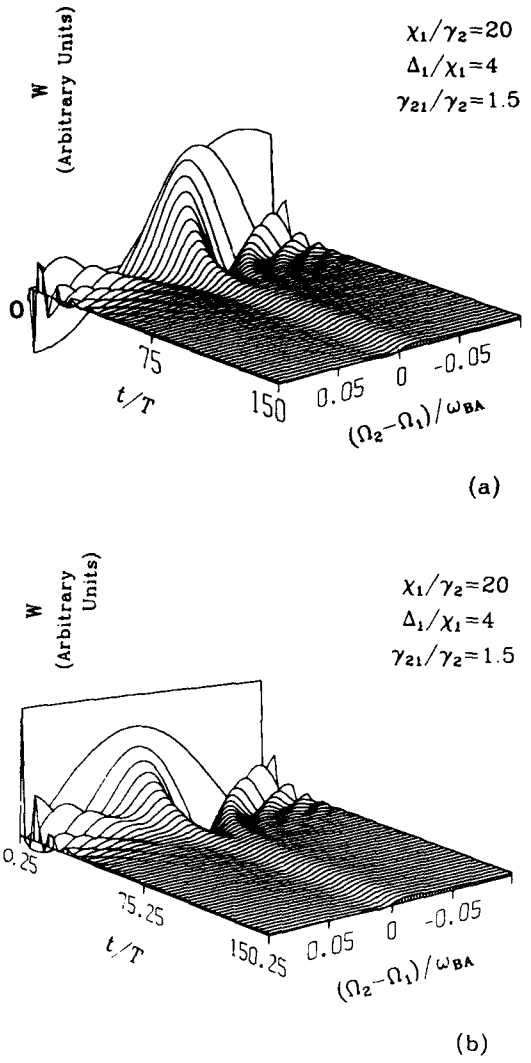

FIG. 14. The central part of transient probe spectra in the presence of collisions ($\gamma_{21}/\gamma_2=1.5$) in the large pump detuning case as a function of both frequency $(\Omega_2-\Omega_1)/\omega_{BA}$ and time t/T ($T=2\pi/\omega_{BA}$) for initial condition $\tilde{\rho}_{11}(0)=1$ and parameters $\chi_1/\gamma_2=20$, $\Delta_1/\chi_1=4$. The step length in time t/T is 3 with starting point (a) $t/T=0$ and (b) $t/T=\frac{1}{4}$, so that the transient spectra do not show oscillatory structure, but only an envelope. The height of the large absorption peak at steady state is about 56 times as high as that of the highest spectral point shown in (a).

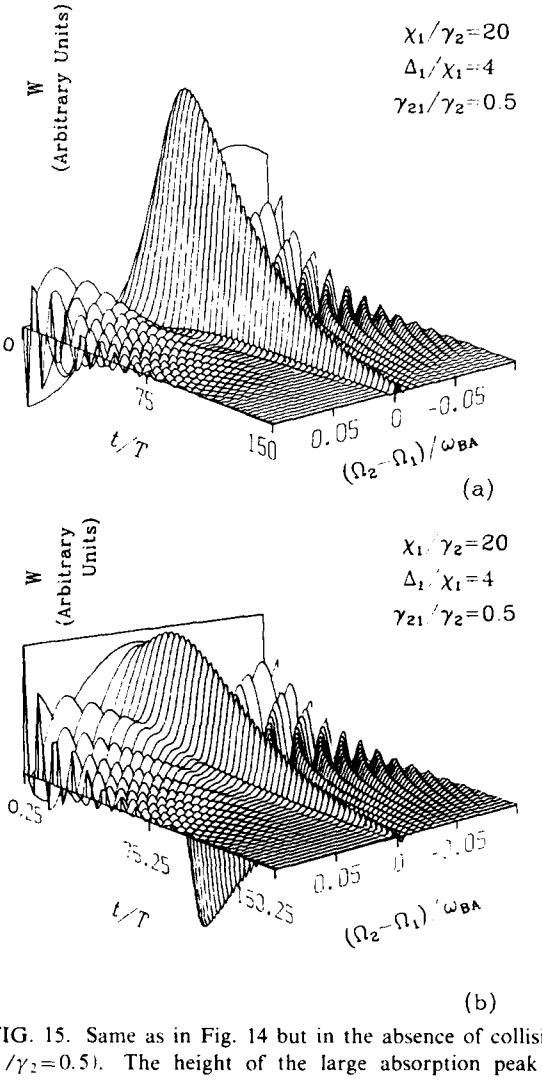

FIG. 15. Same as in Fig. 14 but in the absence of collision ($\gamma_{21}/\gamma_2=0.5$). The height of the large absorption peak at steady state is about 85 times as high as that of the highest spectral point shown in (a).

trum with collisions ($\gamma_{21}=1.5\gamma_2$) in Fig. 14 and that without collisions ($\gamma_{21}=0.5\gamma_2$) in Fig. 15 for the same parameters $\chi_1=20\gamma_2$, $\Delta_1=4\chi_1$. The step length in time in the plotting is $3T$ ($T=2\pi/\omega_{BA}$) with starting value (a) $t=0$ and (b) $t=T/4$, so that the full transient spectra do not show oscillatory structure but only an "envelope." One sees that the dispersion structure may be seen in the presence of collisions only after $\exp(-\gamma_{21}t)\ll 1$.

VII. DISCUSSION

Atoms in the upper (lower) dressed state correspond to the Bloch vector **B** parallel (antiparallel) to the driving vector $\mathbf{\Omega}_B$.[17-19] Preparing atoms in a pure dressed state can be accomplished by a phase-switching method.[12,19] For a resonant pump field, preparing atoms in a pure dressed state is made by an application of a $\pi/2$ pulse followed by a quick $\pi/2$ phase change.[19] For an off-resonant pump field $\Delta_1>0$ ($\Delta_1<0$), preparing atoms in the lower (upper) dressed state can be done by applying a pulse at pump frequency Ω_1 followed by a quick phase change as described in Ref. 12. Preparing atoms in the upper (lower) dressed state with $\Delta_1>0$ ($\Delta_1<0$), however, needs more discussion. If $\chi_1\geq\sqrt{3}|\Delta_1|$, i.e., $|\theta-\pi/2|\leq\pi/6$, a pulse of duration τ at pump frequency Ω_1 followed by a fast phase increase (decrease) $\Delta\phi_1$ aligns the Bloch vector **B** parallel (antiparallel) to the driving vector $\mathbf{\Omega}_B$—atoms in the

upper (lower) dressed state, where

$$\tau=\omega_{BA}^{-1}\ \arccos\{1-[2\cos^2(\tfrac{1}{4}\pi+|\tfrac{1}{4}\pi-\tfrac{1}{2}\theta|)]^{-1}\}$$
$$=\omega_{BA}^{-1}\ \arccos\{1-[1+(\chi_1/\Delta_1)^2]^{1/2}\}^{-1}\ , \tag{7.1}$$

and

$$\Delta\phi_1=\pi-\ \arctan\ \frac{(1-2\sin|\tfrac{1}{2}\pi-\theta|)^{1/2}}{|\cos\theta|}$$
$$=\pi-\ \arctan\ ([1+(\chi_1/\Delta_1)^2]^{1/2}$$
$$\times\{[1+(\chi_1/\Delta_1)^2]^{1/2}-2\})^{1/2}\ . \tag{7.2}$$

If $\Delta_1>0$ ($\Delta_1<0$) and $\chi_1<\sqrt{3}|\Delta_1|$, i.e., $|\theta-\pi/2|>\pi/6$, a pulse at frequency Ω_1 followed by a quick phase change (one pulse–phase-switching cycle) can never put atoms (initially in the level 1) in the upper (lower) dressed state. In this case the preparation of the upper (lower) dressed state can be accomplished by the application of two pulse–phase-switching cycles (for example, the first cycle consists of a pulse of duration π/ω_{BA} with frequency Ω_1 and a π phase change) (when $|\theta-\pi/2|\leq 3\pi/10$) or more such cycles (when $|\theta-\pi/2|>3\pi/10$). It can also be made by first applying a resonant pulse of area π to put atoms in level 2 and then employing one pulse–phase-switching cycle at frequency Ω_1.

In summary, the transient response of two-level atoms in an atomic beam to a step-function weak probe and a strong pump field has been studied. The transient spectra of probe absorption is a sensitive function of the initial conditions of the dressed atoms. When atoms are initially in a superposition of dressed states, the absorption and emission peaks exhibit oscillations as they evolve towards their steady-state values. Moreover, novel spectral features at $\Omega_2=\Omega_1$ can be observed in transient probe spectra, which gives absorption and emission alternately and is totally absent in the steady-state limit. In contrast, when atoms are initially prepared in a pure dressed state, the absorption and emission peaks do not oscillate appreciably as they approach the same steady-state values. For a resonant pump field spectral components at $\Omega_2=\Omega_1\pm\chi_1$, which are absent in the steady-state limit, can be observed in the transient regime. The transient probe spectrum arising from atoms initially prepared in a pure *dressed* state consists of one absorption and one emission component, while that arising from atoms initially in an *atomic* state is symmetric and consists of three oscillatory components. All these can be physically explained by using the conventional dressed-atom picture (DAP). In the secular approximation (i.e., to leading order $|\chi_2|^2\gamma_2^{-1}$), Eq. (4.20) gives quantitative expressions for probe spectra valid in both the transient and steady-state limits.

The effects of collisions on transient probe spectra were also studied. The narrow central hole on the large absorption peak found in the steady state for a resonant weak pump field is formed after $t\gtrsim\gamma_2^{-1}$. The dispersion structure at $\Omega_2=\Omega_1$ found in the steady state of the large pump detuning case may be seen in the presence of collisions only after $t\gg\gamma_{21}^{-1}$.

ACKNOWLEDGMENTS

We would like to thank Professor T. W. Mossberg for several stimulating discussions concerning this work. This research is supported by the U. S. Office of Naval Research and the National Science Foundation under Grant No. PHY-84-15781.

APPENDIX A: EXPRESSION FOR $Z_{lm}(t)$ AND C_{lm}

$$Z_{(0)}=\frac{1-\exp[-(\Gamma_1-i\delta)t]}{\Gamma_1-i\delta}\ , \tag{A1a}$$

$$Z_{\cdot 1,0}=\frac{1-\exp\{-[\Gamma_2-i(\delta\mp\omega_{BA})]t\}}{\Gamma_2-i(\delta\mp\omega_{BA})}\ , \tag{A1b}$$

$$Z_{02}=\frac{\exp(i\delta t)-1}{i\delta}\exp(-\Gamma_1 t)\ , \tag{A1c}$$

$$Z_{\cdot 1,2}=\frac{\exp(-\Gamma_1 t)-\exp\{-[\Gamma_2-i(\delta\mp\omega_{BA})]t\}}{\Gamma_2-\Gamma_1-i(\delta\mp\omega_{BA})}\ , \tag{A1d}$$

$$Z_{\cdot 1,1}=\frac{\exp[-(\Gamma_2\mp i\omega_{BA})t]-\exp[-(\Gamma_1-i\delta)t]}{\Gamma_1-\Gamma_2-i(\delta\mp\omega_{BA})}\ , \tag{A1e}$$

$$Z_{0,\cdot 1}=\frac{\exp(i\delta t)-1}{i\delta}\exp[-(\Gamma_2\mp i\omega_{BA})t]\ , \tag{A1f}$$

$$Z_{\cdot 1,\cdot 1}=\frac{\exp[i(\delta\mp\omega_{BA})t]-\exp(\pm i\omega_{BA}t)}{i(\delta\mp 2\omega_{BA})}\exp(-\Gamma_2 t)\ ; \tag{A1g}$$

$$C_{(0)}=-\tfrac{1}{2}a(\epsilon_{21}-\epsilon_0\cos^2\theta)\sin^2\theta\cos\theta\ , \tag{A2a}$$

$$C_{\pm 1,0}=\pm\tfrac{1}{4}a(1\pm\cos\theta)[i(1\pm\cos\theta)\cos\theta+(\epsilon_{21}-\epsilon_0\cos^2\theta)\sin^2\theta]\ , \tag{A2b}$$

$$C_{02}=\tfrac{1}{4}\epsilon_0\{u(0)\sin\theta-[w(0)+a]\cos\theta\}\sin^2(2\theta)\ , \tag{A2c}$$

$$C_{\pm 1,2}=\pm\tfrac{1}{4}(1\pm\cos\theta)(i\{u(0)\sin\theta-[w(0)+a]\cos\theta-\epsilon_0 v\sin\theta\cos\theta\}(1\pm\cos\theta)$$
$$-2\epsilon_0\{u(0)\sin\theta-[w(0)+a]\cos\theta\}\sin^2\theta\cos\theta)\ , \tag{A2d}$$

$$C_{\pm 1,1}=-\tfrac{1}{4}i\sin\theta\{[u(0)\cos\theta\pm iv(0)+w(0)\sin\theta][(1\pm\cos\theta)(1\mp i\epsilon_0)-2i\epsilon_0\sin^2\theta\cos\theta]$$
$$\pm i\epsilon_2\sin\theta(1\pm\cos\theta)+i\epsilon_0\sin\theta[iv(0)(1\mp\cos\theta)\sin\theta\pm w(0)(1\pm\cos\theta+\tfrac{1}{2}\sin^2\theta)]\}\ , \tag{A2e}$$

$$C_{0,\pm 1}=-\tfrac{1}{4}\sin\theta(i[u(0)\cos\theta\pm iv(0)+w(0)\sin\theta\pm i\epsilon_2\sin\theta](1\mp\cos\theta)$$
$$+\epsilon_0\{\pm(1\pm\cos\theta)(1-3\sin^2\theta)[u(0)\cos\theta\pm iv(0)+w(0)\sin\theta]$$
$$+\tfrac{1}{8}u(0)\sin^2(2\theta)+iv(0)(\tfrac{9}{2}\sin^2\theta-2\pm\sin^2\theta\cos\theta)$$
$$+w(0)(2+3\sin^3\theta-\tfrac{5}{2}\sin^2\theta-\sin\theta\cos\theta\mp 3\sin\theta\cos^2\theta\pm 2\sin^2\theta)\})\ , \tag{A2f}$$

$$C_{\pm 1,-1}=\pm\tfrac{1}{8}\epsilon_0[u(0)\cos\theta\pm iv(0)+w(0)\sin\theta](1\pm\cos\theta)^3\sin\theta\ , \tag{A2g}$$

where

$$\Gamma_1=\gamma_{21}+\gamma_0\cos^2\theta\ , \tag{A3a}$$

$$\Gamma_2=\tfrac{1}{2}(\gamma_2+\gamma_{21}-\gamma_0\cos^2\theta)\ , \tag{A3b}$$

$$\gamma_0=\gamma_2-\gamma_{21}\ , \tag{A3c}$$

$$\cos\theta=\Delta_1/\omega_{BA},\quad \sin\theta=\Upsilon_1/\omega_{BA},\quad 0\le\theta\le\pi \tag{A4}$$

$$a=[\cos^2\theta+(\gamma_{21}/\gamma_2)\sin^2\theta]^{-1}=\gamma_2/\Gamma_1\ , \tag{A5}$$

$$\epsilon_2=\gamma_2/\omega_{BA},\quad \epsilon_{21}=\gamma_{21}/\omega_{BA},\quad \epsilon_0=\gamma_0/\omega_{BA}\ . \tag{A6}$$

APPENDIX B: EXACT SOLUTION OF PROBE ABSORPTION FOR A RESONANT PUMP FIELD

When the pump field is exactly resonant ($\Delta_1=0$), expressions for all the eigenvalues of the matrix L are quite simple. Consequently, $\tilde\rho^{(1)}$ is readily obtained to all orders in γ_2/Υ_1 and γ_{21}/Υ_1 from Eqs. (3.10b). Again, $\tilde\rho_{21}^{(1)}$ can be written in the form

$$\tilde\rho_{21}^{(1)}(t)=\tilde\Upsilon_2 h(t)e^{-i\delta t}+\tilde\Upsilon_2^{*}q(t)e^{i\delta t}\ , \tag{B1}$$

where $q(t)$ gives a four-wave-mixing response and

$$h(t)=\tfrac{1}{2}\sum_{l=-1}^{1}\sum_{m=1}^{2}c_{lm}z_{lm}(t)\ , \tag{B2}$$

$$c_{00}=\tfrac{1}{2}i\epsilon_3\bar\epsilon_{21}\ , \tag{B3a}$$

$$c_{\pm 1,0}=\tfrac{1}{4}\epsilon_3[i\bar\epsilon_{21}\pm\eta(1-\tfrac{1}{2}\bar\epsilon_{21}\bar\epsilon_0)]\ , \tag{B3b}$$

$$c_{02}=0\ , \tag{B3c}$$

$$c_{\pm 1,2}=\pm\tfrac{1}{4}\eta u(0)\ , \tag{B3d}$$

$$c_{\pm 1,1}=-\tfrac{1}{2}(i\eta^{-1}\mp\tfrac{1}{2}\bar\epsilon_0)(\xi\pm i\zeta)\ , \tag{B3e}$$

$$c_{0,\pm 1}=-\tfrac{1}{2}i\eta(\xi\pm i\zeta)\ , \tag{B3f}$$

$$c_{\pm 1,-1}=\pm\tfrac{1}{4}\bar\epsilon_0(1\pm\tfrac{1}{2}i\bar\epsilon_0\eta)(\xi\pm i\zeta)\ , \tag{B3g}$$

where

$$\eta=\Upsilon_1/\sigma,\quad \sigma=(\Upsilon_1^2-\tfrac{1}{4}\gamma_0^2)^{1/2}\ , \tag{B4a}$$

$$\epsilon_3=\bar\epsilon_2/(1+\bar\epsilon_2\bar\epsilon_{21})\ , \tag{B4b}$$

$$\xi=\tfrac{1}{2}\eta[w(0)+\tfrac{1}{2}\bar\epsilon_0 v(0)+\tfrac{1}{2}\epsilon_3(\bar\epsilon_2+\bar\epsilon_{21})]\ ,$$
$$\zeta=\tfrac{1}{2}[v(0)+\epsilon_3]\ , \tag{B4c}$$

z_{lm} are obtained from Z_{lm} [see Eqs. (A1)] by changing ω_{BA} to σ; $\bar\epsilon_2$, $\bar\epsilon_{21}$, and $\bar\epsilon_0$ are the values of ϵ_2, ϵ_{21}, and ϵ_0 at $\Delta_1=0$, respectively.

Probe absorption is proportional to

$$W(t)=2|\Upsilon_2|^2\,\mathrm{Im}h(t)\ , \tag{B5}$$

which has the symmetry relation

$$W(t;\delta,u(0),v(0),w(0))$$
$$=W(t;-\delta,-u(0),v(0),w(0))\ , \tag{B6a}$$

or in terms of the semiclassical dressed-state initial conditions,

$$W(t;\delta,\tilde\rho_{AA}(0),\tilde\rho_{AB}(0))=W(t;-\delta,\tilde\rho_{BB}(0),\tilde\rho_{AB}(0))\ . \tag{B6b}$$

As $t\sim\infty$, W is only a function of δ. Consequently, in steady state the probe absorption spectrum with a resonant pump field is symmetric about $\Omega_2=\Omega_1$.

[1]B. R. Mollow, Phys. Rev. A **5**, 2217 (1972).
[2]S. Haroche and F. Hartmann, Phys. Rev. A **6**, 1280 (1972).
[3]F. Y. Wu, S. Ezekiel, M. Ducloy, and B. R. Mollow, Phys. Rev. Lett. **38**, 1077 (1977).
[4]C. Cohen-Tannoudji and S. Reynaud, J. Phys. B **10**, 345 (1977); in *Multiphoton Processes*, edited by J. H. Eberly and P. Lambropoulos (Wiley, New York, 1978).
[5]M. Sargent III, Phys. Rep. **43**, 223 (1978).
[6]G. S. Agarwal, Phys. Rev. A **18**, 1490 (1978); G. Nienhuis, J. Phys. B **14**, 1963 (1981).
[7]G. S. Agarwal, Phys. Rev. A **19**, 923 (1979).
[8]R. W. Boyd and S. Mukamel, Phys. Rev. A **29**, 1973 (1984).
[9]G. Khitrova, Ph.D. thesis, New York University, 1986.
[10]E. V. Baklanov and V. P. Chebotaev, Zh. Eksp. Teor. Fiz. **60**, 552 (1971) [Sov. Phys.—JETP **33**, 300 (1971)]; **61**, 922 (1971) [**34**, 490 (1972)].
[11]G. Grynberg, E. Le Bihan, and M. Pinard, J. Phys. (Paris) **47**, 1321 (1986).
[12]N. Lu, P. R. Berman, A. G. Yodh, Y. S. Bai, and T. W. Mossberg, Phys. Rev. A **33**, 3956 (1986).
[13]S. H. Autler and C. H. Townes, Phys. Rev. **100**, 703 (1955); A. Schabert, R. Keil, and P. E. Toschek, Appl. Phys. **6**, 181 (1975); J. L. Picqué and J. Pinard, J. Phys. B **9**, L77 (1976); H. R. Gray and C. R. Stroud, Jr., Opt. Commun. **25**, 359 (1978); P. R. Hermmer, B. W. Peuse, F. Y. Wu, J. E. Thomas, and S. Ezekiel, Opt. Lett. **6**, 531 (1981).
[14]Y. S. Bai, T. W. Mossberg, N. Lu, and P. R. Berman, Phys. Rev. Lett. **57**, 1692 (1986).
[15]N. Lu, P. R. Berman, Y. S. Bai, J. E. Golub, and T. W. Mossberg, Phys. Rev. A **34**, 319 (1986).
[16]J. H. Eberly, C. V. Kunasz, and J. Wódkiewicz, J. Phys. B **13**, 217 (1980).
[17]D. Grischkowsky, Phys. Rev. A **14**, 802 (1976).
[18]E. Courtens and A. Szöke, Phys. Rev. A **15**, 1588 (1977).
[19]Y. S. Bai, A. G. Yodh, and T. W. Mossberg, Phys. Rev. Lett. **55**, 1277 (1985).
[20]Pump-field–interaction representation is defined by

$$|\tilde{1}\rangle = \exp[i(\Omega_1 t - \mathbf{k}_1\cdot\mathbf{r} + \phi_1)]\,|1\rangle\ ,$$

$$|\tilde{2}\rangle = |2\rangle\ ,$$

for which

$$\tilde{\rho}_{21} = \rho_{21}\exp[i(\Omega_1 t - \mathbf{k}_1\cdot\mathbf{r} + \phi_1)]\ ,$$

$$\tilde{\rho}_{jj} = \rho_{jj}\ .$$

[21]See, for example, C. Cohen-Tannoudji, in *Frontiers in Laser Spectroscopy*, edited by R. Balian, S. Haroche, and S. Liberman (North-Holland, Amsterdam, 1977).
[22]P. R. Berman and R. Salomaa, Phys. Rev. A **25**, 2667 (1982).
[23]The semiclassical dressed states are defined in terms of bare states in the pump-field–interaction representation as

$$|A\rangle = \cos(\tfrac{1}{2}\theta)\,|\tilde{1}\rangle + \sin(\tfrac{1}{2}\theta)\,|\tilde{2}\rangle\ ,$$

$$|B\rangle = -\sin(\tfrac{1}{2}\theta)\,|\tilde{1}\rangle + \cos(\tfrac{1}{2}\theta)\,|\tilde{2}\rangle\ .$$

[24]R. J. Glauber, Phys. Rev. **131**, 2766 (1963).
[25]Strictly speaking, $\tilde{\rho}_{\mu\nu}$ appearing in Eq. (4.3) changes slightly with n through angle θ defined in Eq. (3.21), since χ_1 should be replaced by $\chi_1(n/\bar{n})^{1/2}$, where $\bar{n} = |\alpha|^2$. The $\tilde{\rho}_{\mu\nu}$'s variation with n, however, may be omitted for n within the width $\Delta n = |\alpha|$ of photon-number distribution centered at $\bar{n}$.
[26]The quantitative relation between the conventional dressed states $|A_n\rangle$ and $|B_n\rangle$ and bare states $|1,n\rangle$ and $|2,n-1\rangle$ is

$$|A_n\rangle = \cos(\tfrac{1}{2}\theta)\,|1,n\rangle + \sin(\tfrac{1}{2}\theta)\,|2,n-1\rangle\ ,$$

$$|B_n\rangle = -\sin(\tfrac{1}{2}\theta)\,|1,n\rangle + \cos(\tfrac{1}{2}\theta)\,|2,n-1\rangle\ .$$

Total probe transition rate between two adjacent doublets is proportional to

$$\sum_{\mu,\nu=A,B} |\langle \nu_{n-1}|\mathbf{p}\cdot\hat{\mathcal{E}}_2|\mu_n\rangle|^2 = |\mathbf{p}_{21}\cdot\hat{\mathcal{E}}_2|^2\ .$$

[27]S. Reynaud, Thèse de troisième cycle, Paris, 1977.
[28]The dressed-state density matrix elements appearing in Eqs. (4.9a) and (4.9b) emerge naturally if one first calculates the transient probe spectra in the semiclassical DAP (rather than in the bare-state picture as we present in the text) and then takes the steady-state limit.
[29]To second order in $\epsilon_0 = \gamma_0/\omega_{BA}$ more accurate positions of the two side peaks are $\delta = \pm\omega_{BA}[1 - \epsilon_0^2\sin^2\theta(1+3\cos^2\theta)/8]$. This indicates that atomic relaxation has an effect of reducing ac Stark (dressed state) splitting of energy levels.
[30]In the Bloch vector space, we may relate the semiclassical dressed-state coherence $\tilde{\rho}_{AB}$ to **B**'s perpendicular component $\mathbf{B}_\perp = \mathbf{B} - (\mathbf{B}\cdot\hat{\Omega}_B)\hat{\Omega}_B$ as

$$2\,\mathrm{Re}\tilde{\rho}_{AB} = \mathbf{B}_\perp\cdot(\mathbf{v}\cdot\hat{\Omega}_B)\ ,$$

$$2\,\mathrm{Im}\tilde{\rho}_{AB} = \mathbf{B}_\perp\cdot\hat{\mathbf{v}}\ ,$$

where $\hat{\mathbf{v}}$ is the unit vector along v axis. When **B** and $\mathbf{\Omega}_B$ are parallel, $\tilde{\rho}_{AB}$ vanishes.